# INVESTIGATIONS ON ENHANCEMENT OF POWER QUALITY OF GRID CONNECTED AND ISLANDED HYBRID DISTRIBUTED GENERATING SYSTEMS

*Submitted to Delhi Technological University*

*In Partial fulfillment of the requirements for the award of degree of*

**DOCTOR OF PHILOSOPHY**

**by**

**DINANATH PRASAD**

**(2K16/PHDEE/19)**

**Department of Electrical Engineering**


**DEPARTMENT OF ELECTRICAL ENGINEERING**
**DELHI TECHNOLOGICAL UNIVERSITY**
**DELHI-110042, INDIA**

**August, 2024**

# CANDIDATE'S DECLARATION

I **Dinanath Prasad** hereby certify that the work which is being presented in this thesis entitled "**Investigations on Enhancement of Power Quality of Grid-connected and Islanded Hybrid Distributed Generating Systems"** in partial fulfillment of the requirements for the award of the Degree of Doctor of Philosophy, submitted in the Department of Electrical Engineering, Delhi Technological University is an authentic record of my own work under the supervision of **Prof. Narendra Kumar**, Department of Electrical Engineering, Delhi and **Prof. Rakhi Sharma**, Professor, School of Engineering and Technology, Indira Gandhi National Open University, Maidan Garhi, New Delhi.

The matter presented in this thesis has not been submitted by me for the award of any other degree of this or any other Institute.

Candidate's Signature

# CERTIFICATE

This is to certify that the thesis entitled "**Investigations on Enhancement of Power Quality of Grid-connected and Islanded Hybrid Distributed Generating Systems"** being submitted by **Mr. Dinanath Prasad (2K16/PHD/EE/19)** for the award of the degree of Doctor of Philosophy in the Department of Electrical Engineering, Delhi Technological University, Delhi, is the record of students own work carried out by him under the supervision of **Prof. Narendra Kumar** and **Prof. Rakhi Sharma** and has fulfilled the requirements which to our knowledge has reached the requisite standard for the submission of this thesis. It is further certified that the work embodied in this thesis has neither partially nor fully submitted any other University or Institution for the award of any degree or diploma.

**Prof. Narendra Kumar**
**(Supervisor)**
Department of Electrical Engineering
Delhi Technological University
Bawana Road, Delhi-110042, India

**Prof. Rakhi Sharma**
**(Co-Supervisor)**
School of Engineering and Technology
Indira Gandhi National Open University
Maidan Garhi, New Delhi- 110068

**Dr. Rachna Garg**
Professor and Head of the Department
Department of Electrical Engineering
Delhi Technological University
Bawana Road, Delhi-110042, India

# ACKNOLEDGEMENTS

I would like to express my deep and sincere gratitude to my supervisors **Prof. Narendra Kumar** and **Prof. Rakhi Sharma** for their valuable guidance and continuous monitoring of my research work. It was great honor for me to pursue my research work under their supervision. Prof. Narendra Kumar has been the main motivating and inspiring force behind my research work. It is his vigor and hunger to perform in adverse situations, which has inspired me to strive for excellence and nothing less. Continuous monitoring by Prof. Rakhi Sharma, valuable guidance, and input have always been a driving force to complete my research work.

I would also like to convey my sincere gratitude to **Dr. Rachna Garg,** Professor and Head of the Department, who taught me the coursework. I would like to thank the SRC members mainly **Prof. P. R. Sharma,** YMCA University of Science and Technology, Faridabad, who have given me valuable guidance and advice to improve the quality of my research work. I am extremely thankful to **Prof. Alka Singh, and Prof. Suman Bhowmick** for their valuable assistance and support. I am extremely thankful to staff members of various labs, DTU, and Delhi for providing me with immense facility and assistance to carry out my research work. I would like to thank other office staff, Central Library and Computer Center staff, for their valuable co-operation and support.

I would like to my sincere thanks to **Dr. Vineet P Chandran**, who has guided me to develop at an initial level of research work. His research publications have guided me during all time of my research work. I am extremely grateful to my research group and friends Hemant Saxena, Saket Gupta, Ambrish Devanshu, Nupur Mittal, Deepak Narang, Harsh Mohan Sharma, Gaurav Srivastava, Ankit Dixit, Rahul Dixit, Praveen

Kumar Dhull, Mahendra Dutt Dwivedi, Mahesh Sharma for their valuable assistance, co-operation, and a great source of learning.

If I get any success today for my research work, the entire credit should go to my mother Smt. Shanti Devi, father Mr. Ajit Kumar, wife Jyotsna Kumari, my elder brother Shambhu Kumar and my sister-in-law Poonam Kumari. I would like to express my deep concern to my daughter, Ananya kumari, and son, Anant Kumar for their consideration for long hours of my absence from home. I would like to thank other family members for supporting me directly and indirectly to carry out my research work. Lastly, I thank almighty, the father of all for his ultimate blessings in accomplishing my research work.

Dinanath Prasad
(2K16/Ph.D/EE/19)

# ABSTRACT

It is not possible to continue using nonrenewable energies like oil, gas, and coal because they release a lot of climate gases. Renewable energies, on the other hand, are better and last longer. The tools to collect and use these powers have also improved. In recent years, they've gotten better, which makes using them more practical and cost-effective. One important way to fight climate change and lessen our reliance on fossil fuels is to use renewable energy sources. Systems that get their power from two or more green sources are called hybrid renewable energy systems. These systems are especially helpful in places that can't connect to the regular power source or where the link is weak or unreliable.

The system that distributes electricity has problems with power quality (PQ), such as low power factor, unbalanced loads, harmonics, uneven voltage and current, and more. Today's electricity systems change so quickly that there are plenty of problems with the quality of the power. In terms of current, voltage, frequency, and other things, Poor power quality is usually caused by problems with the wiring, lightning, bad weather like storms, broken equipment, and other things. However, harmonics are one of the main problems with power quality. This can be caused by several loads that don't behave linearly, such as old loads like transformers, electrical machines, and furnaces,, and new loads like power converters in vapor lights. Also, in the distribution networks' power quality is rapidly declining as a result of the proliferation of power electronic converters in homes, businesses, and factories. There are a lot of issues that are being caused by this, including higher losses, inefficient use of distribution networks, sensitive equipment malfunctioning, and disruption to surrounding customers, protective devices, and communication systems. Injecting intermittent electricity

directly into the distribution grid from renewable sources compounds these issues. Because of the advantages of modern electric equipment, such as reduced maintenance requirements, ease of control, low wear and tear, size and cost reduction, and energy conservation, solid-state controllers have become more prevalent and have exacerbated power quality problems. Because they employ solid-state controllers, electronically controlled energy-efficient commercial and industrial electrical loads are particularly vulnerable to power quality issues and may cause them. In light of the foregoing, this thesis is to help engineers and scientists in the field develop better energy supply systems by identifying, classifying, analyzing, simulating, and quantifying the power quality problems that come along with them.

There is a distinction between the methods used in freshly built and developed equipment and those used to enhance power quality in existing systems that are experiencing power quality issues. Electrical loads and supply systems have distinct types of power quality issues; hence these mitigation approaches are further classed accordingly. Over the last 25 years, there has been a tremendous increase in the amount of time and energy spent studying how to reduce power quality issues. For single-phase two-wire, three-phase three-wire, and three-phase four-wire systems, there has been a lot of study on power filters of different kinds, including passive, active, and hybrid in shunt, series, or a mix of the two configurations, to reduce harmonics and other issues like reactive power, excessive neutral current, and balancing linear and nonlinear loads. Common ways to boost PQ in a distribution system include adding capacitors, changing the taps on transformers, reactors, capacitor banks, and more. But these methods of compensation are slow and don't offer active load compensation, so new special power devices have been made. The technology, called SAPF, is now fully developed and can be used to fix problems with harmonic current, reactive power, and

neutral current in AC distribution networks. In three-phase systems, shunt active power filters are also used to control the voltage at the terminals and stop voltage flicker. Each of these goals can be met on its own or together, based on the needs, the control strategy, and the setup that needs to be chosen correctly. Moreover, improved SAPF dynamic and steady-state performance is now within reach, thanks to advancements in SAPF that allow for the application of various control algorithms. These algorithms include PI (proportional-integral), variable structure, fuzzy logic, and neural network-based control algorithms. These enhancements allow APFs to quickly respond to changing nonlinear loads and take remedial action. More than that, these APFs may counteract harmonics of a higher order, usually up to the 25th harmonic.

As part of the proposed work, design creation and study of both new and old control techniques have been investigated. With both linear and nonlinear loads, simulation and experiment data have been analyzed and put into tables. The sample system has been tried with standard control methods, such as Synchronous Reference Frame Theory (SRFT) and Instantaneous Reactive Power Theory (IPRT).

The SRFT control method with ANN controller is developed and verified with a three phase-four wire SAPF system in MATLAB/Simulink environment. Harmonic current and reactive power adjustment were made possible by the photovoltaic integrated SAPF. Comparisons between the SAPF modified with ANN controller and PI and FLC are made. The DC-link voltage of Shunt APF was maintained constant by the PI, FUZZY, and ANN controllers. The ANN controller-based SAPF delivers better performance than PI and fuzzy controllers. Simulation has been performed in MATLAB/SIMULINK environment.

The other controllers were made for a grid-connected solar/hybrid distribution system. They are referred to as the second-order generalized integrator (SOGI) and the third-order generalized integrator (TOGI). To modify the energy storage of dc-voltage, an artificial neural network controller (ANN), Fuzzy logic is employed with shunt active power filter (SAPF) for PQ improvement. Also, the SAPF is compared and assessed based on PI control, FUZZY controller, and Artificial Neural Network (ANN). Moreover, Fuzzy and ANN techniques are employed with conventional SRFT, SOGI techniques as well as with TOGI control algorithms. As well as being generated in MATLAB/Simulink, the system has also been tested in the real world with a distorted grid and distorted linear and nonlinear loads.

An adaptive fourth-order based frequency locked loop (AFOGI-FLL) controller is developed to provide switching pulses for a three-phase IGBT-based voltage source converter. Accurate frequency synchronization, lower and higher-order harmonic elimination, power quality refinement, and reactive power compensation are some of the features of the proposed controller. In addition, a comparative analysis has been performed between the proposed controller and the third-order generalized integrator (TOGI). The comparative analysis results show that fourth-order generalized integrator have higher DC offset elimination capability, and better dynamic performance as well and THD is less compared with the TOGI controllers. Maximum Solar PV system extraction is achieved using the updated perturb and observed method. The proposed controller robustness is validated by an experimental prototype setup and test results exhibit the performances under nonlinear loading. Additionally, the feasibility of the proposed control scheme is demonstrated by using MATLAB/SIMULINK software. The system is robust. The system is well executed under irradiance variations, load fluctuations, and frequency variations as well. The

laboratory prototype is used to demonstrate the proposed system's simulated behaviour and experimental test results.

Next, the stochastic-gradient-based adaptive control algorithms have been discussed and employed for power quality enhancement in a PV-integrated distribution system. Least mean square (LMS), Least mean fourth (LMF), sign-error LMS and $\epsilon$-Normalized LMS ($\epsilon$-NLMS) have been implemented as control algorithms for the estimation of fundamental load current. The performances of these adaptive algorithms have been compared under steady-state and dynamic conditions under the non-linear load conditions in a closed-loop three-phase system.

The most interesting part of this thesis is how to solve PQ problems in a three-phase grid-connected solar/hybrid distribution system with different SAPF configurations and both new and conventional algorithms.

# TABLE OF CONTENTS

Page No.

*Certificate* ..... *i*

*Acknowledgements* ..... *ii-iii*

*Abstract* ..... *iv-viii*

*Table of Contents* ..... *xi-xiii*

*List of Figures* ..... *xv-xix*

*List of Tables* ..... *xx*

*List of Symbols* ..... *xxi-xxv*

*List of Abbreviations* ..... *xxvi-xxvii*

**CHAPTER-1 : INTRODUCTION** **1-12**

1.0 General 1-3

1.1 The State of the Art in Solar and Wind Energy Recourses 3-5

1.2 State of the Art in Power Quality 5-8

1.3 Objectives and Scope 8-9

1.4 Outline of the Thesis 9-12

**CHAPTER-2 : LITERATURE SURVEY** **13-29**

2.0 General 13-14

2.1 Optimizing Power Quality in Photovoltaic Systems 14-20

2.2 Power Quality Issues and Mitigation Techniques 20-27

2.3 Detailed Research Gaps 27-28

2.4 Objective of the Present Work 28-29

2.5 Conclusions 29

**CHAPTER-3 : MODELING AND SIMULATION OF MICROGRID SOLAR PHOTOVOLTAIC SYSTEM WITH ENERGY STORAGE** **30-46**

3.0 General 30

3.1 The Proposed Grid-Connected Microgrid System 30-31

3.2 Modeling of Microgrid Components 31-36

3.2.1 Modeling and Analysis of PV Cell 31
3.2.2 Equivalent circuit of PV cell 32-36
3.3 Maximum Power Point Tracking Techniques 36
3.4 PV Side Converter 37-38
3.5 Microgrid with Storage 38-46
3.5.1 Storage Connected to DC Grid 38-39
3.5.2 Buck-Boost Converter 39-42
3.5.3 Control of Switching for the Buck-Boost Converter 42-43
3.6 Simulation Results 43-46
3.7 Conclusions 46

**CHAPTER-4 : SRF THEORY BASED SHUNT ACTIVE POWER FILTER FOR POWER QUALITY IMPROVEMENT IN GRID INTERFACED SOLAR PHOTOVOLTAIC SYSTEM 47-60**
4.0 General 47
4.1 The Proposed System 47-48
4.2 Shunt APF 48
4.3 SRF Controller 49
4.4 PV Array with MPPT Technique 49-51
4.4.1 Incremental Conductance MPPT Technique 51
4.5 Comparative Analysis Between Different Controllers 52-54
4.5.1 PI Controller 52
4.5.2 Fuzzy Logic Controller (FLC) 52-53
4.5.3 ANN Controller Scheme 53-54
4.6 Results and Discussion 54-59
4.7 Conclusion 60

**CHAPTER-5 : ANN BASED ADAPTIVE SOGI-FLL CONTROLLER FOR MULTIFUNCTIONAL GRID TIED SOLAR ENERGY CONVERSION SYSTEM 61-76**
5.0 General 61
5.1 System Layouts 61-62
5.2 Control Algorithms 62-68
5.2.1 Incremental Conductance-Based MPPT Controller 63

5.2.2 Adaptive SOGI-FLL Control Scheme 64-68
5.3 Results and Discussion 68-75
5.3.1 Behaviour of System Under Nonlinear Load 68-75
5.4 Conclusions 76

**CHAPTER-6 : GRID INTERFACED SOLAR-WIND HYBRID POWER GENERATING SYSTEMS USING FUZZY-BASED TOGI CONTROL TECHNIQUE FOR POWER QUALITY IMPROVEMENT 77-96**
6.0 General 77
6.1 Proposed layouts 78-80
6.1.1 Design of DC-DC boost converter 79-80
6.2 TOGI Control Technique 80-87
6.2.1 Generation of Reference Grid Current 81-87
6.3 Fundamental Load Current Extraction 88-90
6.3.1 Comparative performance analysis of proposed TOGI with conventional algorithms 88-90
6.4 Results and discussion 90-96
6.4.1 Performance Solar-Wind Hybrid System for Linear Load 91-95
6.4.2 Performance of solar-wind hybrid system for non-linear Load 95-96
6.5 Conclusion 96

**CHAPTER-7 : ADAPTIVE FOURTH-ORDER BASED CONTROLLER FOR GRID-INTERFACED THREE-PHASE SOLAR PV SYSTEM FOR POWER QUALITY ENRICHMENT 97-117**
7.0 General 97-98
7.1 Proposed layouts 98
7.2 VSC Switching 99-105
7.2.1 In-phase and Quadrature-phase unit template estimation 100
7.2.2 The fundamental load (FL) current extraction by Adaptive FOGI-FLL controller 100-103
7.2.3 Reference Grid Currents Generation 103-105
7.3 Comparative Performance Analysis of Proposed AFOGI-FLL With TOGI Control Technique 105-108
7.4 Simulation Results 108-114

7.4.1 Characteristics of the system under fixed solar irradiance 109-111
7.4.2 Characteristics of the system under variable solar Irradiance 111-113
7.4.3 Characteristics of the system under sudden disturbances 113-114
7.5 Hardware Implementation 114-116
7.5.1 Behavior of system having non-linear loading 114-116
7.6 Conclusion 117

**CHAPTER-8 : STOCHASTIC GRADIANT BASED CONTROL ALGORITHMS FOR POWER QULAITY ENHANCEMENT IN SPV INTERFACED THREE-PHASE DISTRIBUTION SYSTEM 118-135**
8.0 General 118
8.1 System Configuration 118-119
8.2 Adaptive Control Algorithms 119-123
8.2.1 Least Mean Square (LMS) 119-121
8.2.2 Sign-Error LMS 121-122
8.2.3 $\epsilon$ −Normalized LMS ($\epsilon$ −NLMS) 122-123
8.2.4 Least Mean Fourth (LMF) 123
8.3 Generation of Switching Pulses For DSTATCOM 124-128
8.3.1 Loss Component Estimation 126
8.3.2 Synchronizing Signals Estimation 126-127
8.3.3 PV Feed-Forward Component 127
8.3.4 Reference Current Estimation 127-128
8. 4 Simulation Performance 129-134
8.5 Conclusion 135

**CHAPTER -9 : MAIN CONCLUSIONS AND FUTURE SCOPE OF WORK 136-140**
9.0 General 136-137
9.1 Main Conclusions 137-139
9.2 Future Scope of Work 140

**Publications 141-142**

**References 143-160**

**Appendix 161**

# LIST OF PUBLICATIONS

**REFERENCES**

**APPENDIX A** : SYSTEM DATA FOR THREE PHASE GRID CONNECTED SOLAR PV SYSTEM

**APPENDIX B** : SYSTEM DATA FOR HYBRID POWER GENERATING SYSTEMS

**APPENDIX C** : SYSTEM DATA FOR ADAPTIVE CONTROL ALGORITHMS FOR GRID-TIED PV SYSTEM

# LIST OF FIGURES


Fig. No.

3.1 Schematic diagram of grid connected system

3.2 Equivalent circuit diagram of PV cell

3.3 PV cell Simulink model

3.4 Control circuit of boost converter

3.5 Microgrid with storage

3.6 Buck-Boost circuit diagram

3.7 Bi-directional converter

3.8 Control diagram for a buck-boost converter

3.9 Matlab/Simulink diagram for PV, battery connected to DC link

3.10(a) PV voltage and DC link Voltage when $R_{load}$ = 60 ohm

3.10(b) PV voltage and DC link Voltage when $R_{load}$ = 240 ohm.

3.11 Grid Voltage

3.12 Grid Current

3.13 Line to line voltage during grid-connected mode

4.1 Illustrative diagram of the presented system

4.2 d-q theory for reference current generation

4.3 PV cell's equivalent circuit

4.4 Characteristics of a typical PV cell

4.5 Structure of FLC

4.6 Artificial Neural Network block

4.7 DC link voltage with PI controller

4.8 DC link voltage with fuzzy logic controller

4.9 DC link voltage with ANN controller

4.10 Reactive power compensation with PI controller

4.11 Reactive power compensation with FLC

4.12 Reactive power compensation with ANN controller

4.13 THD analysis of source current with PI controller

4.14 THD analysis of source current with FLC

4.15 THD analysis of source current with ANN controller

5.1 System Configuration

5.2.(a) Adaptive SOFI-FLL control scheme for the fundamental component of load current extraction from phase 'A'

5.2(b) Adaptive SOGI-FLL control scheme for reference current generation

5.3 Artificial Neural Network block

5.4 (a) Waveforms of G, Vdc, Ipv, Ppv, and Ipvq for non-linear load

5.4 (b) Waveform of Vgabc, Igabc, Ica, iLa, Pg, and Qg at step insolation increase from 700 W/$m^2$ to 1000 W/$m^2$

5.6 (a) Waveforms of G, Vdc, Ipv, Ppv, and Ipvq for linear load

5.6 (b) Waveform of Vgabc, Igabc, Ica, iLa, Pg and Qg at step insolation increase from 700 W/$m^2$ to 1000 W/$m^2$ at t=0.4s

5.7 (a) Behaviour of Solar PV system for intentionally load unbalancing

5.7 (b) Behaviour of solar PV system under varying system frequency

6.1 System Configuration

6.2 Reference current extraction by TOGI control algorithm

6.3 Block diagram of TOGI control algorithm

6.4 (a) Input membership function $\mu e$ (n)

6.4 (b) Change in input membership function $\Delta\mu e$ (n)

6.4 (c) Output membership function Vdc(n)

6.5 (a) Fuzzy logic rule function

6.5 (b) Surface Diagram

6.6 (a) DC link voltage estimation by Fuzzy logic Controller

6.6 (b) DC link voltage estimation by PI Controller

6.7 Fundamental load current extraction from TOGI control strategy

6.8 Frequency response analysis between TOGI and various conventional algorithms

6.9 (a)(b)(c) THD of grid current by Proposed TOGI, DSOGI and SOGI controller

6.10 Sudden connections and disconnection of load for SOGI, DSOGI, TOGI

6.11 Performance of hybrid Solar-Wind system under linear load

6.12 Performance of hybrid Solar-Wind system in PFC mode under linear load

6.13 Performance of hybrid Solar-Wind system in PFC mode under liner load

6.14 Performance of hybrid Solar-Wind system in PFC mode under Nonlinear load

7.1 System Configuration
7.2 Flow chart of MPO control technique
7.3 Basic Linear PLL
7.4 Block diagram of an AFOGI-FLL control algorithm
7.5 AFOGI-FLL algorithm for reference current
7.6 (a) Dynamic behaviour of AFOGI-FLL with conventional TOGI controller under sudden connection and disconnection of load
7.6 (b) In-phase component of current magnitude of FOGI-FLL with the conventional TOGI control algorithm
7. 6 (c) Effectiveness of FOGI-FLL for amplitude estimation under the faulty condition with conventional TOGI algorithm
7. 6 (d) Bode diagram with conventional TOGI and AFOGI-FLL algorithm
7. 6 (e) The THD of the current estimation of AFOGI-FLL with the conventional TOGI control algorithm
7.7 (a) Performance under fixed solar irradiance Vgabc, Igabc, G, iLa, iLb, iLc, ica, icb, icc
7.7 (b) Characteristics under fixed solar irradiance Ppv, Ipv, Vdc, Iff, Pg, Gg, ILPA, ILQA
7.8 Characteristics under variable solar irradiance Vgabc, Igabc, G, Ppv, Ipv, Iff, Vdc, Pg, Qg
7.9 (a) Characteristics under sudden disturbances
7.9 (b) Characteristics under sudden disturbances
7.10 Characteristics of the system at varying system frequency Vgabc, Igabc, Ppv, Vdc, Pg, w
7.11 Experimental behaviors for non-linear loading (a) grid voltage and current (b) grid active and reactive power (c) THD of grid current (d) THD of grid current (e) active and reactive power of load (f) THD of load current (g) compensating voltage and current (h) compensating active and reactive power (i) THD of compensating current (j) THD of compensating voltage (k) DC link voltage and current
7.12 (a),(b) MPPT performance of SPV simulator at 1000 W/$m^2$ and 500 W/$m^2$
8.1 System configuration for three-phase single-stage grid-tied PV system
8.2 Convergence of adaptive algorithms with different learning rates

8.3 Open-loop performance comparison of LMS, Sign-LMS, ϵ-LMS and LMF
8.4 Complete structure of the control of three-phase single-stage grid-tied PV system
8.5 Closed -loop voltage and current performance with LMF control algorithm under variations
8.6 Closed-loop power performance with LMF algorithm
8.7 PV array output and reference DC-link voltage by P & O MPPT
8.8 THD analysis (a) load current (b) grid current by LMS (c) grid current by Sign-error LMS (d) grid current by ϵ-NLMS (b) grid current by LMF

# LIST OF TABLES


Table No.

3.1. Parameters For PV Cell Simulation

3.2 Parameters of Boost Converter

3.3 Parameters of The Buck-Boost Converter

4.1 $V_{dc}$ Settling Time

4.2 Parameters List

6.1 Hybrid Solar-Wind System Parameters

6.2 Fuzzy Control Rule

6.3 Comparative Analysis Between Fuzzy Logic and Conventional Controller

6. 4 Comparative Analysis Between the Proposed TOGI Technique With Conventional Controllers

7.1 Comparative Analysis Between Proposed AFOGI-FLL With Conventional TOGI Control Algorithm

8.1 Comparison of Open-Loop Performance Of LMS, SIGN-Error LMS, $\epsilon$ −NLMS AND LMF

8.2 Closed-Loop Performance of LMF Control Algorithm

# LIST OF SYMBOLS

| | | |
|---|---|---|
| $I_{ph}$ | : | Photon Current |
| $I_d$ | : | Diode Current |
| $\alpha$ | : | Temperature coefficient |
| Voc | : | Open circuit voltage |
| Rsh | : | Shunt resistance |
| $I_s$ | : | Saturation current of the diode |
| k | : | Boltzmann constant |
| n | : | Ideality factor |
| $I_0$ | : | Reverse saturation current |
| $T_{ref}$ | : | Reference temperature |
| $v_g$ | : | Bandgap voltage of the semiconductor |
| $\Delta I$ | : | Ripple current |
| Iref | : | Reference current |
| iLd, iLq | : | Currents of the d-axis and q-axis |
| Rs, Rsh | : | Series and Parallel resistance |
| Isc | : | Short Circuit Current |
| D | : | Diode |
| Kp, Ki | : | Proportional and Integral Gain |
| e(n), ce(n) | : | Crisp values of error and Change in error |
| $V_{dc}$ | : | DC-link capacitor |
| $V_{tm}$ | : | Magnitude of terminal voltage |
| $V_{ga,}V_{gb,}V_{gc}$ | : | Phase voltages |
| $\alpha_{q1}, \alpha_{q2}, \alpha_{q3}$ | : | Quadrature unit template |
| $\alpha_1$, $\alpha_2$ , $\alpha_3$ | : | In-phase unit template signals |
| $I_{Pvq}$ | : | PV-based feed-forward component |
| $V_{dc}^*$, $V_e$(n) | : | Reference DC bus voltage and error in voltage |
| $V_0(n)$ | : | Loss component of voltage |
| $I_{L1,}I_{L2}$*and* $I_{L3}$ | : | In-phase component of load currents |
| $I_{net}$ | : | Net active component of current |

| | | |
|---|---|---|
| $I_{Le}$ | : | Equivalent component of current |
| $I_{sa}, I_{sb}, I_{sc}$ | : | Source Currents |
| G | : | Solar irradiance |
| Ipv | : | SPV Current |
| Ppv | : | SPV Power |
| Vgabc | : | AC Grid Voltage |
| Igabc | : | AC Grid Current |
| Ica | : | Compensating Current |
| iLa | : | Load Current |
| Pg | : | AC Grid Active Power |
| Qg | : | AC grid reactive power |
| Vtm | : | Terminal voltage |
| Wr | : | Frequency |
| $L_f$ | : | Interfacing inductors |
| $L_{B1}$ and $L_{B2}$ | : | Boost converter inductance |
| $d_s$ | : | Minimum Duty Ratio |
| $L_{B1}$ | : | SPV boost converter inductor |
| $d_s$ | : | Duty ratio for SPV |
| $f_s$ | : | Switching frequency of SPV |
| $V_{in}$ | : | SPV output voltage |
| $V_o$ | : | Boost converter output voltage |
| $f_w$ | : | Switching frequency of wind |
| $V_i$ | : | Wind output voltage |
| $\Delta i$ | : | Ripple current |
| $V_t$ | : | Terminal voltage |
| Iploss | : | Loss components of current |
| $U_{qa}, U_{qb}, U_{qc}$ | : | Quadrature phase unit template |
| $U_{pa}, U_{pb}, U_{pc}$ | : | In-phase unit template signals |
| $V_{sa}, V_{sb}, V_{sc}$ | : | Phase voltages |
| $V_{sab}, V_{sbc}, V_{sca}$ | : | Line voltages |

| | | |
|---|---|---|
| $I_{LFA}$ | : | Fundamental load current |
| $I_{Peq}$ | : | Equivalent components of active current |
| $I_{Qeq}$ | : | Reactive current |
| $I_{PA}$ & $I_{QA}$ component | : | Fundamental active and reactive current |
| $I_{Ploss}$ | : | Loss components of current |
| $\mu e$ (n), $\mu e$ (n) | : | Error and change in error |
| $I_{Lpnet}$ | : | Net active current component |
| $I_{Lqnet}$ | : | Net reactive current component |
| $i_{sa}^{*}, i_{sb}^{*}, i_{sc}^{*}$ | : | Reference grid currents |
| $i_{ga}, i_{gb}, i_{gc}$ | : | Grid currents |
| $V_{terminal}$ | : | Terminal voltage |
| $T_{qa,}T_{qb,}T_{qc}$ | : | Quadrature unit templates |
| $T_{pa,}T_{pb,}T_{pc}$ | : | In-phase unit templates |
| $V_{sa}, V_{sb,}V_{sc}$ | : | Sensed line voltages |
| $I_{LA,}I_{LB,}I_{LC}$ | : | Extracted FL currents |
| $PD_o$ | : | Output of the phase detector |
| $\theta_e$ | : | Phase error |
| $I_{LPA,}I_{LPB,}I_{LPC}$ | : | Fundamental in-phase currents |
| $I_{LQA,}I_{LQB,}I_{LQC}$ | : | Quadrature-phase currents |
| $I_{ga}^{*}, I_{gb}^{*}, I_{gc}^{*}$ | : | Reference grid currents |
| $I_{Lpnet}$ | : | Net in-phase current component |
| $I_{Lqnet}$ | : | Net quadrature-phase current component |
| Pc, Qc | : | Compensating Active and Reactive Power |
| $d(0), d(1), d(2)$ | : | Zero-mean random variable $\boldsymbol{d}$ |
| $u_0, u_1, u_2$ | : | Zero-mean random vector $\boldsymbol{u}$ |
| $w^0$ | : | Weight vector |
| $\alpha$ | : | Learning rate |
| $w_{pa}(k)$ | : | Fundamental active component |
| $u_{pa}$ and $u_{qa}$ | : | Unit in-phase and Quadrature-phase templates |
| $e_{La}(k)$ | : | Estimated error |

| | | |
|---|---|---|
| $\epsilon$ | : | Small positive parameter |
| $V_m$ | : | Amplitude of the grid voltage |
| $w_{ff}$ | : | Feed-forward component |
| $w_p, w_q$ | : | Average fundamental active and reactive weights |

# LIST OF ABBREVIATIONS

| | | |
|---|---|---|
| **SPV** | : | Solar Photovoltaic |
| **MPPT** | : | Maximum Power Point Tracking |
| **P&O** | : | Perturbed and observe |
| **IC** | : | Incremental Conductance |
| **PVSC** | : | PV side Converter |
| **PI** | : | Proportional Integral |
| **PWM** | : | Pulse Width Modulation |
| **SAPF** | : | Shunt Active Power Filter |
| **SRF** | : | Synchronous Reference Frame |
| **PV** | : | Photovoltaic |
| **ANN** | : | Artificial Neural Network |
| **THD** | : | Total Harmonic Distortion |
| **VSC** | : | Voltage Source Converter |
| **PCC** | : | Point of Common Coupling |
| **FLC** | : | Fuzzy Logic Controller |
| **SOGI-FLL** | : | Second Order Generalized Integrator Frequency Locked Loop |
| **PMSG** | : | Permanent Magnet Synchronous Generator |
| **TOGI** | : | Third Order Generalized Integrator |
| **PCI** | : | Point of Common Intersection |
| **ZCD** | : | Zero Cross Detector |
| **S&H** | : | Sample & Hold Logic |
| **NH** | : | Negative High |
| **NM** | : | Negative Medium |
| **NS** | : | Negative Small |
| **ZE** | : | Zero |
| **PS** | : | Positive small |
| **PM** | : | Positive Medium |
| **PB** | : | Positive Big |
| **GI** | : | Generalized Integrator |
| **THD** | : | Total Harmonic Distortion |

| | | |
|---|---|---|
| **PFC** | : | Power Factor Correction |
| **PQ** | : | Power Quality |
| **AFOGI-FLL** | : | Adaptive Fourth-Order Based Frequency Locked Loop |
| **PD** | : | Phase Detector |
| **PLL** | : | Phase Look Loop |
| **LF** | : | Loop Filter |
| **DSP** | : | Digital Signal Processor |
| **LMS** | : | Least Mean Square |
| **LMF** | : | Least Mean Fourth |
| **$\epsilon$ −NLMS** | : | $\epsilon$ −Normalized LMS |
| **HCC** | : | Hysteresis Control Technique |

# Chapter 1

# INTRODUCTION

## 1.0 GENERAL

There is an urgent requirement to increase both the quantity and accessibility of power in rural areas to keep up with India's rapidly expanding population. Aside from reducing our emissions on a global scale, an alternative environmentally acceptable option is required to meet the developing world's tremendous need for electricity in light of the treaties'-imposed limitations on emissions.

Conventional energy sources based on oil, coal, and natural gas have proven to be effective economic progress drivers. However, with the rapid depletion of traditional energy sources and increasing energy demand, worldwide primary energy consumption has fallen by 4.5% in 2020 – the largest decline since 1945 [1]. As the world faces an impending dearth of fossil fuels, most immediately oil, alternative sources of energy must be found.

Renewable energy research has focused on improving the efficiency, reliability, and cost-effectiveness of various renewable energy technologies, as well as exploring new technologies and expanding the use of renewable energy to new regions. Policy and economics also play a critical role in the adoption and expansion of renewable energy. The amount of renewable primary energy (including biofuels but excluding hydro) increased by roughly 5.1 EJ in 2021, which is equivalent to a 15% annual growth rate, greater than any other fuel in 2021 and stronger than the 9% growth rate in the previous year [2]. The article Renewable Energy Sources and Climate Change Mitigation examines the role that renewable energy (RE) sources are already playing and their future potential to play in supplying energy services for a sustainable path of social

and economic development. It comprises evaluations of the RE resources and technologies already in use, costs and benefits, integration needs and up scaling impediments, future possibilities, and policy choices [3-5]. With an urgent need for a clean and efficient solution, few renewable sources are promising. Such as solar and wind-based renewable energy sources. With the effective usage of solar and wind energy, India can not only be in a better position in power distribution but also can help in maintaining the stability of the grid as a whole [6-8].

Microgrids have lately gained significance due to the increasing need for decentralised electricity production and consumption. Recently, DERs, or distributed energy resources, have taken the front stage. Microgrids emerged as a solution to the issues of gearbox losses and greenhouse gases as they became more widely recognized [9-14]. The Micro grid has two modes of operation i.e. grid-connected mode and islanded mode [15]. The reliability of grid-connected Micro grids is very high [16]. When operating in isolated mode, the grid relies on microgrid energy storage to meet load demands when renewable energy sources aren't available. However, when the charge of these storage devices drops below a certain critical value, the system becomes less reliable and can't meet the load's power needs [17-20]. In most cases, this happens when the grid goes down or a malfunction occurs [21].

As the number of distributed energy based resources increases, it requires improvement in management and operational strategy to increase the power reliability and quality of supply [22]. The role of power electronics increases tremendously with the applications of distributed generators and in the integration of renewable energy based sources into the electric grid [23]. The main reasons that attract the use of power electronics technology because of their large power handling capability and the

introduction of real-time computer controllers through which we can implement complex control algorithms easily [24-27].

The use of inverter technology is crucial for the safe and dependable connecting of renewable energy installations to the grid. Furthermore, they must be able to deliver high power factor, low harmonic distortion, and high-efficiency conversion. Hence the control policy needs to be taken into account. In this study, the most significant current control techniques are discussed and examined.

## 1.1 THE-STATE-OF-THE ART IN SOLAR AND WIND ENERGY RESOURSES

In this section, we give a quick outline of how solar photovoltaic and wind energy work, as well as other green energy generation and storage systems that were addressed about in general [28-30].

Real-life weather factors usually have an effect on how well PV systems work. People who live in deserts worry that dust build-up is one of the main things that could make PV less efficient. As single-phase distributed power and bigger single-phase loads become more common, it becomes harder to keep voltages steady across distribution networks. In the literature, a reactive power adjustment approach is created that uses spread solar photovoltaic (PV) transformers to fix this kind of voltage imbalance discussed [31]. Using the HOMER simulation to create the first realistic model and test of a unique mixed micro grid that combines solar PV, VRFB storage, wind, and biomass. The two main case studies that are looked at are moderate damage and heavy damage. These are looked at in a range of situations and levels of disturbance and are judged using a number of resilience measures [32-33]. The issue of mixing the production of clean energy with improving the quality of power. The automatic shift also makes sure that important loads always have power, even when the grid is down.

As more green energy sources, like solar photovoltaic (PV), are used, the voltage control of the standard distribution system has to deal with a lot of problems. Because they can respond quickly to changes caused by solar PV, battery energy storage systems (BESS) can help with power control problems [34-35]. It goes into great depth about how well each programme identifies things and how it should be judged. At the end of each method, the found PV parameters are shown, along with the error and the output I-V or P-V curves that were generated. This makes it easier to compare and evaluate the different techniques quantitatively [37-38].

The Learning Modified Salp Swarm Algorithm (OLMSSA) is used to correctly find the two-diode model parameters of the PV cell or module's electrical equivalent circuit. We use six meta-heuristic algorithms to test OLMSSA. One of them is the basic algorithm SSA, which was just released. The standard test PV model of the double diode and a real-world PV module is discussed in article [39]. In the article [40] discussed first to suggest using the Snake optimisation meta-heuristic algorithms to get the details of three types of photovoltaic cells: RTC France, amorphous silicon, and commercial silicon that is mono-crystalline. With the one diode and two diode models, the Snake algorithms are used to get five and seven parameters out of the models, respectively. Moreover, the article [41] suggested an improved teaching–learning-based optimisation (ETLBO) method to figure out the parameters of solar cells. It is suggested that the ETLBO can make the regular TLBO work better and search space smaller by changing the factors that control the explorative and predatory phases to find the right balance. A real set of solar single-diode and double-diode models is used to test the suggested method. The suggested method is also tried on a set of two real PV panels, one with polycrystalline cells and the other with mono-crystalline cells.

A study of the power quality indicators and factors at the point of common connection in a low voltage power grid that simulates solar generation. The Power quality measures are affected by changes in the power from the PV system. These can happen because of changes in the weather, like cloud cover, the amount of shading over a PV panel's surface over time, and the number of PV panels that are covered [42-44].

## 1.2 STATE OF THE ART IN POWER QUALITY

Maintaining sufficiently high-grade energy at the generation and distribution levels is referred to as power quality (PQ). A term used to define the calibre of electrical power delivered is PQ. The quality of electricity may be described by a number of criteria, such as harmonic distortions in the waveforms of the supply voltage and current, the continuity of the electricity, variations in the voltage level, transients in the voltages and currents, and such. Poor PQ may cause a customer's equipment to malfunction or fail, and an electrical load may stop working altogether [45-47].

Power quality (PQ) is an important problem in modern power systems that use a lot of green energy sources and have more power electronics devices built in. To find and rate different operating events in terms of PQ, the proposed method works well. It can also spot a wide range of PQ problems when there is a lot of wind energy [48-50]. As more energy systems are connected, there are higher chances that the quality of the power will get worse at different stages of production, change, delivery, and use [51-52]. A suitable combination of techniques is discussed for enhancing power quality in a micro-grid connected system [53-57]. Additionally, by adding more DG to power systems is one way to get a lot of benefits, such as lower losses, better voltage profiles, and lower peak costs. It also wants to make the system more secure, stable, and reliable. The main goal of optimal distributed generation (ODG) is to make sure that

the benefits listed above happen so that the whole system works more efficiently [58-60].

Electric distribution system power is more reliable and of higher quality when it is controlled by specialised power devices that employ power electronics. At PCC, these devices can be linked various configuration such as in series, shunt, or a combination of series and shunt. An active shunt compensator, also known as a shunt active power filter, is a workable remedy for current distribution-related PQ issues (SAPF). There are many PQ problems, including harmonic distortion, low power factor (PF), unbalanced loads, neutral correction, etc. [61-64]. These PQ issues can be eliminated by using SAPF [65-67]. In order to provide harmonic current compensation, reactive power compensation, and neutral current compensation in an AC distribution network, the SAPF technology has reached maturity. It has many control schemes, solid state devices, and combinations. The shunt compensators and their control methods are extensively discussed in the literature in order to improve PQ at the distribution [68-197]. In a three-phase system, it has also been used to adjust the terminal voltage and reduce voltage flicker. The SAPF may be configured in a variety of different ways, including with two-leg, three-leg, four-leg, and six-leg VSCs, as well as in a variety of various working modes [68-73]. In order to create gating pulses [74] of its VSC and achieve the necessary performance under both steady state and dynamic settings, effective control of the SAPF is required as a precondition.

SAPF works depends extensively on the control method used to derive the basic load current component. To estimate reference supply currents and to create switching pulses for the voltage source converter (VSC) employed as SAPF, the basic active and reactive load current components are also used. Several writers have proposed a variety of approaches to the problem of extracting harmonics from distorted load

current in their respective works [75-113]. Therefore, fast and accurate control algorithms needed to be developed for SAPF operation. Additionally, all algorithms that use SAPF are able to compensate for supply current harmonics, reactive power, and unbalanced currents. The choice of a control method is determined by a number of different considerations, including the following: a low amount of processing time, a low level of mathematical complexity, a quick reaction, steady operation, and simple implementation. Conventional control methods such as synchronous reference frame theory (SRFT), instantaneous reactive power theory (IRPT), and power balance theory (PBT), among others, have been described and documented in the scientific literature [114-153].

There have been recent proposals in the scientific literature for adaptive least mean square control techniques based on adaptive filtering, with both fixed and variable steps [154]. Variable step reduced steady-state error and faster convergence are two ways in which LMS excels. When dealing with PQ issues with SAPF, the LMS techniques could be useful. [155-157]. There are several more control methods that are conceptually comparable to Leaky Least Mean Square [158] and adaptable LMS [159] that can be found in the literature.

During the course of the last several decades, many research articles have been published that discuss the use of fuzzy and neural approaches [160-166] for the control of SAPF. The artificial neural network (ANN), recurrent wavelet artificial neural network, and adaptive neural filtering, among other things, provide the basis for these control systems [167,168]. There are a number of different contemporary control methods that are documented in the literature [169-173]. These methods consist of things like mixed and stationary frame repetitive control [174], Extended Kalman Filter, Optimum Filtering Theory [175], and so on and so forth.

In order to enhance the overall performance of the SAPF. The innovative strategy, which has been offered, is one that makes use of clever neural approaches. Through the use of Matlab simulations and head-to-head comparisons with traditional technical research, the performance of the suggested ANN was evaluated and validated [176-181]. Harmonics brought on by nonlinear loads have resulted in the whole SAPF structure being implanted as a means of compensation. At this stage, comparison investigations between the neural method and the p-q theory, which is one of the most typical ways used to extract the harmonic component of the load current in order to create reference currents, have been completed. Based on the findings that have been obtained, it is possible to declare that the method that is based on neural networks is capable of satisfying all of the identifying goals for harmonic currents. Nevertheless, the benefit of the (p-q theory) is that the latter incorporates an integrated (PI) controller, which was included to regulate the DC voltage of the capacitor in the (SAPF) [183,183]. Second- order generalized integrator (SOGI) and third-order generalized integrator (TOGI)-based frequency estimator is found in the works of literature [184-192] for unknown disturbances as well as higher-order generalized integrators are also mentioned in the kinds of literature [193-197].

**1.3 OBJECTIVES AND SCOPE**

1. The power from the photovoltaic system varies according to climatic conditions. Hence, to obtain maximum power from the PV array, the Maximum Power Point Tracker (MPPT) is used and it is coupled with the SPV system.

2. The photovoltaic energy sources generate power at variable low dc voltage; it requires power conditioning before connecting to DC-link. For this purpose, a DC-DC converter is used. A boost converter is used to realize this operation.

3. Harmonics and reactive power requirements of nonlinear loads are creating serious power quality problems. To compensate for the harmonics and reactive power of nonlinear loads, a 3-phase shunt active power filter has been developed.

4. A Distribution static compensator (DSTATCOM) is proposed for compensation of reactive power and unbalance caused by linear as well as non-linear loads in the distribution system. Therefore, some conventional control algorithms and adaptive control algorithms are evaluated for extracting reference current signals.

5. A PI controller is used to regulate the dc bus voltage to its reference value and compensates for the inverter losses. A low pass filter is used to filter the ripples in the feedback path of the dc-link voltage.

6. Fuzzy logic, ANN, ANFIS-based artificial intelligence controllers have been applied to the design of shunt active filter. The artificial-based controller has advantages over the PI controller such as, it does not need an accurate mathematical model; it can handle nonlinearity and is more robust than the PI controller; it can work with imprecise inputs. Hence, this work validates an enhanced control strategy to improve the power quality of the grid interconnected solar system in terms of harmonic reduction and reactive power compensation.

7. PI and FUZZY logic controllers are used in three-phase shunt active power filters to compensate for harmonics and reactive power produces by nonlinear loads to improve power quality.

## 1.4 OUTLINE OF THE THESIS

The content of the thesis has been divided into the following chapters:

**Chapter 1** begins with an overview and background of hybrid renewable energy resources, power quality issues, and various control algorithms to mitigate the Power quality issues followed by a problem statement and the motivation for conducting research in the design of different control algorithms for mitigation of power quality. This thesis is divided into eight chapters, including an introduction and conclusion. The remaining chapters of the thesis are organized as follows:

**Chapter 2** includes a literature survey on several current harmonics' extraction techniques are used to eliminate harmonics from distorted currents and to extract the fundamental component from load currents. Based on the literature survey significant research gaps are recognized. The difficulties identified for power quality refinement, as well as the need for numerous modifications in conventional algorithms, are also explored.

**Chapter 3** This chapter, presents the modelling of the components of the PV array and uses Maximum Power Point Tracking to utilize the maximum power from the PV array which is connected to energy storage to maintain the DC link voltage using a control strategy. An algorithm for energy management is proposed to connect the Micro-grid to the utility grid. The simulations are carried out, and the results are analysed in Matlab/Simulink environment.

**Chapter 4** In this chapter, the SRF control method with ANN controller is presented and verified with three three-phase-four wire SAPF systems in MATLAB/Simulink environment. Harmonic current and reactive power adjustment were made possible by the photovoltaic integrated SAPF. Comparisons between the SAPF modified with ANN controller and PI and FLC are made. The dc-link voltage of Shunt APF was maintained constant by the PI, fuzzy, and ANN controllers. As a result, the ANN controller-based SAPF delivers better performance than PI and fuzzy controllers.

**Chapter 5** In this chapter a three-phase grid-interfaced solar photovoltaic system (SPV) has been implemented and controlled by using SOGI-FLL based adaptive control scheme. This scheme has been effectively used to extract reference currents and provide gating pulses for VSC. The performance of the control scheme for SPV system has been found satisfactory under linear and nonlinear loads as well as in load unbalancing conditions under varying system frequency. The proposed system along with ANN-based adaptive control scheme has shown better performance in power quality enhancement.

**Chapter 6** In this chapter the TOGI-based fuzzy logic control technique has been designed for a three-phase grids interfaced solar-wind hybrid system. A TOGI control scheme has been presented for reference currents generation and providing pulses for 3-phase VSC. The FLC demonstrates more dynamic performance than the conventional PI controller.

**Chapter 7** In this chapter a fourth-order generalized integrator (FOGI-FLL) based controller is discussed. It provides a satisfactory response for multifunctional objectives such as accurate frequency synchronization, lower and higher-order harmonics elimination, power quality (PQ) refinement, reactive power compensation capability, etc. Regardless of the system dynamic conditions or load disturbances, the proposed technique has strongly rejected harmonics. For the DC bus voltage adjustment, an ANFIS-based controller is successfully implemented with AFOGI-FLL.

**Chapter 8** This chapter discussed and implemented the adaptive control algorithms specifically LMS, Sign-error LMS, $\epsilon-$NLMS and LMF. These control algorithms have been used to track fundamental components from the three-phase non-linear load.

These algorithms have been deployed for reactive power compensation and power quality improvement under different circumstances. The performance of adaptive algorithms has been compared during both dynamic and steady-state conditions.

**Chapter 9** In this chapter briefly reviews the results of the various control algorithms used for SAPF and emphasizes the key findings from this study. Also included after this chapter is a list of the potential future work in the SAPF field.

# Chapter 2
# LITERATURE SURVEY

## 2.0 GENERAL

Growing energy demand causes significant issues including system instability or even outages. As a result, the grid must produce more electricity. Energy production by large plants, however, is not profitable. Additionally, the use of distributed generating is growing quickly. Governments frequently boost the usage of and adoption of renewable energy sources due to rising global warming, resource limitations, and the high expense of fossil fuel sources. The upfront cost versus lifetime energy cost is the primary distinction between systems using renewable energy and those using fossil fuels. Currently, utilities and governments in the majority of developing nations offer a range of incentives to support the growth of the renewable energy sector. Although they are not ideal, renewable energy sources have the potential to be a good alternative to fossil fuels.

Power quality has recently become an important topic of study because more people are becoming aware of it and how it affects customers, makers, and utilities. Electrical equipment needs to work well, but some cost and dependability problems need to be addressed. Power quality issues caused by harmonic currents like characteristic harmonics, no characteristic harmonics, sub harmonics, reactive current, shifting current, uneven currents, and too much neutral current from nonlinear loads can be fixed with SAPFs. In the last few decades, DG using green energy sources has had a big effect on the world's energy input. An electric power system is a very complicated, huge, and always-changing network that makes, sends, and distributes electricity.

Because of too much reactive power demand and noise pollution, the electric power distribution systems are often overloaded and have low voltage issues, which makes them work less efficiently. Power experts all over the world are looking for new ways to solve problems. These SAPFs are the best way to handle nonlinear loads that are fed by current or a mix of current and voltage. They have a middling grade. Because they are cheap, small, light, and loss less power, PWM-based voltage source inverters are best for making SAPFs. Many people think that adding SAPFs is one of the best ways to fix power quality issues caused by complex loads and clean up the AC mains. There is a critical review of the subject matter on SAPF, which is summed up in various categories. This chapter investigates and analyses all the literature that has been written on improving PQ in grid-connected hybrid distributed energy systems. The available energy resources system is first discussed in this chapter. Then the list of different PQ problems that are associated with the distribution system is presented. There are references to international standards that deal with different PQ issues. It is also thought about and studied in depth the possibility of PQ problems in grid-connected PV systems. Additionally, several control algorithms are presented as well to address the PQ issues.

## 2.1 OPTIMIZING POWER QUALITY IN PHOTOVOLTAIC SYSTEMS

A solar PV system uses solar panels to harness the power of the sun to create electricity. The solar panels' photovoltaic cells generate direct current (DC) electricity, which absorb sunlight. In order to power homes, companies, and other applications, the DC electricity is subsequently converted by an inverter into alternating current (AC) electricity. There are several places where solar photovoltaic systems can be deployed, such as on solar farms, rooftops, and the ground. They can run off-grid utilizing batteries to store extra energy produced during the day for use at night or during times

when there is little sunlight, or they can be linked to the electrical grid. Because solar PV systems emit no pollutants and require no fuel, they are a popular source of sustainable energy. They also have no moving parts, require minimal maintenance, and can last for several decades. However, they do require sunlight to produce electricity, so their output is dependent on weather conditions and the time of day. A PV module, or photovoltaic module, is a component of a solar energy system that converts sunlight into electricity. It is also commonly referred to as a solar panel.

A typical PV module is made up of multiple interconnected solar cells, which are made of semiconducting materials, such as silicon.

The electric current produced by the PV module is typically direct current (DC), which can be used to power DC loads, such as batteries or DC motors. However, most household appliances and electrical grids use alternating current (AC), so the DC electricity from the PV module must be converted to AC using an inverter. PV modules can be used in a wide range of applications, from small portable systems to large utility-scale solar farms. They are a key component in the growth of renewable energy and reducing dependence on fossil fuels.

M Yao *et al.*[31] have created a reactive power adjustment plan to lessen this kind of voltage imbalance using dispersed solar photovoltaic (PV) inverters. The proposed approach leverages the Steinmetz concept and was put into practice using both distributed and decentralized control. Through a communication network, the latter manages PV inverters. We evaluate the controllers' performance on both a considerably bigger taxonomy feeder and an IEEE 13-node feeder, taking into account various load and PV system connections.

T Sarkar *et al.*[32] have suggested the first-ever realistic modelling and implementation of a special hybrid micro grid that integrates solar PV, VRFB storage ,wind ,and biomass, Using HOMER simulation, the selection of capacity of various renewable sources for meeting everyday energy use and its technological and business optimization have been carried out. Furthermore, by feeding the model with data from various renewable energy sources, the load profile, and VRFB storage, PSCAD simulation has established the peak load shaving that was a restriction of the model of HOMER.

E Galvan *et al.*[33] have addressed the benefits and drawbacks of using networked microgrids (MGs) to manage DERs specifically, BESS and rooftop solar photovoltaic systems efficiently in order to increase the power distribution system's resilience to natural disasters. Moderate damage and heavy damage are the two main case studies that are examined in varied conditions and disruption levels and are assessed using a range of resilience measures.

S Devassy *et al.*[34] have created an automated system that switches between independent and grid-connected modes of operation for a solar PV array and battery integrated unified power quality conditioner (PV-B-UPQC). The system was presented and examined. This system is made up of a common dc-link connecting a series active filter and a shunt back to back. The system tackles the problem of combining the production of renewable energy with power quality enhancement. Furthermore, the automated transition ensures that key loads always get power, even when the grid is unavailable. One of the major issues resolved was how to implement a PV-B-UPQC system's automated transition while causing the least amount of disruption to the local loads.

T Tewari *et al*.[35] have created a coordinated control technique to guarantee appropriate voltage magnitudes across the distribution feeder by introducing OLTC in addition to BESS. The optimization challenge is designed to minimize the voltage divergence from the necessary values, minimize the count of tap position adjustments, and maximize battery life. For the IEEE 13/33 bus distribution systems, it is shown that employing the newly developed coordinated method over the conventional uncoordinated strategy improves voltage regulation and allows for the best use of available resources.

V Veerapandiyan *et al*.[36] have presented the use of a recurrent neural network-based LSTM technique for the HIF detection in integrated solar PV power systems. For this study, an IEEE 13-bus system was modeled in the MATLAB environment in order to aggregate 300 kW solar PV units for investigation. Initially, features were extracted using the current signal in three phases under both faulty and non-faulty situations. The energy value features of each phase were extracted using the Discrete Wavelet Transform signal processing approach using the db4 mother wavelet in order to train and test the classifiers.

B Yang *et al*.[37] have created heuristic methods and their corresponding variations, which are used for PV cell parameter detection. More specifically, these algorithms were divided into four groups: algorithms based on biology, physics, sociology, and mathematics. In the meantime, each algorithm's identification performance and evaluation criteria are covered in detail. Furthermore, the discovered PV parameters, such as the particular mistake and the output I-V or P-V curves that were simulated, are presented at the end of each method to facilitate a quantitative evaluation and comparison of different algorithms. Furthermore, a thorough synopsis is included to help readers understand and use these strategies in a more targeted manner.

Y Cui *et al*. [38] have suggested to Increasing the PCE of organic photovoltaic (OPV) cells was crucial to expanding their applications. By combining material design with a ternary mixing technique, individual-junction OPV cells can attain a highest PCE of 19.0%. A new low-band gap non-fullerene acceptor (NFA), eC9-2Cl, and a new wide-band gap polymer donor, PBQx-TF, were logically created to build an active layer. A good PCE of 17.7% is displayed by the resulting binary cell with optimum light consumption. Then, as a third component, an NFA F-BTA3 was added to the active layer to simultaneously improve the photovoltaic characteristics.

A Abbassi *et al*.[39] have created a learning modified salp swarm algorithm (OLMSSA) based on opposition for precise identification of the two-diode model parameters of the PV cell/module's electrical equivalent circuit. The performance of OLMSSA is evaluated using six algorithms using meta-heuristics, including the recently published basic algorithm SSA, in conjunction with a realistic PV module and the PV model for the double diode benchmark test.

FBelabbes *et al*.[40] Have developed the application of using the metaheuristic algorithms for Snake optimization to extract the parameters of three solar cells. For the one and two diode models, the Snake algorithms were utilized to extract five and seven parameters, respectively. To demonstrate the effectiveness of the algorithm, a statistical test known as the root mean square error was conducted. The hybrid successive discretization algorithm, one of the best algorithms, requires half the processing time that the modified snake technique requires.

A Ramadan *et al.*[41] have developed an improved ETLBO algorithm, which was used to predict the parameter of solar cells. The ETLBO was developed to enhance the functionality of traditional TLBO and narrow its search space by modifying the parameters that govern the phases of exploration and exploitation to get the appropriate

equilibrium. Using an actual dataset of single- and double-diode photovoltaic models, the proposed technique was verified. Furthermore, two actual PV panels were used as a dataset to evaluate the suggested technique.

O P Quintero *et al.*[42] have developed the influence of emulated PV power injection on several power-quality parameters and indicators (P&I) at the point of common coupling in an LV network. The assessed steady-state P&I values were the RMS voltage (VRMS), non-active power (Q), total and harmonic components of voltage (THDv, Vh) and current (THDi, Ih), voltage imbalance (Desbv), and total rated-current distortion (TRD). Fifteen scenarios were emulated, considering the active power derating, shading percentage over the PV panel surface, and number of shaded PV panels. A PQube3 smart meter was used to measure 256 samples/cycle and store 16 cycles of both voltage and current, for each emulated scenario.

R Boopathi and V Indragandhi[43] have suggested a Shunt Active Power Filter (SAPF) that injects PV energy into a power grid in the presence of nonlinear loads and under various load conditions to maintain power quality and improve power grid capacity. The Perturb and Observe (P&O) algorithm adjusts boost converter duty cycles to track the Maximum Power Point (MPP). The boost converter output was connected to the grid via a SAPF. The effectiveness of SAPF in reducing total harmonic distortion has been investigated using various reference current generation strategies of control methods and improved maximum power factor. The voltage source inverter switches were controlled through hysteresis current control.

S Malathi and J Jayachandran[44] have developed and implemented in Field Programmable Gate Array (FPGA) for Shunt Active Power Filter (SAPF) to enhance Power Quality (PQ) in three-phase four wire distribution system. The PQ enhancement comprises the improvement of power factor, mitigation of harmonics and

compensation of reactive power. The introduced control strategy was simulated in MATLAB/Simulink to determine the reference source currents and weights of active and reactive components. The NN control was developed as individual modules in FPGA. Thus, it can be configured to any other research area which has identical requirements.

## 2.2 POWER QUALITY ISSUES AND MITIGATION TECHNIQUES

One form of renewable energy is wind energy, which uses the wind's force to create electricity. It makes use of wind turbines, which are big, constructions that resemble propellers and rotate in the presence of wind. Generators are powered by the wind's kinetic energy, which is transformed into electrical energy by the turbines' rotating motion. Wind energy is becoming increasingly popular as a source of clean, sustainable energy. It is a renewable energy source, meaning that it is not depleted when used, and it does not produce harmful emissions or pollution. Solar and wind energy is also abundant and widely available, particularly in areas with elevated wind velocities, like coastal regions, mountaintops, and open plains.

A. Khandelwal *et al.*[45] have discussed the benefits over other types of green energy. When linked to the power grid, the photovoltaic (PV) device is very helpful for modern life. Even though there are some problems with the quality of the power when a big PV system is connected to the grid. Having bad or low power quality could cost businesses money and bother end users. Low power quality also causes parts of the power system to get too hot and start working in places they shouldn't, which does a lot of damage.

M. Farhoodnea *et al.*[46] Proposed when big PV system links to the distribution network when the weather is changing, it could really mess up parts of the power

system. The Study includes dynamic power quality analysis of a PV system that is linked to the grid and is part of a distribution system that is affected by different weather conditions. They proposed Matlab/Simulink software, for the 1.8 MW grid-connected PV system in a circular 16 bus test system is designed and simulated with changing amounts of sunlight. The simulations showed that having a lot of PV systems linked to the grid can lead to power quality issues like voltage rise, voltage flicker, and a drop in the power factor.

A. F. Abdul Kadir *et al.* [47] They prosed different kinds of distributed generation (DG) units which affect low voltage distribution systems harmonically. The study looks at what happens when three different kinds of DG units are linked to a power system: a small hydro synchronous generator, a solar system, and a double fed induction generator wind turbine. The PSCAD/EMTDC programme is used to describe the DG units, and tests are run by connecting the DG units to the 2 bus and 13 bus distribution systems. Their findings showed that the total harmonic distortion of the voltage (THDV) in the system is affected by things like the type of DG, how it connects to the utility system, the number of DG units, and where they are placed in the system.

OMahela *et al.*[48] have suggested the benefits of wind energy include reducing greenhouse gas emissions, improving energy security, and creating local jobs. However, wind energy also has some limitations, such as its intermittency, meaning that it was not always available when needed. Wind turbines can also be costly to build and maintain, and they can have visual and noise impacts on local communities. Wind energy was predicted to contribute significantly to supplying the world's energy needs in the ensuing decades, despite these drawbacks. Many countries have set ambitious targets for expanding their wind energy capacity, and technological advancements in

wind turbine design and energy storage were helping to overcome some of the limitations of this important renewable energy source.

M Shoaib *et al.*[49] developed a thorough analysis of the properties of wind and its potential for wind power. Data on wind speed for a three-year period was gathered from Pakistan's Alternate Energy Development Board. Monthly, seasonal, and yearly analyses were conducted by fitting the recorded wind speed data to the Weibull distribution function. The Weibull shape and scale parameters can be found numerically using the Modified Maximum Likelihood Method, the Energy Pattern Factor Method, and the Maximum Likelihood Method. Between the fitted Weibull distribution using the Maximum Likelihood Method estimator and the standard deviation values for the distribution of recorded wind speed data, a very good agreement is found.

P A Østergaard *et al.*[50] have recommended the use of renewable energy sources, with a focus on the development of technologies that make use of them, the assessment of the sources' accessibility, and the level of investigation into the types of systems that can integrate renewable energy sources. Resources and technologies related to sun heating, cooling, and electricity, wind and wave power, wind technology, geothermal energy, and salinity gradient technologies are evaluated. The evaluation of energy systems' environmental performance, effects, and system integration comes last.

S Wang *et al.*[51] have developed a brand-new comprehensive closed-loop method based on a DCNN to identify and categorize power quality issues. The characteristics of the power quality disturbances problem were taken into account when building a unit structure with batch-normalization, pooling, and 1-D convolutional layers. This allowed for the capture of multi-scale features and the reduction of over fitting. Several units were layered in the DCNN that was established in order to automatically extract

features from large disturbance samples. It was demonstrated through comparisons with other cutting-edge deep neural networks and conventional techniques that the proposed approach is capable of overcoming the shortcomings of conventional signal processing and artificial selection of features.

S Ismael *et al.*[52] have suggested the four main aspects of HC: perceptions, performance limitations, historical advances, and augmentation approaches. Additionally, system operators' experiences, the energy markets, and the conclusions drawn from actual case studies were presented and discussed. It was determined that an accurate assessment of hosting capacity is essential for the successful integration of increasingly distributed generating. When the system surpasses its hosting capacity (HC) limit, many issues arise. The HC was a transactive strategy that offers a means of integrating the distribution network with other energy system kinds.

P Rajesh *et al.*[53] have developed a unique control system was created and implemented in order to improve the PQ of RES, including wind turbines, ,fuel cells batteries, and photovoltaic (PV) systems. The recently created hybrid method, which integrated the properties of the Moth Flame Optimization Algorithm (MFOA) and the Improved Bat search Algorithm (IBatMFOA) control strategy, was named the IBatMFOA control strategy. By employing the crossover and mutation processes, the bats' search behavior was modified. In this case, MFOA was used to lower the error function and improve the IBatMFOA technique's searching behavior. "To enhance the PQ depending on active with reactive power variance" was the primary objective of the recently introduced IBatMFOA technique. MFOA was improved to reduce the power variation in order to meet the aim. Furthermore, the operational expenses of REESs are reduced by taking into account daily and weekly data forecasts, which

include grid electricity prices, electrical load, and environmental factors. The IBatMFOA approach improves the overall efficiency of the system.

T Ahilan *et al.* [54] have created a safer method of utilizing solar and wind energy for increasing power efficiency and improving power quality. Custom power devices (CPD) were used to harness wind and solar energy. For the use of solar and wind energy, the most sophisticated CPD device was the interline dynamic voltage restorer (IDVR). Two DVRs were combined to create IDVR, which guards delicate loads in different distribution feeders. Feeder-1 was connected to the solar energy source, and feeder 2 was connected to the wind energy source. Feeder-2 assists feeder -1 by employing IDVR to compensate for reactive power if feeder 1's power requirement is higher, and vice versa. IDVR contributes to the upkeep of feeders 1 and 2's power continuity and quality.

S R Arya *et al*.[55] have raised an issue utilizing a mixed norm-based step size adaptive technique that was developed from optimizations of the $2^{nd}$ and $4^{th}$ orders of error. The recently introduced mixed-norm constraint-based improved proportionate normalized LMS fourth (MNC-IPNLMS/F) management technique generates the reference load voltage and extracts the basic weight quantity from the polluted grid voltage. This technique takes advantage of the improved stability and convergence of dynamic voltage restorers (DVRs). An FOPID controller, or fractional-order proportional-integral-derivative, was used to control the voltages of the dc and ac links. A number of optimizations, including the JAYA method, APSO, and BBO, helped the coefficients of FOPID self-tune.

X Xu *et al*.[56] have presented a hierarchical optimization model intended for active management distribution network planning. The model takes into account all relevant parameters, including cost of carbon emissions, line investment, power purchase cost,

balanced network loss, and governmental subsidies. The NSGA-TS hybrid algorithm, which is renowned for its global and local search capabilities, was used to improve convergence and efficacy. This study offers a strong framework for tackling the complexity brought about by the changing distribution network topologies, which makes a significant contribution to the subject.

Y Liu *et al.*[ 57] have developed into vital issues for power systems' voltage stability and power quality. The AC-DC micro-grid technology preserves voltage stability and enhances system power quality thanks to sophisticated fuzzy controllers. These controllers were distribution static synchronous compensators equipped fuzzy-PI (FPI) and fuzzy-PID (FPID) current-controllers. A pair of case analyses that simulate sudden faults and dynamic load variations on a Hybrid AC-DC micro-grid that gathers various renewable energy sources have utilized the capabilities of the recently proposed system. Furthermore, the power quality problems are resolved and the best dynamic response is produced by the newly implemented fuzzy-based controllers. There are numerical simulations available for in-depth analyses comparing various controllers. ‘It was found that when the tested system was subjected to a three-phase failure, the use of fuzzy-PID and fuzzy-PI, respectively, boosted the dynamic system performance by 12.9% and 8.8% and lowered voltage fluctuation at the D-STATCOM by 7.86% and 4.62%.

M Ali *et al.*[58] have presented a brand-new method for distributed generation (DG) systems and optimal distribution system (DS) planning. This was being done to observe how energy losses and the voltage profile of the system are affected by injections of both reactive and active power. One strategy that offers multiple benefits, including peak savings, loss reduction, and voltage profile improvement, is DG penetration in power systems. Moreover, it aims to improve system security, stability,

and dependability. Optimal distributed generation's (ODG) primary objective was to ensure the above-described benefits in order to raise the overall system efficiency. Analytical methodologies were inadequate and unsuitable for systems that were incredibly large and intricate. Consequently, for large systems, a number of meta-heuristic approaches are preferred in order to improve performance from where convergence and accuracy. The horse's manners were the basis for the recommended approach. In order to evaluate the effectiveness of the IWHO, it was applied to the 23 benchmark functions. The most amazing outcome of the inclusion of DGs is reliability amelioration.

Ferahtia *et al*.[59] have developed the ideal DC microgrid EMS. A commercial building power system featuring a fuel cell (FC), battery storage system, photovoltaic (PV) array, and bidirectional DC/AC grid converter is presented by the system under investigation. Stability, power quality, fuel consumption, and efficiency are among the techno-economic issues that arise from the integration of various power sources, such as renewable energy. Salp Swarm Algorithm (SSA) served as the foundation for the suggested EMS. Due to its many benefits, including its lower computational complexity and convergence features, this algorithm has been put into use. The presented method's meticulous design was described in detail. After that, HIL tests were run to confirm the newly added EMS performances.

J Sharma *et al.* [60] have suggested an original use for affine projection, such as the M-estimate adaptive filtering method. The hybrid AC/DC micro-grid main grid was connected to a medium voltage distribution static compensator that was controlled by an Affine projection similar to the M-estimate adaptive filter.. The efficiency of the newly implemented control method was contrasted with the traditional controls. The control technique that has been developed utilizes the M-estimate cost function to

suppress current harmonics in an IEEE 14 bus system by means of a medium voltage distribution static compensator. When impulsive noise enters the system, the function of M-estimate cost safeguards the filter weights. Additionally, the weight update is directly calculated by the newly introduced affine projection-like method for M-estimation, unlike its parent affine projection algorithm, which occasionally causes instability and computational load.

## 2.3 IDENTIFIED RESEARCH GAPS

The existing research on power quality issues in distribution systems has provided valuable insights into specific components, such as the integration of renewable energy sources, the application of machine learning, and the use of optimization techniques. However, a notable research gap exists due to the absence of a unified and integrated framework that considers the synergies among these various factors. Specifically, there is a need for studies that systematically explore how the integration of renewable energy sources, advancements in machine learning, and the implementation of smart grid technologies collectively influence power quality. Understanding the interconnected influences of these elements is crucial for developing a comprehensive approach to address power quality challenges in distribution systems.

Additionally, while the literature acknowledges the utility of hybrid optimization techniques, there is a lack of a comprehensive comparative analysis of these methods. The research gap lies in the absence of a detailed understanding of the specific contexts in which different hybrid optimization algorithms are most effective. A comparative study could provide insights into the strengths and limitations of these algorithms, offering guidance to practitioners and researchers in selecting the most suitable strategies for mitigating power quality issues.

In summary, the research gap identified is the absence of a unified and interdisciplinary framework that integrates the influences of renewable energy integration, machine learning applications, smart grid technologies, and optimization techniques on power quality in distribution systems. Filling this gap is essential for advancing our understanding of the complex dynamics in distribution systems and for developing comprehensive solutions that address power quality challenges in a synergistic manner.

## 2.4 OBJECTIVE OF THE PRESENT WORK

1. The photovoltaic system's electricity output fluctuates based on the weather. Therefore, the MPPT is utilized in conjunction with the SPV system to extract the maximum power from the PV array.

2. Before connecting to DC-link, the photovoltaic energy sources must undergo power conditioning because they produce power at a fluctuating low DC voltage. A DC-DC converter is utilized for this. This operation is carried out using a boost converter.

3. Reactive power demand and harmonics of nonlinear loads are turning into a major source of pollution for power quality. An active three-phase shunt power filter has been designed to compensate for the reactive power and harmonics of nonlinear loads.

4. It is suggested to employ a Distribution Static Compensator (DSTATCOM) to balance out reactive power and unbalance resulting from both linear and non-linear loads in the distribution system. In order to extract reference current signals, a few traditional control techniques as well as an adaptive control algorithm are tested.

5. The dc bus voltage is regulated to its reference value and the inverter losses are compensated for using a PI controller. The ripples in the dc-link voltage feedback channel are filtered using a low pass filter.
6. Shunt active filter design has made use of artificial intelligence controllers based on fuzzy logic, ANN, and ANFIS. The artificial-based controller offers several advantages over the PI controller, including the ability to operate with imperfect inputs, handling nonlinearity, and not requiring an exact mathematical model. Our analysis therefore validates an enhanced control strategy to enhance the power quality of the grid-connected solar system with respect to harmonic reduction and reactive power compensation.
7. Three-phase shunt active power filters employ PI and FUZZY logic controllers to enhance power quality by compensating for harmonics and reactive power generated by nonlinear loads.

## 2.5 CONCLUSIONS

In this chapter described the enhancement of power quality of grid connected hybrid distributed generating systems. The concise literature review is based on a variety of research tasks, which have recently been done by a number of researchers and scholars who have made some significant contributions to the field of using different algorithms. Problem creation and how to diagnose and reduce the problem are described. Many different techniques can be introduced by researchers.

# Chapter-3

# MODELING AND SIMULATION OF MICROGRID SOLAR PHOTOVOLTAIC SYSTEM WITH ENERGY STORAGE

## 3.0 GENERAL

This chapter, highlights the integrated operations of the photovoltaic system with energy storage device. The variations in the energy produced and the variations in the load, the DC link voltage does vary, which has to be tackled using an energy storage device to maintain the DC link voltage. The battery is used as a storage device that is connected to a bidirectional converter and switching of the bidirectional converter has to be done in such a way that it either charges or discharges the battery depending upon the load conditions. The DC bus is connected to the utility grid, and the power sharing and transfer should be in such a way as to maximize the efficiency. An efficient algorithm is to be used to attain maximum efficiency through an interactive inverter. The SPV generating system with MPPT and boost converter is accomplished with a storage unit, simulations are performed and the results are analysed.

## 3.1 THE PROPOSED GRID-CONNECTED MICROGRID SYSTEM

Fig. 3.1, shows the main circuit topology for grid-connected micro-grid system. This system consists of the PV array and the battery storage system which is connected to the DC bus and then the utility grid using an inverter. The DC bus is connected to the utility grid, for the power-sharing and transfer should be in such a way as to maximize efficiency. An efficient algorithm is to be used to attain maximum efficiency through an interactive inverter. The grid-connected mode is carried out using a 3-leg 3-phase inverter and then switching to the inverter is done with the help of a droop control

technique to generate reference current. PV array is connected through a boost converter are used, to fulfil the objective is to produce reference current by the MPPT algorithm.

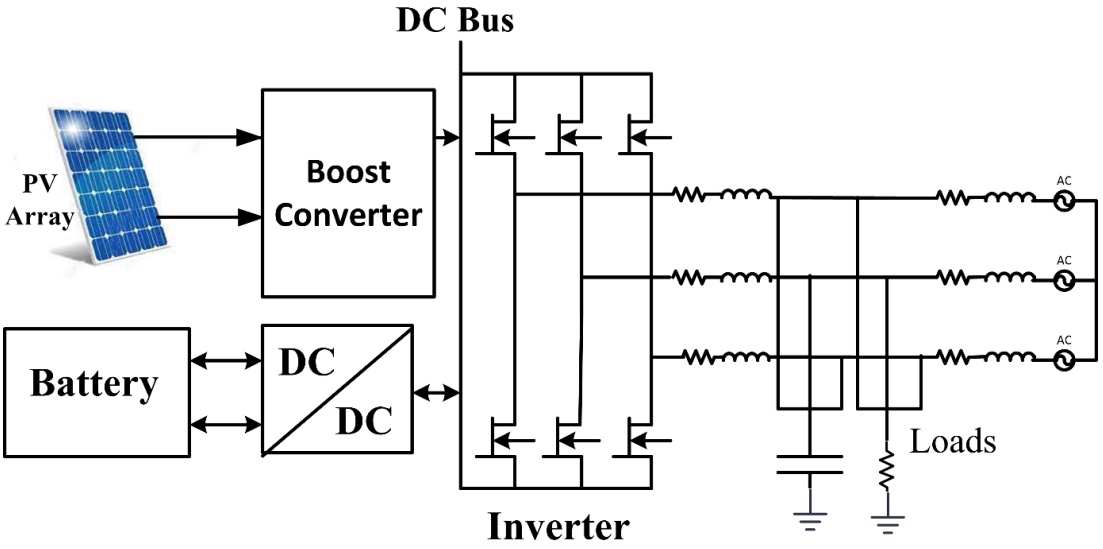


Fig. 3.1 : Schematic diagram of grid connected system

The battery is connected with the help of bi-directional, which can either charge the battery by absorbing the energy from the grid or by discharging the battery by injecting the power into the grid. The bi-directional converter is used for achieving the following, for which the switching has to be done in such a way that it either charges or discharges the battery depending on the load condition. From Fig.3.1, we can observe that solar as a renewable energy source and battery as an energy storage device are connected to the DC bus by which, they are connected to the DC to AC converter.

## 3.2 MODELLING OF MICROGRID COMPONENTS

### 3.2.1 Modelling and Analysis of PV Cell

PV cell is a solid-state device that converts solar energy into electrical energy using the photovoltaic effect. The model of a Photovoltaic cell is developed by analyzing the properties using Matlab/Simulink.

### 3.2.2 Equivalent circuit of PV cell

Fig. 3.2, shows the equivalent circuit of a PV cell, a current source represented by Iph indicates the current caused by the movement of electrons and holes due to the incident light called photons. A diode current $I_d$, is represented parallel to the current source, a shunt resistance $R_{sh}$, represents the leakage of current due to the presence of impurities in the junction diode, and series resistance $R_s$, due to the metallic contacts of the semiconductor.

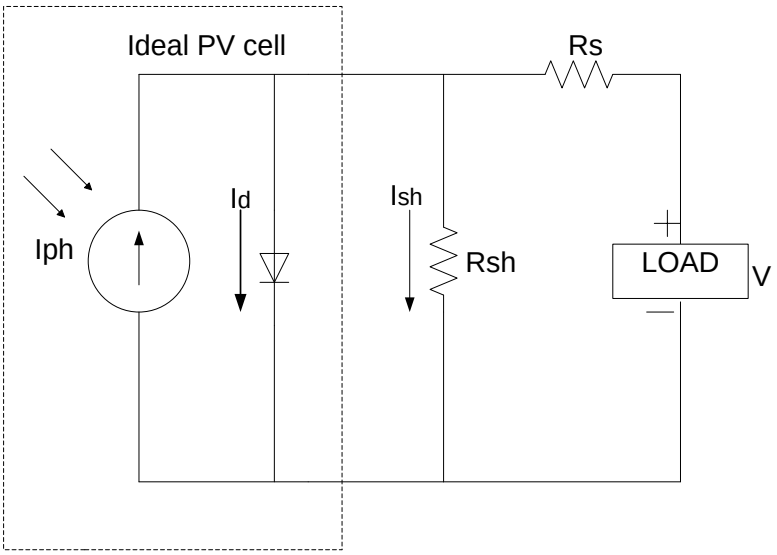


Fig. 3.2 *:* Equivalent circuit diagram of PV cell

$V_{oc}$ is the open circuit voltage which is the voltage produced by the P-N junction diode. $I_{sc}$ is the short circuit current, which is the photon current during short circuit conditions.

Fig. 3.2, shows using Kirchhoff's law

$$I_{pv} = I_{ph} - I_d \tag{3.1}$$

The photon current $(I_{ph})$ *is,*

$$I_{ph} = [(I_{sc} + \alpha(T - T_{ref})]\frac{\beta}{\beta_{ref}} \quad (3.2)$$

Where,

$I_{ph}$ is the photon current (A)

$I_{sc}$ is the photon current at standard conditions (T=298K, $\beta_{ref} = 1000W/m^2$)

$\alpha$ is temperature coefficient

The diode current $I_d = I_s(e^{\frac{qV}{nkT}} - 1)$ (3.3)

Where $I_s$ represents the saturation current of the diode (A), q represents charge of an electron ($1.6*10^{-19}$ C), *n* represents the ideality factor, k is Boltzmann constant ($1.381*10^{-23}$ J/K) and

T is the absolute temperature (K).

The saturation current of the diode varies with temperature as

$$\mathrm{I}_s = I_0(\frac{T}{T_{ref}})^3 e^{\frac{qv_g}{nk}(\frac{1}{T_{ref}} - \frac{1}{T})} \quad (3.4)$$

Where $I_0$ is the reverse saturation current, $T_{ref}$ is the reference temperature (298 K), $v_g$ is the bandgap voltage of the semiconductor (V).

By using initial conditions, $I_{pv}$=0 on the open circuit condition and the constant temperature. Eq. 3.1 can be transformed into

$$0 = I_{sc} - I_d$$

$$I_{sc} = I_s(e^{\frac{qV}{nkT}} - 1)$$

$$I_s = I_0 \, at \, T = T_{ref}$$

$$I_{sc} = I_0(e^{\frac{qV}{nkT}} - 1)$$

$$I_0 = \frac{I_{sc}}{(e^{\frac{qV}{nkT}} - 1)}$$

From Eq. 3.1 the PV current can be expressed by

$$I_{pv} = I_{ph} - I_s(e^{\frac{qV}{nkT}} - 1)$$

Since the voltage across the diode itself is the voltage across the PV cell as $V_d = V_{pv}$

$$I_{pv} = I_{ph} - I_s(e^{\frac{qV_{pv}}{nkT}} - 1) \quad (3.5)$$

So, the output current can be expressed as

$$I_{pv} = [I_{sc} + \alpha(T - T_{ref})]\frac{\beta}{\beta_{ref}} - I_s(e^{\frac{qV_{pv}}{nkT}} - 1) \quad (3.6)$$

By using the above equations, a model which fits the configuration is simulated in the Matlab Simulink environment. The following parameters used for the simulation are tabulated in Table 3.1.

The simulation of the PV array is similar to that of the PV cell, but instead of the current being calculated, from the Eq. 3.6 and operating at the reference temperature

TABLE 3.1 : PARAMETERS FOR PV CELL SIMULATION

| Parameters | Value |
|---|---|
| Open circuit Voltage (Voc) | 0.6 V |
| Short circuit Current (Isc) | 1.8 A |
| Band Gap Voltage (VG) | 1.12 V |
| Diode Ideality Factor | 1.24 |
| Short circuit current temperature coefficient | 2.47*10^3 |

$$Ipv - I_{sc}\frac{\beta}{\beta_{ref}} - I_s(e^{\frac{qVpv}{nkT}} - 1) = 0 \qquad (3.7)$$

Solving the following equation, Vpv can be calculated, which should be the voltage across the PV cell. For the consideration of an array, Eq. 3.7 can be transformed into Eq. 3.8.

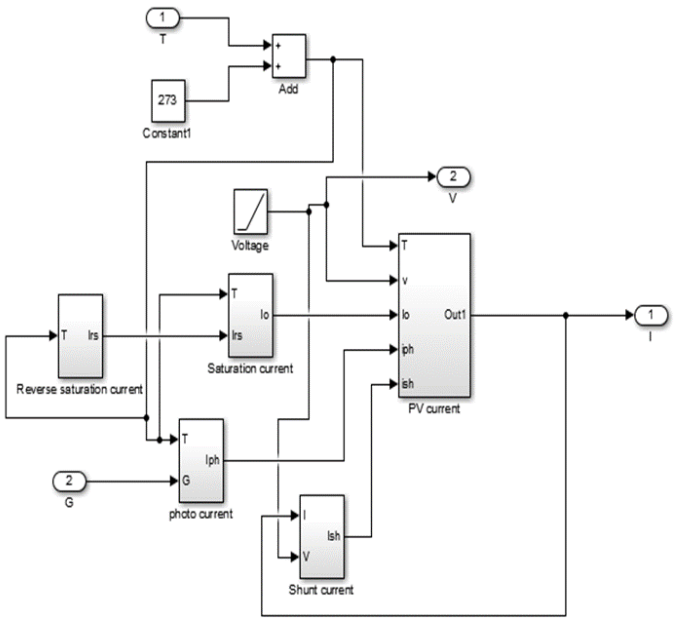


Fig.3.3 : PV cell Simulink model

$$\frac{Ipv}{N_p} - I_{sc}\frac{\beta}{\beta_{ref}} - I_s(e^{\frac{qVpv}{nkTNs}} - 1) = 0$$

$$Ipv = N_p I_{sc} - I_s N_p(e^{\frac{qVpv}{nkTNs}} - 1) - \frac{V_{pv} + I_{pv}R_s}{R_{sh}} \qquad (3.8)$$

The following simulations are carried out for Ns=100 and Np=10.

### 3.3 MAXIMUM POWER POINT TRACKING TECHNIQUES

Maximum power point tracking (MPPT) plays a significant role in renewable energy sources, this chapter focuses on PV systems as a source because of their intermittent nature with the changes in solar irradiance level, ambient temperature, and load the output of the PV array is nonlinear. For the determination of efficient PV output continuously adjust the operating point of the PV array to be around the maximum power point. This process is called MPPT. The available MPPT techniques are perturbed and observe (P&O), Incremental conductance (IC), fractional

Voltage, fractional current, fuzzy logic, feedback control, neural network. The MPPT classifications could be made based on control strategies. Direct, indirect, and probabilistic are three different types that are in use. Perturb and observe (P&O), incremental conductance (IC), fuzzy logic, and neural network are considered direct methods. For estimating the Maximum PowerPoint (MPP), the indirect method is also used. Indirect methods include the look-up table, curve fitting, open circuit, and short circuit methods.

In this chapter perturb and observe (P&O) / Hill-climbing/true-seeking method is modeled for the determination of MPP. Because this algorithm could be easily implemented, the accuracy of the sensors is not needed very high. The disadvantage of this method is that it may result in oscillations of power output near the MPP. The perturbance steps are used for the determination of the oscillation amplitude. The larger the perturbance step, the faster the tracking is, but it serves the fluctuations. Also, if the solar irradiance changes suddenly, the P&O method may become invalid.

### 3.4 PV SIDE CONVERTER

The PV side converter (PVSC) a boost converter is used. The main objective is that the $I_{ref}$ (reference current) produced by the MPPT algorithm is tracked, for that by varying the duty cycle of the boost converter, the maximum power is transmitted and $I_{ref}$ is to be tracked by the PV array.

The value of the inductor and capacitor is calculated from the following Eqs. 3.9 and 3.10. The value of ripple is taken as 5% of the nominal value.

$$L = \frac{V_{pv} * d}{\Delta I * f} \tag{3.9}$$

$$C = \frac{I_o * d}{\Delta V * f} \tag{3.10}$$

The simulation is carried out with the following values, for the duty cycle input is analyzed in the next sections.

The control of boost converter is done for tracking the reference current. The reference current is compared between the MPPT with the actual current in the boost converter; the error is processed by Proportional Integral (PI) controller. The output of the PI controller is further processed to generate Pulse Width Modulation (PWM) signals to the boost converter, by which the current is tracked.

TABLE 3.2 : PARAMETERS OF BOOST CONVERTER

| **Parameter** | **Value** |
|---|---|
| Input value | 200 V |
| Output value | 600 V |
| Frequency | 20 KHZ |
| Maximum Power | 3 KW |

The control circuit of the boost converter is shown in Fig. 3.4

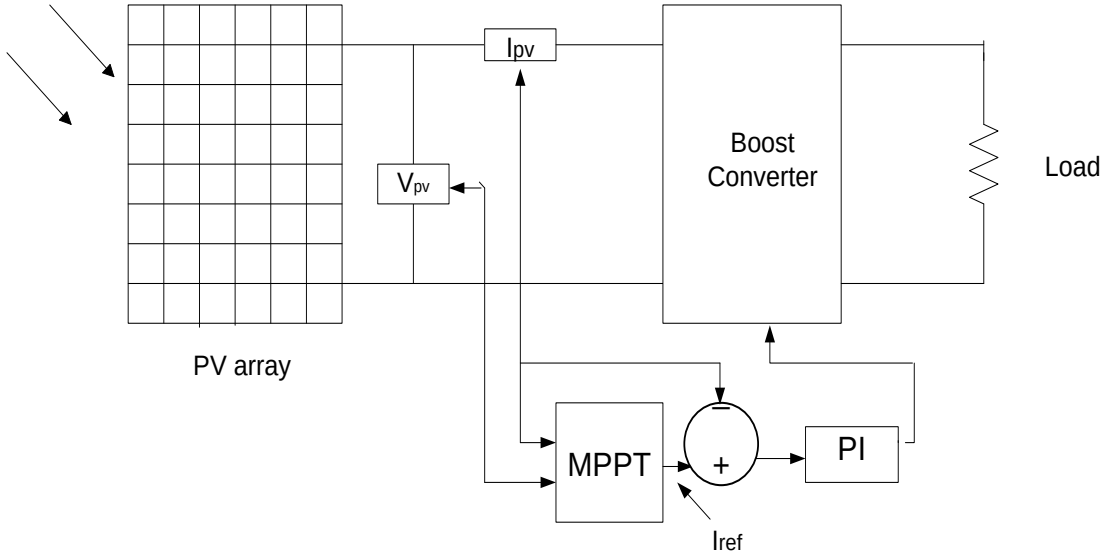


Fig.3.4 : Control circuit of boost converter

### 3.5 MICROGRID WITH STORAGE

It is essential for maintaining the DC grid voltage constant by injecting power if required in the system or conserving the energy by storing the excess amount of energy produced by the PV array. In this section, the operation of the Microgrid is carried out with a storage unit and simulations are carried out and analyzed. Since the battery is to be charged or discharged, depending on whether the power is to be injected or ejected from the DC grid, an algorithm is proposed for the effective maintenance of DC grid voltage.

#### 3.5.1 Storage Connected to DC Grid

In DC grid storage i.e. battery is not directly connected. The function of the battery is to inject power or absorb the power from the grid. So, the battery is connected via bidirectional converter which can either be injecting the power into the grid by discharging the battery or either absorbing the energy from the grid to charge the battery. To fulfill the above requirements, switching of the bidirectional converter has to be in such a way that it either charges or discharges the battery depending upon the

load condition**.** Fig. 3.5 shows the block diagram of the Microgrid with storage connected to the DC bus. The PV array is connected to the grid directly using the boost converter and the battery is connected to the grid using the bidirectional converter. The major bidirectional converter which is commonly used is the Buck-Boost converter. There are many bi-directional converters, but buck-boost is usually selected with the simplicity of its operation and implementation. Using the buck-boost converter, the battery is either charged or discharged, depending on the switching to the converter.

### 3.5.2 Buck-Boost Converter

The Buck-Boost converter is very useful in real-time battery-powered applications, as the name suggests it can act as a buck converter or it can act as a boost converter, that all depends upon the switched to the converter.

For the buck operation or the step-down operation, the power flow from the high voltage side to the low voltage side and for the boost operation or the step-up operation the power flow from the low voltage side to the high voltage side. The power flow can be controlled by suitably choosing the switching to either charge or discharge the battery.

In the specified region of operation, the buck-boost converter parameters are so chosen in such a way that it can get both a buck and boost converter.

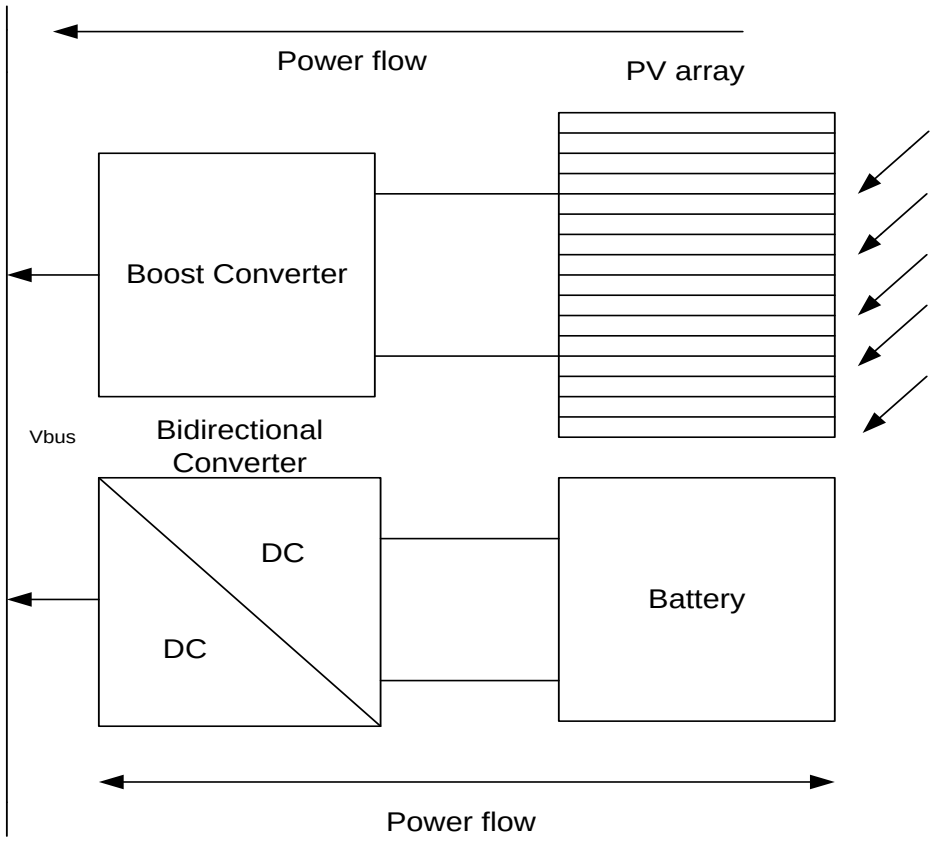


Fig.3.5 Microgrid with storage

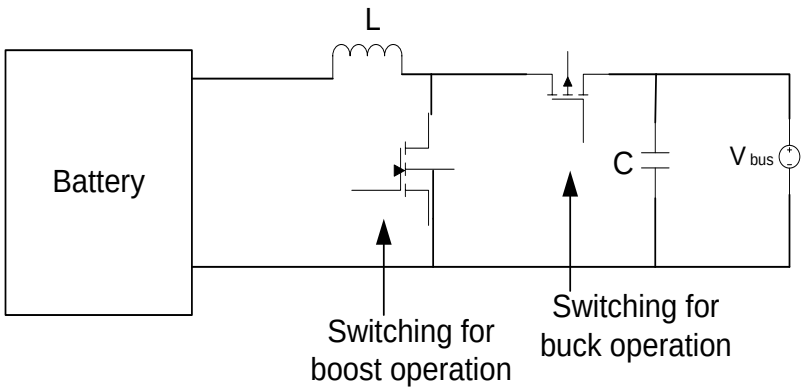


Fig. 3.6 : Buck-Boost circuit diagram

The analysis of buck-boost converter can be done into buck operation and boost operation as the value of the inductor and capacitor are calculated and selected for the lowest ripple value.

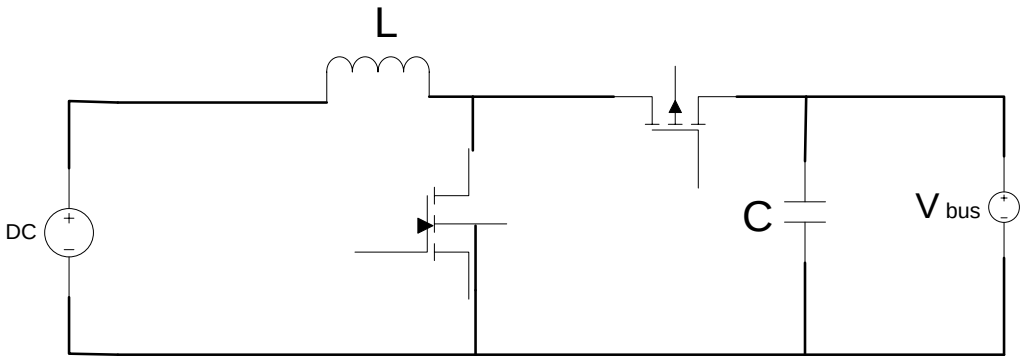


Fig.3.7 : Bi-directional converter

$$(V_{bus} - V_{Battery})T_{ON} = V_{Battery}(T - T_{ON}) \tag{3.11}$$

$$D_1 = \frac{V_{Battery}}{V_{bus}} \tag{3.12}$$

$$D_1 = \frac{T_{ON}}{T} \tag{3.13}$$

The value of inductance (L) can be calculated as follows

$$L = \frac{(V_{bus} - V_{Battery})D_1}{\Delta I * \mathrm{f}} \tag{3.14}$$

The value of capacitance (C) can be calculated as follows

$$\mathrm{C} = \frac{\Delta I}{8 * \Delta V * f} \tag{3.15}$$

For good estimation, the ripple current is 20% to 40% of the output current or $0.2 < \Delta I < 0.4$. The parameters of the boost converter are calculated from the equation, and the value for which the lowest ripple of current and voltage is obtained is selected.

TABLE 3.3 : PARAMETERS OF THE BUCK-BOOST CONVERTER

| PARAMETERS | VALUE |
|---|---|
| VBUS | 600 V |
| $V_{BATTERY}$ | 240 V |
| SWITCHING FREQUENCY | 20 KHZ |
| INDUCTANCE (L) | 14 MH |
| CAPACITANCE (C) | 100μ F |

The power to be injected or to be absorbed from the grid is decided from the selection of Buck/Boost converter which is very important for the following a selection mechanism is required. If it is to be noted that solar PV power is greater than the load, then the voltage of the DC bus increases above the desired value, hence to maintain the DC voltage steady at the required voltage should be absorbed. And when solar PV power is less than the load, then the voltage of the DC bus decreases from the required voltage, hence to maintain the DC voltage steady at the required voltage power should be injected.

### 3.5.3 Control of Switching For the Buck-Boost Converter

The switching for the buck-boost converter should be done so that the voltage reference is maintained at the DC voltage bus. To acquire the above, the voltage of the DC bus is sensed and the error in voltage between the DC grid voltage and the reference voltage is fed to a PI controller from which a reference current (Iref) is generated.

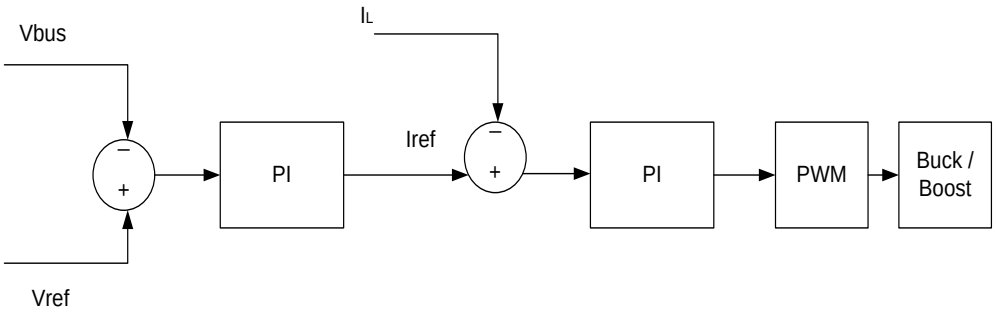


Fig.3.8 : Control diagram for a buck-boost converter

### 3.6 SIMULATION RESULTS

The Simulations are carried out for different cases when the microgrid system is connected to the DC link with and without storage unit. Microgrids without storage units can also be classified into two different sections; either the load power at 600V is greater than the power produced by the PV array or when the load power at 600V is less than the PV array. So for the case when power required by the load at 600V is more than power by the PV array with the maximum rated power at around 3KW, the load resistance is taken at 120 ohms, for that load resistance at which the nominal value of about 600V is reached. Now for the load less than 120 ohms, to maintain the voltage of 600V, additional power is to be injected into the DC grid, but due to the lack of a storage unit connected to the grid, the bus lack power, and the voltage drops from the nominal value. The following simulation is carried out with a load of 60 ohms for which to maintain the 600V nominal value of the DC bus, 6KW of power should be transmitted by the PV array. The maximum power from the PV array is around 3KW, so the DC bus voltage drops below the 600V mark. It settles around 400V. This is a very unsuitable case without the storage unit system in the DC bus.

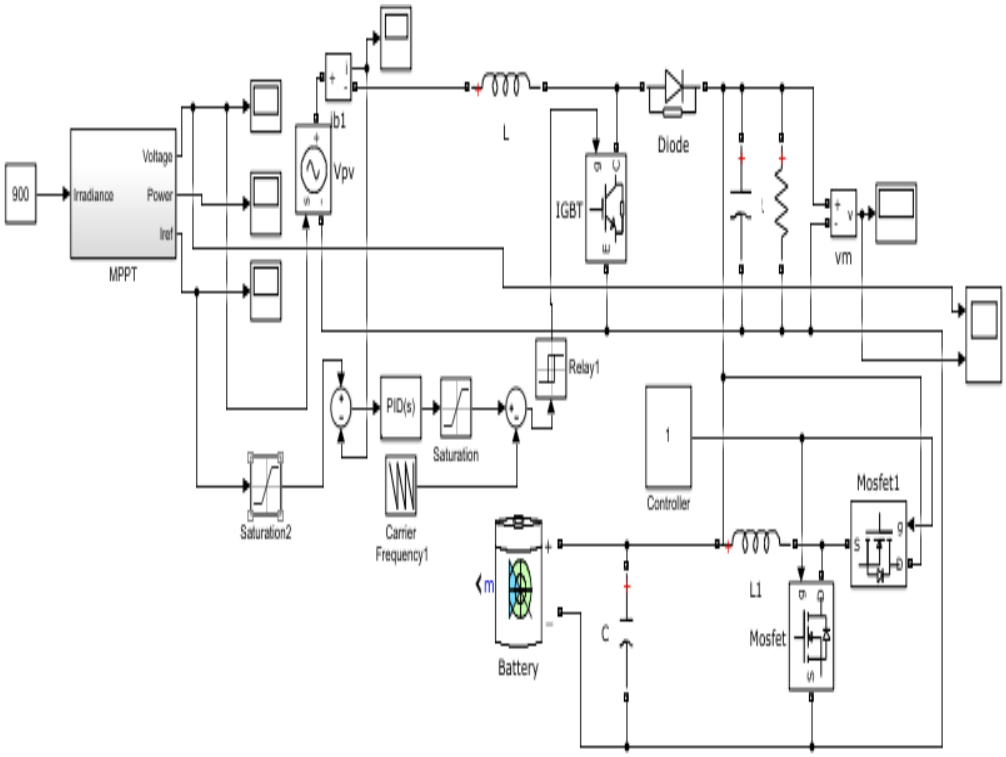


Fig.3.9 : MATLAB/Simulink diagram for PV, battery connected to DC link

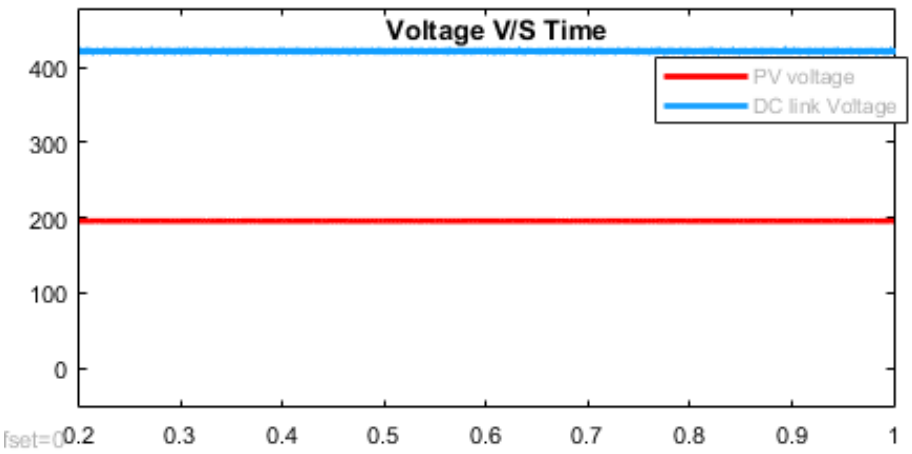


Fig. 3.10(a) : PV voltage and DC link Voltage when $R_{load}$ = 60 ohm

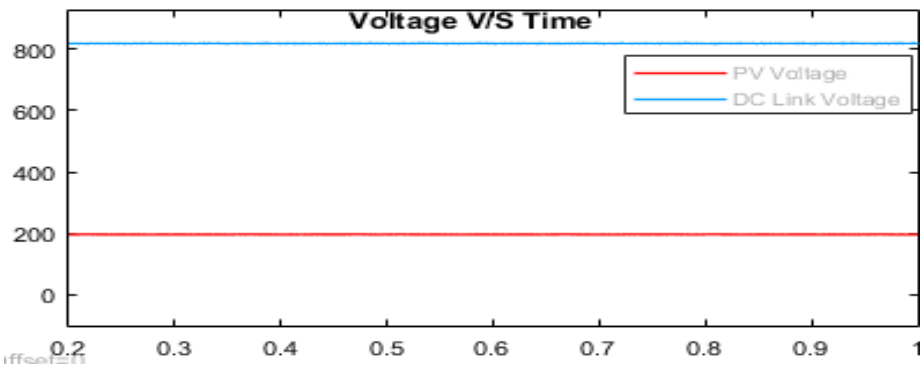


Fig. 3.10 (b) : PV voltage and DC link Voltage when $R_{load}$ = 240 ohm.

The DC link grid voltage has to be maintained at about 600V, but from the Fig 3.10(a), the DC grid voltage is approx. 400V. The same situation is carried out with a load of 240 ohms, and since the load power at 600V is 1.5KW but the power generated by the PV array is around 3KW. Since there is an excess generation of power than the load power, the voltage instead of maintaining at 600V will increase and reach a voltage around 850V which is shown in Fig 3.10 (b).

From the following, we can conclude that an energy source is essential for the maintenance of the DC link grid at a constant voltage. If the following DC bus is connected to the energy source, which can inject/eject the remaining power to maintain the voltage level at 600V. The other simulation is carried out where the PV array and the storage device are connected to the utility grid using an inverter and the switching to the inverter is executed by the droop control method. The inverter is connected to the grid and the required power is transmitted to the grid.

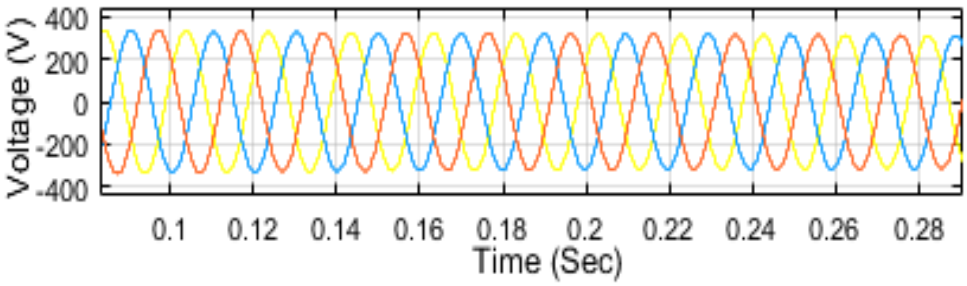


Fig.3.11 : Grid Voltage

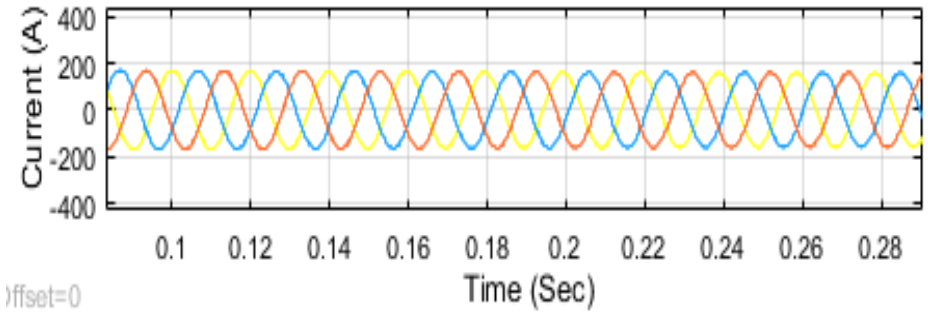


Fig.3.12 : Grid Current

The following system was tested under the following conditions: Vs= 415 V, switching frequency = 10 kHz, Vdc= 600 V, line impedance Ls= 2.6 MH, Rs= 0.6 ohms, filter inductance $L_L$ = 0.6 MH, filter capacitance = 1500 μF, a linear load of 75 KW.

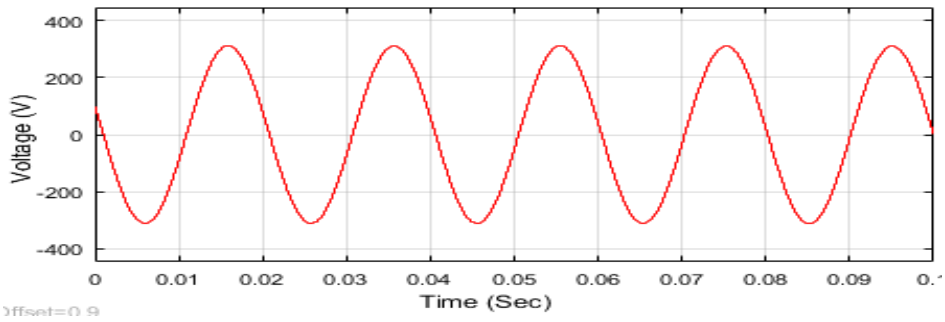


Fig. 3.13 : Line to line voltage during grid-connected mode

Grid voltage and grid current in the respective Figs. 3.11 and 3.12 demonstrate system performance and Fig. 3.13 shows the line-to-line voltage during grid-connected mode.

### 3.7 CONCLUSION

The Microgrid integration with the utility grid will help in the effective utilization of renewable sources for improving the quality of the grid. This chapter, explains the modelling of the components of the PV array and uses Maximum Power Point Tracking to utilize the maximum power from the PV array which is connected to energy storage to maintain the DC link voltage using a control strategy. An algorithm for energy management is proposed to connect the Microgrid to the utility grid. The simulations are carried out, and the results are analysed in Matlab/Simulink environment.

# Chapter 4

# SRF THEORY BASED SHUNT ACTIVE POWER FILTER FOR POWER QUALITY IMPROVEMENT IN GRID INTERFACED SOLAR PHOTOVOLTAIC SYSTEM

## 4.0 GENERAL

In this chapter uses Shunt Active Power Filter (SAPF) in a polluted and unbalanced mains voltage for the compensation of current harmonics along with the reactive power. During compensation, the reference current is calculated by the theory of Synchronous Reference Frame (SRF). This study utilizes Photovoltaic (PV) energy, a renewable energy source, for which a maximum power point tracking (MPPT) method, an incremental conductance (InCnd), is employed. To modify the energy storage of dc-voltage, an artificial neural network controller (ANN) is used. The power system toolbox of MATLAB/SIMULINK is used to simulate the system being proposed. The SAPF is compared and assessed on the basis of PI control, FUZZY controller, and Artificial Neural Network (ANN). The results demonstrate the ANN control's efficiency in optimizing the DC capacitor energy storage, sinusoidal form of the current, and reactive power compensation. A low Total Harmonic Distortion (THD) will be achieved with the proposed system which shows the efficacy of the method presented.

## 4.1 THE PROPOSED SYSTEM

The use of diodes, triacs, thyristors and other semiconductor switches to regulate AC power is commonly used to feed regulated power to electrical loads, solid-state AC-voltage controllers, lighting systems, electrochemical industries, and power supplies

(UPS), etc. These solid-state converters, like nonlinear loads, extract harmonic currents in addition to the current's reactive component from the AC mains. They can also trigger unbalanced currents and draw too much neutral current in three-phase power systems. The injected reactive power burden, harmonic currents, excessive and unbalance neutral current are responsible for low efficiency in distribution system. Fig. 4.1 shows the presented system's schematic diagram.

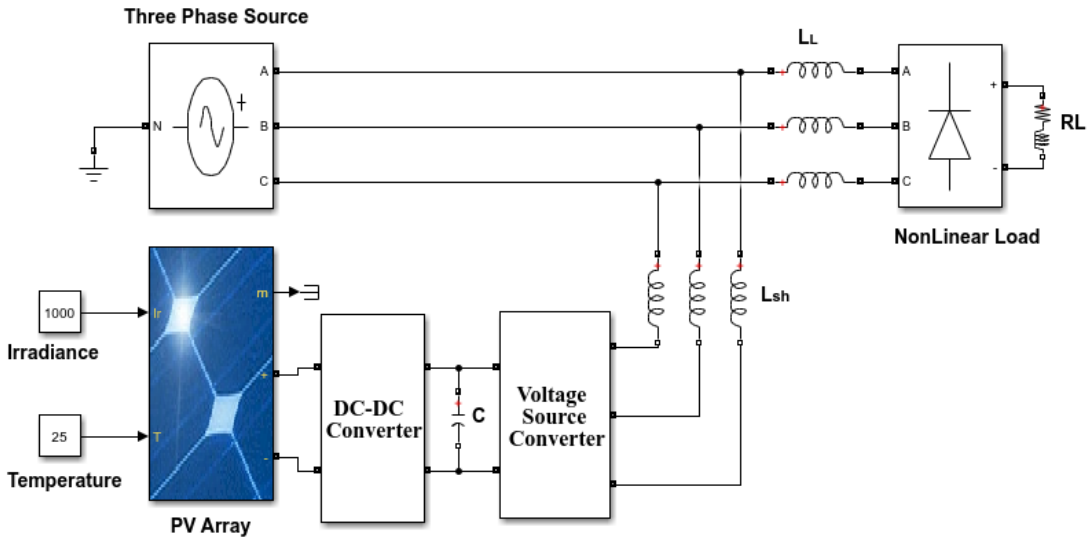


Fig.4.1 : Illustrative diagram of the presented system

## 4.2 SHUNT APF

Today, SAPF technology is a mature technology to provides AC distribution networks with reactive power compensation, harmonic current, and neutral current compensation. In three-phase systems, SAPFs are often used to control the terminal voltage and prevent voltage flicker. SAPF is considered to be the best system for dealing with power quality issues. These filters are divided into three categories: 1: single phase-two wire, 2: three phase-three wire, and 3: three phase-four wire configurations, to satisfy the needs of the nonlinear loads of supply systems. Here we use three phase-four wire SAPF.

## 4.3 SRF CONTROLLER

The SRF theory is used for the regulation of VSC of APF and its control scheme is depicted in Fig.4.2. The DC bus voltage, point of common coupling (PCC) voltages, and load currents are some of the feedback signals for the APF. Using Park's transformation, the following load currents are transformed into a dq0 frame:

$$\begin{bmatrix} i_{Ld} \\ i_{Lq} \end{bmatrix} = \sqrt{\frac{2}{3}} \begin{bmatrix} cos\theta & \cos\left(\theta - \frac{2\pi}{3}\right) & \cos\left(\theta + \frac{2\pi}{3}\right) \\ -sin\theta & -\sin\left(\theta - \frac{2\pi}{3}\right) & -\sin\left(\theta + \frac{2\pi}{3}\right) \end{bmatrix} \begin{bmatrix} i_{La} \\ i_{Lb} \\ i_{Lc} \end{bmatrix} \quad (4.1)$$

A phase-locked loop coordinates these feedback signals with voltages at a common coupling point. The components of d–q current are next sent through low pass filters obtaining the DC components of $i_{\mathrm{Ld}}$ and $i_{\mathrm{Lq}}$. The currents of the d-axis and q-axis consist of fundamental components and harmonic components as

$$i_{Ld} = \bar{\imath}_{Ld} + \bar{\imath}_{Ld} \quad (4.2)$$

$$i_{Lq} = \bar{\imath}_{Lq} + \bar{\imath}_{Lq} \quad (4.3)$$

$$\begin{bmatrix} i_a^* \\ i_b^* \\ i_c^* \end{bmatrix} = \sqrt{\frac{2}{3}} \begin{bmatrix} cos\theta & -sin\theta \\ \cos\left(\theta - \frac{2\pi}{3}\right) & -\sin\left(\theta - \frac{2\pi}{3}\right) \\ \cos\left(\theta + \frac{2\pi}{3}\right) & -\sin\left(\theta + \frac{2\pi}{3}\right) \end{bmatrix} \begin{bmatrix} i_{Ld} \\ i_{Lq} \end{bmatrix} \quad (4.4)$$

The harmonic components are converted into the three-phase values using the inverse Clark's transformation. After the transmission of these reference values to the hysteresis controller, voltage source inverter (VSI) gate pulses are generated.

## 4.4 PV ARRAY WITH MPPT TECHNIQUE

A photovoltaic array, which converts solar and photovoltaic energy into electrical energy, is the primary part of a PV system. The solar irradiance of PV array changes for several reasons like time variation in a day and climatic effects like clouds, etc.

Therefore, MPPT strategies are employed on DC/DC boost converter to manage the PV array's output current and voltage and to extract maximum power from PV array even during solar irradiance variations. The boost converter helps to step-up the PV output voltage making it compatible with electrical loads.

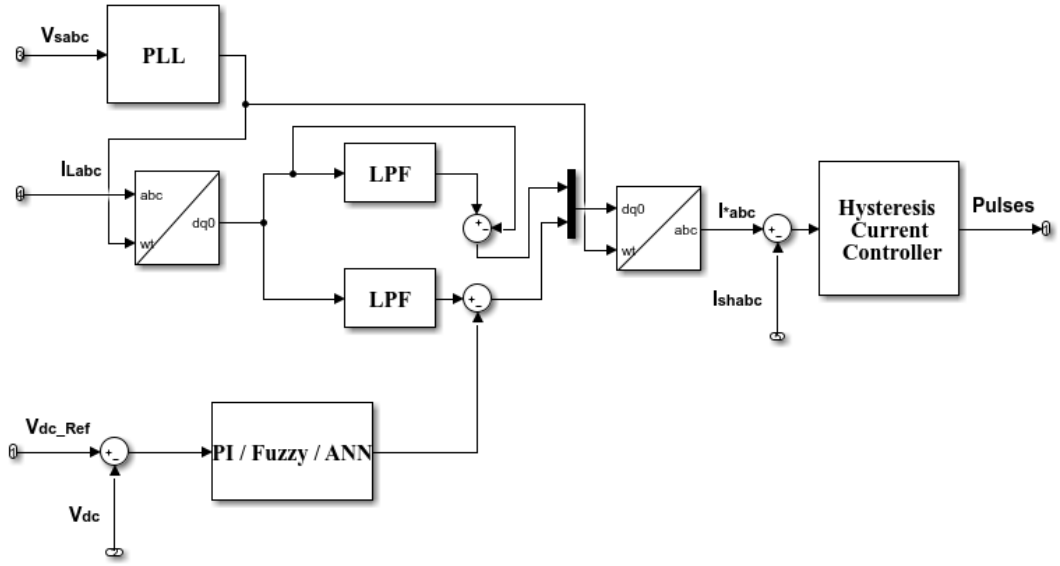


Fig. 4.2 : d-q theory for reference current generation

The PV cell's equivalent circuit is depicted in Fig. 4.3. and describes the source current ($I_L$), diode (D), and series resistance ($R_s$) representing the internal resistance of current flow and parallel resistance ($R_{sh}$) indicating the leakage current.

Fig. 4.4 depicts the current-voltage and power-voltage (I-V and P-V) dynamics of a PV array as they change with solar irradiance and temperature. When no load is attached to PV cell, the open circuit ($V_{oc}$) voltage is generated at terminals. During short circuit at PV cell, the short circuit ($I_{sc}$) current is produced. In both the above scenario, zero power is generated.

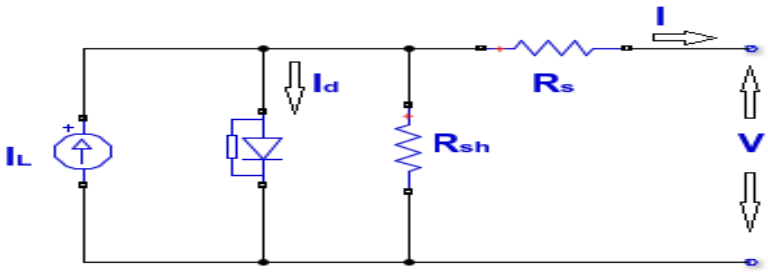


Fig.4.3 : PV cell's equivalent circuit

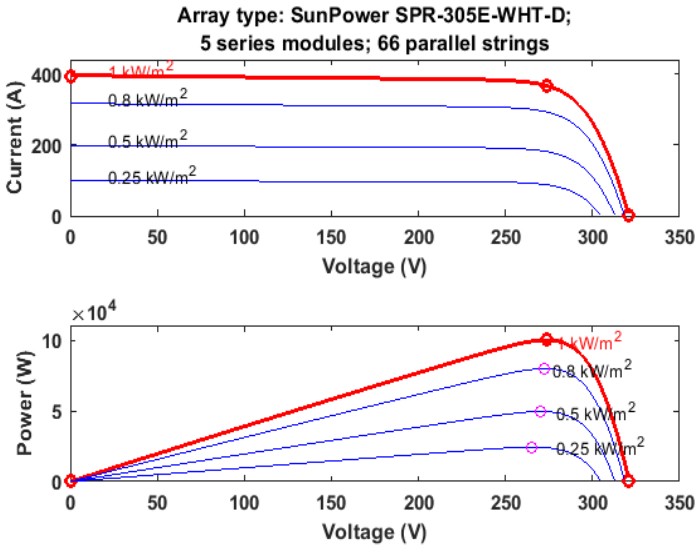


Fig. 4.4 : Characteristics of a typical PV cell

### 4.4.1 Incremental conductance MPPT Technique

Because of the features like simplicity and good performance during the lowest solar irradiation levels or the rapid change of the irradiance, the InCnd MPPT technology is broadly used in PV systems. This method is used for sensing the voltage and current output of solar arrays using sensors.

In this method, the voltage at the terminal array ($V_{PV}$) is always adjusted to the maximum power point of the photovoltaic array. And at this point i.e., at MPP the derivative of power with respect to voltage ($dP_{pv}/dV_{pv}$) equals zero. Furthermore, this derivative is positive on the MPP's left side ($dP_{pv}/dV_{pv} > 0$) and negative on the right side ($dP_{pv}/dV_{pv} < 0$).

## 4.5 COMPARATIVE ANALYSIS BETWEEN DIFFERENT CONTROLLERS

### 4.5.1 PI Controller

A PI controller typically modifies the voltage of the dc-link capacitor to eliminate steady-state errors and reduce ripple voltage. The proportional constant (Kp) governs the dynamic responsiveness of the dc-link voltage, while an integral constant governs its settling time (Ki). The values of $K_p$ and $K_i$ have to be selected properly for ensuring the control performances aforementioned. The energy-balance principle is employed for calculating $K_p$, and the $K_i$ value is determined observationally. The voltage of the dc-link capacitor is adjusted by changing the flow of a small amount of power into the dc-link capacitor, which compensates for losses in conduction and switching. $K_p$ and $K_i$ have the proper setting to the actual $V_{vsc}$ and reference $V_{vsc\text{-}ref}$ across the capacitor. In addition to the determination of $P_{loss}$, the dc voltage regulator also corrects power compensation errors. Finally, the ripple voltage of the PWM-controlled VSC is reduced by PI controller. In this system, the $K_p$ and $K_i$ values are 2 and 20.

### 4.5.2 Fuzzy Logic Controller (FLC)

In 1965, Professor Lotfi Zadeh projected the idea of FLC first as a means to process data by enabling partial membership rather than crisp membership. Shortly, for many system control applications it was proved to be an excellent choice. The fuzzy logic controller (FLC) is currently used in many sectors of industries, power systems, and science for compensating reactive power and harmonic current. The structure of the FLC system is shown in Fig. 4.5. In the fuzzification block, the crisp values of error e(n) and change in error ce(n) are transformed into fuzzy values, determined by linguistic variables like low, medium, high, big, slow, etc. The rule elevator evaluates the fuzzy rules by fuzzy set operations like AND, OR, and NOT indicating intersection,

union, and complement respectively. These fuzzy rules are stored in the rule base. The linguistic variables are then transformed to crisp values by defuzzification block. The membership functions needed by fuzzification and defuzzification are stored in the database.

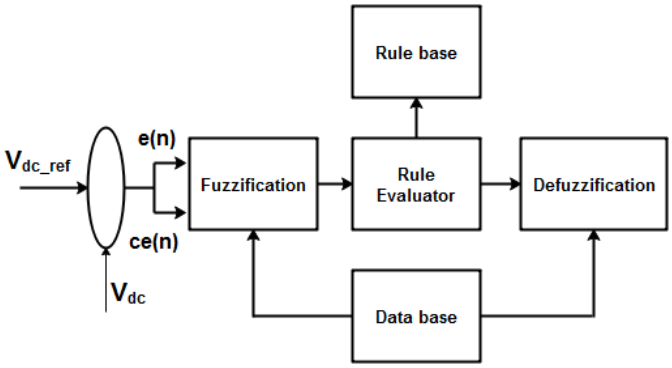


Fig. 4.5 : Structure of FLC

### 4.5.3 ANN Controller Scheme

Artificial Neural Networks (ANN), together with SAPF, have recently impressed many applications. This methodology is measured as a modern tool for the development of SAPF control circuits. ANN is a theoretical model that uses biological neural networks to motivate. It includes a linked artificial neuron collection. Without the need to create a dynamic system model, artificial intelligence problems are fixed by ANN. The single-layer feed network (trained by the backpropagation method) is employed to improve the SAPF performance. This network consists of two layers of neuron connections. The input layer contains 1 neuron for getting input, and 20 hidden layers, supplied with every input processed. The output layer consists of 1 neuron with output $P_{loss}$. For every layer to be trained, activation functions are assigned. The input and output layers' activation functions are provided to Tan-sigmoidal and Pos linear functions, respectively. Fig. 4.6 shows the ANN block, at 'n' and ‘n-1’ intervals, large data of dc-link voltage are collected and stored in the workspace of Matlab by

the traditional method. This data is used to train ANN and retrieve data from the Matlab workspace using the training algorithm. The input/output layer neurons are almost in fixed volumes, while the precise ANN operation depends on the neurons amount present in the hidden layer.

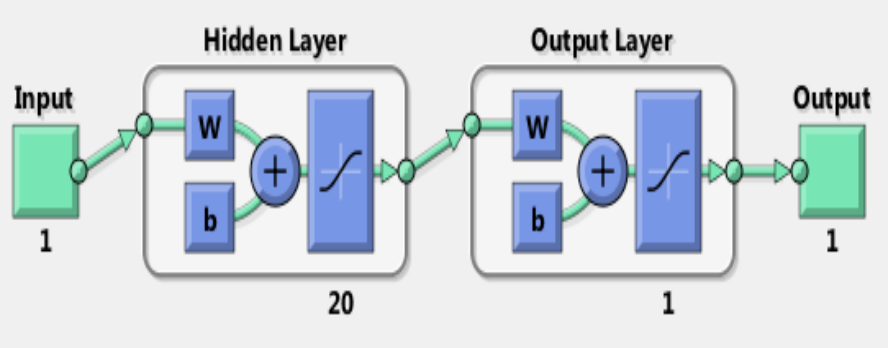


Fig. 4.6 : Artificial Neural Network block

## 4.6 RESULTS AND DISCUSSION

The suggested system is modeled and simulated in Matlab/Simulink environment. Table 4.2 provides the suggested settings for the system parameters. The simulation's findings are on par with those of three PI, fuzzy logic, and ANN controllers. The figures analyzed and provided descriptions of the reactive power compensation, THD, and DC link voltage scenarios.

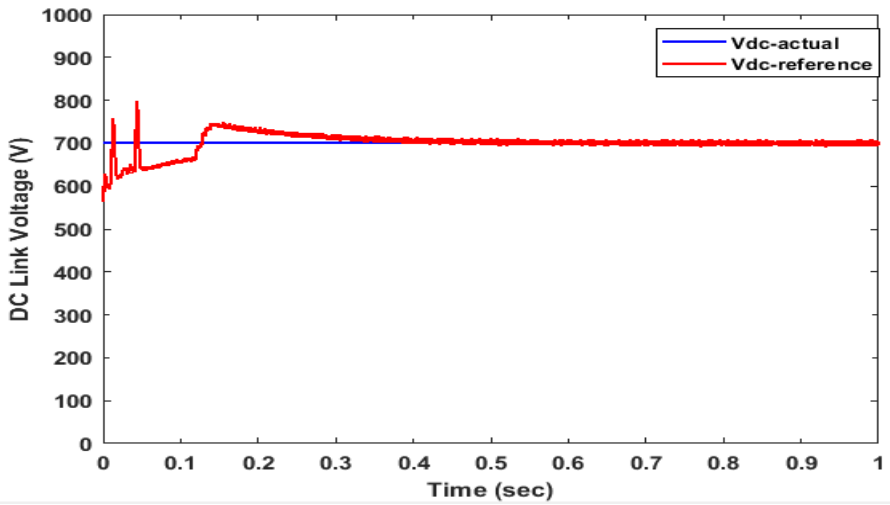


Fig 4.7 : DC link voltage with PI controller

The PI control scheme for the dc link capacitor voltage is compared with both the FLC and the ANN control schemes. The dc-link voltage response for three control schemes (PI, FLC, and ANN) at different times shows in Fig. 4.7, 4.8, and 4.9 respectively. The dc-link voltage setting times with PI controller, Fuzzy logic controller, and ANN controller are 0.15sec, 0.08sec, and 0.01sec respectively as listed in Table 4.1

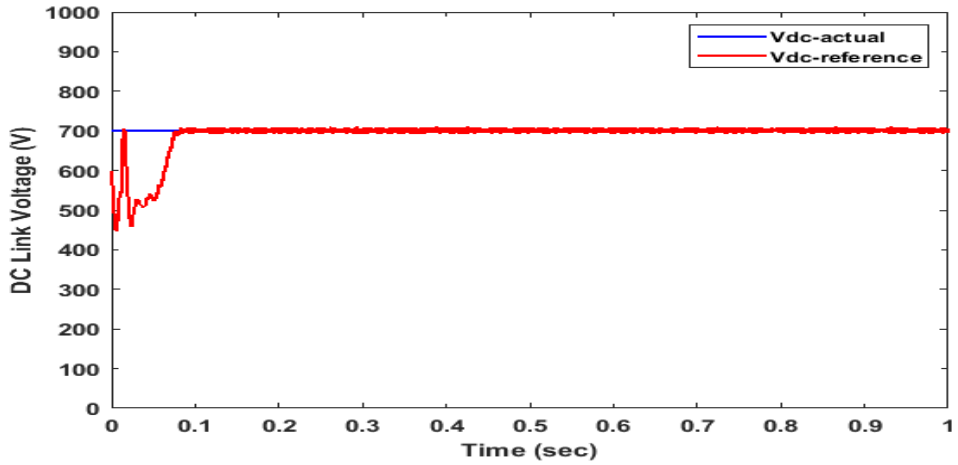


Fig. 4.8 : DC link voltage with fuzzy logic controller

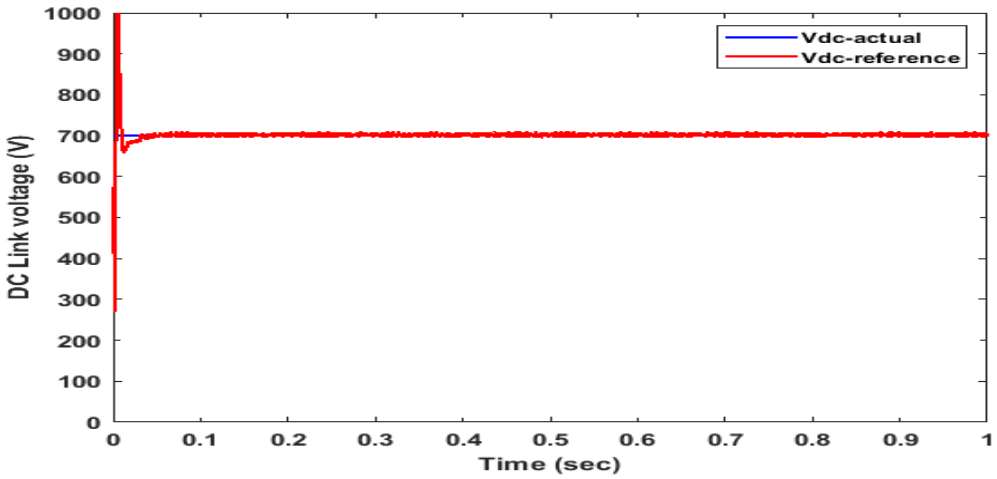


Fig. 4.9 : DC link voltage with ANN controller

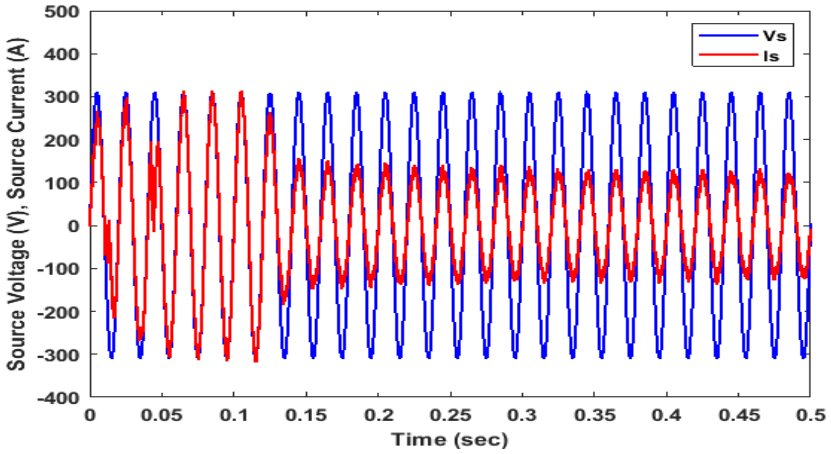


Fig. 4.10 : Reactive power compensation with PI controller

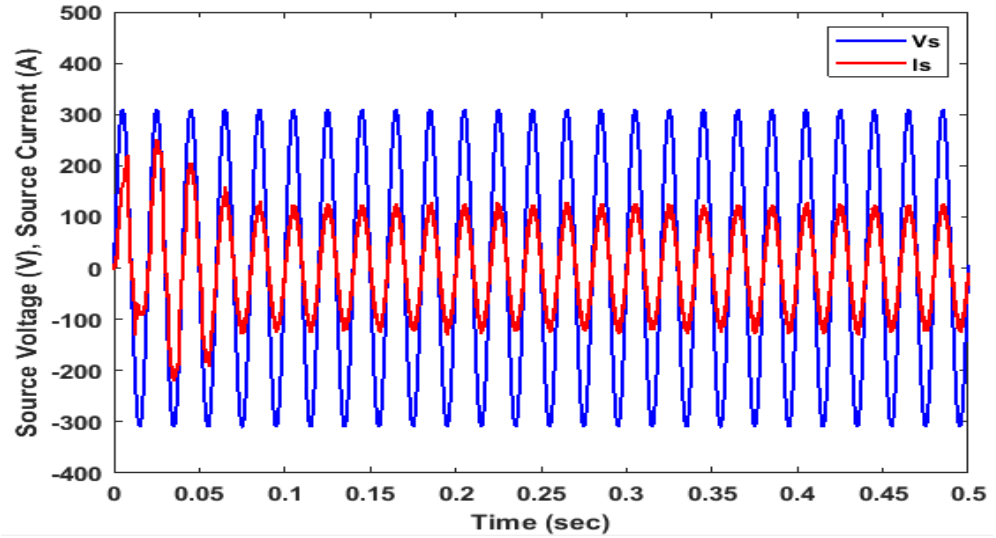


Fig. 4.11 : Reactive power compensation with FLC

According to the data, SAPF's ANN-based dc-link voltage control outperforms PI and FLC. Particularly the dc link voltage is less oscillating with ANN than with applications with PI and FLC. Also, when the two other controllers are used, the time period until the voltage of the DC link is returned to steady status is smaller. The reactive power compensation with PI, FLC, and ANN controller applications is shown in Figs. 4.10, 4.11, and 4.12 respectively. The ANN produces better results among the three different controllers for reactive power compensation.

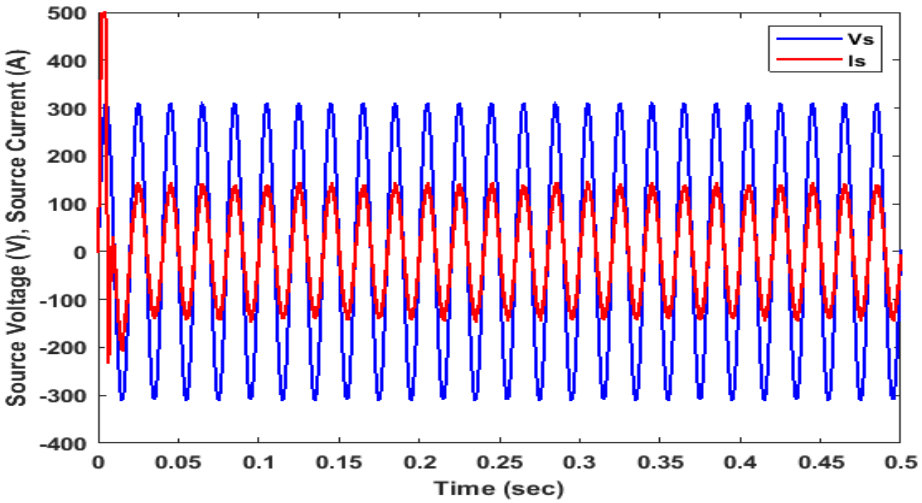


Fig. 4.12 : Reactive power compensation with ANN controller

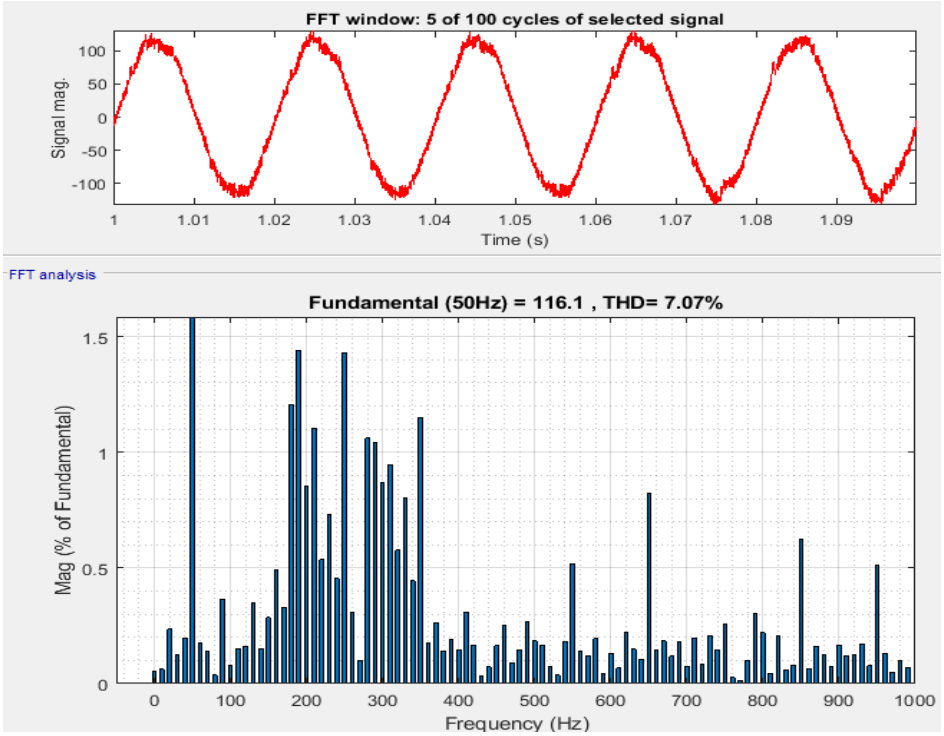


Fig. 4.13 : THD analysis of source current with PI controller

TABLE 4.1 : $V_{dc}$ SETTLING TIME

| **Controller** | **Settling Time** |
|---|---|
| PI Controller | 0.15 sec |
| Fuzzy Logic Controller | 0.08 sec |
| ANN Controller | 0.01 sec |

In Fig. 4.13, Fig. 4.14, and Fig. 4.15 the THD of the system for PI, FLC, and ANN control schemes are shown respectively. Compared with the two other control systems, the proposed system using an ANN controller provides better sources of THD, which means the THD percentage is decreased from 7.07% to 4.97% whereas using the FLC, and the ANN controller is down to 4.12%.

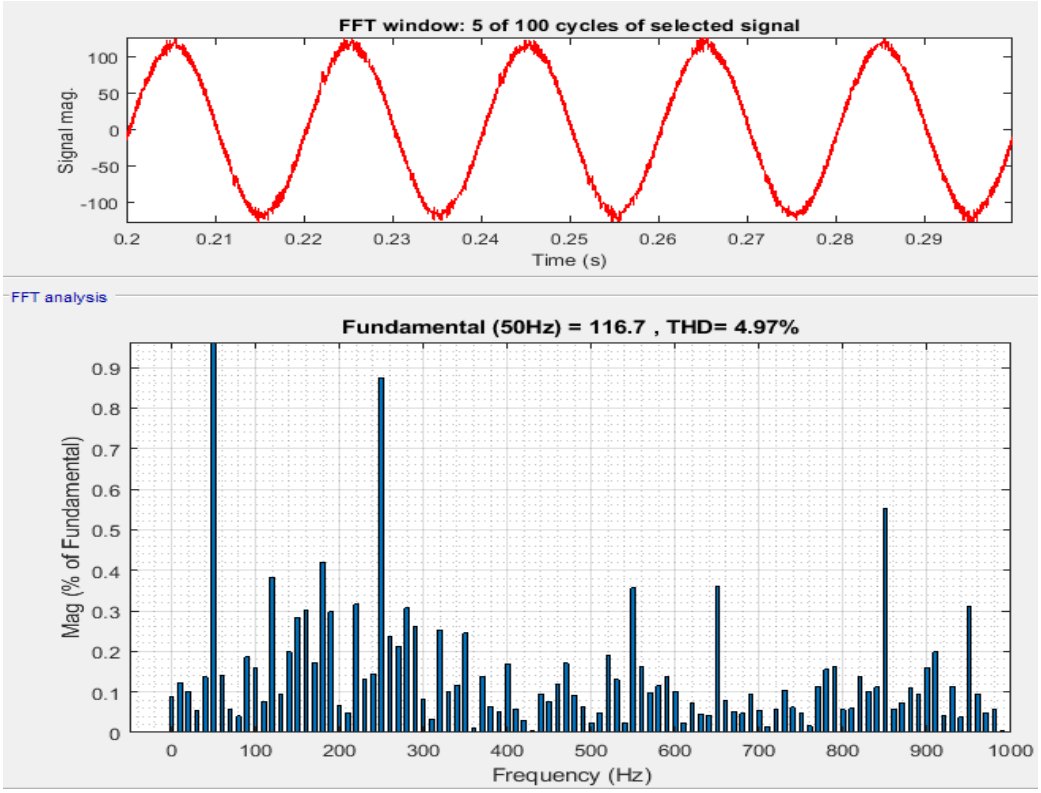


Fig. 4.14 : THD analysis of source current with FLC

TABLE 4.2 : PARAMETERS LIST

| **Parameters** | **Values** |
|---|---|
| Source Voltages | 220 V |
| System Frequency (f) | 50 Hz |
| Rectifier Load | 5 ohm, 8mH |
| Load Inductance ($L_L$) | 0.1 mH |
| Filter Inductance ($L_{sh}$) | 1 mH |
| DC voltage | 700 V |
| Capacitor Voltage | 2580 µF |

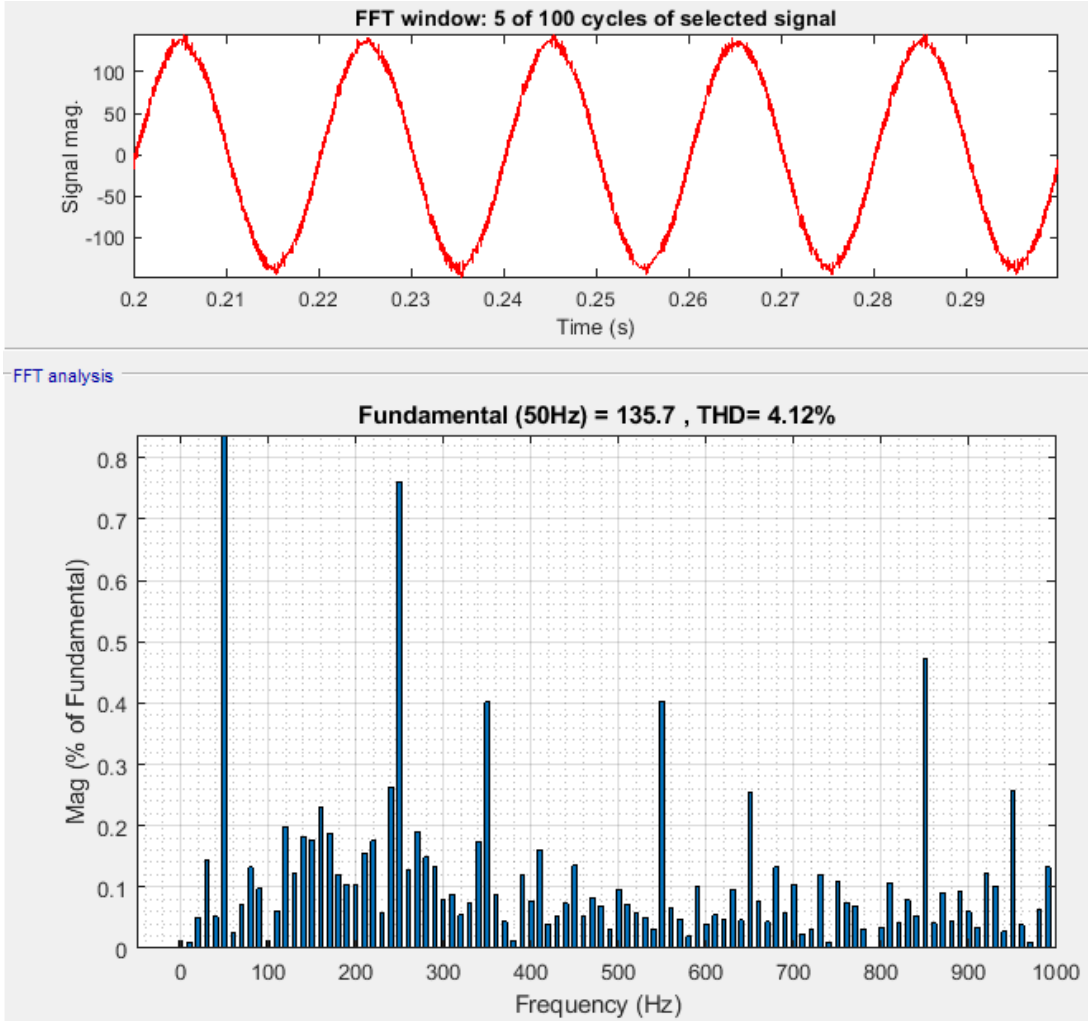


Fig. 4.15 : THD analysis of source current with ANN controller

## 4.7 CONCLUSION

In this chapter, the SRF control method with ANN controller is presented and verified with three phase-four wire SAPF system in MATLAB/Simulink environment. Harmonic current and reactive power adjustment were made possible by the photovoltaic integrated SAPF. Comparisons between the SAPF modified with ANN controller and PI and FLC are made. The dc-link voltage of Shunt APF was maintained constant by the PI, FUZZY, and ANN controllers. As a result, the ANN controller-based SAPF delivers better performance than PI and fuzzy controllers. Additionally, by using ANN controller the source current THD and, settling time are reduced.

# Chapter 5

# ANN BASED ADAPTIVE SOGI-FLL CONTROLLER FOR MULTIFUNCTIONAL GRID TIED SOLAR ENERGY CONVERSION SYSTEM

## 5.0 GENERAL

In this chapter presents an Artificial neural network (ANN) based adaptive second order generalized integrator frequency locked loop (SOGI-FLL) control technique for grid-tied solar photovoltaic (SPV) system. The system includes a boost converter, and the duty ratio of the boost converter is regulated by a maximum power point tracker (MPPT) system. An incremental conductance-based MPPT controller is incorporated for maximum power extraction from SPV system. The three-leg voltage source converter (VSC) is connected to SPV array via a DC link capacitor. The proposed ANN-based adaptive SOGI-FLL control scheme is designed to generate reference grid currents. The proposed system exhibits multifunctional applications such as power quality enrichment, balancing of load, reactive power compensation, voltage regulation, etc. An ANN-based controller is utilized for maintaining DC link voltage. The PV feed-forward technique is incorporated in the proposed controller for dynamic performance enhancement. The proposed system is implemented in Matlab/Simulink environment and the simulation results exhibit high-value performance for microgrid applications.

## 5.1 SYSTEM LAYOUTS

Fig.5.1 presents the proposed configuration system. The system contains SPV array for the source of renewable energy. The proposed SPV system is interfaced to a 3-phase grid along with non-linear load. Voltage source converter (VSC) and ripple

filters are coupled at the point of common coupling point (PCC). The VSC is utilized for supplying power to the distribution system and ripple filters are used for elimination of switching ripples. The SPV system includes SPV array, DC-DC boost converter for step the DC voltage, maximum point tracking (MPPT) unit for utilization of maximum power from SPV array.

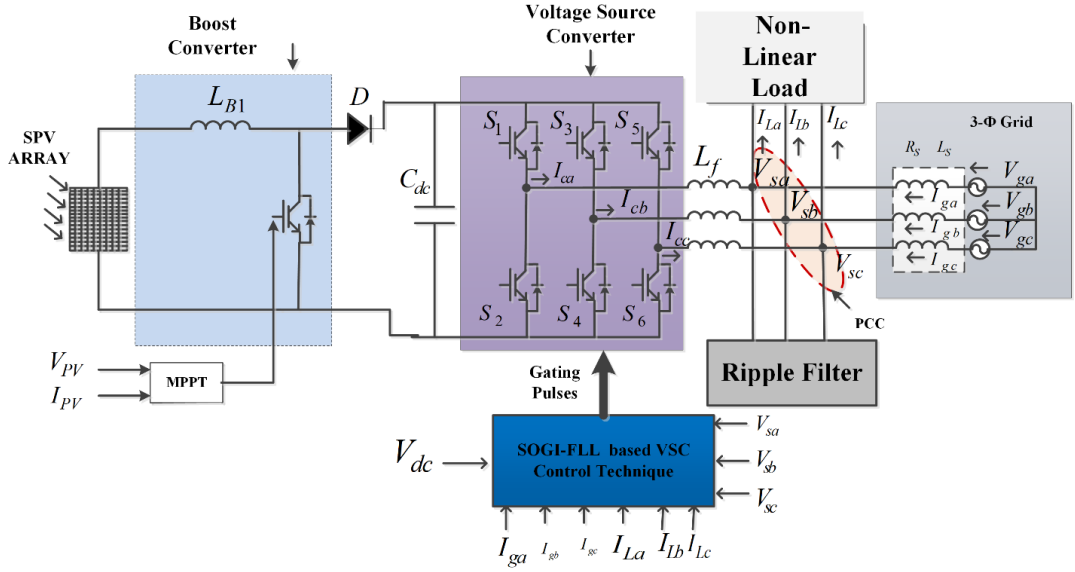


Fig.5.1 : System Configuration

## 5.2 CONTROL ALGORITHMS

The control algorithms are applied for boost converter of SPV as well as for voltage source converter (VSC). However, pulses of SPV boost converter are regulated by the incremental conductance (INC) based MPPT controller. The energy of SPV is fed to DC-link capacitor ($V_{dc}$) of VSC. Furthermore, fuzzy logic controller (FLC) is utilized for maintaining constant DC-Bus voltage and loss computation for VSC. The pulses of VSC are extracted by SOGI-FLL-based controller. The function of VSC is to power

quality improvement as well it can be utilized to power conversion. The parameters of the SPV system are mentioned in the appendix.

### 5.2.1 Incremental Conductance Based MPPT Controller

The incremental conductance (InC) based maximum power point tracker (MPPT) is utilized to extract maximum power from the solar array. It is easier to implement, has fast maximum tracking capability, and good dynamic behavior kind of attracting features to choose as an MPPT controller. Therefore, based controller is applied to extract maximum power from the proposed SPV array. The basic mathematics describe the operation of this MPPT controller as,

$$P = V_{PV} \times I_{PV} \tag{5.1}$$

$$\frac{\partial P}{\partial V} = \frac{\partial \left( V_{PV} \times I_{PV} \right)}{\partial V} \approx I_{PV} + V_{PV} \frac{\partial I_{PV}}{\partial V} \tag{5.2}$$

Now, compare the array conductance with increment conductance to find the maximum power point.

$$\begin{aligned} &left\ of\ MPP\ \ when,\ \frac{\partial I_{PV}}{\partial V_{PV}} > \frac{-I_{PV}}{V_{PV}} \\ &Right\ of\ MPP\ when, \frac{\partial I_{PV}}{\partial V_{PV}} < \frac{-I_{PV}}{V_{PV}} \\ &\&\ at\ MPP\ when, \frac{\partial I_{PV}}{\partial V_{PV}} = \frac{-I_{PV}}{V_{PV}} \end{aligned} \tag{5.3}$$

Hence, Eq. 5.3 concludes that the maximum power point is tracked when incremental conductance will be equal to the array conductance.

### 5.2.2 ADAPTIVE SOGI-FLL CONTROL SCHEME

The proposed controller is presented in Fig. 5.2 (a). The applied control scheme is utilized for the accurate generation of switching pulses for VSC. In this section step by step, procedures are presented for the generation of switching pulses. Moreover, various silent signals are utilized for the generation of switching pulses for VSC, the signals are:

1. Magnitude of terminal voltage
2. In-phase and quadrature-phase unit templete
3. Feed-forward component of current
4. Loss component of current
5. Equivalent component of current
6. Net active component of current

1. Magnitude of terminal voltage ($V_{tm}$):- The magnitude of terminal voltage is computed as,

$$V_{tm}=\sqrt{\frac{2(V_{ga}^2+V_{gb}^2+V_{gc}^2}{3}}$$

Where, $V_{ga,}V_{gb,}V_{gc}$ are the phase voltages

2. In-phase and quadrature-phase unit templete:- The quadrature unit template ( $\alpha_{q1},\alpha_{q2},\alpha_{q3}$) and the in-phase unit template signals ( $\alpha_1$, $\alpha_2$ , $\alpha_3$) are utilized for VSC switching algorithm.

In-phase unit templates are, $\alpha_1=\frac{V_{ga}}{V_{tm}}$, $\alpha_2=\frac{V_{gb}}{V_{tm}}$, $\alpha_3=\frac{V_{gc}}{V_{tm}}$ (5.4)

The quadrature unit template is estimated as,

$$\alpha_{q1}=\frac{\alpha_3-\alpha_2}{\sqrt{3}},\ \alpha_{q2}=\frac{\alpha_1-\alpha_3}{\sqrt{3}},\ \alpha_{q3}=\frac{\alpha_2-\alpha_1}{\sqrt{3}} \tag{5.5}$$

3. Feed-forward component of current: - The feed-forward loop is utilized for the reference current generation ($I_{pf}$), which helps in dynamic response improvement. The PV-based feed-forward component is estimated by this equation as, $I_{Pvq}=\frac{2}{3}*\frac{P_{pv}}{V_{tm}}$

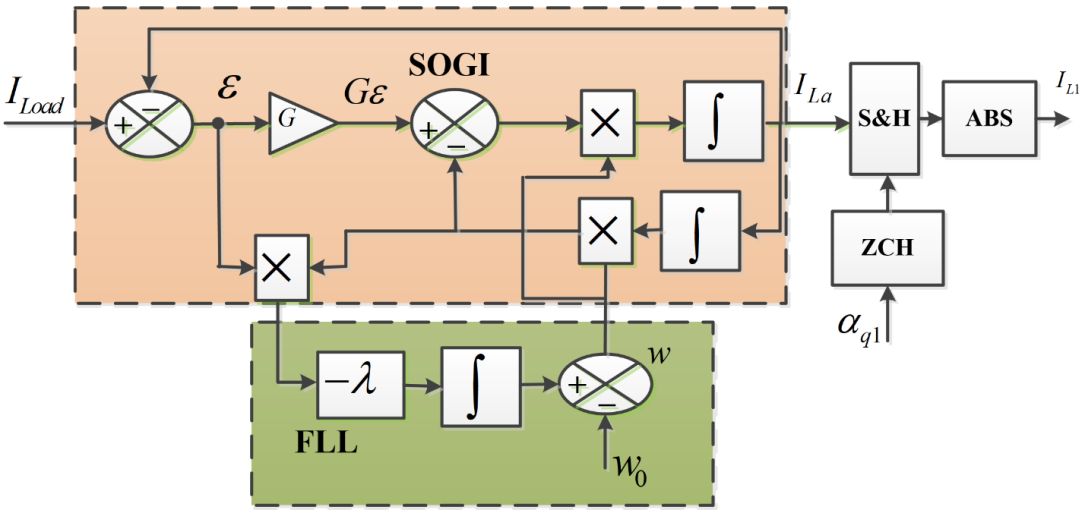


(a)

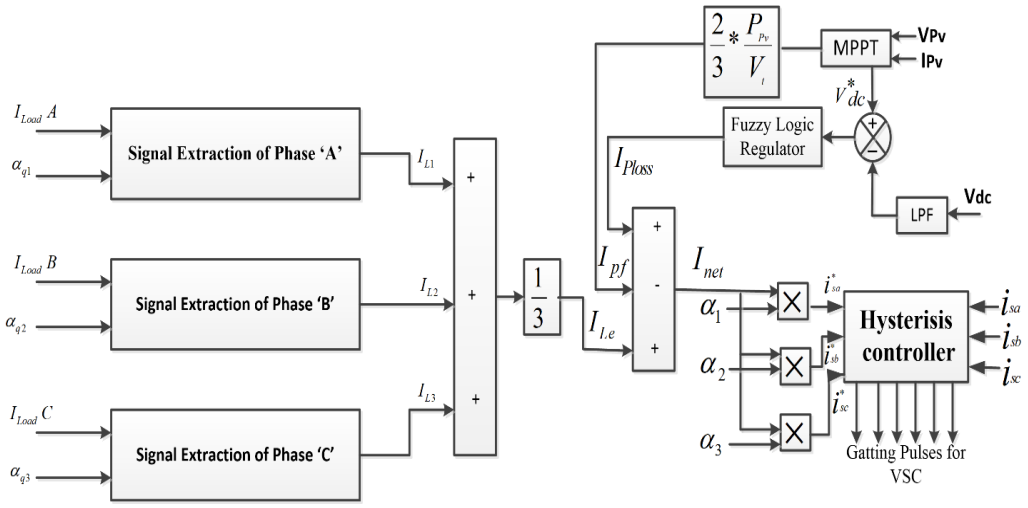


(b)

Fig. 5.2. (a) : Adaptive SOFI-FLL control scheme for the fundamental component of load current extraction from phase 'A', (b) Adaptive SOGI-FLL control scheme for reference current generation

4. Loss component of current: - The artificial neural network (ANN) based controller is utilized to maintain the DC bus voltage constant as well as for the loss component of current estimation. As efficient and fast it maintains the constant value and minimizes the losses in the converter. This technique is measured to be the latest tool to improve the dynamic performance design control circuits of adaptive SOGI-FLL. Moreover, ANN is a mathematical model motivated by biological neural networks. It comprises an interconnected collection of artificial neurons.

Here, $V_{dc}^{*}$ is the reference DC bus voltage and $V_{dc}$ the sensed DC bus voltage. So, the error in voltage ($V_e(\mathrm{n})$) is represented as, $V_e(\mathrm{n}) = V_{dc}^{*} - V_{dc}(n)$. Moreover, the loss component of voltage error y(n) is represented as,

$$\mathrm{y(n)} = \mathrm{V_0}(n) - V_0(n-1) \tag{5.6}$$

Here, $\mathrm{V_0}(n)$ is the output to compute the loss component of current.

The following procedure algorithm is adapted for ANN to regulate the DC-bus voltage.

Initialize neural network toolbox

- Define input and target parameters with the help of PI controller
- Import input and target data from MATLAB workspace
- Create a network
- Define data in the network as input data, target data, training function, performance function, number of layers, and number of transfer functions.
- Train the network
- Check performance

If the training regression value is near one then import the network otherwise update the weights and do again training up to when performance gets the satisfactory result.

To improve the performance, a feed-forward network of a single layer (trained by the back propagation method) is used. This network comprises two layers with their respective neuron interconnections. The input layer has 1 neuron for receiving input and the hidden layer has 20 neurons which are fed by each processed input. The activation functions are designated to every layer for training purposes. The artificial neural network block is shown in Fig. 3 for the intervals of 'n' and 'n-1', the huge data of DC link voltage is collected and stored in MATLAB workspace from the PI controller. Using this data, training of ANN is performed and the training algorithm is used for retrieving the stored data from the workspace. The neurons of the input layer and output layer are almost in a fixed quantity, whereas the accuracy of ANN operation is dependent on the number of neurons in the hidden layer.

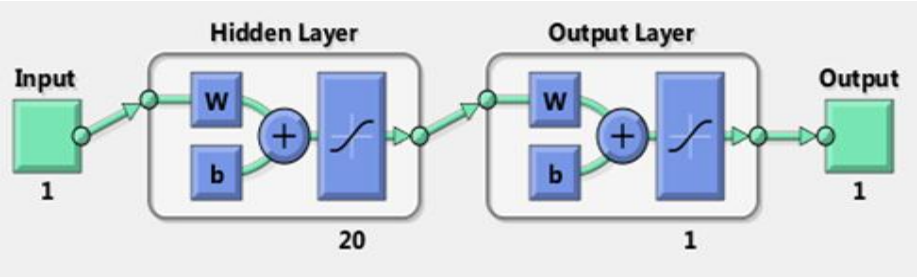


Fig. 5.3 : Artificial Neural Network block

5. Equivalent component of current: - The equivalent component of in-phase and quadrature-phase current is calculated as follows

$$I_{Le} = \frac{I_{L1} + I_{L2} + I_{L3}}{3} \tag{5.7}$$

Were, $I_{L1,} I_{L2} and\ I_{L3}$ in-phase component of load currents.

6. Net active component of current: - The net active component of current is computed as, $I_{net} = (I_{Ploss} - I_{pvq} + I_{Le})$ (5.8)

Where, $I_{Ploss}$ = loss component of current

$I_{pvq}$ = feed-forward component of current

$I_{Le}$ = Equivalent component of current

Furthermore, reference grid currents are compared with the source currents ($I_{sa}, I_{sb}, I_{sc}$) by using hysteresis current controllers. A not gate logic is used to convert these three reference grid currents to six gating pulses to control the grid-tied IGBT's based VSC.

## 5.3 RESULTS AND DISCUSSION

The simulation is carried out with varying operating conditions to illustrate the behavior of the proposed methodology using Matlab/Simulation software. The results have been carried out by considering linear as well as non-linear loads at the point of common coupling. For the performance analysis of the proposed system, simulation results include solar irradiance (G), DC link bus voltage (Vdc), SPV current (Ipv), SPV power (Ppv), feed-forward current (Ipvq), AC grid voltage (Vgabc), AC grid current (Igabc), compensating current (Ica), load current (iLa), AC grid active power (Pg), AC grid reactive power (Qg), terminal voltage (Vtm) and frequency (wr).

### 5.3.1 Behavior of System Under Nonlinear Load

Figs. 5.4 (a), and (b) present the behavior of the Solar PV system under non-linear load at variable insolation. Fig. 5.4 (a) shows the waveforms of G, Vdc, Ipv, Ppv, and Ipvq. Fig. 5.4 (b) shows the waveform of Vgabc, Igabc, Ica, iLa, Pg, and Qg at step insolation increase from 700 W/m2 to 1000 W/$m^2$ at t=0.4s.

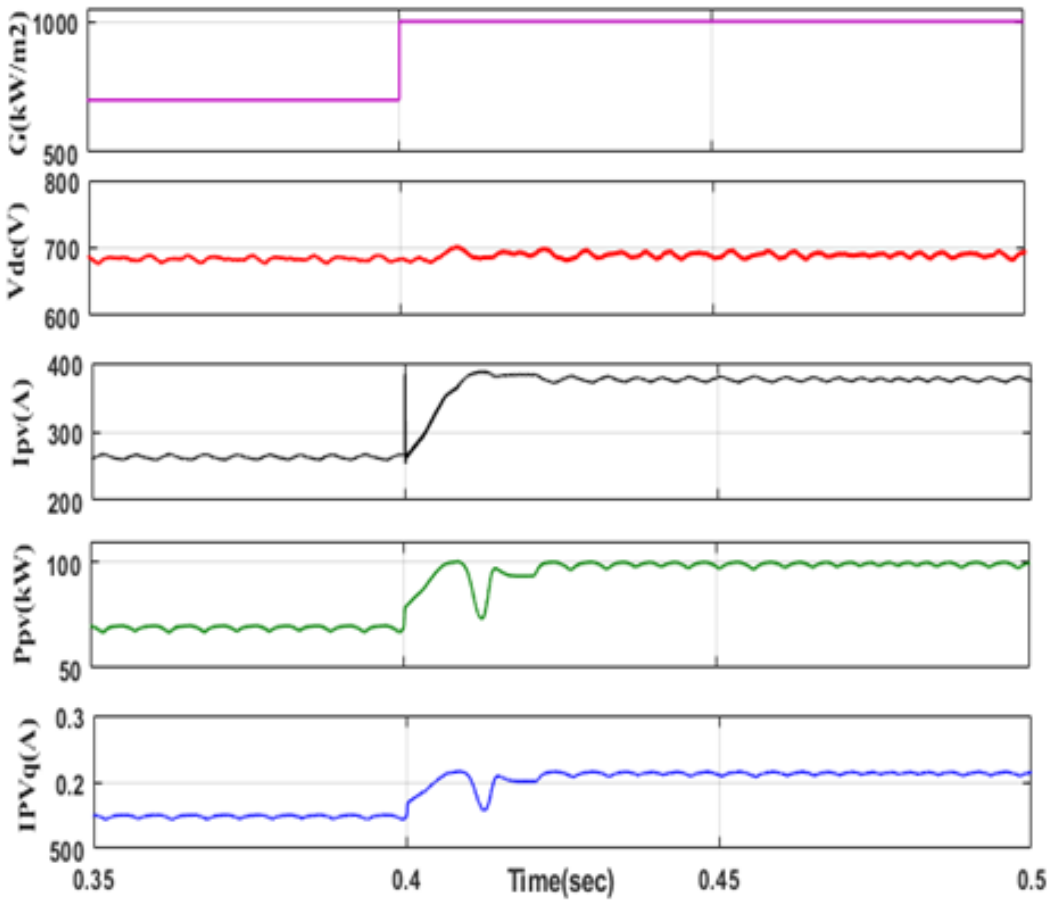


(a)

The grid current (Igabc) and voltage (Vgabc) are perfectly sinusoidal. It is noticed that as solar insolation increases at t=0.4 s, SPV array power (Ppv) and SPV current (Ipv ) are increased. The DC link voltage is maintained constant and very minute oscillation is observed in it. The feed-forward current is also increased, because of the increment in SPV power. Therefore, it causes low oscillations observed in grid current. Moreover, it is observed that as insolation increases at t=0.4s, the power generation from the solar power system is increased and therefore, active power flow and grid current are decreased because load power is constant in this operation. The system is carried on at unity power factor, as reactive power (Qg) is zero as shown in Fig.5.4 (b).

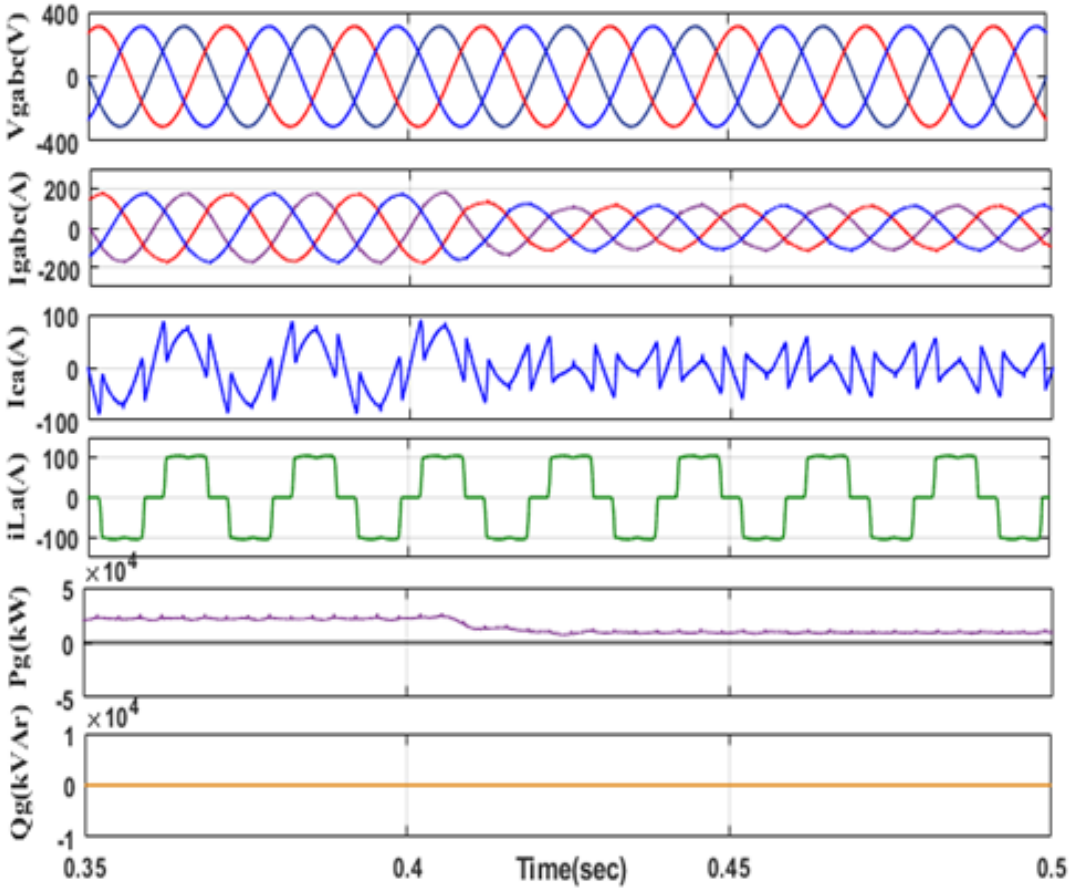


(b)

Fig. 5.5 (a) presents the behavior of the Solar PV system for intentionally load unbalancing of one phase under load non-linear load conditions. Fig. 5.4 (a) shows the waveform of G, Vgabc, Igabc, iLa, Ica, Vdc, Pg, and Vt. In this case, assume that the solar array is constantly operated at 1000 W/m2 insolation but, phase 'a' intentionally removed at (t= 0.4 - 0.5s). The grid currents are observed balanced and perfectly sinusoidal in both steady-state conditions (before t=0.4s and after t=0.5s), as well as in unbalanced conditions at (t= 0.4-0.5s). During the unbalancing period, the active power demand and load balancing criterion are fulfilled by Solar PV generating system. However, with this unbalancing condition, the DC bus voltage of VSC is maintained constant at 700 V.

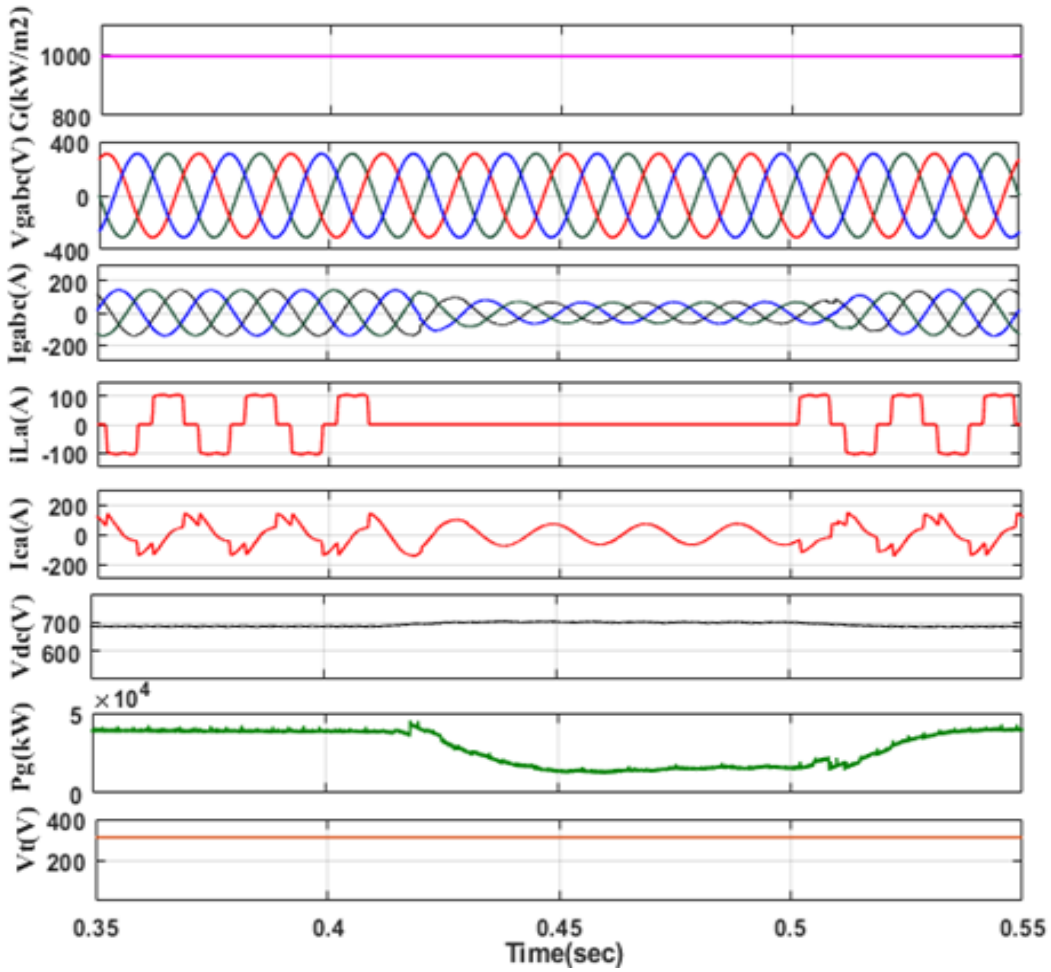


(a)

Fig. 5.5 (b) presents the dynamic behavior of solar PV system for varying system frequencies 49.5 Hz to 50.5 Hz. Fig. 5.5 (b) depicts the waveform of Vgabc, Igabc, iLa, Ica, Ipvq, Vdc, and wr. With the system frequency variation, it is observed that the grid current and voltage are balanced and sinusoidal. The DC link voltage and feed-forward current are remains unaffected irrespective of system frequency variations.

Figs. 5.6 (a), (b) present the behaviour of Solar PV system under linear load at variable insolation. Fig. 5.6 (a) shows the waveforms of G, Vdc, Ipv, Ppv, and Ipvq. Fig. 5.6 (b) shows the waveform of Vgabc, Igabc, Ica, iLa, Pg and Qg at step insolation increase from 700 W/m2 to 1000 W/m2 at t=0.4s. The grid current (Igabc) and voltage (Vgabc) are perfectly sinusoidal.

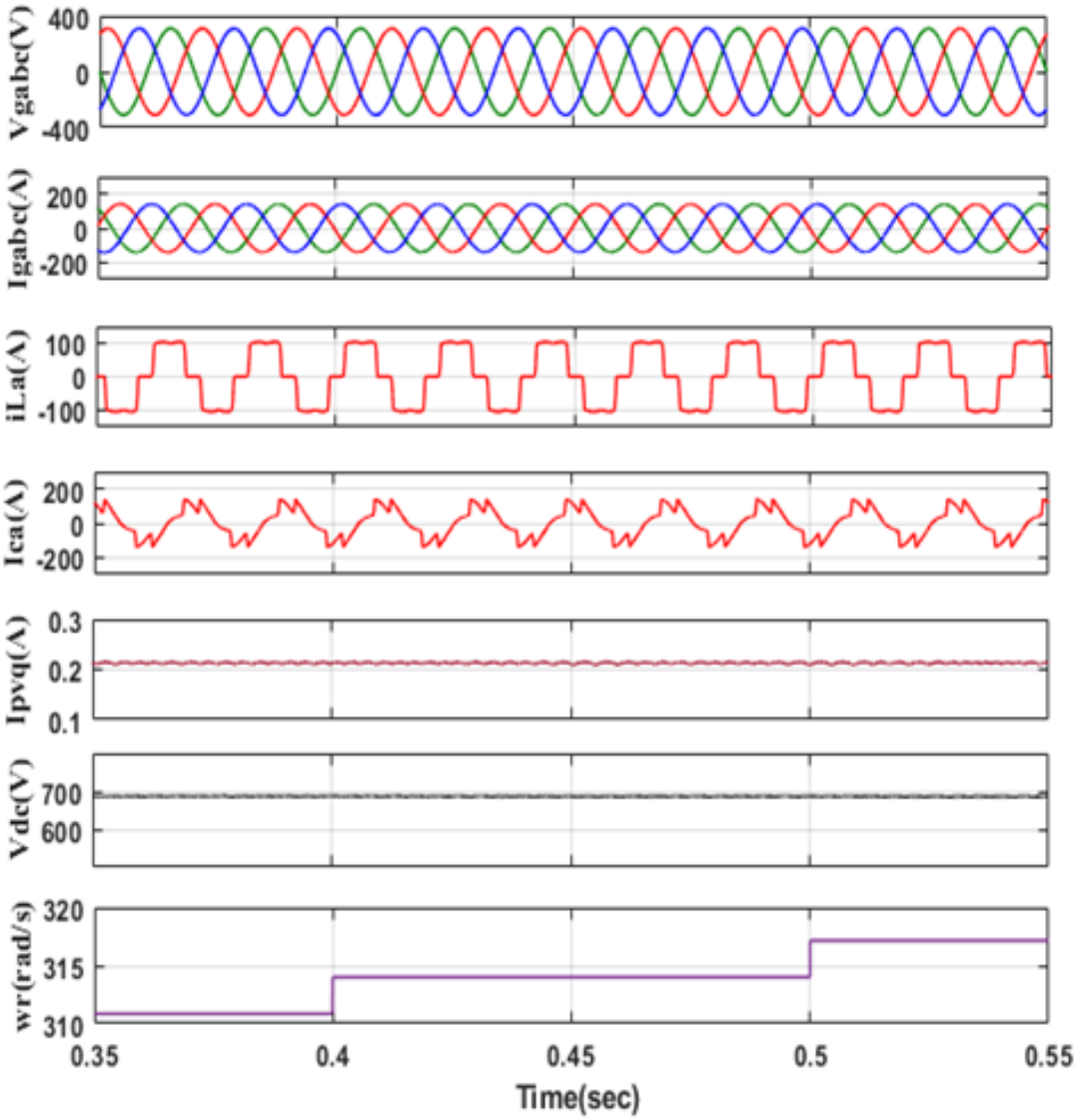


(b)

It is notice that as solar insolation increases at t=0.4 s, SPV array power (Ppv) and SPV current are increased. The DC link voltage is maintained constant and very low oscillation is observed in it.

The feed-forward current component is also increased, because of the increment in SPV power. Therefore, it causes low oscillations to be observed in grid current. Moreover, it is observed that as insolation increases at t=0.4s, the power generation from solar power system is increased and therefore, active power flow and grid current are decreased because of load power is constant in this operation.

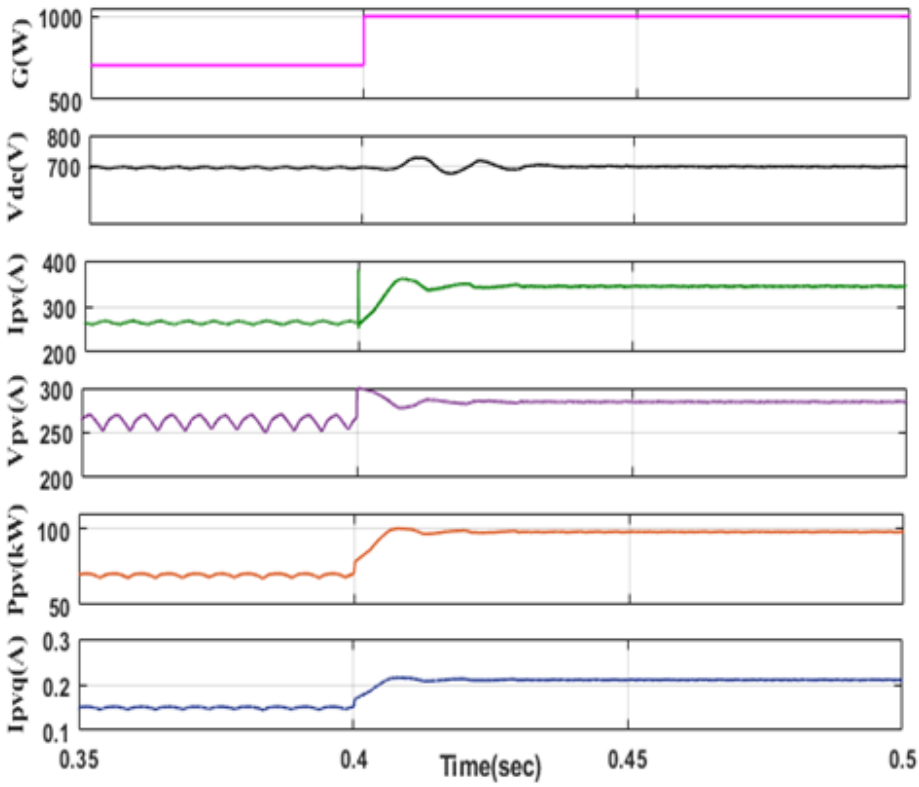


(a)

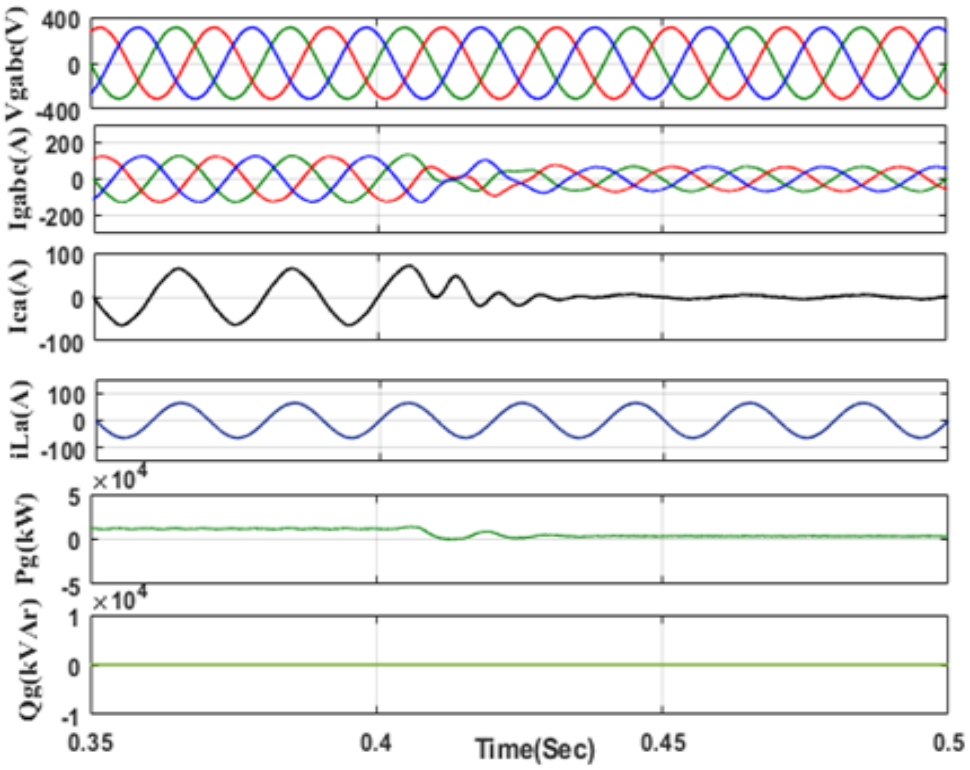


(b)

Fig.5.6 : Behaviour of system (a) under load unbalancing, (b) under variable system frequency

The system is carried on at unity power factor, as reactive power (Qg) is zero as shown in Fig. 5.6(b).

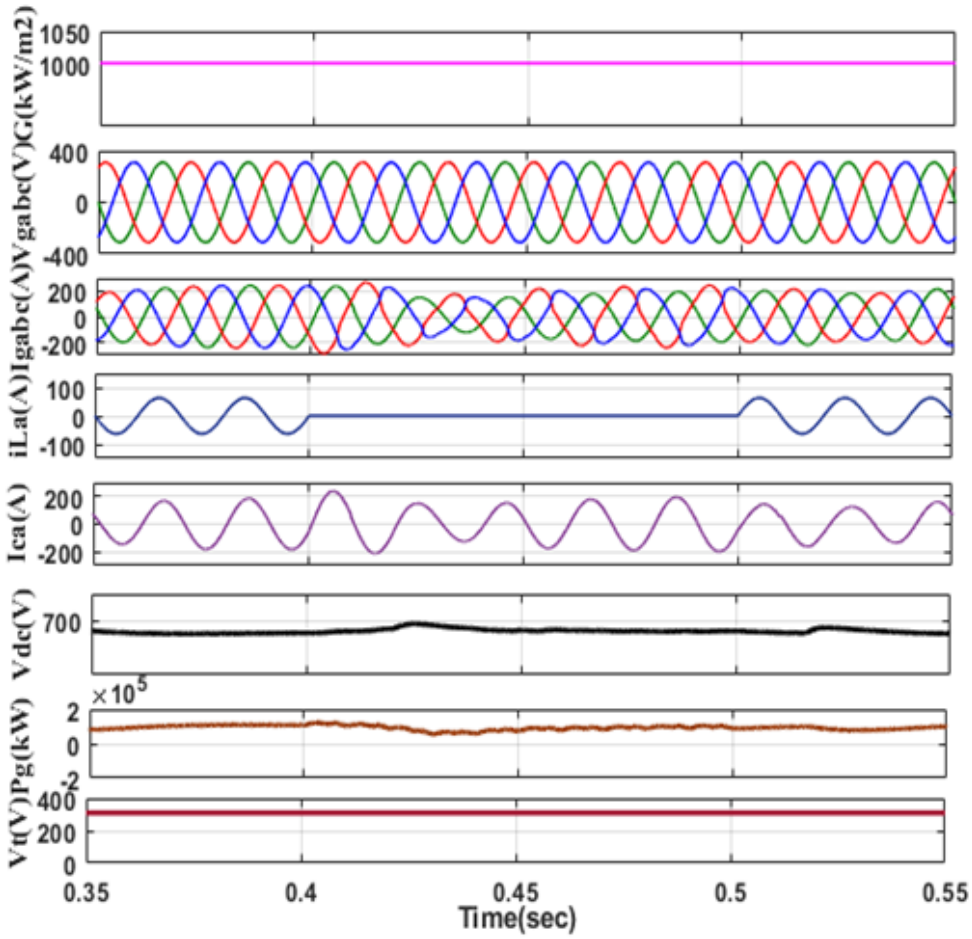


(a)

Fig. 5.7 (a) presents the behavior of Solar PV systems for intentional load unbalancing of one phase under load non-linear load conditions. It shows the waveform of G, Vgabc, Igabc, iLa, Ica, Vdc, Pg, and Vt. In this case, assume that the solar array constantly operates at 1000 W/m2 irradiance but, phase 'a' intentionally removed at (t= 0.4 - 0.5s). The grid currents are observed perfectly sinusoidal in both steady-state conditions (before t=0.4s and after t=0.5s), as well as in unbalanced conditions at (t= 0.4-0.5s). During the unbalancing period, the active power demand and load balancing criterion are fulfilled by the Solar PV generating system. However, with this

unbalancing condition, the DC link voltage of VSC is maintained constant with small oscillations.

Fig. 5.7 (b) presents the behavior of solar PV systems under varying system frequencies 49.5 Hz to 50.5 Hz. Fig. 5.7 (b) depicts the waveform of Vgabc, Igabc, iLa, Ica, Ipvq, Vdc and wr. With the system frequency variation, it is observed that the grid current and voltage are perfectly sinusoidal. The DC link voltage is approximately constant to its reference value.

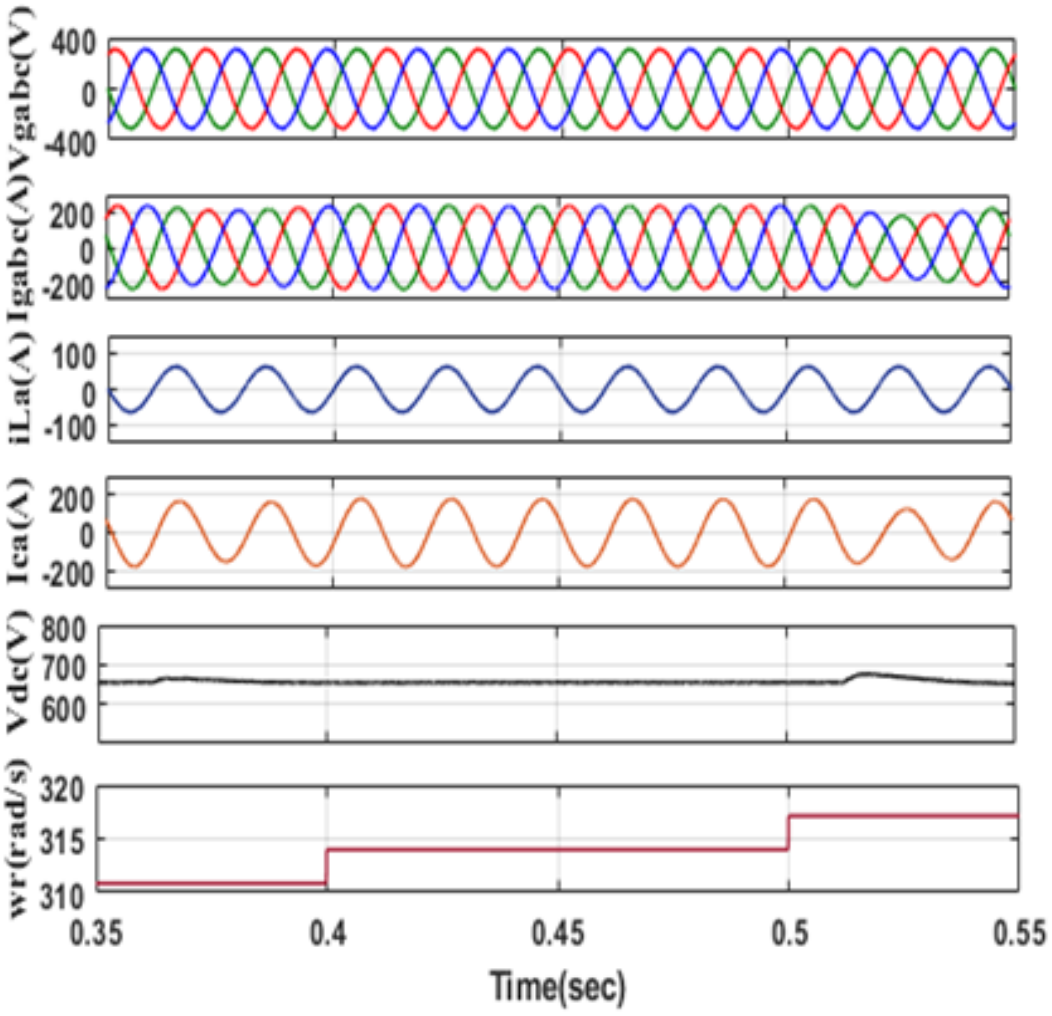


(b)

Fig. 5.7 (a) : Behavior of system under load unbalancing, (b) system under variable frequency

## 5.4 CONCLUSIONS

A three-phase grid-interfaced solar photovoltaic system (SPV) has been implemented and controlled by using SOGI-FLL-based adaptive control scheme. This scheme has been effectively used to extract reference currents and provide gating pulses for VSC. The performance of the control scheme for SPV system has been found satisfactory under linear and nonlinear loads as well as in load unbalancing conditions under varying system frequency. The proposed system along with ANN-based adaptive control scheme has shown better performance in power quality enhancement. The effectiveness of the feed-forward component has been presented for dynamic performance improvement. ANN controller is incorporated accurately with an adaptive control scheme for converter loss component estimation. The THD has been reduced much better using ANN controller ensuring good operation of the shunt active power filter thus resulting in improved power quality. The proposed system was simulated using Matlab/Simulink software and the results demonstrate the harmonic free source current.

# Chapter 6

# GRID INTERFACED SOLAR-WIND HYBRID POWER GENERATING SYSTEMS USING FUZZY-BASED TOGI CONTROL TECHNIQUE FOR POWER QUALITY IMPROVEMENT

## 6.0 GENERAL

This chapter presents the grid interfaced solar-wind hybrid renewable energy system, feeding three-phase loads. The proposed system includes solar photovoltaic, permanent magnet synchronous generator (PMSG), DC-DC boost converter, incremental conductance based maximum power point tracker (MPPT), three phases IGBT based voltage source converter (VSC), with a third order generalized integrator (TOGI) control technique. This control technique bestows multifunctional capabilities such as harmonic mitigations, load balancing, and reactive power compensation. A fundamental component of load current is extracted by TOGI based controller, and further it is utilized to generate the switching pulses to VSC for power quality enrichment. The fuzzy logic based controller is used for loss computation of VSC as well as for maintaining DC link voltage. Moreover, fuzzy logic provides better dynamic performance compared to conventional PI controllers. The results are presented in many aspects for linear and nonlinear loads such as, the intermittent nature of solar and wind as well as disturbances in the system. A comparative analysis between proposed TOGI based controller and conventional control algorithm has been presented. Test results are performed with the help of MATLAB/ Simulink environment and demonstrate, grid current is maintained well within the IEEE-519 standard.

## 6.1 PROPOSED LAYOUTS

The proposed layout of the system is illustrated in Figure 6.1. The system comprises a solar photovoltaic array (SPV) system and wind as a hybrid renewable energy source. Table 6.1 presents the parameters of hybrid solar-wind system. The hybrid system interfaced with a 3-phase utility grid along-with linear and nonlinear load with series impedance $R_s$ and $L_s$ voltage source converter (VSC) is interfaced at the point of common coupling (PCC) through series interfacing inductors $L_f$ . Ripple filters are coupled at the PCC for removing switching ripples. The hybrid sources are coupled to the VSC at the DC side. Moreover, the output of SPV and wind system, by conversion of DC-AC and AC-DC/DC-AC is integrated on the AC side parallel to feed power to the grid as well as loads. The SPV system consists of a PV array, DC-DC boost converter, IGBTs based three-leg semiconductors device as VSC. Moreover, the wind energy system consists of a permanent magnet synchronous generator (PMSG), rectifiers, and DC-DC boost converters.

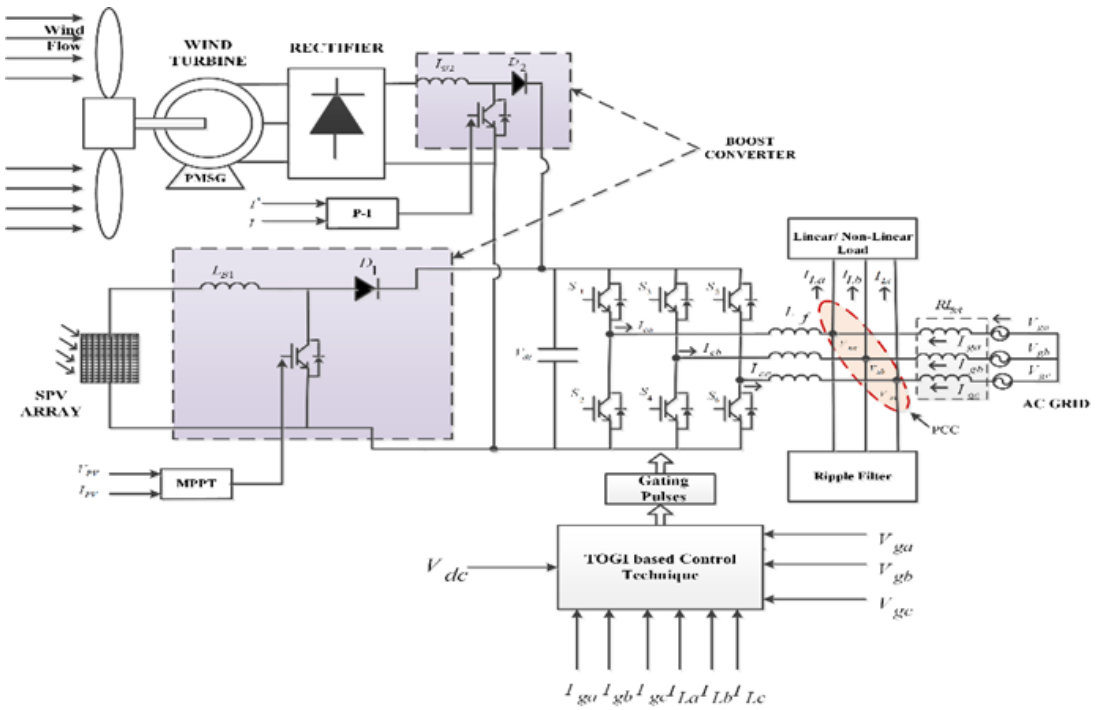


Fig. 6.1 : System Configuration

TABLE 6.1 : HYBRID SOLAR-WIND SYSTEM PARAMETERS

| **Parameter** | **Value** | **Parameter** | **Value** |
|---|---|---|---|
| SPV power | 100 kW | | |
| Voc | 64.2 V | Rated Power | 400 kW |
| Isc | 5.96 A | Rated speed | 1500 rpm |
| Vmp | 54.7 V | Permanent magnet flux linkages | 0.52Wb |
| Imp | 5.58 A | Stator phase resistance Rs | 0.01 ohm |
| IL | 6 A | Armature inductance | 7e-5 H |
| Io | $6.3014e^{-12}$ | | |
| Cells per module | 96 | | |
| Np | 66 | | |
| Ns | 5 | | |

### 6.1.1 Design of DC-DC Boost Converter

The value of inductor and generation of switching pulses govern the design of DC-DC boost converter. Fig. 6.1 shows $L_{B1}$ and $L_{B2}$ corresponds to boost converter inductance of solar and wind respectively. Furthermore, the value of inductance is selected based on the maximum allowed ripple current ( $\Delta i$ ), input voltage ( $V_{PV}$ ), and minimum duty ratio ( $\mathrm{d}_s$ ). The value of inductance ( $L_{B1}$ ) of SPV boost converter is mathematically calculated as:

$$L_{B1} = \frac{V_{PV}\,\mathrm{d}_s}{2\Delta i * f_s} \tag{6.1}$$

The duty ratio for SPV is calculated as,

$$d_s = 1 - \frac{V_{in}}{V_o} = 1 - \frac{270}{700} = 0.6 \tag{6.2}$$

Furthermore, generating a switching action has to be performed by comparing the reference duty ratio with the saw-tooth waveform. The reference duty ratio of solar boost converter ( $d_i$ ) is computed as,

Where, $f_s$ : switching frequency of SPV is 5kHz, $V_{in}$ : SPV output voltage is 270 V, $V_o$ : Boost converter output is 700 V

Similarly, the wind connected boost converter inductance

$$L_{B2} = \frac{V_W \, \mathrm{d}_w}{2\Delta i * f_w} \tag{6.3}$$

The duty ratio for wind is calculated as,

$$d_w = 1 - \frac{V_i}{V_{ow}} = 1 - \frac{540}{700} = 0.3 \tag{6.4}$$

Where, $f_w$ : switching frequency of wind is 5kHz, $V_i$ : wind output voltage is 540V, $V_{ow}$ : Boost converter voltage is 700V.

The ripple current ( $\Delta i$ ) for both SPV and wind is taken as 10% of the input current. Finally, by putting all these parameters boost converter inductance is

$$d_i = 1 - \frac{V_{ref\,(i)}}{V_{dc(i)}} \tag{6.5}$$

The converter finally converters the wind and SPV voltage to a fixed DC voltage for regulating the output voltage.

## 6.2 TOGI CONTROL TECHNIQUE

The proposed TOGI based control algorithm is shown in Fig. 6.2. The objective of the control algorithm is to generate switching pulses for the VSC. The feed-forward loop is utilized for the reference current generation ($I_f$), this will be utilized for improving dynamic response. Moreover, solar photovoltaic power ($P_{pv}$) and the terminal voltages ($V_t$) are used for the estimation of the reference current. The feed-forward component of PV, loss components of current (Iploss), quadrature phase unit template ($U_{qa}, U_{qb}, U_{qc}$), and the in-phase unit template signals. ($U_{pa}, U_{pb}, U_{pc}$) are utilized for the VSC switching algorithm.

### 6.2.1 Generation of Reference Grid Current

Fig. 6.3 presents the building blocks TOGI controller. The magnitude of terminal voltage ( $V_t$ ) at point of common intersection (PCI) is determined using phase voltages ( $V_{sa}, V_{sb,} V_{sc}$ ). Moreover, line voltages ( $V_{sab}, V_{sbc,} V_{sca}$ ) are sensed to determine the phase voltages. So, the terminal voltage is calculated as,

$$V_t = \sqrt{\frac{2}{3} * (V_{sa}^2 + V_{sb}^2 + V_{sc}^2)} \tag{6.6}$$

The in-phase ( $U_{pa,} U_{pb,} U_{pc}$ ) and quadrature-phase ( $U_{qa,} U_{qb,} U_{qc}$ ) unit templates are calculated as,

$$U_{pa} = \frac{V_{sa}}{V_t}, U_{pb} = \frac{V_{sb}}{V_t} \& U_{pc} = \frac{V_{sc}}{V_t} \tag{6.7}$$

$$U_{qa} = \frac{1}{\sqrt{3}} * \left[ U_{pc} - U_{pb} \right], U_{qb} = \frac{1}{\sqrt{3}} * \left[ U_{pa} - U_{pc} \right],$$
$$\& \quad U_{qc} = \frac{1}{\sqrt{3}} * \left[ U_{pb} - U_{pc} \right] \tag{6.8}$$

Furthermore, fundamental load current ( $I_{LFA}$ ) is extracted from the TOGI control algorithm presented in the next section.

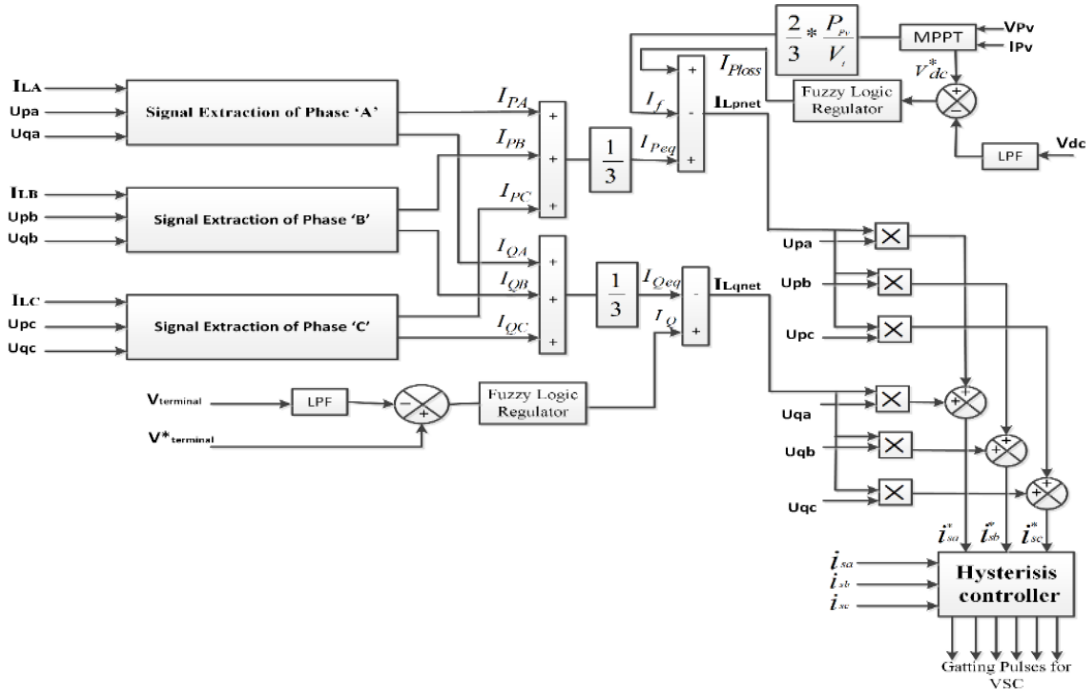


Fig. 6.2 : Reference current extraction by TOGI control algorithm

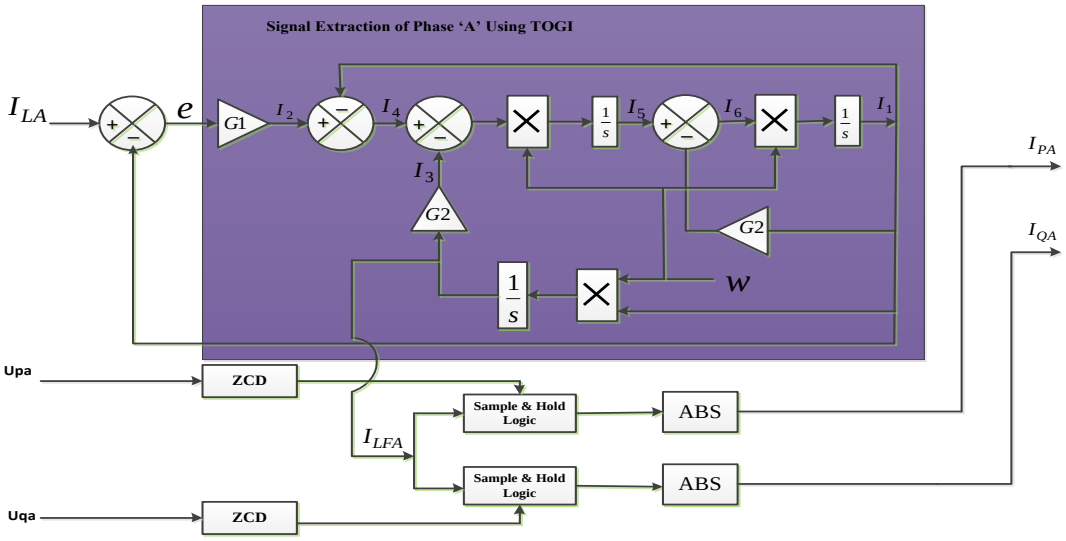


Fig. 6.3 : Block diagram of TOGI control algorithm

Now, equivalent components of active current ($I_{Peq}$) and reactive current ($I_{Qeq}$) components are calculated by the addition of active component and the reactive current component of all phases divided by three. Hence, equivalent components of currents are represented as,

$$I_{Peq} = \frac{I_{PA} + I_{PB} + I_{PC}}{3} \tag{6.9}$$

$$I_{Qeq} = \frac{I_{QA} + I_{QB} + I_{QC}}{3} \tag{6.10}$$

Fig. 6.3 presents the basic blocks for the extraction of fundamental load current. Moreover, Eq. 6.23 shows extracted fundamental load current by solving a nonlinear control system, which is in the phase of the point of interconnection voltage. The point of interconnection voltage is to be determined by zero cross detector (ZCD) block, sample & hold logic (S&H), and absolute block are used to determination of fundamental active and reactive current components ( $I_{PA}$ & $I_{QA}$ ) computations for phase 'a' as shown in Fig. 6.3. Similarly, for phase 'b' ( $I_{PB}$ & $I_{QB}$ ) and phase 'c' ( $I_{PC}$ & $I_{QC}$ ) are computed.

The loss components of current ( $I_{Ploss}$ ), are evaluated by a fuzzy logic regulator. Table 6.3, shows a 7*7 (49) rule base fuzzy logic control system. For the implementation of the control technique DC link capacitor voltage ($V_{dc}$) is compared with the reference value of capacitor voltage ($V_{dc}^{*}$).

TABLE 6.2 : FUZZY CONTROL RULE

| *e(n)/ce(n)* | *NB* | *NM* | *NS* | *ZE* | *PS* | *PM* | *PB* |
|---|---|---|---|---|---|---|---|
| *NB* | NB | NB | NB | NB | NM | NS | ZE |
| *NM* | NB | NB | NB | NM | NS | ZE | PS |
| *NS* | NB | NB | NM | NS | ZE | PS | PM |
| *ZE* | NB | NM | NS | ZE | PS | PM | PB |
| *PS* | NM | NS | ZE | PS | PM | PB | PB |
| *PM* | NS | ZE | PS | PM | PB | PB | PB |
| *PB* | ZE | PS | PM | PB | PB | PB | PB |

The error, $\mu e$ (n) and change in error, $\Delta\mu e$ (n) are inputs for the fuzzy processing. Fig. 6.4 (a)-(c) presented the fuzzy logic membership functions of $\mu e$ (n), $\Delta\mu e$ (n) and Vdc(n). The seven linguistic variables such as Negative High (NH), Negative Medium (NM), Negative Small (NS), Zero (ZE), Positive small (PS), Positive Medium (PM), Positive Big (PB) are used in the process of fuzzification.

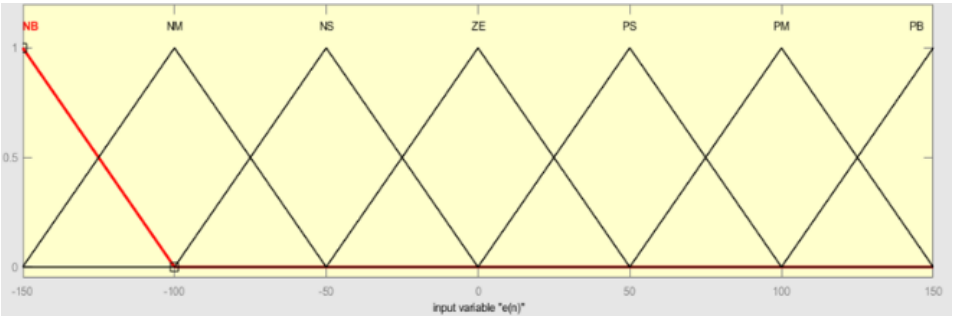


Fig. 6.4 (a) : Input membership function $\mu e$ (n)

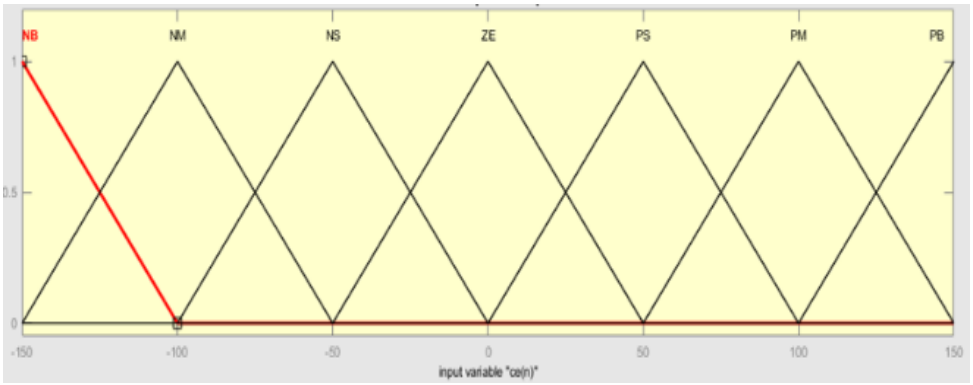


Fig. 6.4 (b) : Change in input membership function $\Delta\mu e$ (n)

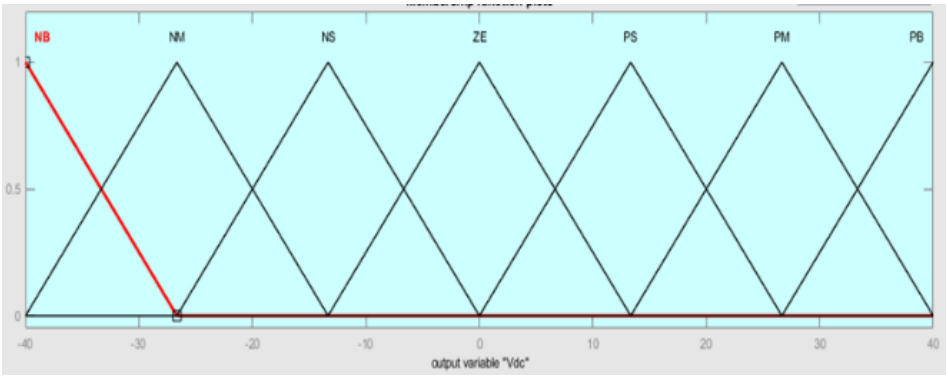


Fig. 6.4 (c) : Output membership function Vdc(n)

Fig. 6.4 (a)-(c) Membership function of input $\mu e$ (n), change in input $\Delta\mu e$ (n), output Vdc(n)

The different linguistic control rules consist of rule bases which are required by rule evaluator to compute loss computation. Fig. 6.5 (a)- 6.5 (b) depict the fuzzy rules for loss calculation of VSC and surface diagram of fuzzy function.

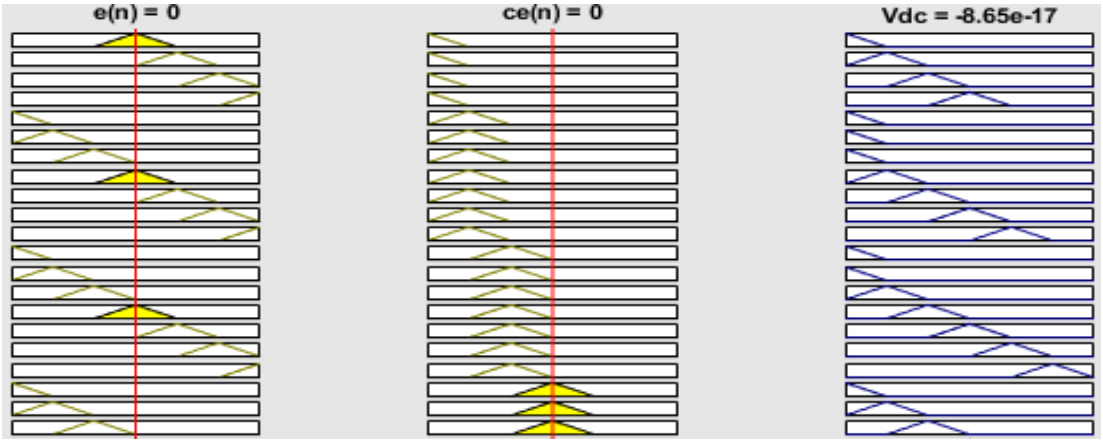


Fig. 6.5 (a) : Fuzzy logic rule function

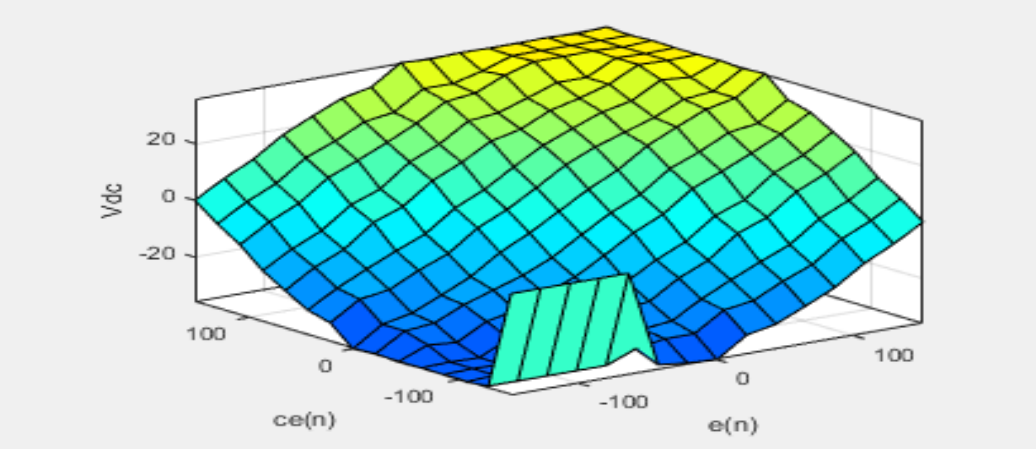


Fig. 6.5 (b) : Surface Diagram

Fig. 6.5 (a), (b) : Fuzzy logic rule and surface diagram

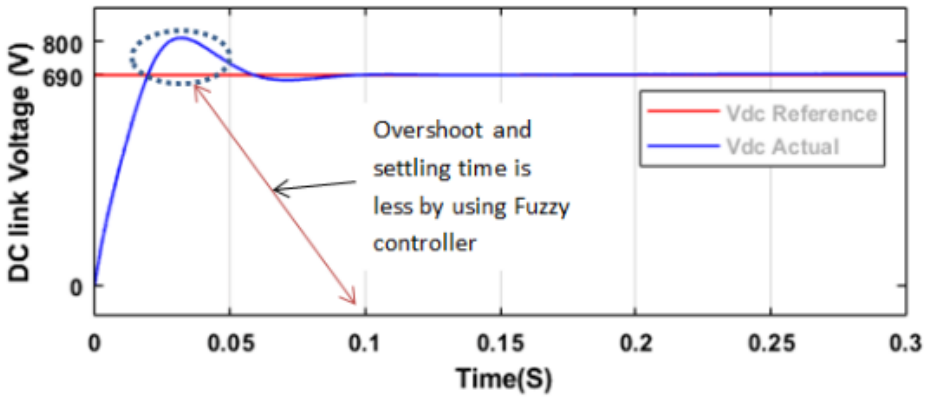


Fig. 6.6 (a) : DC link voltage estimation by Fuzzy controller

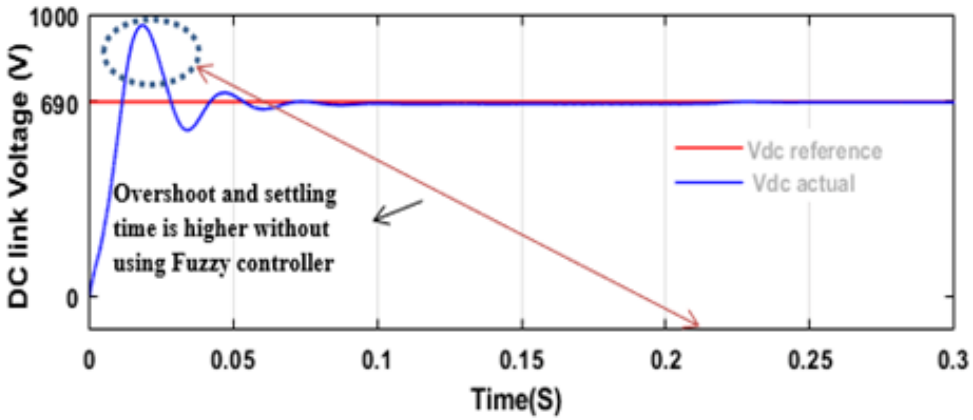


Fig. 6.6 (b) : DC link voltage estimation by PI Controller

Fig. 6.6 (a)- (b) : DC link voltage estimation by Fuzzy controller and conventional PI Controller

Figs. 6.6 (a) – 6.6 (b) presents the DC link voltage estimation by fuzzy logic and conventional PI controller. Moreover, Table 6.3 presents the comparative analysis showing that fuzzy logic-based TOGI outperforms then PI based controller.

TABLE 6.3 : COMPARATIVE ANALYSIS BETWEEN FUZZY LOGIC AND CONVENTIONAL CONTROLLER

| **Controller** | **Maximum Overshoot** | **Settling Time** | **DC Link Actual Voltage** |
|---|---|---|---|
| Fuzzy Logic | Lower | Less (0.11sec) | Less Oscillation |
| PI | Higher | Higher (0.23sec) | High Oscillation |

The additional PV feed-forwarding compensation ( $I_f$ ) is utilized for the minimization of % overshoot in the DC link bus voltage and disturbances in the AC side grid current as,

Feed-forward current $I_{fe} = \frac{2}{3} * \left[ \frac{P_{pv}}{V_{te}} \right]$ (6.11)

So, the net active current component ( $I_{Lpnet}$ ) is calculated as,

$$I_{Lpnet} = I_{Peq} - I_{fe} + I_{Ploss} \quad (6.12)$$

Similarly, the net reactive current component ( $I_{Lqnet}$ ) is calculated as,

$$I_{Lqnet} = I_{Qeq} - I_Q \quad (6.13)$$

Where, $I_Q$ the loss component of the DC link voltage is evaluated again with the rule base fuzzy logic regulator as same $I_{ploss}$ estimation.

The reference grid currents ( $i_{sa}^*, i_{sb}^*, i_{sc}^*$ ) is determined by net active and reactive power component with the active and reactive unit templates and add them together to generate reference grid currents as,

$$\begin{aligned} i_{sa}^* &= I_{Lpnet} * W_{pa} + I_{Lqnet} * W_{qa} \\ i_{sb}^* &= I_{Lpnet} * W_{pb} + I_{Lqnet} * W_{qb} \\ i_{sc}^* &= I_{Lpnet} * W_{pc} + I_{Lqnet} * W_{qc} \end{aligned} \quad (6.14)$$

Furthermore, these reference grid currents are compared with the grid currents ( $i_{ga}, i_{gb}, i_{gc}$ ) by using hysteresis current controllers. A not gate is used to convert these three-reference grid current to six gating pulses to control the grid-tied IGBT's based VSC.

## 6.3 FUNDAMENTAL LOAD CURRENT EXTRACTION

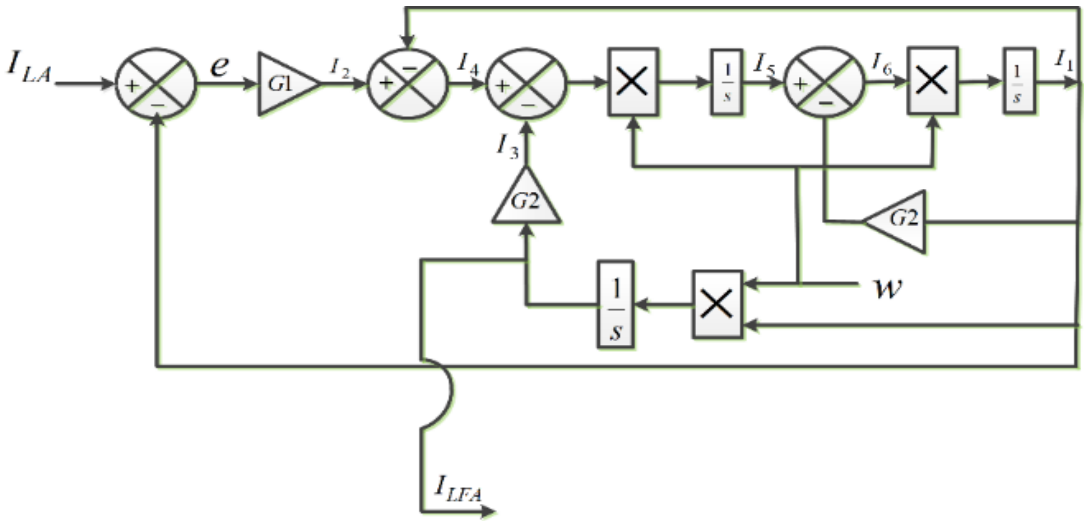


Fig. 6.7 : Fundamental load current extraction from TOGI control strategy

Therefore, for the realization of TOGI control technique the analysis of extracted fundamental load current ($I_{LFA}$), need to be expressed properly. The parameters (G1&G2), of control strategy, are properly tuned for better dynamic capability and good filtering ability. Moreover, extracted fundamental load current ($I_{LFA}$), are is in phase with the point of interconnection (PIC) voltage.

### 6.3.1 Comparative Performance Analysis of Proposed TOGI with Conventional Algorithms

This section provides a detailed comparative analysis of the Proposed TOGI control technique along-with conventional control technique. Fig. 6.8 presents the frequency domain analysis between generalized integrator (GI), SOGI and TOGI control algorithm. It is clearly illustrated that proposed TOGI controller having better filtering capability of both lower and higher order harmonics and DC offset rejection capability then conventional controllers.

Figs. 6.9 (a) - 6.9 (c) presents the proposed technique as having better dynamic performance and lower harmonic distortions. THDs of grid current of all techniques are tabulated in Table 6.3.

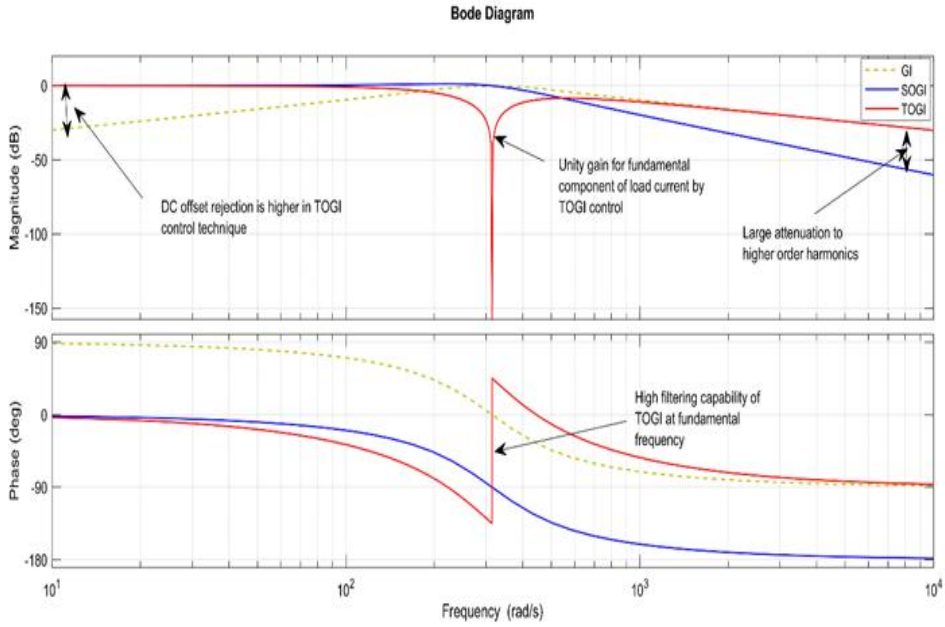


Fig. 6.8 : Frequency response analysis between TOGI and various conventional algorithms

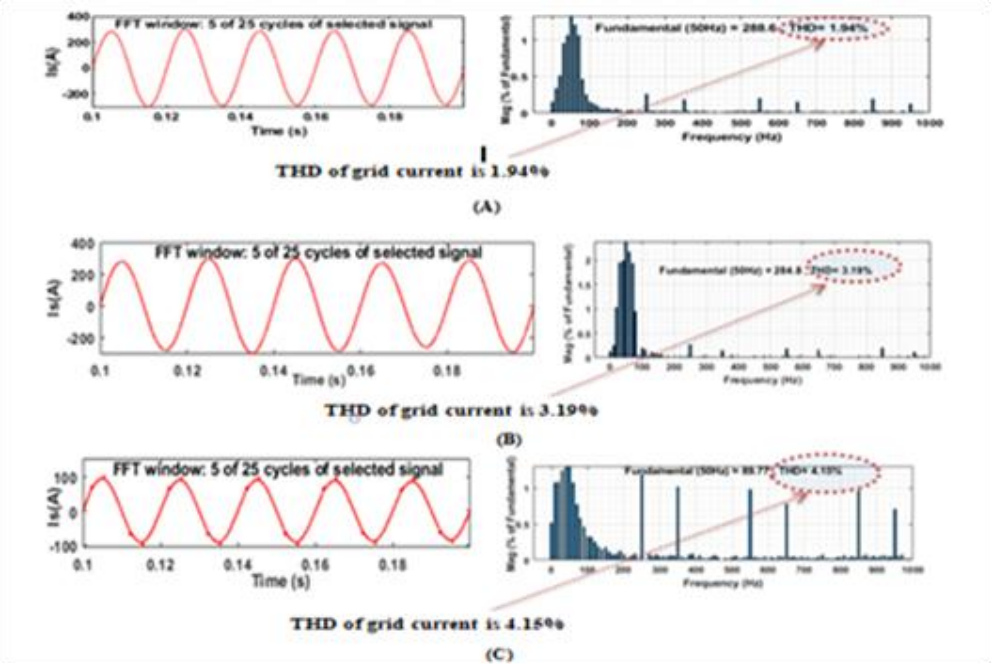


Fig. 6.9 (a)-(c) : THD of grid current by Proposed TOGI, DSOGI and SOGI controller

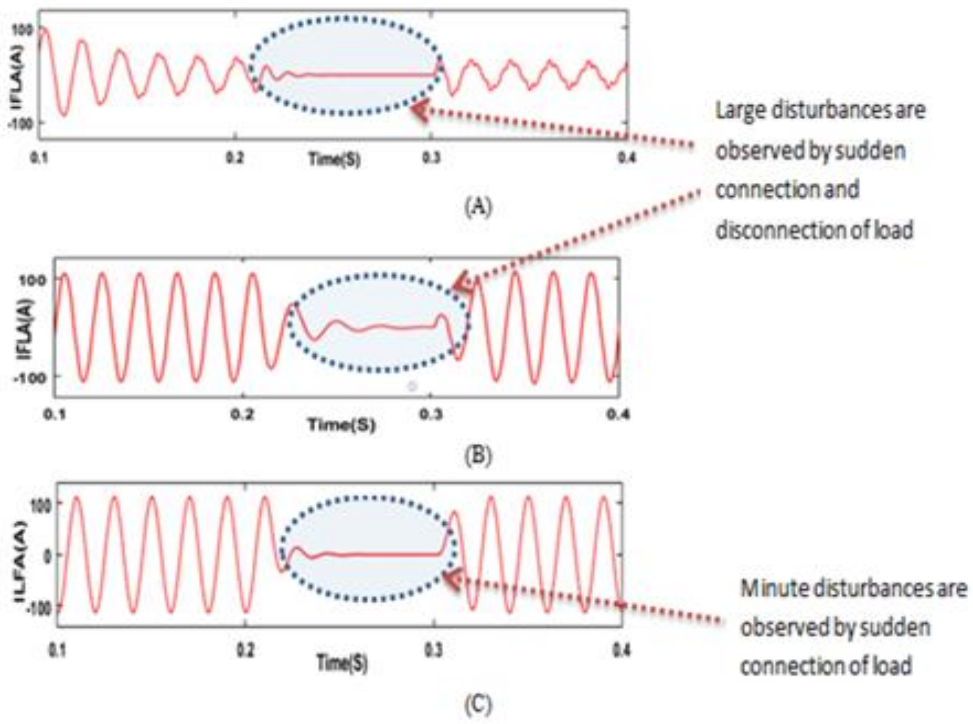


Fig. 6.10 : Sudden connections and disconnection of load (a) SOGI (b) DSOGI (c) TOGI

TABLE 6. 4 : COMPARATIVE ANALYSIS BETWEEN THE PROPOSED TOGI TECHNIQUE WITH CONVENTIONAL CONTROLLERS

| **Controllers** | **FC of load current** | **DC offset** | **Dynamic behaviour** | **Order of harmonic** | **Grid Current THD** | **Complexity** |
|---|---|---|---|---|---|---|
| TOGI | High | Eliminated | Best | Higher | 1.94% | Medium |
| DSOGI | Average | Present | Better | Lower | 3.19% | Medium |
| SOGI | Low | Present | Good | Lower | 4.15% | Low |

## 6.4 RESULTS AND DISCUSSION

A detailed simulation of the proposed TOGI based control algorithm is carried out to illustrate the behavior of the system using Matlab/Simulink environment. The results include a solar-wind hybrid system operating at various operating scenarios such as solar irradiance, temperature, wind speed, and varying load conditions. The purpose of the proposed hybrid system is apart from feeding power to the grid only but it also aids in power quality improvement in distribution systems. To bestow these features

Fig. 6.10 presents the sudden connection and disconnection of load, SOGI and DSOGI possesses a large transition whereas, TOGI has a smooth transition of PQ improvement, both linear as well nonlinear loads are considered and it is connected to the AC grid.

The comprehensive data for modelling hybrid systems is provided in the appendix. Results illustrate the operation under varying operating conditions as shown in Figs. 6.11- 6.14.

### 6.4.1 Performance Solar-Wind Hybrid System for Linear Load

Fig. 6.11 depicts the dynamic behaviour execution of the solar-wind hybrid system in power factor correction with the linear load connected to AC grid. The results include waveforms of grid voltage (Vsabc), grid current (Ig), DC bus voltage, load currents, as well as compensating currents are shown in the Fig. 6.11. The Grid voltages (Vsabc) at the point of common point of three phases i.e phase ‘a’, ‘b’, ‘c’, and AC side grid current (Ig). Moreover, phase ‘a’, ‘b’ and ‘c’ are represented by red, black, and blue colors respectively. At steady state before (t=0.4s) at fixed wind speed (12 km/s) and solar irradiance of (1000 w/$m^2$), temperature ($25^0$c), grid current is balanced and DC link voltage is constant to its desired value of 690V. As other parameters are kept constant and solar irradiance is reduced to 600 w/$m^2$ at (t=0.4 s), therefore, power generation from solar PV systems gets reduced from 100 kW to 60 kW. Therefore, the remaining power is supplied by the wind energy and by AC grid, and DC link voltage is maintained to its desired value with very minute fluctuations. Moreover, due to the sudden disturbance of one-phase ‘a’ is disconnected at (t=0.6s to t=0.7s).

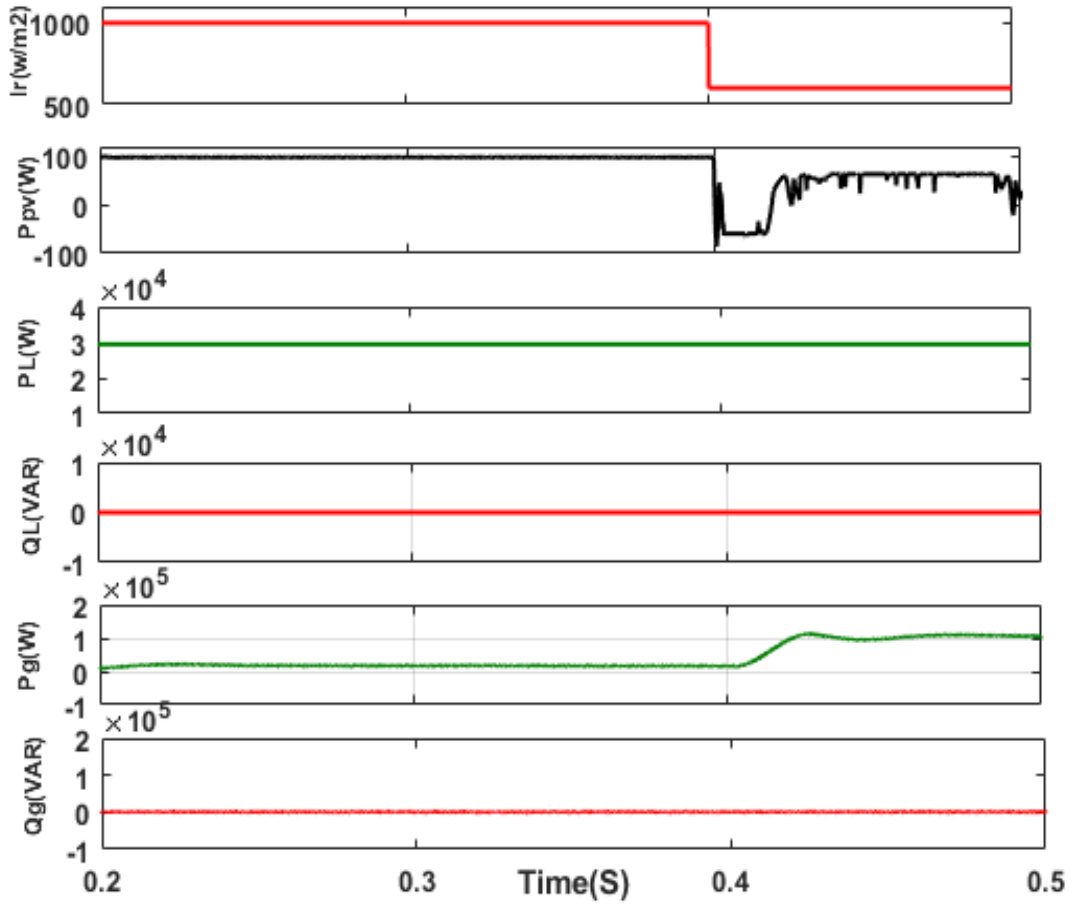


Fig. 6.11 : Performance of hybrid Solar-Wind system under linear load

During this disturbance period, it is noticed that converter currents are unbalanced to produce grid currents balanced and sinusoidal. The load unbalancing during this duration and shortage of power demand of load can be fulfilled by combined solar-wind sources. Moreover, after t=0.7s, phase ‘a’ of the load is connected and DC link voltage is settled within a cycle.

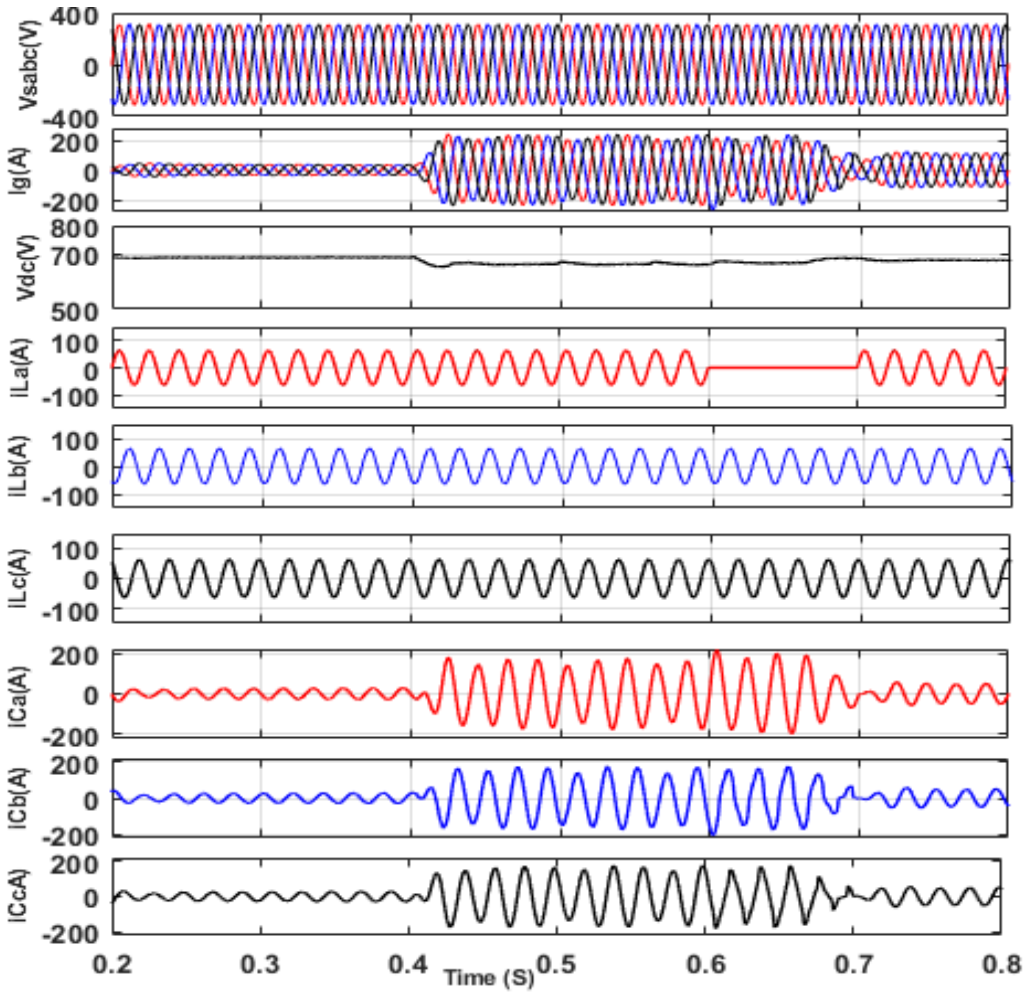


Fig. 6.12 : Performance of hybrid Solar-Wind system in PFC mode under linear load

Fig. 6.12. depicts that SPV system where net power is decreased after at time=0.4s, to 60%, owing to reduction in irradiance intensity from 1000 W/m$^2$ to 600 W/m$^2$. Hence, because of the variation of irradiance, remaining active power of load is catered by the AC grid and therefore, there is a very minute burden of reactive power is observed on the AC grid.

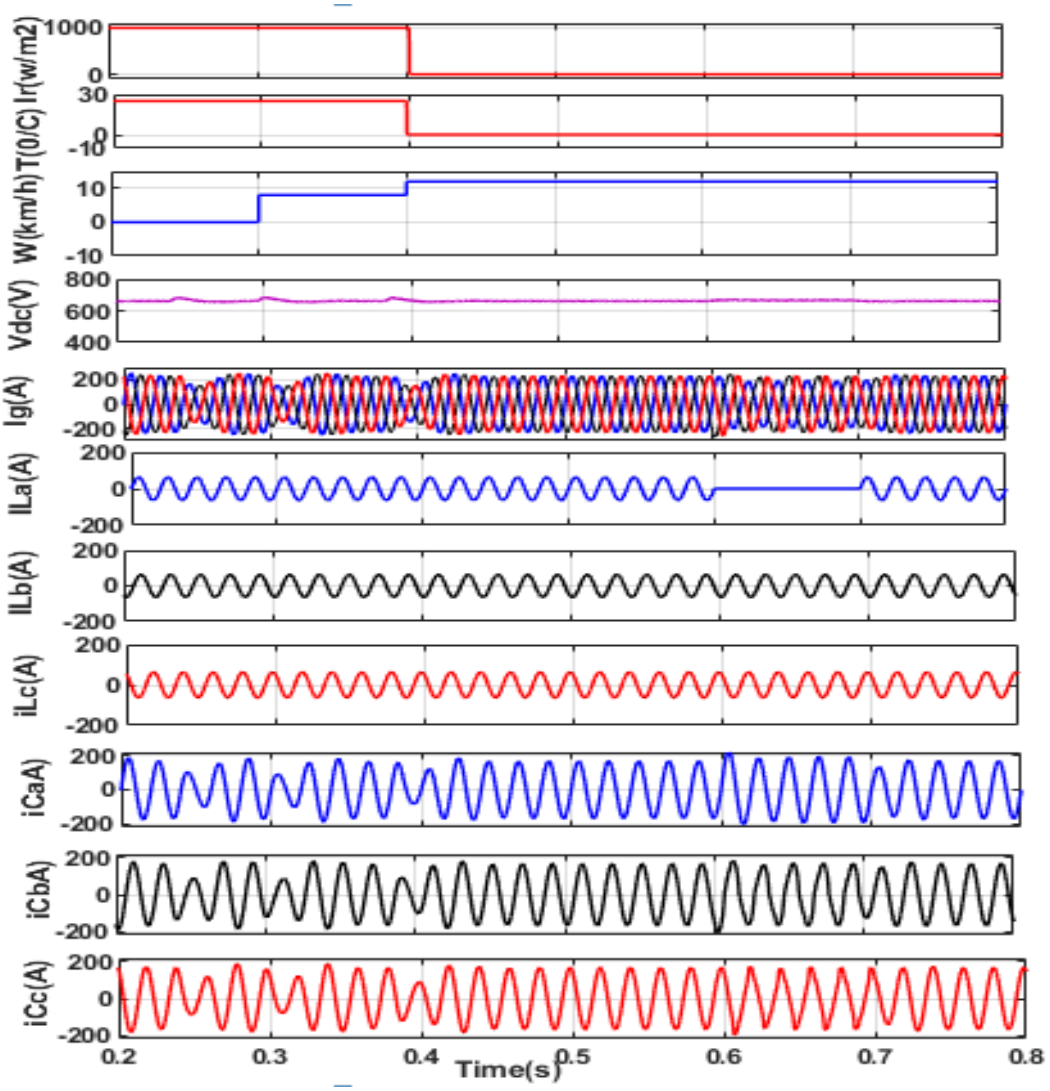


Fig. 6.13 : Performance of hybrid Solar-Wind system in PFC mode under liner load

Fig. 6.13. depicts the case when time=0.4sec, solar irradiance, and temperature of the solar photovoltaic system are suddenly reduced to zero. That means, there is no effect of solar PV generating systems only wind energy systems will play as a source of power generation. Moreover, wind speed is taken as a variable nature for the sake of simulation study, its speed is 8 km/s between time=0.2sec-0.4sec, and 12km/s after time=0.4sec, as depicted in Fig. 6.13. In view of such intermittency of solar and wind systems, the AC side grid-current is perfectly balanced and sinusoidal in nature also, DC link voltage is sustaining to its desired value with very slight oscillations is

observed in Fig. 6.13. Furthermore, an unbalancing is introduced in the simulation between time=0.6sec- 0.7sec. Along with this, when phase ‘a’ is detach at t=0.6 sec-0.7sec. During this disturbance period, it is noticed that converter currents are unbalanced to produce grid currents balanced and sinusoidal. Furthermore, the active power demand and balancing of load are gratified by the wind energy system and by the AC grid.

### 6.4.2 Performance of Solar-Wind Hybrid System For Nonlinear Load

Fig. 6.14 depicts the dynamic behaviour execution of the solar-wind hybrid system in power factor correction (PFC) mode with the nonlinear load interfaced to the grid. At steady state before time=0.4sec at fixed wind speed (12 km/s) and solar irradiance of (1000 W/$m^2$), temperature ($25^0$ C), grid current is balanced and DC bus voltage is maintained constant to its desired value of 690V.

As other parameters are kept constant and solar irradiance is reduced to 600 W/$m^2$ at time=0.4sec, which consequences power generation from solar PV systems gets reduced from 100 kW to 60 kW around. Therefore, the remaining power is supplied by the wind energy and AC grid, and DC link voltage is maintained to its reference value with very minute fluctuations. Moreover, a sudden disturbance scenario is introduced when phase ‘a’ is removed time=0.6 sec -t=0.7sec. During this period, it is observed that converter currents are unbalanced to produce AC-side grid currents balanced and sinusoidal. The load unbalancing during this duration and shortage of power demand of load can be fulfilled by combined solar-wind sources. Moreover, after time=0.7sec, phase ‘a’ of the load is connected and dc-link voltage is settled within a cycle. Harmonic analysis has been done for THD calculation for nonlinear load and waveforms are depicted in Table 6.4.

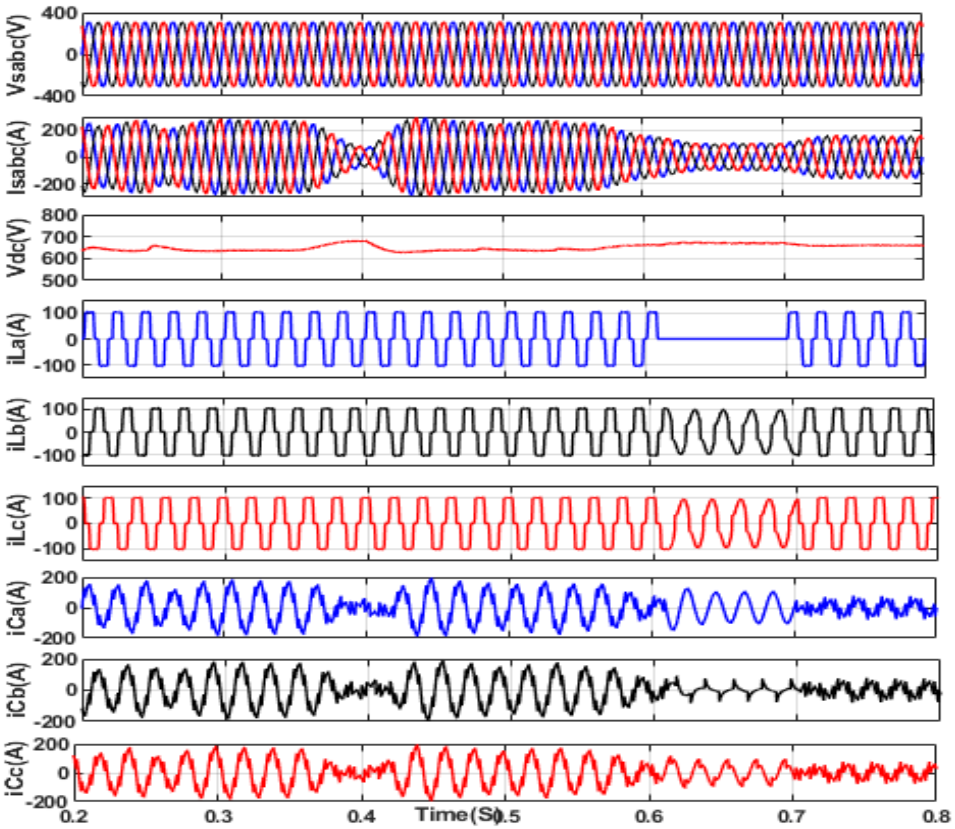


Fig. 6.14 : Performance of hybrid Solar-Wind system in PFC mode under nonlinear load

### 6.5 Conclusion

The TOGI based fuzzy logic control technique has been designed for three phase grids interfaced solar-wind hybrid system. A TOGI control scheme has been presented for reference currents generation and providing pulses for 3-phase VSC. The FLC demonstrates more dynamic performance than the conventional PI controller. The proposed system with TOGI controller is verified satisfactorily for multifunctional objectives such as power quality (PQ) enrichment, load balancing, reactive power compensation capability, etc. A brief comparative result has been presented of TOGI control scheme with conventional control schemes. The presented result shows that the designed controller is well executed irrespective of system intermittency, and load disturbances and it provides excellent harmonic filtering capability compared to conventional controllers.

# Chapter 7

# ADAPTIVE FOURTH-ORDER BASED CONTROLLER FOR GRID-INTERFACED THREE-PHASE SOLAR PV SYSTEM FOR POWER QUALITY ENRICHMENT

## 7.0 GENERAL

An adaptive fourth-order based frequency locked loop (AFOGI-FLL) controller is proposed to provide switching pulses for a three-phase IGBT-based voltage source converter. Accurate frequency synchronization, lower and higher-order harmonic elimination, power quality refinement, and reactive power compensation are some of the features of the presented controller. As a renewable energy solution to meet energy demands, grid-interfaced photovoltaic systems are described in this paper. In addition, a comparative analysis has been performed between the proposed controller and the third-order generalized integrator (TOGI). The comparative analysis results show that fourth-order generalized integrator have higher DC offset elimination capability, and better dynamic performance as well and THD is less compared with the TOGI controllers. The THD of the proposed controller is 1.10% which is less than the IEEE standard. Moreover, the fundamental current extraction from the fourth-order generalized integrator is described mathematically in detail for better understanding. Maximum Solar PV system extraction is achieved using the updated perturb and observed method. The proposed controller robustness is validated by an experimental prototype setup and test results exhibit the performances under nonlinear loading. Additionally, the feasibility of the proposed control scheme is demonstrated by using MATLAB/SIMULINK software. The system is robust. The system is well executed

under irradiance variations, load fluctuations, and frequency variations as well. The laboratory prototype is used to demonstrate the proposed system's simulated behaviour and experimental test results.

## 7.1 PROPOSED LAYOUTS

Fig. 7.1 shows the suggested setup for the machine. Photovoltaic solar panels are part of the system as a sustainable energy source for changing energy. The SPV system is connected to a three-phase grid and a non-linear load via series resistance (Rs) and inductance (Ls). At the point of common crossing (PCI), the voltage source converter (VSC) and the ripple filters are connected. The ripple filters eliminate switching pulses when the VSC supplies power to the distribution system. Through the DC bus, the solar PV system is linked to VSC. The SPV system has a 32 kW SPV array, a boost converter, an MPPT unit to get the most power from the array, and a 3-leg VSC based on IGBTs for converting power. The MPO-based control method is used to keep track of the highest power level from different amounts of sunlight. Fig. 7.2 also shows the process of MPO-based MPPT.

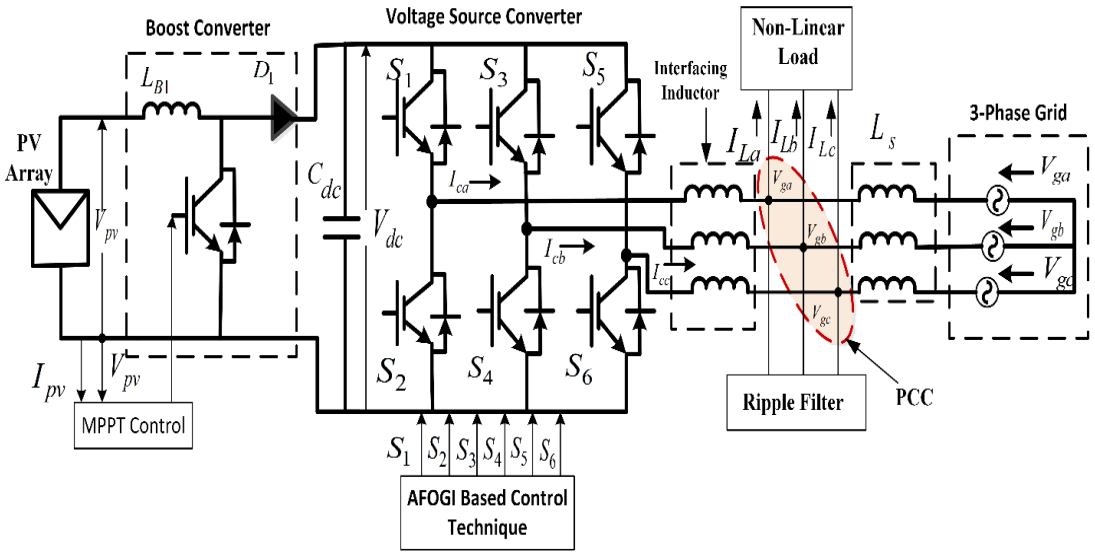


Fig. 7.1 : System Configuration

## 7.2 VSC SWITCHING

The role of grid interfaced VSC is for multi-objective functions such as THD reduction, compensation of reactive power, PFC, DC link voltage stabilization, etc. All the above objectives can be fulfilled by an accurate getting switching pulse for VSC by an AFOGI-FLL-based controller. The extracted fundamental component of load currents, feed-forward compensation term ($I_{ff}$), terminal voltage ($V_{ter\,min\,al}$), loss component of current ($I_{Ploss}$), quadrature unit templates ($T_{qa,}T_{qb,}T_{qc}$), and the in-phase unit templates signals ($T_{pa,}T_{pb,}T_{pc}$) are utilized for the generation of grid reference currents ($I_{sa}^{*}, I_{sb}^{*}, I_{sc}^{*}$) to VSC.

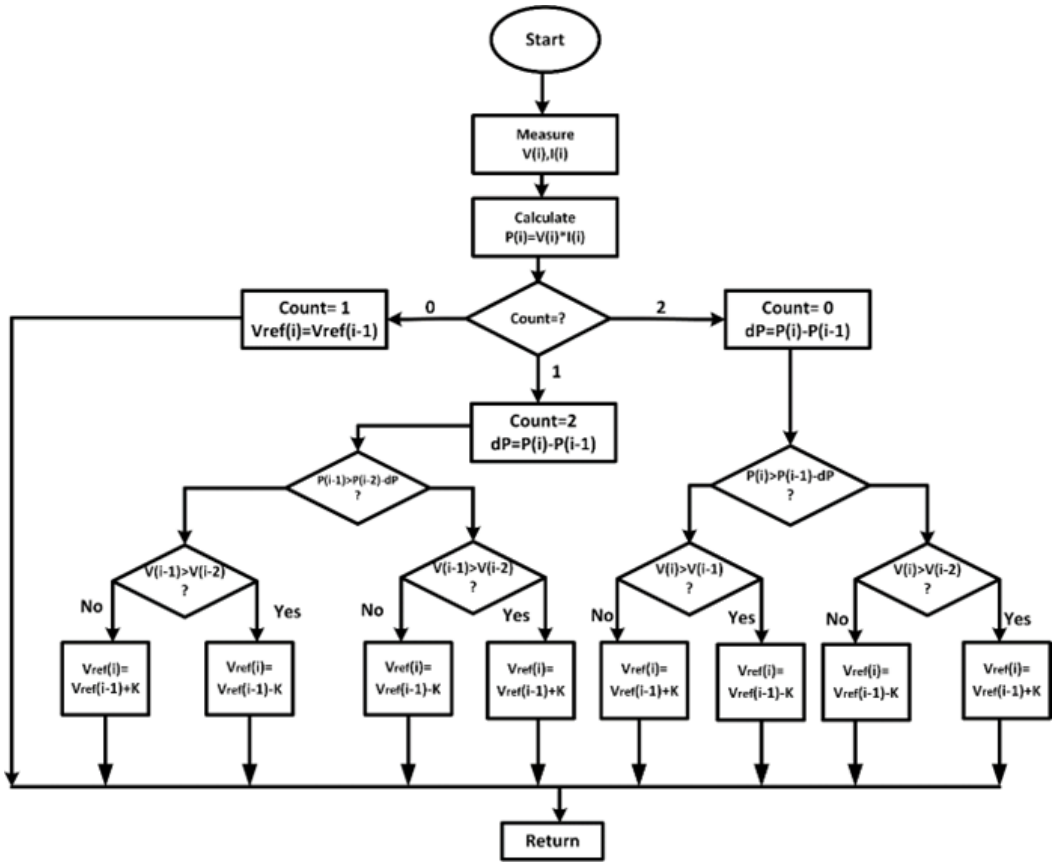


Fig. 7.2 : Flow chart of MPO control technique

### 7.2.1 In-Phase and Quadrature-Phase Unit Template Estimation

The terminal voltage ($V_t$) magnitude at PCI is determined using the sensed line voltages ($V_{sa}, V_{sb,} V_{sc}$) as,

$$\begin{bmatrix} V_{sa} \\ V_{sb} \\ V_{sc} \end{bmatrix} = \frac{1}{3}\begin{bmatrix} 21 \\ -11 \\ -12 \end{bmatrix}\begin{bmatrix} V_{sa} \\ V_{sb} \end{bmatrix}$$

$$V_{tt} = \sqrt{\frac{2}{3} * (V_{sa}^2 + V_{sb}^2 + V_{sc}^2)} \tag{7.1}$$

However, phase voltage ($V_{sa}$,$V_{sb}$) is computed from the sensed line voltages. The in-phase ($T_{pa,}T_{pb,}T_{pc}$) and quadrature-phase ($T_{qa,}T_{qb,}T_{qc}$) unit templates are calculated as,

$$T_{pa} = \frac{V_{sa}}{V_{tt}}, T_{pb} = \frac{V_{sb}}{V_{tt}} \& T_{pc} = \frac{V_{sc}}{V_{tt}} \tag{7.2}$$

$$T_{qa} = \frac{1}{\sqrt{3}} * \left[U_{pc} - U_{pb}\right], T_{qb} = \frac{1}{\sqrt{3}} * \left[U_{pa} - U_{pc}\right],$$

$$T_{qc} = \frac{1}{\sqrt{3}} * \left[U_{pb} - U_{pc}\right] \tag{7.3}$$

### 7.2.2 The Fundamental Load (FL) Current Extraction by Adaptive FOGI-FLL Controller

The AFOGI-FLL is utilized to extract FL currents ($I_{LA,}I_{LB,}I_{LC}$), from all three phases. The proposed technique having excellent harmonics elimination capability and DC offset rejection capability than the conventional SOGI-FLL technique. The structured control system transfer function is represented in Eq.7.4 which is the ratio of the in-phase component of fundamental load current ($I_{LA1}$) for phase 'a' to the sensed load current ($I_{LA}$). An appropriate parameter selection procedure of the AFOGI-FLL algorithm is presented by the pole-zero plot and unit-step response analysis.

$$\frac{I_{LA1}(s)}{I_{LA}(s)} = \frac{G_1 G_2 w^2 s}{s^4 + G_2 w s^3 + (2 + G_1 G_2) w^2 s^2 + G_2 w^3 s + w^4} \tag{7.4}$$

Fig. 7.3 presents the kernel of FLL which is a phase detector (PD), the output of the phase detector is the product of error (e) with the quadrature-phase component of load current ($I_{LQ}$). The error (e) is the difference between load current ($I_L$) and the in-phase component (IPC) of load current ($I_{L1}$). The load current ($I_L$) consists of fundamental as well as odd harmonics which is mathematically represented as,

$$I_L = I_m \sin(w_k t + \theta_k) + f(3w_k, 5w_k \ldots\ldots) \tag{7.5}$$

Suppose, the IPC of load current ($I_{L1}$) = $I_m \sin(w_i t + \theta_i)$ and the quadrature-phase-component (QPC) of load current ($I_{LQ}$) =$I_m \cos(w_i t + \theta_i)$. The output of the phase detector ($PD_o$) is represented as,

$$PD_o = e \times I_{LQ} \tag{7.6}$$

$$PD_o = \frac{I_m^2}{2}\sin(w_k t + \theta_k - w_i t - \theta_i) + \frac{I_m^2}{2}\sin(w_k t + \theta_k + w_i t + \theta_i) + f(3w_k, 5w_k, 7w_k \ldots\ldots)$$

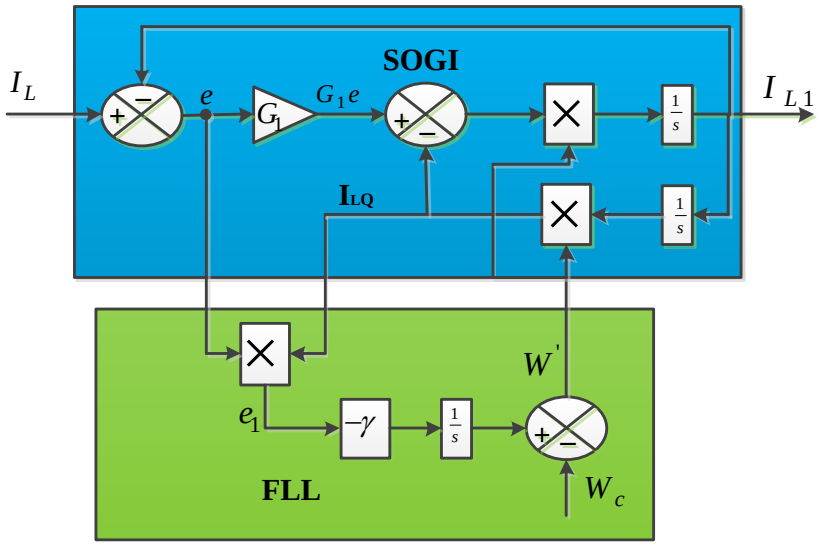


Fig. 7.3 : Basic Linear PLL

The PLL is assumed to be locked, in steady state condition, with this condition $w_k = w_i$and $\theta_k \approx \theta_i$ ,

So, the phase detector output can be approximated as,

$$PD_o = \frac{I_m^2}{2} sin(w_k t + \theta_k - w_i t - \theta_i) + \frac{I_m^2}{2} sin(w_k t + \theta_k + w_i t + \theta_i) +$$

$$f(3w_k, 5w_k, 7w_k \ldots\ldots \quad (7.7)$$

In steady-state condition, PLL is assumed to be locked, under this condition $w_k = w_i$and $\theta_k \approx \theta_i$, So, the output of the phase detector is approximated as,

$$PD_o \approx \frac{I_m^2}{2} sin(\theta_k - \theta_i) + \frac{I_m^2}{2} sin(2w_k t + 2\theta_k) + f(3w_k, 5w_k, 7w_k \ldots\ldots) \quad (7.8)$$

$$PD_o \approx (\theta_e) + f\, sin(2w_k t + 2\theta_k) + f(3w_k, 5w_k, 7w_k \ldots\ldots) \quad (7.9)$$

Where, $(\theta_k - \theta_i) \approx (\theta_e)$

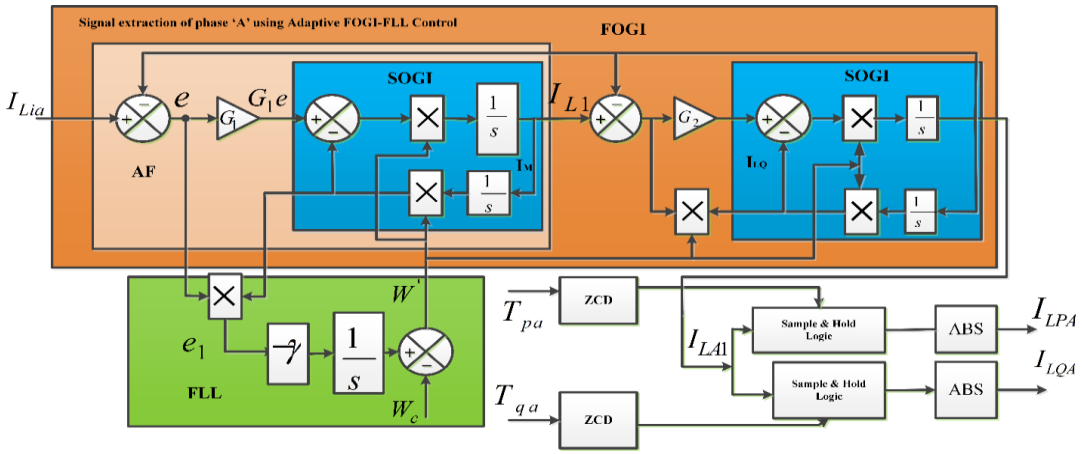


Fig. 7.4 : Block diagram of an AFOGI-FLL control algorithm

From Eq. 7.9 it is observed that in steady-state the output of phase detector (PD) contains phase error $(\theta_e)$ component as well as even and odd components of harmonics. Therefore, these generated harmonics will distort the output of PD. The proper tuning of phase error component $(\theta_e)$, as well as the calculation of generated harmonics are done by the loop filter (LF). The loop filter is a PI-based filter that is provided to minimize the current distortions generated in PD and it provides a tuned signal to VCO. The LP provides a good dynamic response so that it helps in the

extraction of the fundamental component of load currents. The AFOGI-FLL based controller is utilized for its accurate frequency estimation under variable system frequency variation as well as its lower and higher-order harmonics elimination capability. Two SOGI filters are connected in cascaded fashion as shown in Fig.7.4, FLL is used for grid synchronization and to construct the internal AFOGI filter structure. The control parameters of AFOGI-FLL are tuned for its better performance and good dynamic performance. The proposed AFOGI-FLL presents excellent characteristics of distortion current elimination and fundamental load current (FLC) extraction. The amplitude of fundamental in-phase currents ($I_{LPA,}I_{LPB,}I_{LPC}$) and quadrature-phase currents ($I_{LQA,}I_{LQB,}I_{LQC}$) are estimated by utilizing zero-cross detector, sample, and hold logic block.

### 7.2.3 Reference Grid Currents Generation

The Fig. 7.5, illustrates the reference current generation from the proposed controller. For the generation of reference grid currents ($I_{ga}^{*}, I_{gb}^{*}, I_{gc}^{*}$), firstly evaluate the net in-phase current component ($I_{Lpnet}$) and net quadrature-phase current component ($I_{Lqnet}$) is computed as,

$$I_{Lpnet}= I_{Peq} - I_{ff} + I_{Ploss} \tag{7.10}$$

$$I_{Lqnet} = I_{Qeq} - I_{Q} \tag{7.11}$$

Here, $I_{Peq}$ &$I_{Qeq}$is the equivalent component of in-phase and quadrature-phase current

$I_{ff}$ : feed-forward current compensation component

$I_{Ploss}$: Loss component of the current

$I_{Q}$ : Loss component of DC-link voltage

So, using this formula, we can determine the in-phase and quadrature-phase current's equivalent component.

$$I_{Peq} = \frac{I_{LPA}+I_{LPB}+I_{LPC}}{3} \tag{7.12}$$

$$I_{Qeq} = \frac{I_{LQA}+I_{LQB}+I_{LQC}}{3} \tag{7.13}$$

($I_{LPA,}I_{LPB,}I_{LPC}$) & ($I_{LQA,}I_{LQB,}I_{LQC}$) are the magnitude of the in-phase and quadrature-phase component of load currents. The term feed-forward current compensation ($I_{ff}$) is utilized to improving the dynamic performance of the system. The computations of this compensation component are as follows,

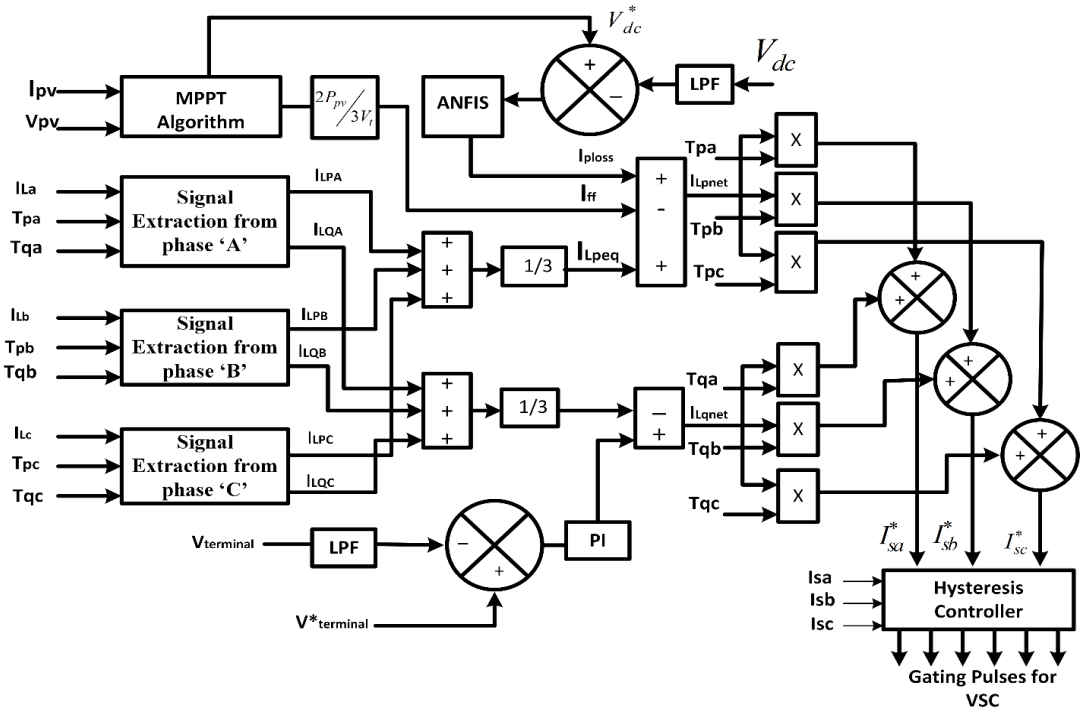


Fig. 7.5 : AFOGI-FLL algorithm for reference current

$$I_f = \frac{2}{3} \times \frac{P_{pv}}{V_{tt}} \tag{7.14}$$

Where, he term $I_Q$& $I_{Ploss}$ is the loss components, which is described in the next section. Therefore, the reference grid currents ($I_{ga}^*, I_{gb}^*, I_{gc}^*$) is determined by net in-phase current component and net quadrature-phase current component and add them together to generate

$$I_{ga}^* = I_{Lpnet} * T_{pa} + I_{Lqnet} * T_{qa}$$

$$I_{gb}^* = I_{Lpnet} * T_{pb} + I_{Lqnet} * T_{qb}$$

$$I_{gc}^* = I_{Lpnet} * T_{pc} + I_{Lqnet} * T_{qc} \quad (7.15)$$

Hysteresis current controls are also used to match these reference grid currents ($I_{ga}, I_{gb}, I_{gc}$) with the source currents. To regulate the grid-tied IGBT-based VSC, the three-reference grid current is converted into six gating pulses using a not gate logic.

## 7.3 COMPARATIVE PERFORMANCE ANALYSIS OF PROPOSED AFOGI-FLL WITH TOGI CONTROL TECHNIQUE

Figs. 7.6 (a)- 7.6 (e) depicts the comparative analysis of the proposed AFOGI-FLL with the TOGI control technique and tabulated in Table 7.1. Moreover, the structure of TOGI is referred from literature. It is shown that the AFOGI-FLL control technique exhibits superior performance concerning DC offset elimination capability, accuracy, and harmonics elimination capability. Fig. 7.6 (a) depicts the dynamic behavior of AFOGI-FLL and TOGI behavior when one phase ‘a’ is suddenly removed at (t=0.3s - 0.5s). Under this scenario, it is observed that sudden fault at (t=0.3s), the fundamental component of load current is settled within a cycle of disconnection in the AFOGI-FLL technique. However, TOGI control technique takes two cycles to settle after the disconnection of the load. Fig. 7.6 (b) depicts the in-phase magnitude estimation by TOGI and AFOGI-FLL control algorithms. It is observed that there are no oscillations found in the AFOGI-FLL control algorithm, however; in the TOGI algorithm, the DC

offset component is there in the load side current. Fig. 7.6 (c) depicts the characteristics of magnitude estimation in TOGI and FOGI-FLL control algorithms. It is observed that TOGI based control possesses oscillations whereas, no oscillations are observed in FOGI-FLL steady-state condition. However, during load unbalancing in the phase 'a' it is observed that TOGI control scheme has a steady-state error which results in wrong amplitude estimation. Fig. 7.6 (d) presents the frequency domain analysis between TOGI and the proposed AFOGI-FLL control scheme.

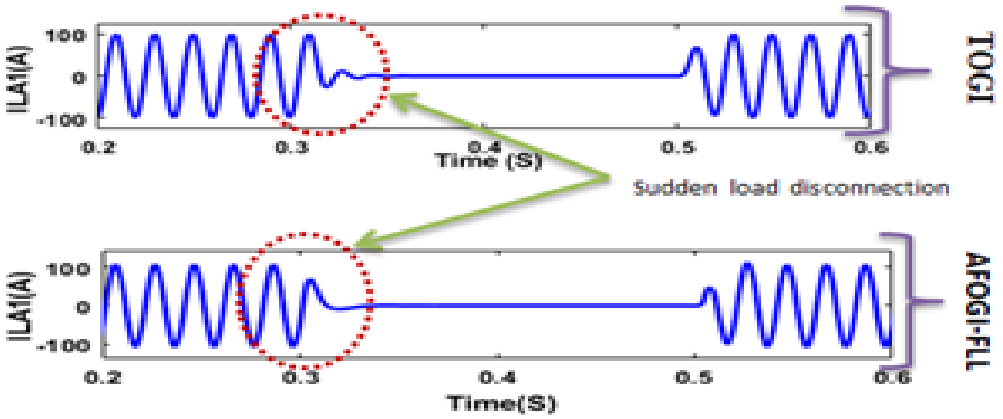


Fig. 7.6 (a) : Dynamic behaviour of AFOGI-FLL with conventional TOGI controller under sudden connection and disconnection of load

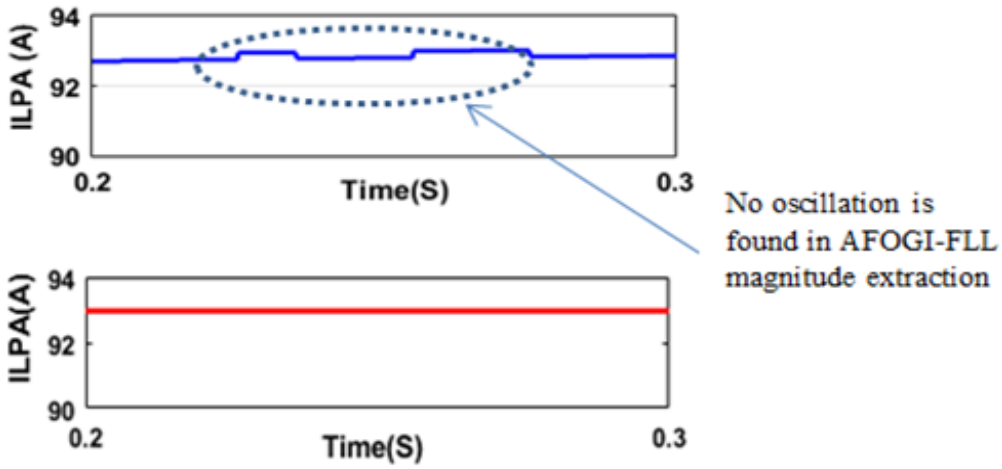


Fig. 7.6 (b) : In-phase component of current magnitude of FOGI-FLL with the conventional TOGI control algorithm

It is observed that AFOGI-FLL having the capability of higher and lower order harmonic rejection capability as well as DC offset rejection capability as compared to TOGI control algorithm. Figure 7.6 (e) presents the FFT analysis to determine the % THD estimation in the AC grid current in the proposed AFOGI-FLL and TOGI control scheme. It is found that both systems having %THD under the IEEE range. Moreover, the AFOGI-FLL control scheme having lower THD (1.10%) as compared to the TOGI control scheme THD (1.23%).

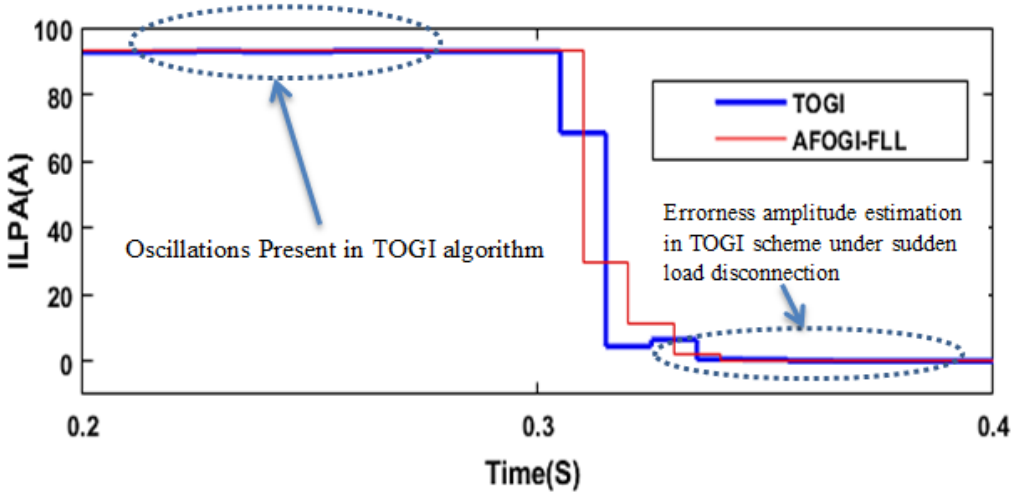


Fig. 7. 6 (c) : Effectiveness of FOGI-FLL for amplitude estimation under the faulty condition with conventional TOGI algorithm

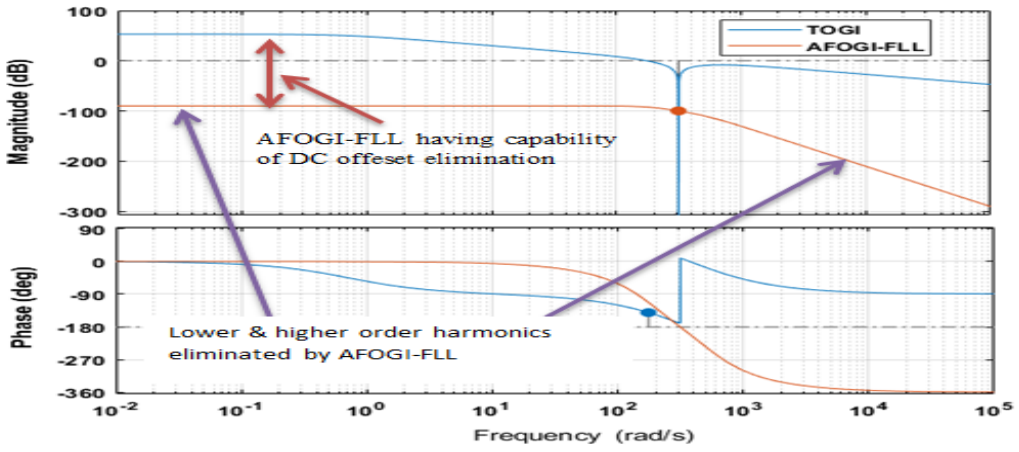


Fig. 7. 6 (d) : Bode diagram with conventional TOGI and AFOGI-FLL algorithm

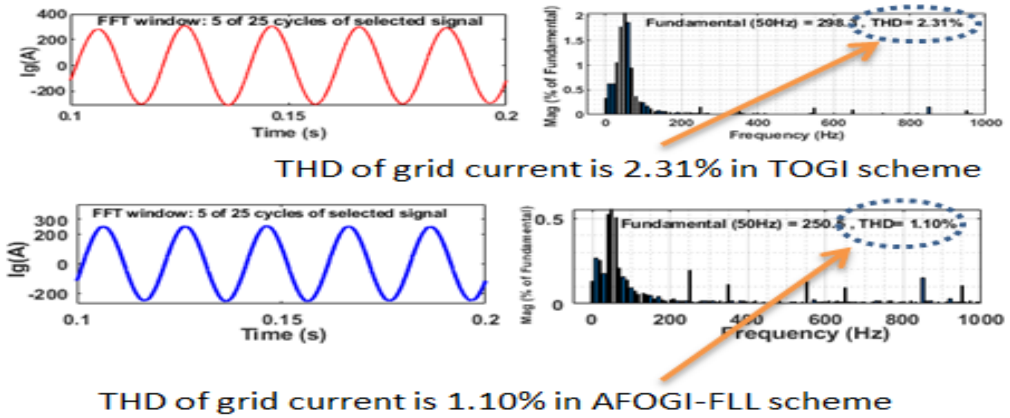


Fig. 7. 6 (e) : The THD of the current estimation of AFOGI-FLL with the conventional TOGI control algorithm

TABLE 7.1 : COMPARATIVE ANALYSIS BETWEEN PROPOSED AFOGI-FLL WITH CONVENTIONAL TOGI CONTROL ALGORITHM

| AFOGI-FLL | TOGI |
|---|---|
| DC Offset Eliminated | DC Offset Present |
| Best Dynamic Performance | Better Dynamic Performance |
| THD is 1.10% | THD is 2.31% |
| Complexity Level Medium | Complexity Level Lower |
| High Filtering Capability | Medium Filtering Capability |
| Four Integrators Used | Three Integrator Used |

## 7.4. SIMULATION RESULTS

The various performances of AFOGI-FLL are analyzed in MATLAB-Simulink environment by simulating the proposed system. The system consists of a solar PV system interfaced to a three-phase AC grid incorporating a diode bridge rectifier with R-L-based nonlinear load. The system is analyzed for various dynamic conditions such as fixed as well in variable isolations, intentionally load unbalancing, and variable frequency conditions. The PQ improvements such as compensated reactive power,

load balancing, and power factor correction (UPF) are also achieved by adaptive control. The parameters of the presented system are provided in appendix-A.

### 7.4.1 Characteristics of the System under Fixed Solar Irradiance

Fig. 7.7 (a) -7.7 (b) presents the characteristics of AFOGI-FLL controller with the fixed irradiance.

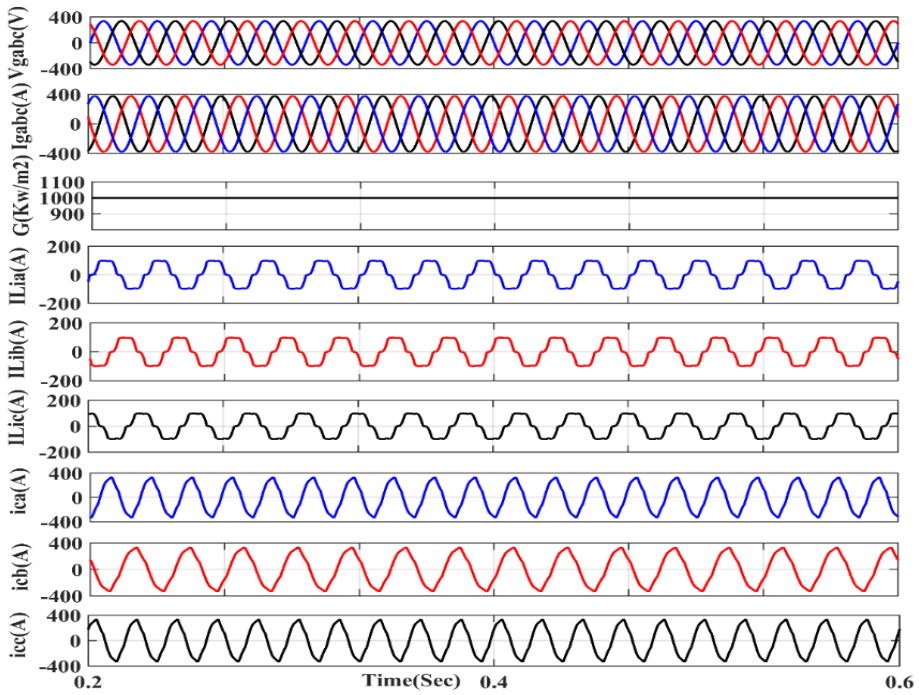


Fig. 7.7 (a) : Performance under fixed solar irradiance Vgabc, Igabc, G, iLa, iLb, iLc, ica, icb, icc

The Fig. 7.7 (a) shows grid voltage and current dynamics (Vgabc, Igabc), load currents (ILa, ILb, ILc), and compensating currents (ica, icb, icc). Grid voltage and current are shown to be in unison and perfectly sinusoidal with a constant solar irradiation of 1000 W/m$^2$. In addition, at a constant irradiance, Fig. 7.7 (b) displays the other performances, including the power and current from solar PV (Ppv, Ipv), DC link voltage (Vdc), feed-forward component of current (Iff), grid active and reactive power (Pg, Qg), and the magnitude of IPC and QPC currents (ILPA, ILQA).

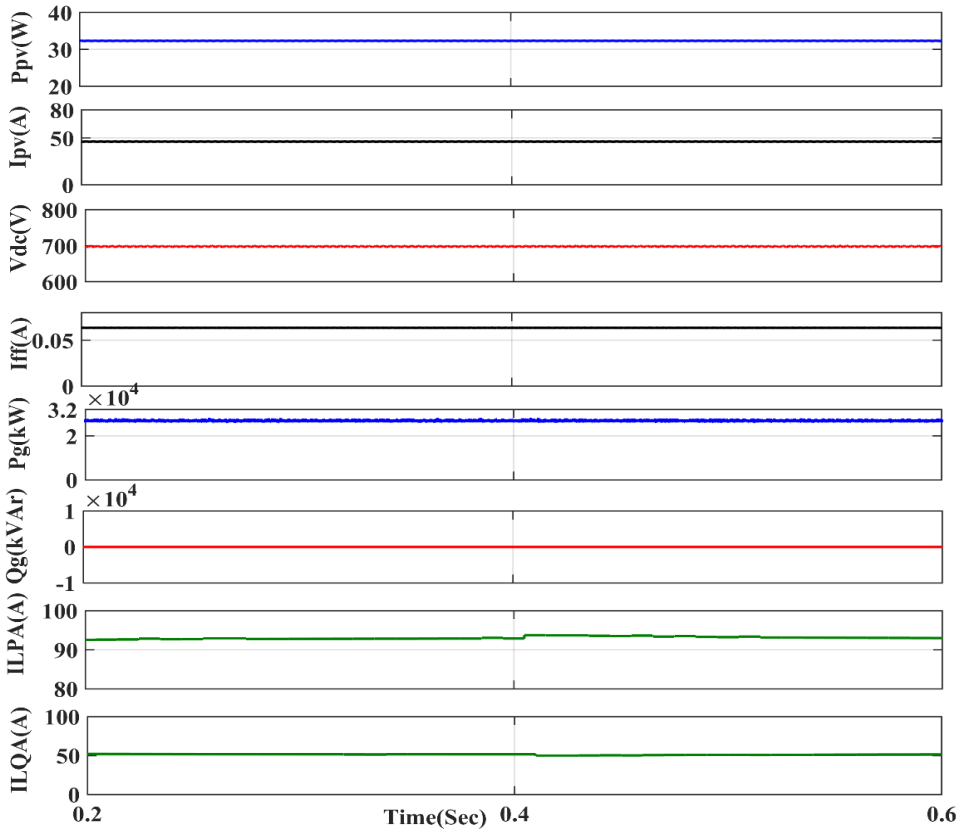


Fig. 7.7 (b) : Characteristics under fixed solar irradiance Ppv, Ipv, Vdc, Iff, Pg, Gg, ILPA, ILQA

### 7.4.2 Characteristics of the System under Variable Solar Irradiance

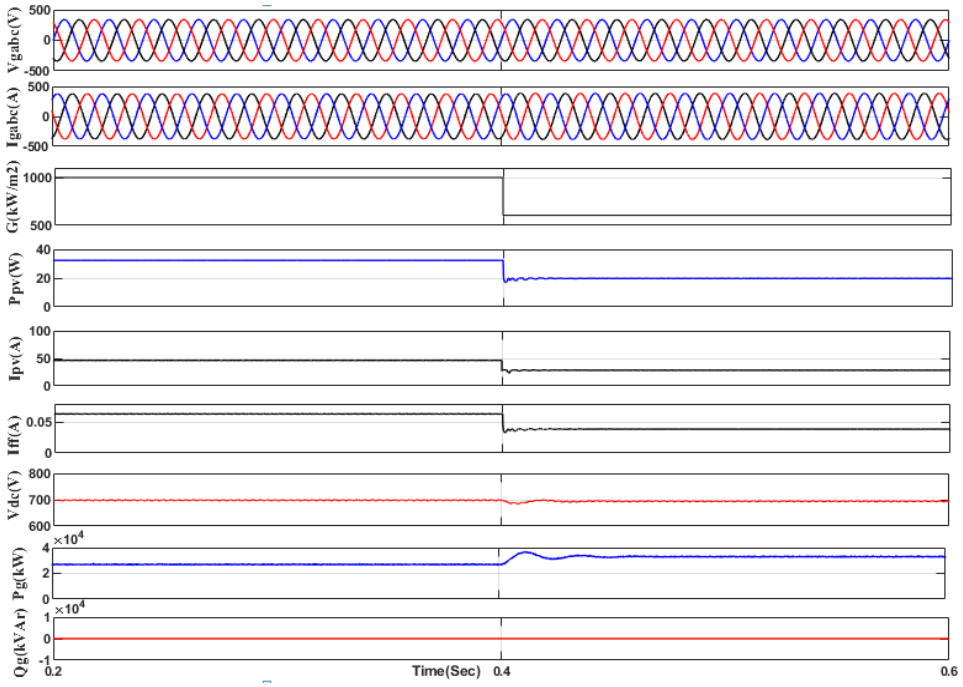


Fig. 7.8 : Characteristics under variable solar irradiance Vgabc, Igabc, G, Ppv, Ipv, Iff, Vdc, Pg, Qg

The Fig. 7.8 illustrates the dynamic characteristics of a PV system with varying solar irradiance and a nonlinear load attached to the utility grid. The simulation results present the waveforms of three-phase voltages (Vgabc), currents (Igabc) of grid side, solar PV power and current (Ppv, Ipv), feed-forward current (Iff), DC bus voltage (Vdc), and active power (Pg) and reactive power (Qg). Initially at the steady-state before at (t=0.4s) and with the fixed solar irradiance i.e. of (1000 W/$m^2$) at temperature (25$^o$C), AC side three-phase grid currents are perfectly balanced and sinusoidal. Moreover, the DC bus voltage (Vdc) is sustained to its reference value of 700V. In this case, the solar irradiance is reduced to 600 W/$m^2$ at (t=0.4 s), thus decreasing the output power from the SPV system from 32 kW to 20 kW approximately. Furthermore, the remaining power, i.e. 12 kW, is used to supply the AC grid. Moreover, it is also very interesting to notice the DC link voltage is constant with very minute fluctuations to its reference value. As solar irradiance decreases at (t=0.4s) the feed-forward component of current is also decreasing, which tends to reduce fluctuations in AC grid current. Moreover, due to the sudden drop in irradiance, it is analyzed that the source side grid currents and voltages are balanced and grid power is increased at (t=0.4s), to maintain the load power constant. Due to that, there is no reactive power burden is observed in the AC grid. Moreover, AC grid voltage and current are in the same phase with UPF operation.

### 7.4.3 Characteristics of the System under Sudden Disturbances

The waveforms of Vgabc, Igabc, G, ILa, ILb, ILc, Ica, Icb, and Icc may be seen in Fig. 7.9 (a).

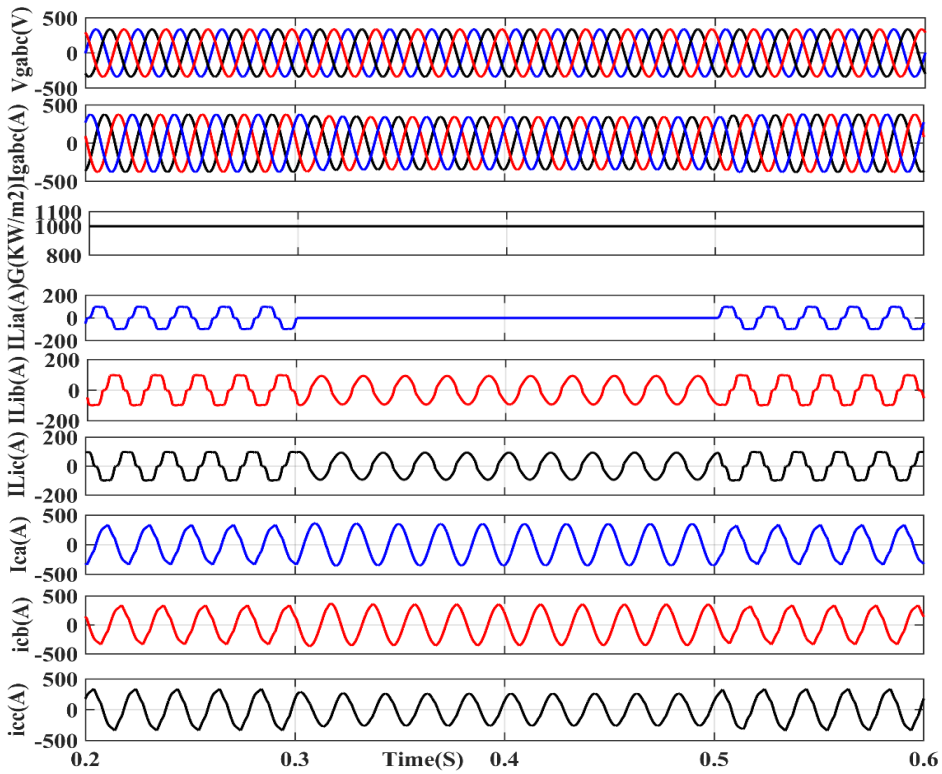


Fig. 7.9 (a) : Characteristics under sudden disturbances

The Fig. 7.9 (b) shows the waveform of Ppv, Ipv, Vdc, Iff, Pg, Qg, $I_{LPA,}$ and $I_{LQA.}$ The grid currents are perfectly balanced and sinusoidal if one of the phases 'a' is intentionally removed at the time (t=0.3s to t=0.5s). With this intentional disturbance, it is also noticed that the converter currents (Ica, Icb, Icc) are unbalanced. Also, the grid voltage and the currents are in the same phase with UPF operation. There are no noticeable changes to the DC link voltage. In addition, the AC grid provides the active power (Pg), meets the demand, and balances the load. The magnitude of ILPA, ILQA currents are reduced to zero at (t=0.3s), and constant at fixed irradiance.

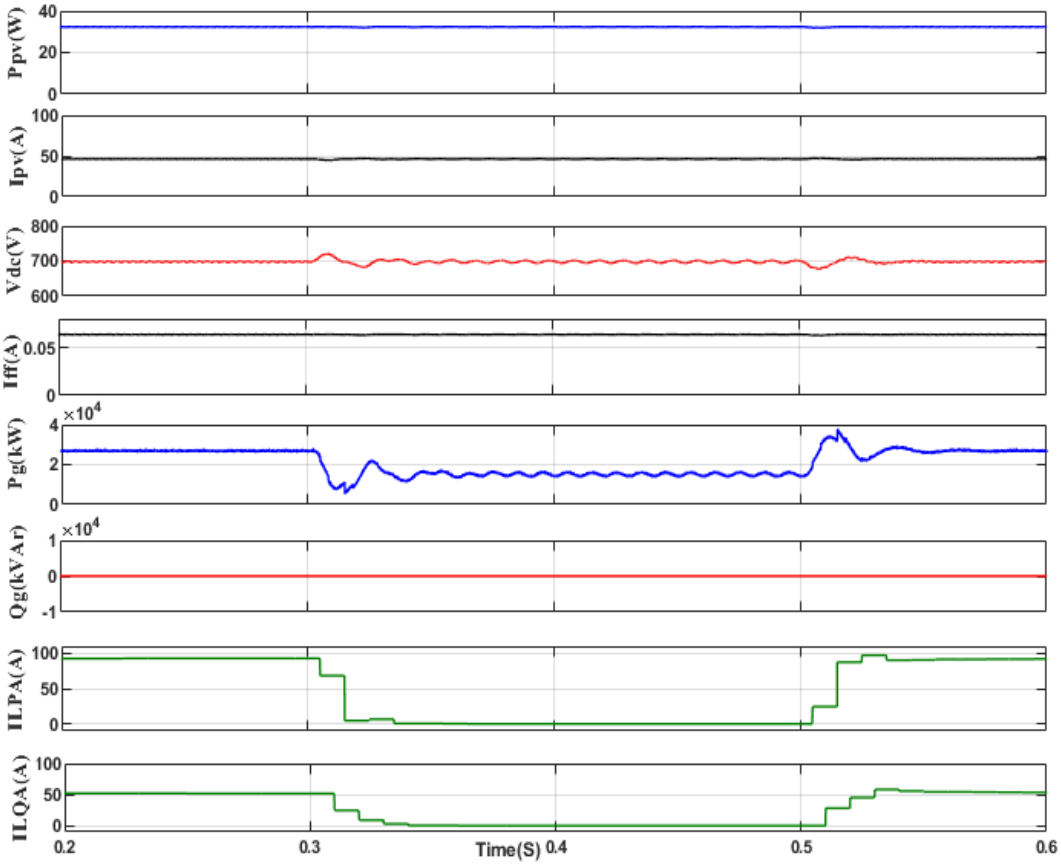


Fig. 7.9 (b) : Characteristics under sudden disturbances

### 7.4.4 Characteristics of the System Due to Variable Frequency

Fig. 7.10 depicts the characteristics of the system as Vgabc, Igabc, Ppv, Vdc, and Pg at variable system frequency (w). The system frequency varies from 49.5 Hz to 50.5 Hz at (t= 0.4 s to t=0.5 s), as depicted in Fig. 7.10. The Grid voltages and currents are balanced and sinusoidal with varying system frequencies. Additionally, the maximum power extraction of the SPV array also remains unaffected. However, very minute oscillations are observed in DC bus voltage with variations in system frequency. Hence, it is observed that the overall control algorithm exhibits reliable operation under system frequency variation.

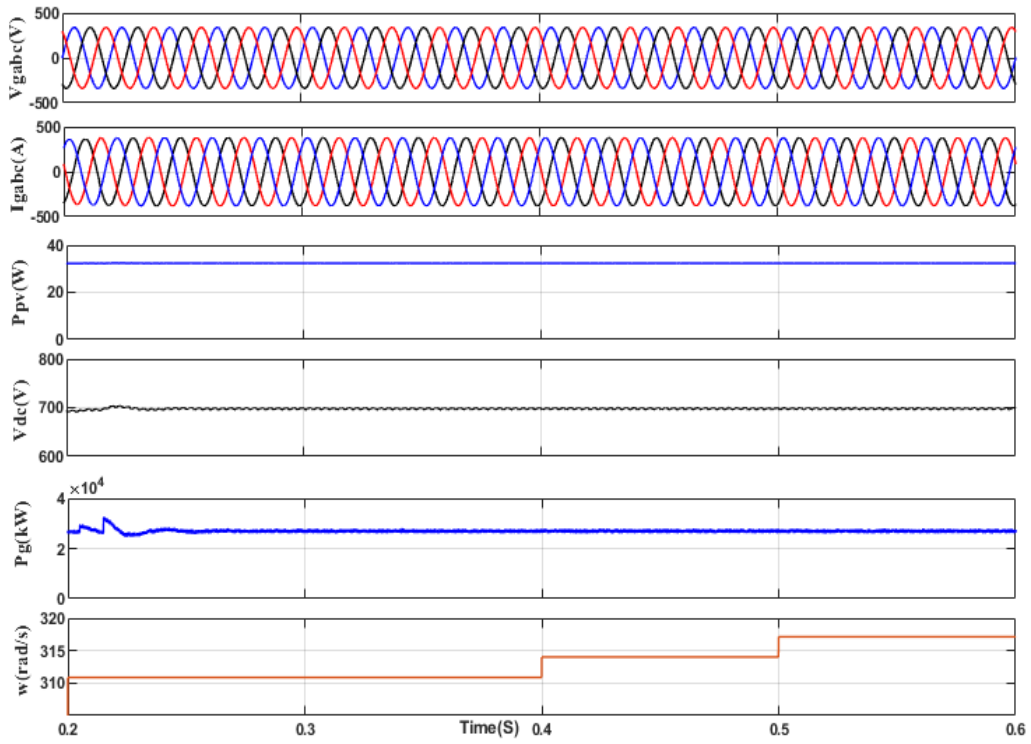


Fig. 7.10 : Characteristics of the system at varying system frequency Vgabc, Igabc, Ppv, Vdc, Pg, w

## 7.5 HARDWARE IMPLEMENTATION

A prototype hardware set-up is developed for the implementation of proposed control algorithm. Also, solar-array simulator having 2.5 kW capacity is utilized to generate the PV power. The MPPT performance at variable solar irradiance is analyzed through SPV simulator and it is shown in Fig. 7.12 (a),(b). The volage and current sensors are utilized to sense grid voltage and grid current respectively. The digital signal processor (DSP), is used to convert analog current and voltage signals to discrete signals which are further utilized in AFOGI-FLL control algorithm to generate the reference current signal. Further, these generated reference source currents are compared with the grid currents for getting pulses for the VSC.

### 7.5.1 Behavior of System Having Non-Linear Loading

In the Fig. 7.11, the performance of system shown under steady-state conditions for the 2.33kW of non-linear load. The Figs. 7.11 (a-d) shows the grid voltage (Vg), current (Ig), active power (Pg), reactive power (Qg), and THD of grid voltage and grid current respectively. In the Figs. 7.11 (e-f), depicts the active and reactive power of the load and THD of the load current. Moreover, it is depicted in Fig. 11 (e), out of 2.33kW grid power 1.69 kW is consumed by non-linear load as shown in the figure. Figs.7.11 (g-k) depicts the compensating voltage (Vc) and current (Ic), compensating active (Pc) and reactive power (Qc), compensating current THD and compensating voltage THD and DC link voltage, current respectively.

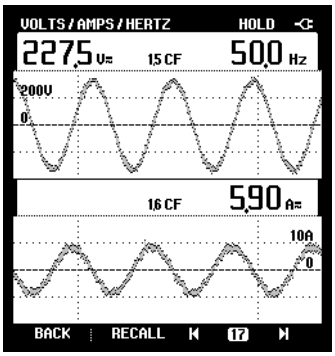


(a)

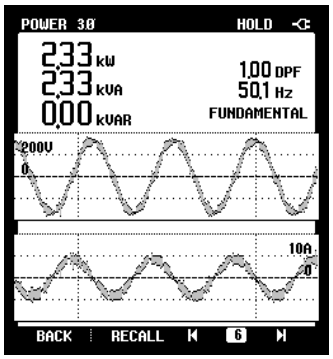


(b)

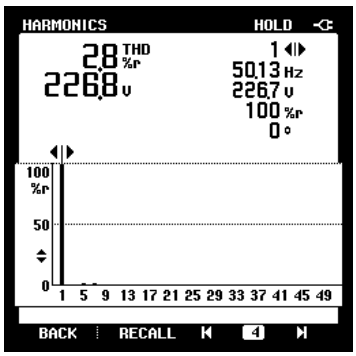


(c)

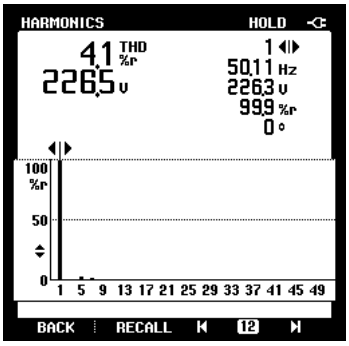


(d)

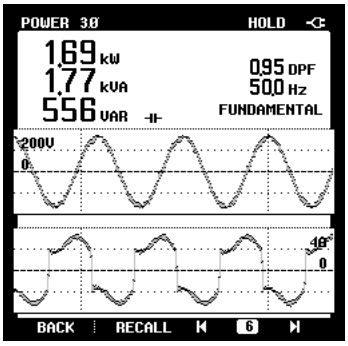


(e)

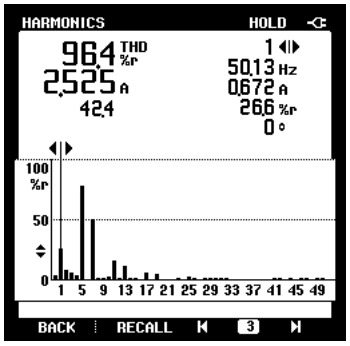


(f)

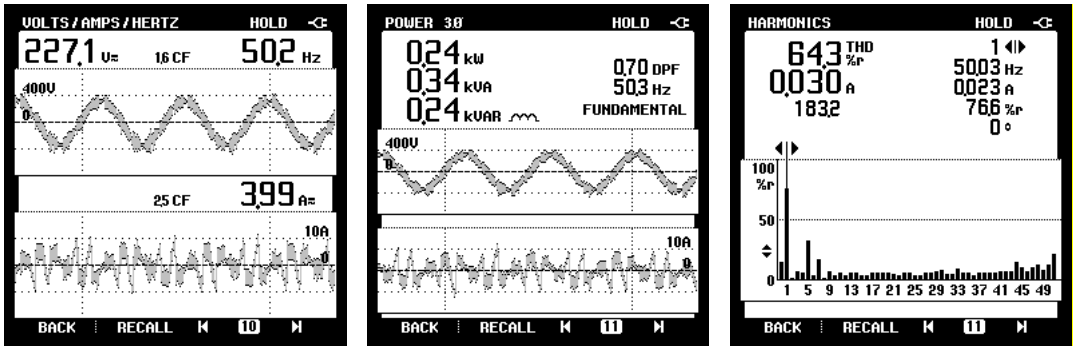


(g) (h) (i)


(j) (k)

Fig. 7.11 Experimental behaviors for non-linear loading (a) grid voltage and current (b) grid active and reactive power (c) THD of grid current (d) THD of grid current (e) active and reactive power of load (f) THD of load current (g) compensating voltage and current (h) compensating active and reactive power (i) THD of compensating current (j) THD of compensating voltage (k) DC link voltage and current

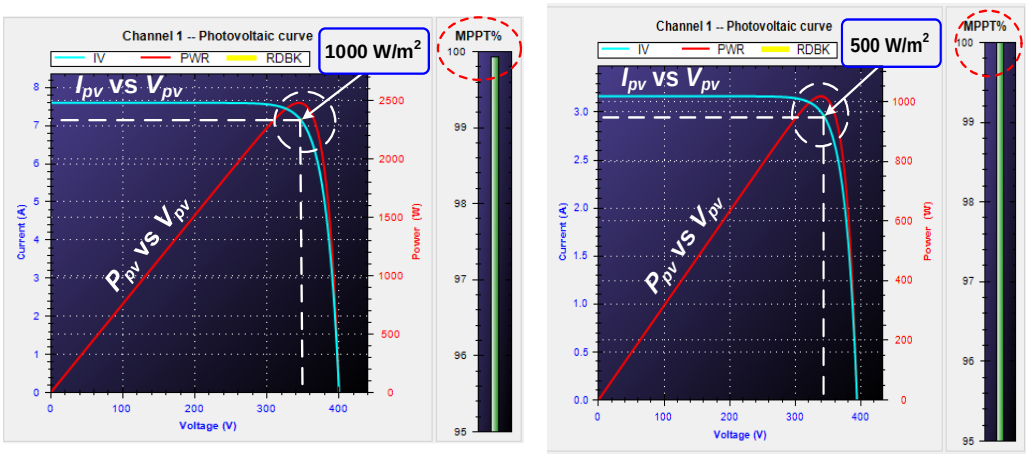


(a) (b)

Fig. 7.12 (a), (b) : MPPT performance of SPV simulator at 1000 W/m$^2$ and 500 W/m$^2$

## 7.6 CONCLUSION

The Adaptive FOGI-FLL based control strategy has been described for three phase grid interfaced Solar PV system. The goal of this scheme is to harvest the greatest amount of electricity from solar PV arrays while simultaneously improving the power quality of the distribution network. The presented controller provides a satisfactory response for multifunctional objectives such as accurate frequency synchronization, lower and higher-order harmonics elimination, power quality (PQ) refinement, reactive power compensation capability, etc. Regardless of the system dynamic conditions or load disturbances, the proposed technique has strongly rejected harmonics. Frequency domain investigation has shown how successful the DC offset rejection capabilities and higher order harmonics rejection capabilities are in separating the fundamental component from load current. Moreover, under fluctuating solar insolation, the MPO algorithm is utilized to collect the highest amount of electricity possible from a solar PV array while maintaining an efficiency of one hundred percent. Additionally, AFOGI-FLL outperforms the TOGI controller on a number of parameters, including DC offset elimination, dynamic performance, complexity, and lower and higher-order filtering capabilities. Furthermore, the AFOGI-FLL control scheme has a lower THD (1.10%) than the TOGI control scheme (1.23%). The proposed controller robustness can be verified with the hybrid energy sources. An FPGA-based HLL is used to validate the proposed method on a real-time simulator.

# Chapter 8

# STOCHASTIC GRADIANT BASED CONTROL ALGORITHMS FOR POWER QULAITY ENHANCEMENT IN SPV INTERFACED THREE-PHASE DISTRIBUTION SYSTEM

## 8.0 GENERAL

In this research paper, stochastic-gradient-based adaptive control algorithms have been discussed and employed for power quality enhancement in a PV integrated distribution system. Least mean square (LMS), Least mean fourth (LMF), sign-error LMS and $\epsilon$ −Normalized LMS ($\epsilon$ −NLMS) have been implemented as control algorithms for the estimation of fundamental load current. The performances of these adaptive algorithms have been compared under steady-state and dynamic conditions under the non-linear load conditions in a closed-loop three-phase system. The main aim of implementing these algorithms is reactive power compensation, power quality enhancement and load balancing in a single-stage three-phase grid-tied PV system. The hysteresis control technique (HCC) has been used to generate switching pulses for the three-phase DSTATCOM. An MPPT has also been employed to ensure maximum power delivery from the solar PV array. PV integrated three-phase single-stage distribution system with adaptive control algorithms has been implemented in MATLAB/Simulink environment as well as in experimental environment to achieve the goals per standard IEEE-519.

### 8.1 SYSTEM CONFIGURATION

The three-phase grid-tied PV system consists of a 415V, 50Hz supply feeding the non-linear load. Three-phase VSC has a self-sustained DC-link, and its AC side is

connected to the point of common coupling (PCC) via the passive filter or the interfacing inductor. The non-linear load model is modeled by connecting the R-L load to the DC-side of a rectifier. PV array of 5.95kW power rating is directly connected to the DC-link of the DSTATCOM. MPPT technique has been used to achieve maximum power from the PV array. Parameters of the single-stage three-phase grid-tied PV system are given in the appendix. Fig. 8.1 shows the system configuration for single-stage three-phase grid-tied PV systems and is simulated in MATLAB/Simulink.

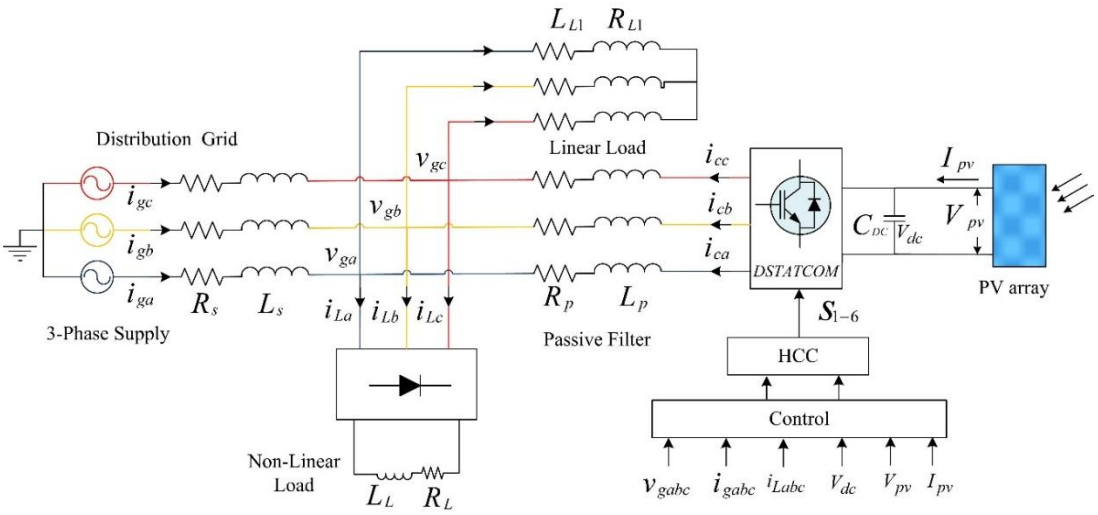


Fig. 8.1 System configuration for three-phase single-stage grid-tied PV system

## 8.2 ADAPTIVE CONTROL ALGORITHMS

### 8.2.1 Least Mean Square (LMS)

Assume that we have access to desired random variables $\boldsymbol{d}$ and $\boldsymbol{u}$ as the unit templates, which can be estimated from three-phase voltage signals. Zero-mean random variable $\boldsymbol{d}$ is realized as $\{d(0), d(1), d(2), \ldots\ldots\}$ and zero-mean random vector $\boldsymbol{u}$ is realized as $\{u_0, u_1, u_2, \ldots\ldots\}$ respectively. The optimal weight vector $w^0$ that solves

$$\min_{w} E|\boldsymbol{d} - \boldsymbol{u}w|^2 \qquad (8.1)$$

The above equation can be solved iteratively by the LMS recursion, as shown in equation (8.2).

$$w(k) = w(k-1) + \alpha u^*(k)[d(k) - u^*(k)w(k-1)], \quad k \geq 0, \quad w_{-1} = \text{initial guess} \tag{8.2}$$

$$w(k) = w(k-1) + \alpha u(k)e(k) \tag{8.3}$$

Here, $w(k)$ is the weight estimate at iteration $k$, $u(k)$ is the regressor at iteration at $k$. In Eq. 8.2, $\alpha$ (usually a small positive value) is called as learning rate or intelligent factor or step-size, and $e(k)$ is the output estimation error at iteration $k$.

The LMS method can estimate the fundamental load current component, which can be used as a three-phase grid-tied PV system control algorithm. Considering the phase-a element in the load current contain harmonics and can be written as-

$$i_a = \sum_{n=1}^{N} I_m \sin(n\omega t + \phi) \tag{8.4}$$

Using the LMS algorithm, a weight updating method extracts the fundamental active and reactive components of the non-linear load current. The fundamental active and reactive component of the non-linear load current of phase-a is expressed as:

$$w_{pa}(k) = w_{pa}(k-1) + \alpha u_{pa}(k)e_{La}(k) \tag{8.5}$$

$$w_{qa}(k) = w_{qa}(k-1) + \alpha u_{qa}(k)e_{La}(k) \tag{8.6}$$

Here, $w_{pa}(k)$ is the fundamental active component at iteration $k$, $w_{qa}(k)$ is the fundamental reactive component at iteration $k$, $u_{pa}$ and $u_{qa}$ are the unit in-phase and quadrature-phase templates. $e_{La}(k)$ is the estimated error and can be obtained by subtracting the non-linear load current by the estimated current.

$$e_{La}(k) = i_{La}(k) - i_{Lae}(k) \tag{8.7}$$

The load current is estimated by using equation (8.8).

$$i_{Lae}(k) = w_{pa}(k)u_{pa}(k) + w_{qa}(k)u_{qa}(k) \tag{8.8}$$

Similarly, the fundamental active and reactive components of phase-b and phase-c are estimated as:

For phase-b,

$$w_{pb}(k) = w_{pb}(k-1) + \alpha u_{pb}(k)e_{Lb}(k) \tag{8.9}$$

$$w_{qb}(k) = w_{qb}(k-1) + \alpha u_{qb}(k)e_{Lb}(k) \tag{8.10}$$

For phase-c

$$w_{pc}(k) = w_{pc}(k-1) + \alpha u_{pc}(k)e_{Lc}(k) \tag{8.11}$$

$$w_{qc}(k) = w_{qc}(k-1) + \alpha u_{qc}(k)e_{Lc}(k) \tag{8.12}$$

### 8.2.2 Sign-Error LMS

Consider a zero-mean random variable $\boldsymbol{d}$ realizations $\{d(0), d(1), d(2), \dots\dots\}$, and a zero-mean random row vector $\boldsymbol{u}$ with realizations $\{u_0, u_1, u_2, \dots\dots\}$. The optimal weight vector $w^0$ that solves

$$\min_{w} E|\boldsymbol{d} - \boldsymbol{u}w| \tag{8.13}$$

And it can be approximated iteratively via the recursion

$$w(k) = w(k-1) + \alpha u^*(k)\text{csgn}[d(k) - u^*(k)w(k)], \;\; k \geq 0 \tag{8.14}$$

Where $\alpha$ is usually a small-positive value. In the above statement, the sign of a complex number $z = z_r + jz_i$ is defined as

$$\text{csgn}(z) \triangleq \text{sign}(z_r) + j\text{sign}(z_i), \;\; j = \sqrt{-1} \tag{8.15}$$

Where the notation $sign$ denotes the sign of a real number and is defined as

$$\text{sign}(z_r) \triangleq \begin{cases} +1 & if\ a > 0 \\ -1 & if\ a < 0 \\ 0 & if\ a = 0 \end{cases} \tag{8.16}$$

Similarly, as discussed earlier, the fundamental active and reactive components of phase-a load current are estimated as:

$$w_{pa}(k) = w_{pa}(k-1) + \alpha u_{pa}(k)\text{sgn}\, e_{La}(k) \tag{8.17}$$

$$w_{qa}(k) = w_{qa}(k-1) + \alpha u_{qa}(k)\text{sgn}\, e_{La}(k) \tag{8.18}$$

### 8.2.3 $\epsilon$ −Normalized LMS ($\epsilon$ −NLMS)

Consider a zero-mean random variable $\boldsymbol{d}$ realizations $\{d(0), d(1), d(2), \ldots\ldots\}$, and a zero-mean random row vector $\boldsymbol{u}$ with realizations $\{u_0, u_1, u_2, \ldots\ldots\}$. The optimal weight vector $w^0$ that solves:

$$\min_{w} E|\boldsymbol{d} - \boldsymbol{u}w|^2 \tag{8.19}$$

The above equation can be solved iteratively by the $\epsilon$ −NLMS recursion, as shown in equation (8.20).

$$w(k) = w(k-1) + \frac{\alpha}{\epsilon + ||u(k)||^2} u^*(k)[d(k) - u^*(k)w(k)],\ \ i \geq 0,\ \ w_{-1} = \text{initial guess} \tag{8.20}$$

Where, $\alpha$ is a positive step-size and $\epsilon$ is a small positive parameter. Similarly as discussed earlier, the fundamental active and reactive components of phase-a load current are estimated as:

$$w_{pa}(k) = w_{pa}(k-1) + \frac{\alpha}{\epsilon + ||u(k)||^2} u_{pa}(k) e_{La}(k) \tag{8.21}$$

$$w_{qa}(k) = w_{qa}(k-1) + \frac{\alpha}{\epsilon + ||u(k)||^2} u_{qa}(k) e_{La}(k) \tag{8.22}$$

### 8.2.4 Least Mean Fourth (LMF)

Optimal weight vector for LMF that solves

$$\min_{w} E|\boldsymbol{d} - \boldsymbol{u}w|^4 \tag{8.23}$$

It can be approximated iteratively via the recursion

$$w(k) = w(k-1) + \alpha u^*(k) e(k) |e(k)|^2, \;\; k \geq 0 \tag{8.24}$$

Where $\alpha$ is usually a small-positive value. In a similar fashion as discussed earlier the fundamental active and reactive components of phase-a are estimated as:

$$w_{pa}(k) = w_{pa}(k-1) + \alpha u_{pa}(k) e_{La}(k) |e_{La}(k)|^2 \tag{8.25}$$

$$w_{qa}(k) = w_{qa}(k-1) + \alpha u_{qa}(k) e_{La}(k) |e_{La}(k)|^2 \tag{8.26}$$

Fundamental component estimated by the LMS, Sign-error LMS, $\epsilon$ −NLMS, and LMF has been shown in Fig. 8.2 at different learning rates and optimized values have been considered for optimal performance. Figure 8.3 shows the comparison performance at optimized learning rates. During the unbalanced load and sudden change in load demand. Detailed analysis of the open-loop performance of LMS, Sign-error LMS, $\epsilon$ −NLMS and LMF during dynamic and steady-state conditions have been tabulated in Table 8.1. From Table 8.1, it can be seen that LMF shows a faster response with a very low steady-state peak-to-peak value than LMS, Sign-error LMS, and $\epsilon$ −NLMS.

## 8.3 GENERATION OF SWITCHING PULSES FOR DSTATCOM

The hysteresis current control technique has been used to generate all six necessary pulses for the DSTATCOM. HCC block requires the reference current and the grid current. Estimation of reference currents requires the fundamental load component, loss component of the DSTATCOM, synchronizing signal, and the PV feed-forward weight component. Estimation of the fundamental component has been discussed in the previous section and the estimation of other components will be discussed in this section.

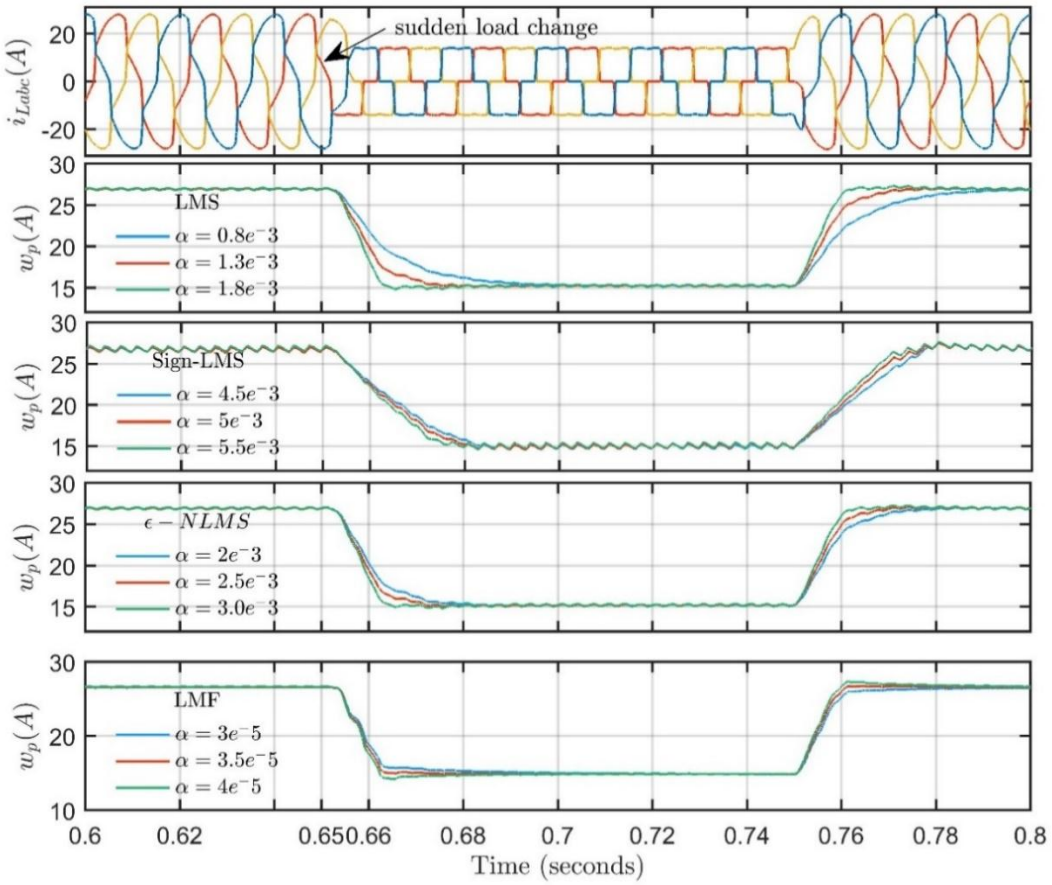


Fig. 8.2 : Convergence of adaptive algorithms with different learning rates

Table 8.1 : COMPARISON OF OPEN-LOOP PERFORMANCE OF LMS, SIGN-ERROR LMS, $\epsilon$ −NLMS And LMF

| Parameters | Control Algorithms | | | |
|---|---|---|---|---|
| | LMS | Sign-error LMS | $\epsilon$-NLMS | LMF |
| | Dynamic performance | | | |
| Rise time (ms) | 7.959 | 17.078 | 8.102 | 6.596 |
| Settling time (ms) | 19.465 | 30.005 | 19.497 | 16.861 |
| Preshoot (%) | 1.559 | 4.945 | 1.520 | 0.262 |
| Overshoot (%) | 2.604 | 4.945 | 2.604 | 4.851 |
| Undershoot (%) | 1.994 | 5.370 | 1.993 | 1.988 |
| | Steady-state performance | | | |
| Fundamental current ($w_p$)(A) peak-peak | 0.292 | 0.783 | 0.286 | 0.099 |
| RMS (A) | 26.96 | 26.83 | 26.94 | 26.64 |

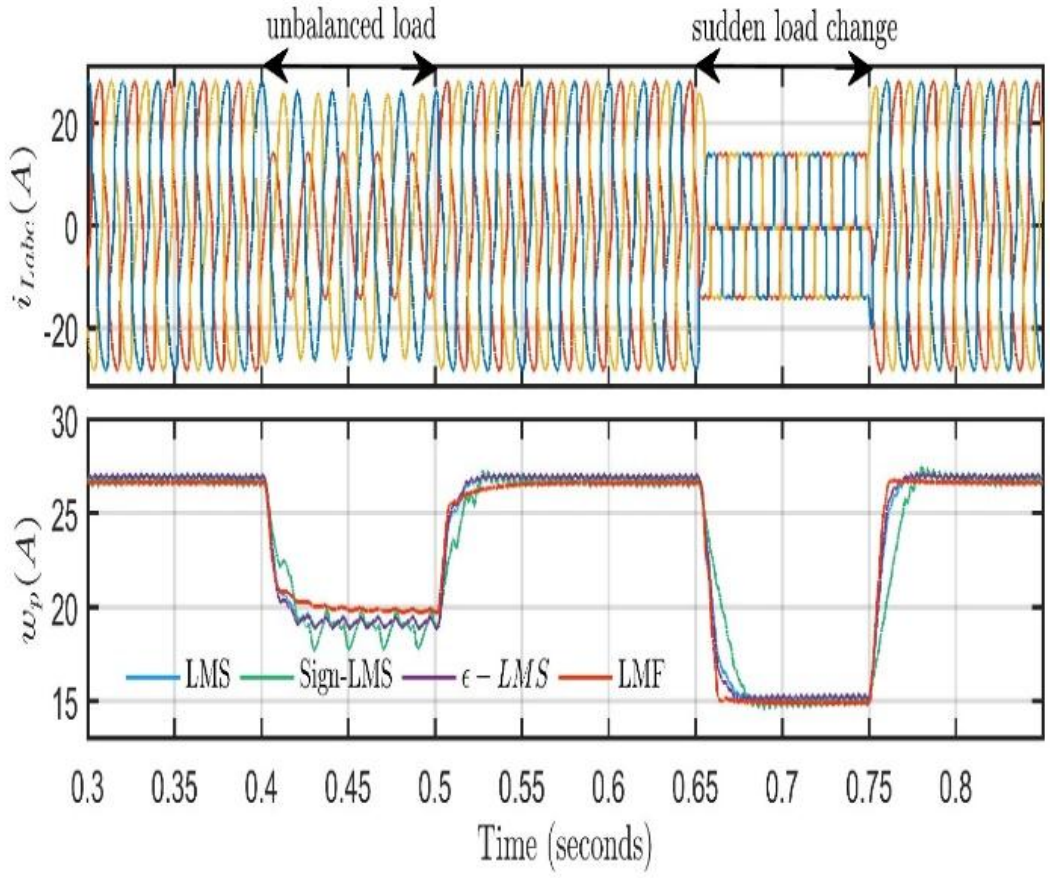


Fig. 8.3 : Open-loop performance comparison of LMS, Sign-LMS, $\epsilon - LMS$ and LMF

### 8.3.1 Loss Component Estimation

DC-link voltage has been regulated by the proportional-integral (PI) controller. It requires reference DC-link voltage and measuring DC-link voltage. Perturb-observe (P&O) MPPT technique is used to generate reference DC-link voltage and achieve maximum power from the PV array. Equations for the P&O MPPT technique are discussed below:

$$\text{If } \Delta P_{pv} \times \Delta V_{pv} > 0 \Rightarrow V_{ref} = V_{old} + \Delta V \tag{8.27}$$

$$\text{And if } \Delta P_{pv} \times \Delta V_{pv} < 0 \Rightarrow V_{ref} = V_{old} - \Delta V \tag{8.28}$$

$$\text{At MPPT, } \Delta P_{pv} \times \Delta V_{pv} = 0 \Rightarrow V_{ref} = V_{old} \tag{8.29}$$

Here, $V_{ref}$ is the DC-link reference voltage and DC-link voltage will be regulated at this reference voltage. The loss component of the DSTATCOM is estimated as:

$$w_{loss}(n+1) = w_{loss}(n) + k_p\{V_{dce}(n+1) - V_{dce}(n)\} + k_i V_{dce}(n+1) \tag{8.30}$$

In above, equation $V_{dce}$ is the error in DC-link voltage and is calculated as $V_{ref} - V_{dc}$.

### 8.3.2 Synchronizing Signals Estimation

For estimating the synchronizing signal, the unit-template method is very simple and easy to implement. Unit templates of each phase from the grid voltage are estimated by dividing the individual phase voltages by the amplitude of the grid voltage ($V_m$).

$$V_m = \sqrt{\frac{2}{3}(v_{ga}^2 + v_{gb}^2 + v_{gc}^2)} \tag{8.31}$$

Unit templates of individual phases are:

$$u_{pa} = \frac{v_{ga}}{V_m}, u_{pb} = \frac{v_{gb}}{V_m}, u_{pc} = \frac{v_{gc}}{V_m} \tag{8.32}$$

Unit quadrature templates can be estimated by:

$$u_{qa} = -\frac{1}{\sqrt{3}}u_{pb} + \frac{1}{\sqrt{3}}u_{pc} \tag{8.33}$$

$$u_{qb} = \frac{\sqrt{3}}{2}u_{pa} + \frac{1}{2\sqrt{3}}\left(u_{pb} - u_{pc}\right) \tag{8.34}$$

$$u_{qb} = \frac{\sqrt{3}}{2}u_{pa} + \frac{1}{2\sqrt{3}}\left(u_{pb} - u_{pc}\right) \tag{8.35}$$

### 8.3.3 PV Feed-Forward Component

Power generated from the PV is transferred to the grid or the load depends on the load demand and PV generation. If PV power is more than load demand it is transferred to the grid via VSC. Therefore, a feed-forward component ($w_{ff}$) of PV array is considered to improve the transient response of the system during the variation of environmental conditions or change in the load demand.

Instantaneous peak power generated from the PV array is calculated as,

$$P_{pv} = V_{pv}I_{pv} \tag{8.36}$$

PV power reflected at AC side is calculated by,

$$P_{ac} = 3V_{rms}I_{rms} = 3\frac{V_m}{\sqrt{2}}\frac{I_m}{\sqrt{2}} \tag{8.37}$$

Ideally, $P_{pv} = P_{ac}$

Hence, PV feed-forward weight component is estimated as,

$$w_{ff} = I_m = \frac{2P_{pv}}{3V_m} \tag{8.38}$$

### 8.3.4 Reference Current Estimation

Once the fundamental active and reactive components of the three-phase are calculated and then the average fundamental active ($w_p$) and reactive weights ($w_q$) can be

computed as:

$$w_p = \frac{w_{pa}+w_{pb}+w_{pc}}{3} \tag{8.39}$$

$$w_q = \frac{w_{qa}+w_{qb}+w_{qc}}{3} \tag{8.40}$$

The net reference active weight component is estimated by the equation (8.41).

$$w_{net} = w_p + w_{loss} - w_{ff} \tag{8.41}$$

Net reference active weight is used to estimate the three-phase reference current and is written as:

$$i_{ga}^* = w_{net}u_{pa}, i_{gb}^* = w_{net}u_{pb}, i_{gc}^* = w_{net}u_{pc} \tag{8.42}$$

Further, the measured grid currents and estimated reference current are given to the hysteresis current controller (HCC) to generate the necessary switching pulses of the three-phase DSTATCOM. Complete control of the proposed system has been shown in Fig. 8.4.

TABLE 8.2 CLOSED-LOOP PERFORMANCE OF LMF CONTROL ALGORITHM

| **System conditions** | **G=500W/m² At t = 0 0.16s** | | **G=1000W/m² At t = 0.35s** | **Unbalanced load At t=0.45s** | **Load decrease t =0.73** |
|---|---|---|---|---|---|
| **Active power ($kW$)** | $P_L$ | 13.69 | 13.69 | 9.44 | 7.74 |
| | $P_g$ | 10.76 | 7.98 | 4.37 | 2.31 |
| | $P_c$ | 2.93 | 5.71 | 5.06 | 5.42 |
| **Reactive power ($kVar$)** | $Q_L$ | 4.98 | 4.98 | 4.19 | 0.926 |
| | $Q_g$ | 0.006 | 0.003 | 0 | 0.078 |
| | $Q_c$ | 4.98 | 4.98 | 4.19 | 0.934 |

## 8. 4 SIMULATION PERFORMANCE

This section discusses the performance of different adaptive control algorithms for the single-stage three-phase grid-tied PV system. A combination of linear lagging and non-linear load is connected to the distribution grid. PV array of 5.954kW is directly connected to the DC-link of DSTATCOM. Here, in single-stage DC-DC converter is not employed and in double-stage, a DC-DC converter is used. Single-stage configuration is advantageous over double-stage configuration as the DC-DC converter cost has been eliminated.

Figs. 8.5-8.7 show the closed-loop performance under various conditions such as irradiance change, load unbalancing, and sudden change in load. Figure 8.5 shows the voltage and current performance of the grid, load and

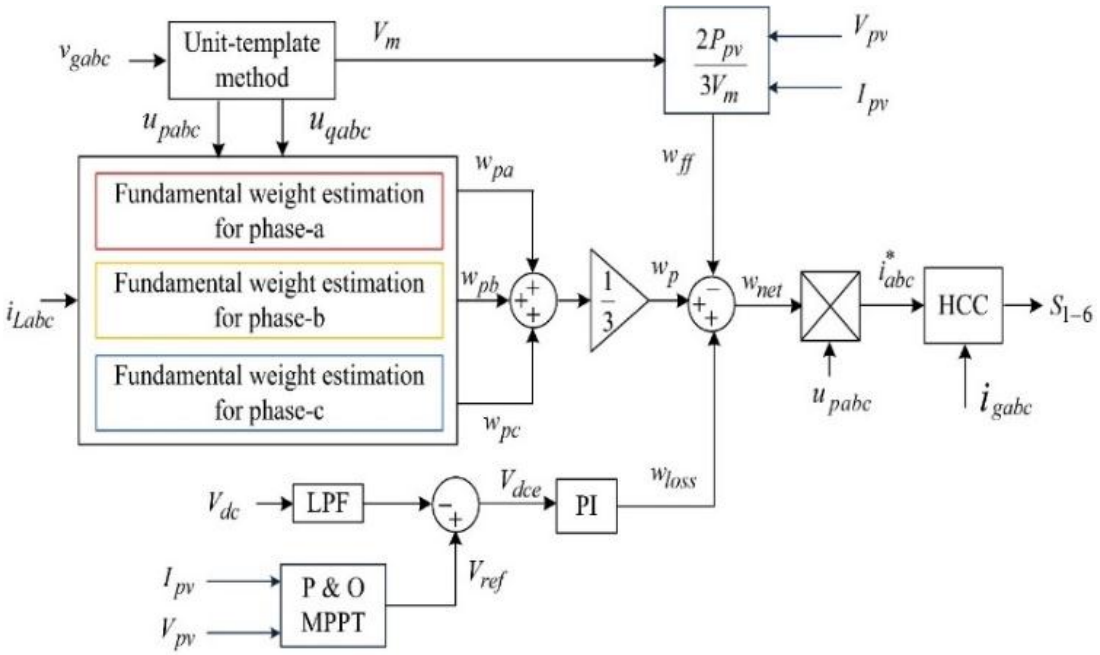


Fig. 8.4 : Complete structure of the control of three-phase single-stage grid-tied PV system

Compensator. Initially, the irradiance level is $500W/m^2$ and then increased to $1000W/m^2$. As the irradiance increased active power demanded by the grid current is

decreased. During the unbalanced load conditions from $t = 0.4s$ to $t = 0.5s$ the grid current is sinusoidal. At $t = 0.65s$, the load has been suddenly decreased and hence grid current also decreased. The DC-link reference voltage is maintained at the reference DC-link voltage by the PI action and the reference voltage is estimated by the P & O MPPT algorithm.

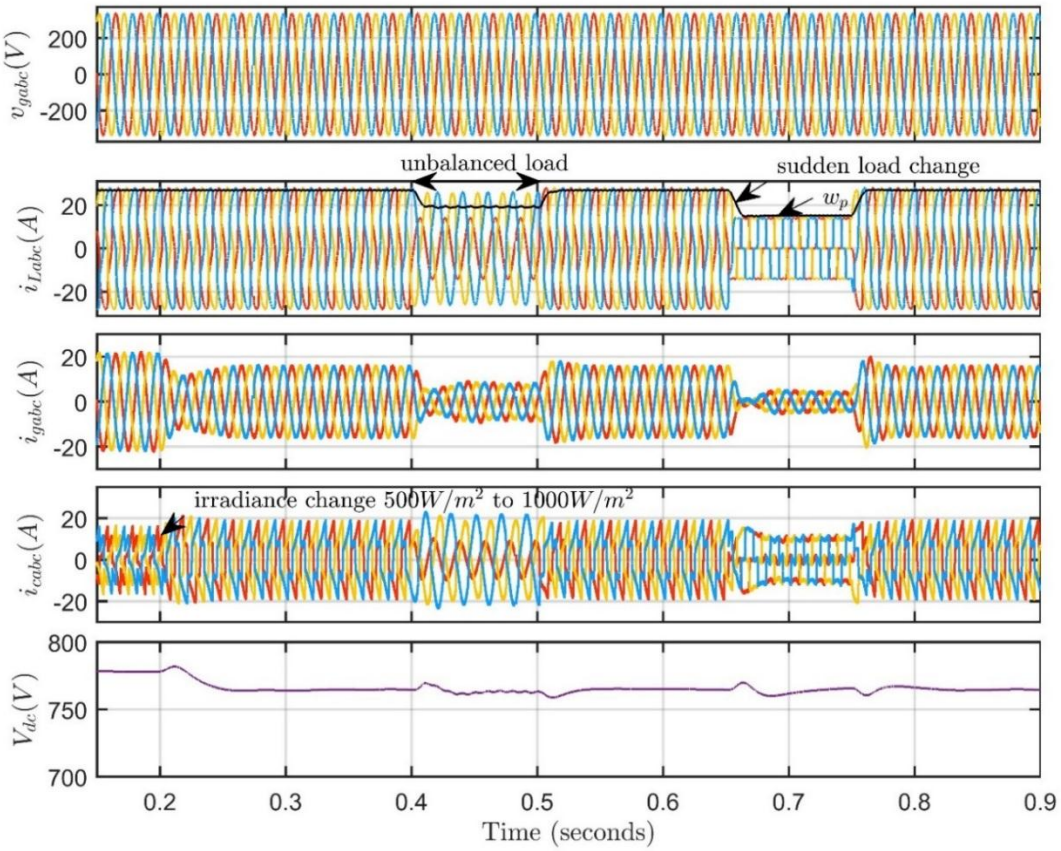


Fig. 8.5 : Closed -loop voltage and current performance with LMF control algorithm under variations

Fig. 8.6 shows the closed-loop power performance with the LMF control algorithm. Active and reactive power has been measured under different load and irradiance conditions. Initially, at $t = 0.16s$ when the irradiance level is $500W/m^2$ the load demand is 13.69kW and PV transfers 2.93kW to load. The extra power of 10.76kW required by the load is fulfilled by the distribution grid. At time $t = 0.35s$, when the irradiance level is $1000W/m^2$ power generated by PV via compensator is 5.71kW

and extra power demand of 7.98kW is supplied by the grid. While, during this condition, all the reactive power of 4.98kVar demanded by the load is supplied by the grid. During the unbalanced load condition, load demand is decreased to 9.44kW and in this case, 5.06 kW of active power is supplied by the PV via compensator, and the rest of the demand is fulfilled by the grid itself at $t = 0.73s$, when the total load is decreased to 7.74kW the compensator power is 5.42kW, and power delivered by the grid is 2.31kW. Reactive power demand also reduces to 0.926kVar and it is supplied by the compensator. The precise details of active power and reactive power at different irradiance and load conditions are tabulated in Table 8.2.

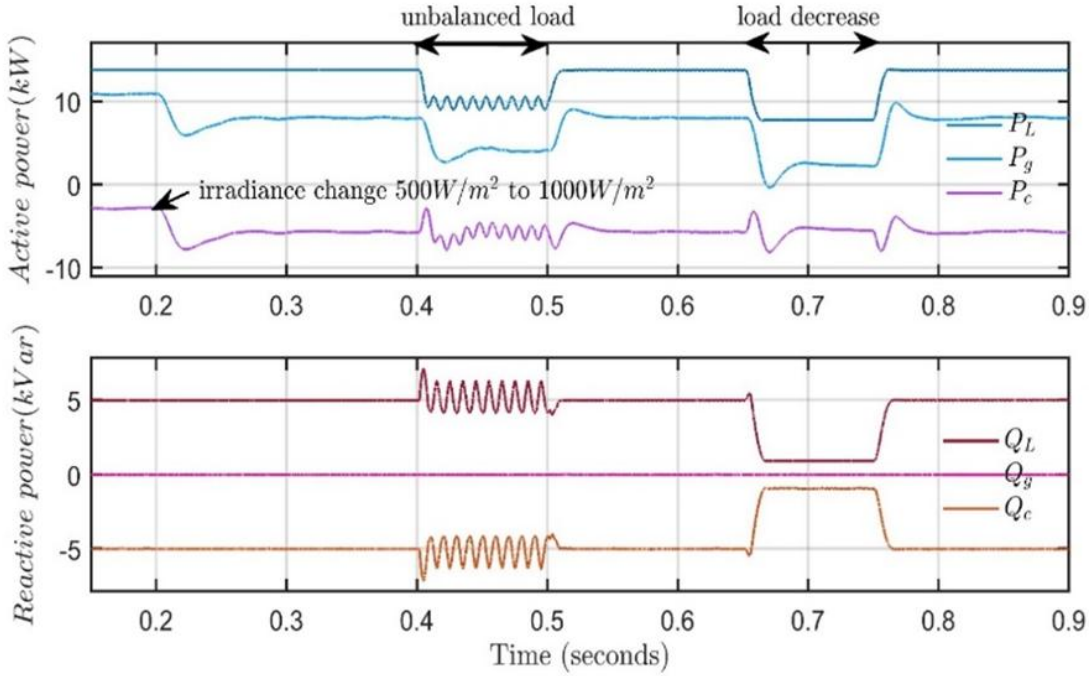


Fig. 8.6 : Closed-loop power performance with LMF algorithm

Fig. 8.7 shows the PV performance at different irradiance levels and the effect on PV output voltage due to the load side disturbances. Initially, the irradiance level is $500W/m^2$ and changed to $1000W/m^2$ at $t = 0.2s$. Power has also been almost doubled as the irradiance has been increased. The reference DC-link voltage has been estimated by the P&O MPPT algorithm. It is tracked precisely to the standard

maximum power point voltage at different irradiance levels which assure maximum power achieved from the PV array.

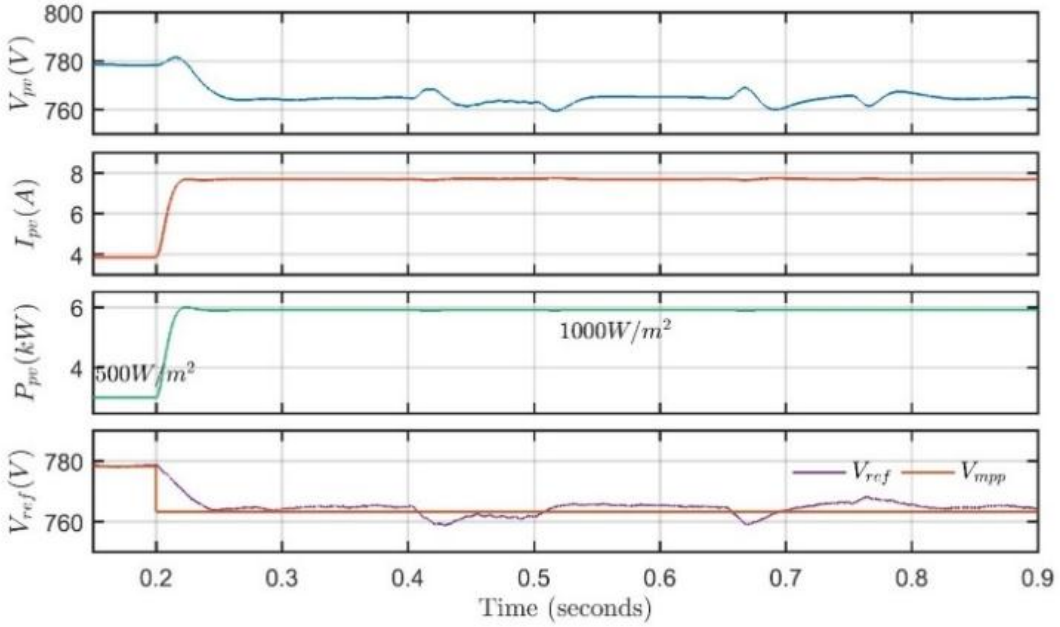


Fig. 8.7 : PV array output and reference DC-link voltage by P & O MPPT

Fig. 8.8 shows the THD analysis of the load current and the THD of grid current achieved by different control algorithms. THD of the load current is 14.18% as shown in Figure 8.8(a).

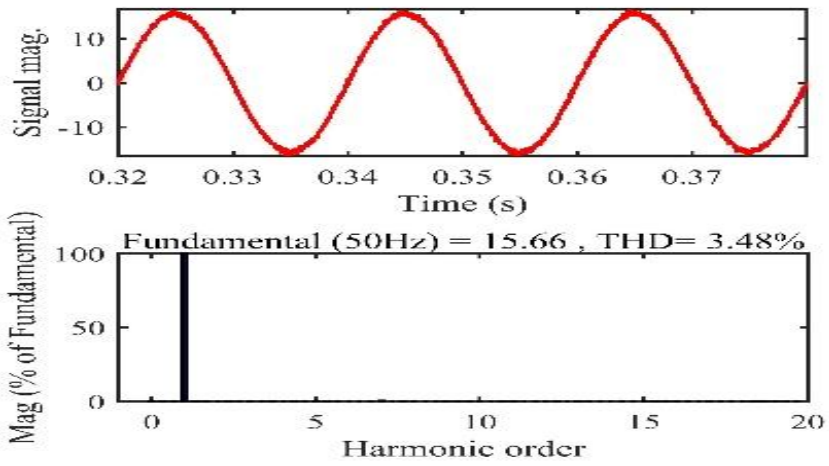


(a)

THD of the grid current obtained by LMS, Sign-error LMS, $\epsilon$ −NLMS and LMF is 3.48%, 3.71%, 3.51% and 3.44% respectively for the same non-linear load condition. Harmonic analysis of grid current achieved by different adaptive algorithms shows the LMF gives better results than other discussed adaptive algorithms.

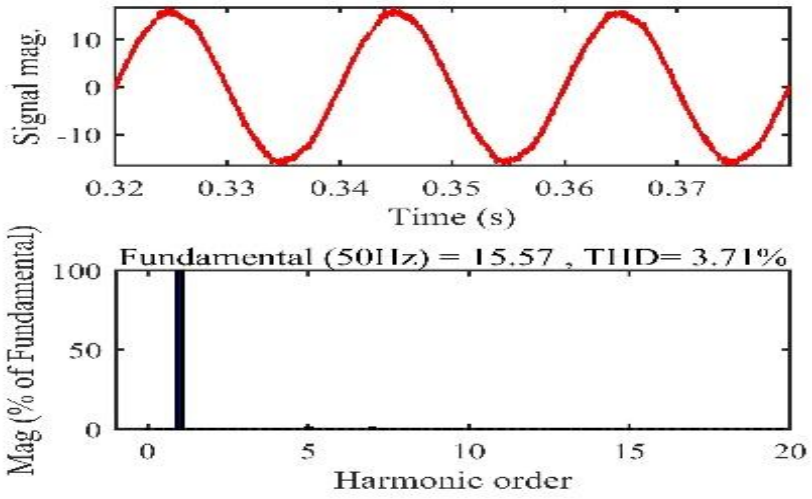


(b)

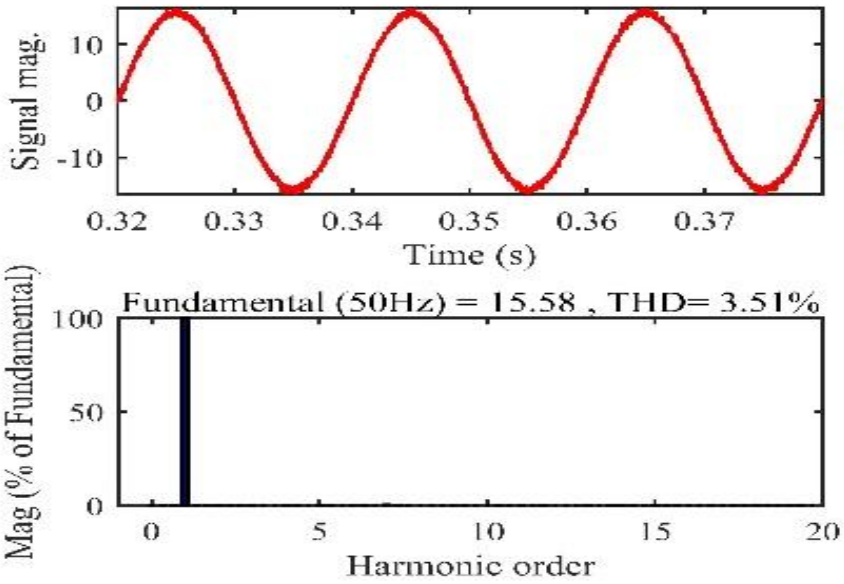


(c)

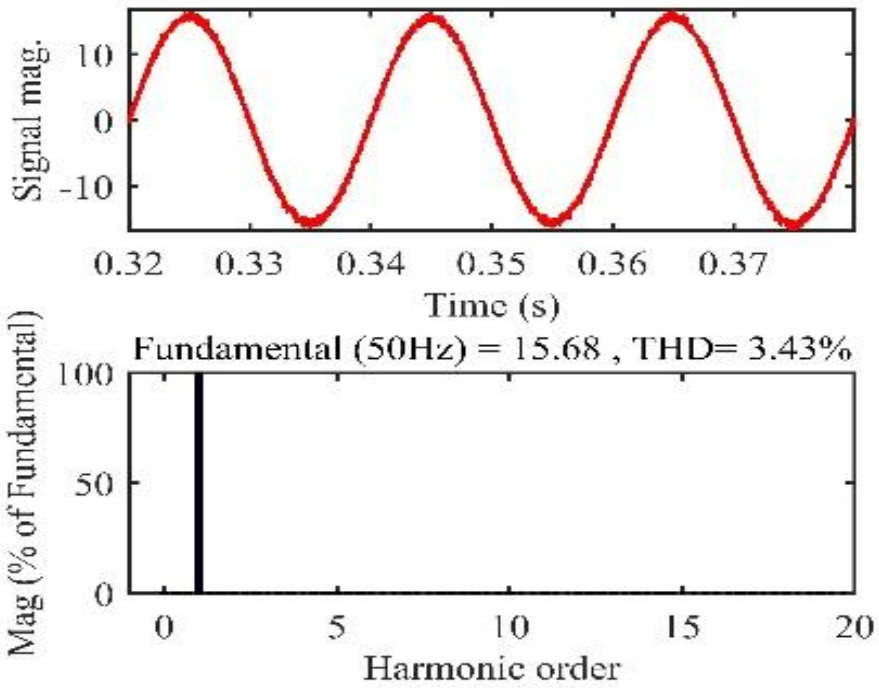


(d)

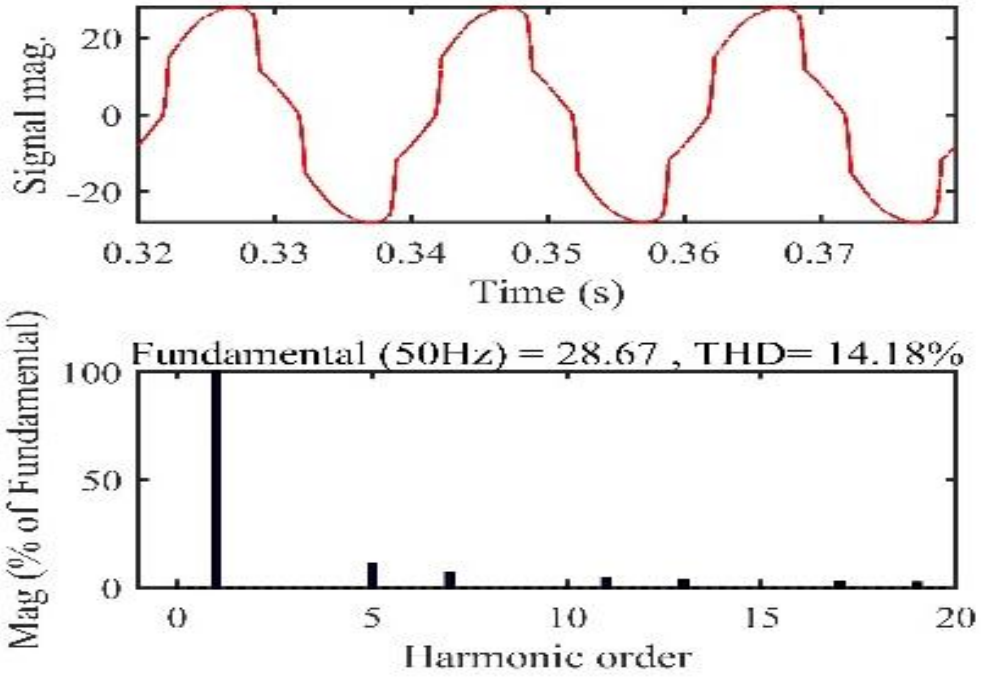


(e)

Fig. 8.8 THD analysis (a) load current (b) grid current by LMS (c) grid current by Sign-error LMS (d) grid current by $\epsilon$ −NLMS (b) grid current by LMF

## 8.5 CONCLUSION

This chapter has discussed and implemented the adaptive control algorithms specifically LMS, Sign-error LMS, $\epsilon$ −NLMS and LMF. These control algorithms have been used to track fundamental components from the three-phase non-linear load. These algorithms have been deployed for reactive power compensation and power quality improvement under different circumstances. The performance of adaptive algorithms has been compared during both dynamic and steady-state conditions. LMF shows a faster response during sudden load change than other adaptive algorithms. Ripples during steady-state conditions are also less than LMS, $\epsilon$-NLMS and Sign-error LMS. Sign-error LMS shows poorer performance in both steady-state and dynamic conditions. During the closed-loop operation, discussed adaptive control algorithms work as per standard IEEE-519 but LMF improves to pure sinusoidal grid current under non-linear conditions. As per the open-loop and closed-loop performance of discussed adaptive algorithms, LMF shows superior performance for a single-stage three-phase grid-tied PV system.

# Chapter 9

# MAIN CONCLUSIONS AND FUTURE SCOPE OF WORK

## 9.0 GENERAL

This thesis addresses PQ problems in Grid-interfaced solar systems and hybrid distributed systems, as well as ways to resolve them using both old and new control methods. For 3-phase grid-connected systems, PQ problems have been investigated in extensive detail in the MATLAB/SIMULINK environment. Simulink models based on MATLAB have been created and performed over PQ issues, including varying solar energy, changing wind speed, unbalanced loads, PF improvement, varying frequencies, and more. MPPT controller is incorporated for maximum power extraction from SPV system. For the study of the SAPF system with the new control technique, both linear and nonlinear load combinations were taken into account. The suggested controllers can be used for many purposes, like improving power quality, managing loads, compensating reactive power, controlling voltage, and more. The PI control, the FUZZY controller, and the Artificial Neural Network (ANN) are used to compare and evaluate the SAPF. The performance was studied by looking at the THD drop in source current and the time it took for the dc-link voltage to settle down. The PI, fuzzy, and ANN controls kept the dc-link voltage of the Shunt APF stable. It has been discussed the method to analyze the performance of filtering methods for distorted grid power and making synchronizing signals. Comparative analysis has been performed between the conventional controller and modern controller. The stochastic-gradient-based adaptive control algorithms have been discussed and employed for power quality enhancement in a PV integrated distribution

system. Several control algorithms have been successfully used for controlling the VSC to lower the PQ and get real power from the PV source.

## 9.1 MAIN CONCLUSIONS

The work of this thesis has been broadly classified into five parts. In the first part the SRF control method with ANN controller is presented and verified with three phase-four wire SAPF system in MATLAB/Simulink environment. Harmonic current and reactive power adjustment were made possible by the photovoltaic integrated SAPF. Comparisons between the SAPF modified with ANN controller and PI and FLC are made. The dc-link voltage of Shunt APF was maintained constant by the PI, FUZZY, and ANN controllers. As a result, the ANN controller-based SAPF delivers better performance than PI and fuzzy controllers. The proposed system using an ANN controller provides better sources of THD, which means the THD percentage is decreased from 7.07% to 4.97% whereas using the FLC, and the ANN controller is down to 4.12%.

In the second part of thesis work, a three-phase grid interfaced solar photovoltaic system (SPV) has been implemented and controlled by using SOGI-FLL based adaptive control scheme. This scheme has been effectively used to extraction of reference currents and providing gating pulses for VSC. The performance of control scheme for SPV system has been found satisfactory under linear and nonlinear loads as well as in load unbalancing conditions under varying system frequency. The proposed system along with ANN based adaptive control scheme has shown better performance in power quality enhancement. The effectiveness of feed-forward component has been presented for dynamic performance improvement. ANN controller is incorporated accurately with adaptive control scheme for converter loss component estimation. The THD has been reduced much better using ANN controller

ensuring good operation of shunt active power filter thus resulting in improved power quality. The proposed system was simulated using Matlab/simulink software and the results demonstrate the harmonic free source current.

In the third part of the thesis, the TOGI based fuzzy logic control technique has been designed for three phase grids interfaced solar- wind hybrid system. A TOGI control scheme has been presented for reference currents generation and providing pulses for 3-phase VSC. The FLC demonstrate dynamic performance than the conventional PI controller. The proposed system with TOGI controller is verified satisfactory for multifunctional objective such as power quality (PQ) enrichment, load balancing, reactive power compensation capability, etc. A brief comparative result has been presented of TOGI control scheme with conventional control schemes. The presented result shows that the designed controller is well executed irrespective of system intermittency, load disturbances and it provides excellent harmonic filtering capability compared to conventional controllers.

In the fourth part of the thesis, The Adaptive FOGI-FLL based control strategy has been described for three phase grid interfaced Solar PV system. The goal of this scheme is to harvest the greatest amount of electricity from solar PV arrays while simultaneously improving the power quality of the distribution network. The presented controller provides a satisfactory response for multifunctional objectives such as accurate frequency synchronization, lower and higher-order harmonics elimination, power quality (PQ) refinement, reactive power compensation capability, etc. Regardless of the system dynamic conditions or load disturbances, the proposed technique has strongly rejected harmonics. Frequency domain investigation has shown how successful the DC offset rejection capabilities and higher order harmonics rejection capabilities are in separating the fundamental component from load current.

Moreover, under fluctuating solar insolation, the MPO algorithm is utilized to collect the highest amount of electricity possible from a solar PV array while maintaining an efficiency of one hundred percent. Additionally, AFOGI-FLL outperforms the TOGI controller on a number of parameters, including DC offset elimination, dynamic performance, complexity, and lower and higher-order filtering capabilities. Furthermore, the AFOGI-FLL control scheme has a lower THD (1.10%) than the TOGI control scheme (1.23%). The proposed controller robustness can be verified with the hybrid energy sources. An FPGA-based HLL is used to validate the proposed method on a real-time simulator.

In the fifth part of the thesis, discussed and implemented the adaptive control algorithms specifically LMS, Sign-error LMS, $\epsilon -$NLMS and LMF. These control algorithms have been used to track fundamental components from the three-phase non-linear load. These algorithms have been deployed for reactive power compensation and power quality improvement under different circumstances. The performance of adaptive algorithms has been compared during both dynamic and steady-state conditions. LMF shows a faster response during sudden load change than other adaptive algorithms. Ripples during steady-state conditions are also less than LMS, $\epsilon$-NLMS and Sign-error LMS. Sign-error LMS shows poorer performance in both steady-state and dynamic conditions. During the closed-loop operation, discussed adaptive control algorithms work as per standard IEEE-519 but LMF improves to pure sinusoidal grid current under non-linear conditions. As per the open-loop and closed-loop performance of discussed adaptive algorithms, LMF shows superior performance for a single-stage three-phase grid-tied PV system.

## 9.2 FUTURE SCOPE OF WORK

In this thesis, a SAPF with a standard two-level VSC is examined. SAPF having three or multilevel VSC configuration can be used to mitigate PQ problems in grid interface solar PV system. For applications requiring larger voltage and power levels, multilevel VSC based SAPF can be utilised.

To get the maximum power from a solar PV system, the standard P&O and incremental conductance-based MPPT method is used. For MPPT, new and present-day control techniques can be used that work better than traditional control methods in terms of difficulty and number of uses. This study just covers three-phase grid-connected systems. The development of single-phase grid-connected systems allows for more efficient operation of power systems. Several renewable energy systems, including PV and wind, are linked to three-phase and single-phase distribution networks; these systems include biomass and hydro. In the thesis work fuzzy logic, ANN based technologies are applied for power quality enhancement. ANFIS technique and machine learning application, smart grid technologies, and optimization techniques on power quality in distribution systems can be applied. There is scope to implement this work through low-cost FPGA based DSP development.

Following are the publications in journals and conferences have been published.

## ❖ Publications in International Journals

[1] **Dinanath Prasad**, Narendra Kumar, Rakhi Sharma. "Grid Interfaced Solar-wind Hybrid Power Generating Systems Using Fuzzy based TOGI Control Technique for Power Quality Improvement", Journal Intelligent & Fuzzy Systems, vol. 42, no. 2, pp. 1127-1139, doi: 10.3233/JIFS-189777. 2022.

[2] **Dinanath Prasad,** Narendra Kumar, Rakhi Sharma "A novel ANROA based control approach for grid-tied multi-functional solar energy conversion system" Energy Reports, Volume 9, pages 2044-2057, ISSN 2352-4847, doi: 10.10.16/j.egyr.2023.01.039. 2023.

[3] **Dinanath Prasad**, Narendra Kumar, Rakhi Sharma "Adaptive fourth-order GI based controller for 3-phase grid-tied solar photovoltaic system" IETE Journal of research, doi: 10.1080/03772063.2024.2389188. 2024, (In press).

## ❖ Publications in National/International Conferences

[1] **Dinanath Prasad**, Narendra Kumar and Rakhi Sharna, "Modeling and Simulation of Microgrid Solar Photovoltaic System with Energy Storage" 2018, 2nd IEEE International Conference on Power Electronics, Intelligent Control and Energy Systems (ICPEICES), pp. 623-629, doi: 10.1109/ICPEICES.2018.8897355. 2018.

[2] **Dinanath Prasad** and Narendra Kumar, ANN based Adaptive SOGI-FLL controller for multifunctional grid tied solar conversion system, 35th Indian engineering congress, Page: 713-723, 978-81-950662-0-9. Dec-2020.

[3] **Dinanath Prasad**, Narendra Kumar and Rakhi Sharma, Shunt Active Power Filter based on Synchronous Reference Frame Theory Connected to SPV for Power Quality Enrichment, 2nd International conference on machine learning, Advances in computing, Renewable Energy and communication, MARC-2020, 17-18 Dec 2020.

[4] **Dinanath Prasad**, Narendra Kumar and Rakhi Sharma, "Adaptive Control Technique for Grid Integrated PV Generating System for Power Quality Enrichment" TUBA World Conference on Energy Science and Technology (TUBA WCEST-2021) 8-12 August 2021.

[5] **Dinanath Prasad**, Narendra Kumar and Rakhi Sharma, "SRF theory-based shunt active power filter for power quality improvement in grid-interfaced solar photovoltaic system" Journal of Physics: Conference Series, AKGEC 2023, Vol. 2570, doi: 10.1088/1742-6596/2570/1/012024. Aug 2023.

[6] **Dinanath Prasad**, Narendra Kumar and Rakhi Sharma, "Adaptive fourth order based controller for grid-interfaced three-phase solar PV system for power quality enrichment" presented in Springer nature's International conference SIGMAA-2023, held on 15th-16th December 2023.

# REFERENCES


[1] BP Statistical Review of World Energy, ⟨bp.com/statistical review⟩; June 2020. 69th edition.

[2] N.L. Panwar, S.C. Kaushik, Surendra Kothari, "Role of renewable energy sources in environmental protection: A review", Renewable and Sustainable Energy Reviews, Volume 15, Issue 3, 2011, Pages 1513-1524, ISSN 1364-0321, https://doi.org/10.1016/j.rser.2010.11.037.

[3] Omar Ellabban, Haitham Abu-Rub, Frede Blaabjerg, Renewable energy resources: Current status, future prospects and their enabling technology, Renewable and Sustainable Energy Reviews, Volume 39, 2014, Pages 748-764, ISSN 1364-0321, https://doi.org/10.1016/j.rser.2014.07.113.

[4] Chen, G.Q. & Yang, Qing & Zhao, Y.H. & Wang, Z.F. "Non-renewable energy cost and greenhouse gas emissions of a 1.5 Â MW solar power tower plant in China". Renewable and Sustainable Energy Reviews. 2011, 15. 1961-1967. 10.1016/j.rser.2010.12.014.

[5] Santosh Singh Raghuwanshi & Rajesh Arya "Renewable energy potential in India and future agenda of research", International Journal of Sustainable Engineering, 12:5, 2019, 291-302, DOI: 10.1080/19397038.2019.1602174.

[6] Roy, P.; He, J.; Zhao, T.; Singh, Y.V. Recent Advances of Wind-Solar Hybrid Renewable Energy Systems for Power Generation: A Review. IEEE Open J. Ind. Electron. Soc. 2022, 3, 81–104.

[7] Nema, P.; Nema, R.K.; Rangnekar, S. A Current and Future State of Art Development of Hybrid Energy System Using Wind and PV-Solar: A Review. Renew. Sustain. Energy Rev. 2008, 13, 2096–2103.

[8] Rashid Al Badwawi, Mohammad Abusara & Tapas Mallick (2015) A Review of Hybrid Solar PV and Wind Energy System, Smart Science, 3:3, 127-138, DOI: 10.1080/23080477.2015.11665647.

[9] Moslem Uddin, Huadong Mo, Daoyi Dong, Sondoss Elsawah, Jianguo Zhu, Josep M. Guerrero, Microgrids: "A review, outstanding issues and future trends, Energy Strategy Reviews", Volume 49, 2023, 101127, ISSN 2211-467X, https://doi.org/10.1016/j.esr.2023.101127.

[10] Thirunavukkarasu, Gokul & Seyedmahmoudian, Mehdi & Jamei, Elmira & Horan, B. & Mekhilef, Saad & Stojcevski, Alex. "Role of optimization techniques in microgrid energy management systems—A review". Energy Strategy Reviews. 43., 2022, 100899. 10.1016/j.esr.2022.100899.

[11] A. Cagnano, E. De Tuglie, P. Mancarella, Microgrids: Overview and guidelines for practical implementations and operation, Applied Energy, Volume 258, 2020, 114039, ISSN 0306-2619, https://doi.org/10.1016/j.apenergy.2019.114039.

[12] S. Parhizi, H. Lotfi, A. Khodaei and S. Bahramirad, "State of the Art in Research on Microgrids: A Review," in IEEE Access, vol. 3, pp. 890-925, 2015, doi: 10.1109/ACCESS.2015.2443119.

[13] W.A. Lidula, A.D. Rajapakse, Microgrids research: A review of experimental microgrids and test systems, Renewable and Sustainable Energy Reviews, Volume 15, Issue 1, 2011, Pages 186-202, ISSN 1364-0321, https://doi.org/10.1016/j.rser.2010.09.041.

[14] Hatziargyriou, Nikos & Asano, Hiroshi & Iravani, Reza & Marnay, Chris. "Microgrids". Power and Energy Magazine, IEEE. 5. 78 – 94, 2007, 10.1109/MPAE.2007.376583.

[15] O. Palizban and K. Kauhaniemi, "Microgrid control principles in island mode operation," 2013 IEEE Grenoble Conference, Grenoble, France, 2013, pp. 1-6, doi: 10.1109/PTC.2013.6652453.

[16] Adrian Nocoń, Stefan Paszek, "Transient states and island mode operation of industrial electricity networks", 2016 13th Selected Issues of Electrical Engineering and Electronics (WZEE), pp.1-6, 2016.

[17] X. Liu, T. Zhao, H. Deng, P. Wang, J. Liu and F. Blaabjerg, "Microgrid Energy Management with Energy Storage Systems: A Review," in CSEE Journal of Power and Energy Systems, vol. 9, no. 2, pp. 483-504, March 2023, doi: 10.17775/CSEEJPES.2022.04290.

[18] S. H. Yao, P. Wang and T. Y. Zhao, "Transportable energy storage for more resilient distribution systems with multiple microgrids", *IEEE Transactions on Smart Grid*, vol. 10, no. 3, pp. 3331-3341, May 2019.

[19] C. Q. Ju, P. Wang, L. Goel and Y. Xu, "A two-layer energy management system for microgrids with hybrid energy storage considering degradation costs", IEEE Transactions on Smart Grid, vol. 9, no. 6, pp. 6047-6057, Nov. 2018.

[20] P. Lyu, X. J. Liu, J. Qu, J. T. Zhao, Y. T. Huo, Z. G. Qu, et al., "Recent advances of thermal safety of lithium-ion battery for energy storage", *Energy Storage Materials*, vol. 31, pp. 195-220, Oct. 2020.

[21] X. Liu, P. Wang and P. C. Loh, "A hybrid AC/DC microgrid and its coordination control", IEEE Transactions on Smart Grid, vol. 2, no. 2, pp. 278-286, Jun. 2011.

[22] Thomas Navidi, Abbas El Gamal, Ram Rajagopal, coordinating distributed energy resources for reliability can significantly reduce future distribution grid upgrades and peak load, Joule, Volume 7, Issue 8, 2023, Pages 1769-1792, ISSN 2542-4351, https://doi.org/10.1016/j.joule.2023.06.015.

[23] B. Singh, A. Chandra, K. Al-Haddad, "Power Qulaity: Problems and mitigation Techniques", John Wiley and Sons, U.K., 2015.

[24] E. Acha, V.G. Agelids, O. Anaya-Lara, T.J.E. Miller, "Power Electronic Control in Electric Systems", Newness Power engineering series, 1st Edition, Oxford, 2002.

[25] G. Arindam and L. Gerard, "Power Quality Enhancement using Custom Power Devices", Springer International Edition ed. Delhi, India: Springer, 2009.

[26] Antonio Moreno-Munoz, "Power Quality: Mitigation Technologies in a Distributed Environment", Springer-Verlag London limited, London, 2007.

[27] Ewald F. Fuchs and Mohammad A. S. Mausoum, Power Quality in Power Systems and Electric Machines", Elsevier Academic Press, London, UK, 2008.

[28] Sheldon Wang, Ernuel Tong, Isaac Sekanyo and Elijah Portmann, "On the state-of-the -art of solar, wind, and Other Green Energy Resources and Their Respective Storage Systems" *Eng* 2023, *4*(1), 857-883; https://doi.org /10.3390/eng4010052

[29] Ahmad Zahedi, Sustainable Power Supply Using Solar Energy and Wind Power Combined with Energy Storage, Energy Procedia, Volume 52, 2014, Pages 642-650, ISSN 1876-6102, https://doi.org/10.1016/j.egypro.2014.07.120.

[30] Liu, Quanhua & Miao, Qinxian & Liu, Jue & Yang, Wenli. (2009). Solar and wind energy resources and prediction. Journal of Renewable and Sustainable Energy. 1. 10.1063/1.3168403.

[31] M. Yao, I. A. Hiskens and J. L. Mathieu, "Mitigating Voltage Unbalance Using Distributed Solar Photovoltaic Inverters," in IEEE Transactions on Power Systems, vol. 36, no. 3, pp. 2642-2651, May 2021, doi: 10.1109/TPWRS.2020.3039405.

[32] Tathagata Sarkar, Ankur Bhattacharjee, Hiranmay Samanta, Konika Bhattacharya and Hiranmay Saha, "Optimal design and implementation of solar PV-wind-biogas-VRFB storage integrated smart hybrid microgrid for ensuring zero loss of power supply probability" Energy Conversion and Management, Volume 191, 2019, Pages 102-118, ISSN 0196-8904, https://doi.org /10.1016/j.enconman.2019.04.025.

[33] Eric Galvan, Paras Mandal and Yuanrui Sang, "Networked microgrids with roof-top solar PV and battery energy storage to improve distribution grids resilience to natural disasters, International Journal of Electrical Power & Energy Systems, Volume 123, 2020, 106239, ISSN 0142-0615, https://doi.org/10.1016 /j.ijepes.2020.106239.

[34] S. Devassy and B. Singh, "Performance Analysis of Solar PV Array and Battery Integrated Unified Power Quality Conditioner for Microgrid Systems," in IEEE Transactions on Industrial Electronics, vol. 68, no. 5, pp. 4027-4035, May 2021, doi: 10.1109/TIE.2020.2984439.

[35] T. Tewari, A. Mohapatra and S. Anand, "Coordinated Control of OLTC and Energy Storage for Voltage Regulation in Distribution Network with High PV Penetration," in IEEE Transactions on Sustainable Energy, vol. 12, no. 1, pp. 262-272, Jan. 2021, doi: 10.1109/TSTE.2020.2991017.

[36] V. Veerasamy et al., "LSTM Recurrent Neural Network Classifier for High Impedance Fault Detection in Solar PV Integrated Power System," in IEEE Access, vol. 9, pp. 32672-32687, 2021, doi: 10.1109/ACCESS.2021.3060800.

[37] Wang, Jingbo & Zhang, Xiaoshun & Tao, YU & Yao, Wei & Shu, Hongchun & Zeng, Fang & Sun, Liming. "Comprehensive overview of meta-heuristic algorithm applications on PV cell parameter identification". Energy Conversion and Management. 208. 2020, 112595. 10.1016/j.enconman.2020.112595.

[38] Zhu, L., Zhang, M., Xu, J. et al. Single-junction organic solar cells with over 19% efficiency enabled by a refined double-fibril network morphology. Nat. Mater. 21, 656–663, 2022, https://doi.org/10.1038/s41563-022-01244-y.

[39] Abdelkader Abbassi, Rabeh Abbassi, Ali Asghar Heidari, Diego Oliva, Huiling Chen, Arslan Habib, Mohamed Jemli, Mingjing Wang, Parameters identification of photovoltaic cell models using enhanced exploratory salp chains-based approach, Energy, Volume 198, 2020, 117333, ISSN 0360-5442, https://doi.org /10.1016/j.energy.2020.117333.

[40] Fatima Belabbes, Daniel T. Cotfas, Petru A. Cotfas, Mourad Medles, Using the snake optimization metaheuristic algorithms to extract the photovoltaic cells parameters, Energy Conversion and Management, Volume 292, 2023, 117373, ISSN 0196-8904, https://doi.org/10.1016/j.enconman.2023.117373.

[41] Ramadan, A., Kamel, S., Korashy, A. et al. Photovoltaic Cells Parameter Estimation Using an Enhanced Teaching–Learning-Based Optimization Algorithm. Iran J Sci Technol Trans Electr Eng 44, 767–779, 2020, https://doi.org/10.1007/s40998-019-00257-9.

[42] Oscar Pinzón-Quintero, Daniel Gaviria-Ospina, Alejandro, Rusber Rodríguez-Velásquez, German Osma-Pinto, Assessment of power quality parameters and indicators at the point of common coupling in a low voltage power grid with photovoltaic generation emulated, Electric Power Systems Research, Volume 203, 2022, 107679, ISSN 0378-7796, https://doi.org /10.1016/ j.epsr. 2021. 107679.

[43] Rajendran Boopathi, Vairavasundaram Indragandhi, “Comparative analysis of control techniques using a PV-based SAPF integrated grid system to enhance power quality, e-Prime - Advances in Electrical Engineering, Electronics and Energy, Volume 5, 2023, 100222, ISSN 2772-6711, https://doi.org /10.1016/j.prime.2023.100222.

[44] S. Malathi, J. Jayachandran, “FPGA implementation of NN based LMS–LMF control algorithm in DSTATCOM for power quality improvement, Control Engineering Practice”, Volume 98, 104378, ISSN 0967-0661, https://doi.org /10.1016/j.conengprac 2020, 104378.

[45] A. Khandelwal and P. Neema, "State of Art for Power Quality Issues in PV Grid Connected System," 2019 International Conference on Nascent Technologies in Engineering (ICNTE), Navi Mumbai, India, 2019, pp. 1-4, doi: 10.1109/ICNTE44896.2019.8945829.

[46] M. Farhoodnea, A. Mohamed, H. Shareef and H. Zayandehroodi, "Power quality impact of grid-connected photovoltaic generation system in distribution networks," 2012 IEEE Student Conference on Research and Development (SCOReD), Pulau Pinang, Malaysia, 2012, pp. 1-6, doi: 10.1109 /SCOReD.2012.6518600.

[47] A. F. Abdul Kadir, A. Mohamed and H. Shareef, "Harmonic impact of different distributed generation units on low voltage distribution system," 2011 IEEE International Electric Machines & Drives Conference (IEMDC), Niagara Falls, ON, Canada, 2011, pp. 1201-1206, doi: 10.1109/IEMDC.2011.5994774.

[48] O. P. Mahela, B. Khan, H. H. Alhelou and P. Siano, "Power Quality Assessment and Event Detection in Distribution Network with Wind Energy

Penetration Using Stockwell Transform and Fuzzy Clustering," in IEEE Transactions on Industrial Informatics, vol. 16, no. 11, pp. 6922-6932, Nov. 2020, doi: 10.1109/TII.2020.2971709.

[49] Shoaib, Muhammad & Siddiqui, I. & Khan, Shamim & Alhems, Luai. "Assessment of wind energy potential using wind energy conversion system". Journal of Cleaner Production. 2019, 216. 10.1016/j.jclepro.2019.01.128.

[50] Poul Alberg Østergaard, Neven Duic, Younes Noorollahi, Hrvoje Mikulcic, Soteris Kalogirou, Sustainable development using renewable energy technology, Renewable Energy, Volume 146, 2020, Pages 2430-2437, ISSN 0960-1481, https://doi.org/10.1016/j.renene.2019.08.094.

[51] Shouxiang Wang, Haiwen Chen, "A novel deep learning method for the classification of power quality disturbances using deep convolutional neural network" Applied Energy, Vol. 235, 2019, Pages 1126-1140, ISSN 0306-2619, https://doi.org/10.1016/j.apenergy. 2018.09.160.

[52] Sherif M. Ismael, Shady H.E. Abdel Aleem, Almoataz Y. Abdelaziz, Ahmed F. Zobaa, State-of-the-art of hosting capacity in modern power systems with distributed generation, Renewable Energy, Volume 130, 2019, Pages 1002-1020, ISSN 0960-1481, https://doi.org/10.1016/j.renene.2018.07.008.

[53] P. Rajesh, Francis H. Shajin, B. Rajani, " An optimal hybrid control scheme to achieve power quality enhancement in micro grid connected system" 2022, https://doi.org/10.1002/jnm.3019.

[54] Ahilan, T., Suresh, P., Cheren, S.E., Ramya, G. "Power Quality Enhancement Using Interline Dynamic Voltage Restorer in Renewable Energy System". In: Subramani, C., Vijayakumar, K., Dakyo, B., Dash, S.S. (eds) Proceedings of International Conference on Power Electronics and Renewable Energy Systems. Lecture Notes in Electrical Engineering, vol 795. Springer, 2022, https://doi.org/10.1007/978-981-16-4943-1_47.

[55] S. R. Arya, K. D. Mistry and P. Kumar, "Least Mean Mixed Norm Square/Fourth Adaptive Algorithm with Optimized FOPID Gains for Voltage Power Quality Mitigation," in IEEE Journal of Emerging and Selected Topics in Power Electronics, vol. 11, no. 3, pp. 2632-2640, June 2023, doi: 10.1109/JESTPE.2023.3240712.

[56] Xiaomin Xu, Dongxiao Niu, Luyao Peng, Shipeng Zheng, Jinpeng Qiu, "Hierarchical multi-objective optimal planning model of active distribution network considering distributed generation and demand-side response, Sustainable Energy Technologies and Assessments, Volume 53, Part A, 2022, 102438, ISSN 2213-1388, https://doi.org/10.1016/j.seta.2022.102438.

[57] Yichen Liu, Dragan Ćetenović, Haiyu Li, Elena Gryazina, Vladimir Terzija, "An optimized multi-objective reactive power dispatch strategy based on improved genetic algorithm for wind power integrated systems," International Journal of Electrical Power & Energy Systems, Volume 136, 2022, 107764, ISSN 0142-0615, https://doi.org/10.1016/j.ijepes.2021.107764.

[58] Mohammed Hamouda Ali, Salah Kamel, Mohamed H. Hassan, Marcos Tostado-Véliz, Hossam M. Zawbaa, "An improved wild horse optimization algorithm for reliability based optimal DG planning of radial distribution

networks, Energy Reports, Volume 8, 2022, Pages 582-604, ISSN 2352-4847, https://doi.org /10.1016/j.egyr.2021.12.023.

[59] Seydali Ferahtia, Ali Djeroui, Hegazy Rezk, Azeddine Houari, Samir Zeghlache, Mohamed Machmoum, "Optimal control and implementation of energy management strategy for a DC microgrid," Energy, Volume 238, Part B, 2022, 121777, ISSN 0360-5442, https://doi.org/10.1016/j.energy.2021.121777.

[60] Jayant Sharma, C.K. Sundarabalan, R. Sitharthan, C. Balasundar, N.S. Srinath, "Power quality enhancement in microgrid using adaptive affine projection controlled medium voltage distribution static compensator," Sustainable Energy Technologies and Assessments, Volume 52, Part B, 2022, 102185, ISSN 2213-1388, https://doi.org/10.1016/j.seta.2022.102185.

[61] F.F Ewald and A. S. M. Mohammad, "Power Quality in Power Systems and Electrical Machines. London, U.K.: Elsevier Academic Press, 2008.

[62] N. G. Hingorani, L. Gyugyi, 1999, ''Understanding FACTS: Concepts and Technology of Flexible AC Transmission System, "IEEE Press, New York.

[63] K. R. Padiyar, "FACTS Controllers in Power Transmission and Distribution," New Age International (P) Limited, Publishers, New Delhi, 2007.

[64] M. Thamizh Thentral, R. Palanisamy, S. Usha, Mohit Bajaj, Hossam M. Zawbaa, Salah Kamel, Analysis of Power Quality issues of different types of household applications, Energy Reports, Volume 8, 2022, Pages 5370-5386, ISSN 2352-4847, https://doi.org/10.1016/j.egyr.2022.04.010.

[65] A. Cavallini and G. C. Montanari, "Compensation strategies for shunt active-filter control," in IEEE Transactions on Power Electronics, vol. 9, no. 6, pp. 587-593, Nov. 1994, doi: 10.1109/63.334773.

[66] H. Pinheiro and C. A. Zeferino, "A simple control strategy for shunt power line conditioner with inductive energy storage," Proceedings of IECON '93 - 19th Annual Conference of IEEE Industrial Electronics, Maui, HI, USA, 1993, pp. 1093-1098 vol.2, doi: 10.1109/IECON.1993.339122.

[67] S. K. Kadem, M. Basu and M.F. Conlon, "Harmonic power compensation capacity of shunt active power filter and its relationship with design paraments," in IET Power Electronics, vol. 7, no.2, pp. 418-430, February 2014. Doi: 10.1049/iet-pel.2013.0098.

[68] B. Singh, P. Jayaprakash and D. P. Kothari, "Isolated H-bridge VSC Based 3-phase 4- wire DSTATCOM for power quality improvement, "2008 IEEE International Conference on Sustainable Energy Technologies, Singapore, 2008, pp. 366-371. Doi: 10.1109/ICSET.2008.4747034.

[69] S. Kumar, B. Singh, "Control of 3 Leg VSC Based 3 Phase 4 Wire DSTATCOM using Modified Instantaneous Symmetrical Component Theory,'' in International Journal of Automation and Power engineering (IJAPE) Vol. 2 No. 6, September 2013.

[70] M. I. M. Montero, E. R. Cadaval and F. B. Gonzalez, "Comparison of Control Strategies for Shunt Active Power Filters in Three-Phase Four-Wire Systems," in IEEE Transactions on Power Electronics, vol. 22, no. 1, pp. 229-236, Jan. 2007, doi: 10.1109/TPEL.2006.886616.

[71] San-Yi Lee, Wei-Nan Chang and Chi-Jui Wu, "A compact algorithm for three-phase three-wire system reactive power compensation and load balancing," Proceedings 1995 International Conference on Energy Management and Power Delivery EMPD '95, Singapore, 1995, pp. 358-363 vol.1, doi: 10.1109/EMPD.1995.500753

[72] C. A. Quinn, N. Mohan and H. Mehta, "A four-wire, current-controlled converter provides harmonic neutralization in three-phase, four-wire systems," Proceedings Eighth Annual Applied Power Electronics Conference and Exposition, San Diego, CA, USA, 1993, pp. 841-846, doi: 10.1109/APEC.1993.290773.

[73] M. Aredes and E. H. Watanabe, "New control algorithms for series and shunt three-phase four-wire active power filters," in IEEE Transactions on Power Delivery, vol. 10, no. 3, pp. 1649-1656, July 1995, doi: 10.1109/61.400952.

[74] R. Panigrahi, P.C. Panda and B. D. Subudhi, "Comparison of performances of hysteresis and dead-beat controllers in active power filtering, "2012 IEEE Third International Conference on Sustainable Energy Technology (ICSET), Kathmandu, 2012, pp. 287-292. doi: 10.1109/ICSET.2012.6357413.

[75] P. F. Wojciak and D. A. Torrey, "The design and implementation of active power filters based on variable structure system concepts," Conference Record of the 1992 IEEE Industry Applications Society Annual Meeting, Houston, TX, USA, 1992, pp. 850-857 vol.1, doi: 10.1109/IAS.1992.244308.

[76] Elango Sundaram, Manikandan Venugopal, "On design and implementation of three phase three level shunt active power filter for harmonic reduction using synchronous reference frame theory, International Journal of Electrical Power & Energy Systems, Volume 81, Pages 40-47, ISSN 0142-0615, https://doi.org/10.1016 /j.ijepes.2016.02.008.

[77] C. E. Lin, C. L. Chen and C. L. Huang, "Calculating approach and implementation for active filters in unbalanced three-phase system using synchronous detection method," Proceedings of the 1992 International Conference on Industrial Electronics, Control, Instrumentation, and Automation, San Diego, CA, USA, 1992, pp. 374-380 vol.1, doi: 10.1109/IECON.1992.254577.

[78] M. Cirrincione, M. Pucci, G. Vitale and A. Miraoui, "Current Harmonic Compensation by a Single-Phase Shunt Active Power Filter Controlled by Adaptive Neural Filtering," in IEEE Transactions on Industrial Electronics, vol. 56, no. 8, pp. 3128-3143, Aug. 2009, doi: 10.1109/TIE.2009.2022070.

[79] D. Wenjin and H. Taiyang, "Design of Single-phase Shunt Active Power Filter Based on ANN," 2007 IEEE International Symposium on Industrial Electronics, Vigo, Spain, 2007, pp. 770-774, doi: 10.1109/ISIE.2007.4374694.

[80] A. Timbus, M. Liserre, R. Teodorescu and F. Blaabjerg, "Synchronization methods for three phase distributed power generation systems - An overview and evaluation," 2005 IEEE 36th Power Electronics Specialists Conference, Dresden, Germany, 2005, pp. 2474-2481, doi: 10.1109/PESC.2005.1581980.

[81] K. M. Tsang , W. L. Chan & Xin Tang tangxin, "Multi-level Shunt Active Power Filter Using Modular Cascade H-bridge and Delay Firing", Electric

Power Components and Systems, 41:6, 605-618, DOI: 10.1080 /15325008. 2013.763307.

[82] V. B. Bhavaraju and P. N. Enjeti, "Analysis and design of an active power filter for balancing unbalanced loads," in IEEE Transactions on Power Electronics, vol. 8, no. 4, pp. 640-647, Oct. 1993, doi: 10.1109/63.261037.

[83] L. Malesani, L. Rossetto and P. Tenti, "Active filter for reactive power and harmonics compensation," 1986 17th Annual IEEE Power Electronics Specialists Conference, Vancouver, BC, Canada, 1986, pp. 321-330, doi: 10.1109/PESC.1986.7415577.

[84] C. A. Quinn and N. Mohan, "Active filtering of harmonic currents in three-phase, four-wire systems with three-phase and single-phase nonlinear loads," [Proceedings] APEC '92 Seventh Annual Applied Power Electronics Conference and Exposition, Boston, MA, USA, 1992, pp. 829-836, doi: 10.1109 /APEC.1992.228328.

[85] P. Enjeti, W. Shireen, P. Packebush and I. Pitel, "Analysis and design of a new active power filter to cancel neutral current harmonics in three phase four wire electric distribution systems," Conference Record of the 1993 IEEE Industry Applications Conference Twenty-Eighth IAS Annual Meeting, Toronto, ON, Canada, 1993, pp. 939-946 vol.2, doi: 10.1109/IAS.1993.299011.

[86] S. Saetieo, R. Devaraj and D. A. Torrey, "The design and implementation of a three-phase active power filter based on sliding mode control," in IEEE Transactions on Industry Applications, vol. 31, no. 5, pp. 993-1000, Sept.-Oct. 1995, doi: 10.1109/28.464511.

[87] A. Cavallini and G. C. Montanari, "Compensation strategies for shunt active-filter control," in IEEE Transactions on Power Electronics, vol. 9, no. 6, pp. 587-593, Nov. 1994, doi: 10.1109/63.334773.

[88] Uceda, J., Aldana, F., and Martinez, P. “Active filters for static power converters”, Proceedings of the IEEE, 130(5), 347–354, 1983.

[89] P. Enjeti, W. Shireen and I. Pitel, "Analysis and design of an active power filter to cancel harmonic currents in low voltage electric power distribution systems," Proceedings of the 1992 International Conference on Industrial Electronics, Control, Instrumentation, and Automation, San Diego, CA, USA, 1992, pp. 368-373 vol.1, doi: 10.1109/IECON.1992.254578.

[90] Kawahira, H., Nakamura, T., Nakazawa, S., and Nomura, M. “Active power filter”, IPEC-Tokyo, Institute of Electrical Engineers of Japan, pp. 981–992, 1983.

[91] Hsu, C.Y. and Wu, H.Y. “A new single-phase active power filter with reduced energy storage capacity”, IEEE Proceedings: Electric Power Applications, 143(1), 25–30, 1996.

[92] Mohan, N., Peterson, H.A., Long, W.F. et al. “Active filters for AC harmonic suppression”, IEEE PES Winter Meeting, pp. 168–174, 1977.

[93] H. Akagi, A. Nabae and S. Atoh, "Control Strategy of Active Power Filters Using Multiple Voltage-Source PWM Converters," in IEEE Transactions on Industry Applications, vol. IA-22, no. 3, pp. 460-465, May 1986, doi: 10.1109/TIA.1986.4504743.

[94] H. Akagi, "Trends in active power line conditioners," in IEEE Transactions on Power Electronics, vol. 9, no. 3, pp. 263-268, May 1994, doi: 10.1109/63.311258.

[95] Choe, G.H., Wallace, A.K., and Park, M.H. “Control technique of active power filter for harmonic elimination, reactive power control”, IEEE-IAS Annual Meeting Record, pp. 859–866, 1988.

[96] F. Z. Peng, H. Akagi and A. Nabae, "A new approach to harmonic compensation in power systems-a combined system of shunt passive and series active filters," in IEEE Transactions on Industry Applications, vol. 26, no. 6, pp. 983-990, Nov.-Dec. 1990, doi: 10.1109/28.62380.

[97] H. Pinheiro and C. A. Zeferino, "A simple control strategy for shunt power line conditioner with inductive energy storage," Proceedings of IECON '93 - 19th Annual Conference of IEEE Industrial Electronics, Maui, HI, USA, 1993, pp. 1093-1098 vol.2, doi: 10.1109/IECON.1993.339122.

[98] A. Nakajima et al., "Development of active filter with series resonant circuit," PESC '88 Record., 19th Annual IEEE Power Electronics Specialists Conference, Kyoto, Japan, 1988, pp. 1168-1173 vol.2, doi: 10.1109/PESC.1988.18258.

[99] S. Fukuda and M. Yamaji, "Design and characteristics of active power filter using current source converter," Conference Record of the 1990 IEEE Industry Applications Society Annual Meeting, Seattle, WA, USA, 1990, pp. 965-970 vol.2, doi: 10.1109/IAS.1990.152301.

[100] Fukuda, S. and Endoh, J. “Control method and characteristics of active power filters”, EPE Conference Record, pp. 139–144, 1993.

[101] F. Z. Peng, H. Akagi and A. Nabae, "A study of active power filters using quad-series voltage-source PWM converters for harmonic compensation," in IEEE Transactions on Power Electronics, vol. 5, no. 1, pp. 9-15, Jan. 1990, doi: 10.1109/63.45994.

[102] H. Akagi, "Trends in active power line conditioners," in IEEE Transactions on Power Electronics, vol. 9, no. 3, pp. 263-268, May 1994, doi: 10.1109/63.311258.

[103] C. Pahmer, G. A. Capolino and H. Henao, "Computer-aided design for control of shunt active filter," Proceedings of IECON'94 - 20th Annual Conference of IEEE Industrial Electronics, Bologna, Italy, 1994, pp. 669-674 vol.1, doi: 10.1109/IECON.1994.397857.

[104] P. Verdelho and G. D. Marques, "Design and performance of an active power filter and unbalanced current compensator," Proceedings of IECON'94 - 20th Annual Conference of IEEE Industrial Electronics, Bologna, Italy, 1994, pp. 422-427 vol.1, doi: 10.1109/IECON.1994.397815.

[105] Jou, H.L. “Performance comparison of the three-phase active power-filter algorithms”, IEE Proceedings of the Generation, Transmission and Distribution, Volume 142, Issue 6, November 1995, p. 646 – 652 , 10.1049/ip-gtd:19952247.

[106] S. Bhattacharya and D. Divan, "Active filter solutions for utility interface of industrial loads," Proceedings of International Conference on Power

Electronics, Drives and Energy Systems for Industrial Growth, New Delhi, India, 1996, pp. 1078-1084 vol.2, doi: 10.1109/PEDES.1996.537025.

[107] J. W. Dixon, J. J. Garcia and L. Moran, "Control system for three-phase active power filter which simultaneously compensates power factor and unbalanced loads," in IEEE Transactions on Industrial Electronics, vol. 42, no. 6, pp. 636-641, Dec. 1995, doi: 10.1109/41.475504.

[108] Seung-Gi Jeong and Myung-Ho Woo, "DSP based active power filter with predictive current control," Proceedings of IECON '95 - 21st Annual Conference on IEEE Industrial Electronics, Orlando, FL, USA, 1995, pp. 645-650 vol.1, doi: 10.1109/IECON.1995.483484.

[109] Chin Lin Chen, Chen E. Lin and C. L. Huang, "An active filter for unbalanced three-phase system using synchronous detection method," Proceedings of 1994 Power Electronics Specialist Conference-PESC'94, Taipei, Taiwan, 1994, pp. 1451-1455 vol.2, doi: 10.1109/PESC.1994.373875.

[110] B. Singh, P. Jayaprakash, D. P. Kothari, A. Chandra and K. A. Haddad, "Comprehensive Study of DSTATCOM Configurations," in IEEE Transactions on Industrial Informatics, vol. 10, no. 2, pp. 854-870, May 2014, doi: 10.1109/TII.2014.2308437.

[111] S. K. Jain & P.A "Design Simulation and Experimental Investigations, on a Shunt Active Power Filter for Harmonics, and Reactive Power Compensation, Electric Power Components and Systems", 31:7, 671-692, DOI: 10.1080/15325000390203674, 2003.

[112] A. Govind, V. Kumar Tayal and R. K. Kumawat, "Comparison of Current Controlling Methods for Shunt Active Power Filters to Improve Power Quality," 2022 10th International Conference on Reliability, Infocom Technologies and Optimization (Trends and Future Directions) (ICRITO), Noida, India, 2022, pp. 1-5, doi: 10.1109/ICRITO56286.2022.9965182.

[113] S. Kumaresan and H. Habeebullah Sait, " Embedded System Implementation of Shunt Active Power Filter with Direct Compensation Component Generation Using Linear Operational Amplifiers", Journal of Circuits, Systems and ComputersVol. 29, No. 10, 2050166 (2020), https://doi.org /10.1142/S0218126620501662.

[114] H. Akagi, Y. Kanazawa and A. Nabae, "Instantaneous Reactive Power Compensators Comprising Switching Devices without Energy Storage Components," in IEEE Transactions on Industry Applications, vol. IA-20, no. 3, pp. 625-630, May 1984, doi: 10.1109/TIA.1984.4504460.

[115] R. S. Herrera, P. Salmer and H. Kim, "Instantaneous Reactive Power Theory Applied to Active Power Filter Compensation: Different Approaches, Assessment, and Experimental Results," in IEEE Transactions on Industrial Electronics, vol. 55, no. 1, pp. 184-196, Jan. 2008, doi: 10.1109/TIE.2007.905959.

[116] Vijayakumar Gali, Nitin Gupta & R. A. Gupta "PTF-based control algorithm for three-phase interleaved inverter-based SAPF", International Journal of Electronics, 2019, 106:7, 1060-1084, DOI: 10.1080/00207217.2019.1582706.

[117] Monfared, M.; Golestan, S.; Guerrero, J.M. A new synchronous reference frame-based method for single-phase shunt active power filters. J. Power Electron. 2013, 13, 692–700.

[118] Elango Sundaram, Manikandan Venugopal, “On design and implementation of three phase three level shunt active power filter for harmonic reduction using synchronous reference frame theory, International Journal of Electrical Power & Energy Systems, Volume 81, 2016, Pages 40-47, ISSN 0142-0615, https://doi.org/10.1016/j.ijepes.2016.02.008.

[119] S. Devassy and B. Singh, "Design and performance analysis of three-phase solar PV integrated UPQC," 2016 IEEE 6th International Conference on Power Systems (ICPS), New Delhi, India, 2016, pp. 1-6, doi: 10.1109/ICPES.2016.7584022.

[120] B. Singh, C. Jain and S. Goel, "ILST Control Algorithm of Single-Stage Dual Purpose Grid Connected Solar PV System," in IEEE Transactions on Power Electronics, vol. 29, no. 10, pp. 5347-5357, Oct. 2014, doi: 10.1109/TPEL.2013.2293656.

[121] M. Kesler and E. Ozdemir, "Synchronous-Reference-Frame-Based Control Method for UPQC Under Unbalanced and Distorted Load Conditions," in IEEE Transactions on Industrial Electronics, vol. 58, no. 9, pp. 3967-3975, Sept. 2011, doi: 10.1109/TIE.2010.2100330.

[122] B. Singh, S. Dwivedi, I. Hussain and A. K. Verma, "Grid integration of solar PV power generating system using QPLL based control algorithm," 2014 6th IEEE Power India International Conference (PIICON), Delhi, India, 2014, pp. 1-6, doi: 10.1109/POWERI.2014.7117785.

[123] B. Singh, D. T. Shahani and A. K. Verma, "Power balance theory-based control of grid interfaced solar photovoltaic power generating system with improved power quality," 2012 IEEE International Conference on Power Electronics, Drives and Energy Systems (PEDES), Bengaluru, India, 2012, pp. 1-7, doi: 10.1109/PEDES.2012.6484359.

[124] M. Karimi-Ghartemani, H. Karimi and M. R. Iravani, "A magnitude/phase-locked loop system based on estimation of frequency and in-phase/quadrature-phase amplitudes," in IEEE Transactions on Industrial Electronics, vol. 51, no. 2, pp. 511-517, April 2004, doi: 10.1109/TIE.2004.825282.

[125] R. I. Bojoi, L. R. Limongi, D. Roiu and A. Tenconi, "Enhanced Power Quality Control Strategy for Single-Phase Inverters in Distributed Generation Systems," in IEEE Transactions on Power Electronics, vol. 26, no. 3, pp. 798-806, March 2011, doi: 10.1109/TPEL.2010.2103572.

[126] M. Saitou and T. Shimizu, "Generalized theory of instantaneous active and reactive powers in single-phase circuits based on Hilbert transform," 2002 IEEE 33rd Annual IEEE Power Electronics Specialists Conference. Proceedings (Cat. No.02CH37289), Cairns, QLD, Australia, 2002, pp. 1419-1424 vol.3, doi: 10.1109/PSEC.2002.1022375.

[127] M. Gonzalez, V. Cardenas and F. Pazos, "DQ transformation development for single-phase systems to compensate harmonic distortion and reactive power," 9th IEEE International Power Electronics Congress, 2004. CIEP 2004, Celaya, Mexico, 2004, pp. 177-182, doi: 10.1109/CIEP.2004.1437575.

[128] F. Blaabjerg, R. Teodorescu, M. Liserre and A. V. Timbus, "Overview of Control and Grid Synchronization for Distributed Power Generation Systems," in IEEE Transactions on Industrial Electronics, vol. 53, no. 5, pp. 1398-1409, Oct. 2006, doi: 10.1109/TIE.2006.881997.

[129] Guan-Chyun Hsieh and J. C. Hung, "Phase-locked loop techniques. A survey," in IEEE Transactions on Industrial Electronics, vol. 43, no. 6, pp. 609-615, Dec. 1996, doi: 10.1109/41.544547.

[130] Se-Kyo Chung, "A phase tracking system for three phase utility interface inverters," in IEEE Transactions on Power Electronics, vol. 15, no. 3, pp. 431-438, May 2000, doi: 10.1109/63.844502.

[131] A. Timbus, M. Liserre, R. Teodorescu and F. Blaabjerg, "Synchronization methods for three phase distributed power generation systems - An overview and evaluation," 2005 IEEE 36th Power Electronics Specialists Conference, Dresden, Germany, 2005, pp. 2474-2481, doi: 10.1109/PESC.2005.1581980.

[132] L. N. Arruda, S. M. Silva and B. J. C. Filho, "PLL structures for utility connected systems," Conference Record of the 2001 IEEE Industry Applications Conference. 36th IAS Annual Meeting (Cat. No.01CH37248), Chicago, IL, USA, 2001, pp. 2655-2660 vol.4, doi: 10.1109/IAS.2001.955993.

[133] H. Akagi, E H Watanabe and M Aredes, "Instantaneous power theory and applications to power conditioning, John Wiley & Sons, New Jersey, USA, 2007.

[134] S. Devassy and B. Singh, "Design and performance analysis of three-phase solar PV integrated UPQC," 2016 IEEE 6th International Conference on Power Systems (ICPS), New Delhi, India, 2016, pp. 1-6, doi: 10.1109/ICPES.2016.7584022.

[135] B. Singh, C. Jain and S. Goel, "ILST Control Algorithm of Single-Stage Dual Purpose Grid Connected Solar PV System," in IEEE Transactions on Power Electronics, vol. 29, no. 10, pp. 5347-5357, Oct. 2014, doi: 10.1109/TPEL.2013.2293656.

[136] M. Kesler and E. Ozdemir, "Synchronous-Reference-Frame-Based Control Method for UPQC Under Unbalanced and Distorted Load Conditions," in IEEE Transactions on Industrial Electronics, vol. 58, no. 9, pp. 3967-3975, Sept. 2011, doi: 10.1109/TIE.2010.2100330.

[137] B. Singh, S. Dwivedi, I. Hussain and A. K. Verma, "Grid integration of solar PV power generating system using QPLL based control algorithm," 2014 6th IEEE Power India International Conference (PIICON), Delhi, India, 2014, pp. 1-6, doi: 10.1109/POWERI.2014.7117785.

[138] B. Singh, D. T. Shahani and A. K. Verma, "Power balance theory-based control of grid interfaced solar photovoltaic power generating system with improved power quality," 2012 IEEE International Conference on Power Electronics, Drives and Energy Systems (PEDES), Bengaluru, India, 2012, pp. 1-7, doi: 10.1109/PEDES.2012.6484359.

[139] M. Karimi-Ghartemani, H. Karimi and M. R. Iravani, "A magnitude/phase-locked loop system based on estimation of frequency and in-phase/quadrature-

phase amplitudes," in IEEE Transactions on Industrial Electronics, vol. 51, no. 2, pp. 511-517, April 2004, doi: 10.1109/TIE.2004.825282.

[140] R. I. Bojoi, L. R. Limongi, D. Roiu and A. Tenconi, "Enhanced Power Quality Control Strategy for Single-Phase Inverters in Distributed Generation Systems," in IEEE Transactions on Power Electronics, vol. 26, no. 3, pp. 798-806, March 2011, doi: 10.1109/TPEL.2010.2103572.

[141] M. Saitou and T. Shimizu, "Generalized theory of instantaneous active and reactive powers in single-phase circuits based on Hilbert transform," 2002 IEEE 33rd Annual IEEE Power Electronics Specialists Conference. Proceedings (Cat. No.02CH37289), Cairns, QLD, Australia, 2002, pp. 1419-1424 vol.3, doi: 10.1109/PSEC.2002.1022375.

[142] M. Gonzalez, V. Cardenas and F. Pazos, "DQ transformation development for single-phase systems to compensate harmonic distortion and reactive power," 9th IEEE International Power Electronics Congress, 2004. CIEP 2004, Celaya, Mexico, 2004, pp. 177-182, doi: 10.1109/CIEP.2004.1437575.

[143] F. Blaabjerg, R. Teodorescu, M. Liserre and A. V. Timbus, "Overview of Control and Grid Synchronization for Distributed Power Generation Systems," in IEEE Transactions on Industrial Electronics, vol. 53, no. 5, pp. 1398-1409, Oct. 2006, doi: 10.1109/TIE.2006.881997.

[144] Guan-Chyun Hsieh and J. C. Hung, "Phase-locked loop techniques. A survey," in IEEE Transactions on Industrial Electronics, vol. 43, no. 6, pp. 609-615, Dec. 1996, doi: 10.1109/41.544547.

[145] Se-Kyo Chung, "A phase tracking system for three phase utility interface inverters," in IEEE Transactions on Power Electronics, vol. 15, no. 3, pp. 431-438, May 2000, doi: 10.1109/63.844502.

[146] S. Bhattacharya and D. Divan, "Synchronous frame-based controller implementation for a hybrid series active filter system," IAS '95. Conference Record of the 1995 IEEE Industry Applications Conference Thirtieth IAS Annual Meeting, Orlando, FL, USA, 1995, pp. 2531-2540 vol.3, doi: 10.1109/IAS.1995.530625.

[147] H. Akagi, Y. Kanazawa and A. Nabae, "Instantaneous Reactive Power Compensators Comprising Switching Devices without Energy Storage Components," in IEEE Transactions on Industry Applications, vol. IA-20, no. 3, pp. 625-630, May 1984, doi: 10.1109/TIA.1984.4504460.

[148] R. S. Herrera, P. Salmer and H. Kim, "Instantaneous Reactive Power Theory Applied to Active Power Filter Compensation: Different Approaches, Assessment, and Experimental Results," in IEEE Transactions on Industrial Electronics, vol. 55, no. 1, pp. 184-196, Jan. 2008, doi: 10.1109 /TIE.2007.905959.

[149] Vijayakumar Gali, Nitin Gupta & R. A. Gupta “PTF-based control algorithm for three-phase interleaved inverter-based SAPF”, International Journal of Electronics, 2019, 106:7, 1060-1084, DOI: 10.1080/00207217.2019.1582706.

[150] Monfared, M.; Golestan, S.; Guerrero, J.M. A new synchronous reference frame-based method for single-phase shunt active power filters. J. Power Electron. 2013, 13, 692–700.

[151] R. S. Herrera, P. Salmeron and H. Kim, "Instantaneous reactive power theory applied to active power filter compensation: Different approaches assessment and experimental results", IEEE Trans. Ind. Electron., vol. 55, no. 1, pp. 184-196, Jan. 2008.

[152] L. N. Arruda, S. M. Silva and B. J. C. Filho, "PLL structures for utility connected systems," Conference Record of the 2001 IEEE Industry Applications Conference. 36th IAS Annual Meeting (Cat. No.01CH37248), Chicago, IL, USA, 2001, pp. 2655-2660 vol.4, doi: 10.1109/IAS.2001.955993.

[153] C. Jain and B. Singh, "An assessment of RAD based control algorithm for single-stage multitasking grid tied SECS," 2014 Innovative Applications of Computational Intelligence on Power, Energy and Controls with their impact on Humanity (CIPECH), Ghaziabad, India, 2014, pp. 273-278, doi: 10.1109/CIPECH.2014.7019060.

[154] N. Sireesha, K. Chithra and T. Sudhakar, "Adaptive filtering based on least mean square algorithm," 2013 Ocean Electronics (SYMPOL), Kochi, India, 2013, pp. 42-48, doi: 10.1109/SYMPOL.2013.6701910.

[155] S. Haykin and T. Kailath, "Adaptive Filter Theory", Pearson education, New Delhi, India, 2003.

[156] A. Singh, M. Badoni and B. Singh, "Application of least means square algorithm to shunt compensator: An experimental investigation," 2014 IEEE International Conference on Power Electronics, Drives and Energy Systems (PEDES), Mumbai, India, 2014, pp. 1-6, doi: 10.1109/PEDES.2014.7042044.

[157] Goran S. Nikolić, Tatjana R. Nikolić & Goran Lj. Djordjević, "Adaptive Control Based on LMS Algorithm for Grid Connected Inverters", Electric Power Components and Systems, 2023, 51:7, 656 - 668, DOI: 10.1080/ 15325008. 2023.2180815.

[158] S. R. Arya and B. Singh, "Performance of DSTATCOM Using Leaky LMS Control Algorithm," in IEEE Journal of Emerging and Selected Topics in Power Electronics, vol. 1, no. 2, pp. 104-113, June 2013, doi: 10.1109/JESTPE.2013.2266372.

[159] M. Badoni, A. Singh and B. Singh, "Comparative Performance of Wiener Filter and Adaptive Least Mean Square-Based Control for Power Quality Improvement," in IEEE Transactions on Industrial Electronics, vol. 63, no. 5, pp. 3028-3037, May 2016, doi: 10.1109/TIE.2016.2515558.

[160] S. Malathi, J. Jayachandran, "FPGA implementation of NN based LMS–LMF control algorithm in DSTATCOM for power quality improvement", Control Engineering Practice, Volume 98, 2020, 104378, ISSN 0967-0661, https://doi.org/10.1016/j.conengprac.2020.104378.

[161] Vanaja N. & Senthil Kumar N." Interval type-2 fuzzy controller-based power quality enhancement in HSES grid-Integrated scheme, Automatika, 2023, 64:3, 577-592, DOI: 10.1080/00051144.2023.2203563.

[162] J. Jayachandran and R. Murali Sachithanandam, "Neural Network-Based Control Algorithm for DSTATCOM Under Nonideal Source Voltage and Varying Load Conditions," in Canadian Journal of Electrical and Computer

Engineering, vol. 38, no. 4, pp. 307-317, Fall 2015, doi: 10.1109/CJECE.2015.2464109.

[163] Jayachandran, J., Sachithanandam, R.M. Performance investigation of artificial intelligence-based controller for three phase four leg shunt active filter. Front. Energy 9, 446–460 (2015). https://doi.org/10.1007/s11708-015-0378-2.

[164] M. Qasim, P. Kanjiya and V. Khadkikar, "Artificial-Neural-Network-Based Phase-Locking Scheme for Active Power Filters," in IEEE Transactions on Industrial Electronics, vol. 61, no. 8, pp. 3857-3866, Aug. 2014, doi: 10.1109/TIE.2013.2284132.

[165] K. Kumar Pedapenki, "Power Quality with ANN and Hysteresis controllers," 2019 2nd International Conference on Intelligent Computing, Instrumentation and Control Technologies (ICICICT), Kannur, India, 2019, pp. 328-334, doi: 10.1109/ICICICT46008.2019.8993197.

[166] K. A. Naushad Ahmed, K. C. Obula Reddy and P. Bhakre, "Fuzzy Based Active Filter for Power Quality Mitigation," 2018 IEEE International Conference on System, Computation, Automation and Networking (ICSCA), Pondicherry, India, 2018, pp. 1-4, doi: 10.1109/ICSCAN.2018.8541247.

[167] M. A. M. Radzi and N. A. Rahim, "Neural Network and Bandless Hysteresis Approach to Control Switched Capacitor Active Power Filter for Reduction of Harmonics," in IEEE Transactions on Industrial Electronics, vol. 56, no. 5, pp. 1477-1484, May 2009, doi: 10.1109/TIE.2009.2013750.

[168] L.-T. Teng, F.-J. Lin, H.-C. Chiang and J.-W. Lin, "Recurrent wavelet neural network controller with improved particle swarm optimisation for induction generator system", Volume 3, Issue 2, March 2009, p. 147 – 159, DOI: 10.1049/iet-epa:20080038.

[169] A. Bhattacharya and C. Chakraborty, "Predictive and Adaptive ANN (Adaline) Based Harmonic Compensation for Shunt Active Power Filter," 2008 IEEE Region 10 and the Third international Conference on Industrial and Information Systems, Kharagpur, India, 2008, pp. 1-6, doi: 10.1109/ICIINFS.2008.4798496.

[170] L. H. Tey, P. L. So, and Y. C. Chu, "Neural network-controlled unified power quality conditioner for system harmonics compensation," IEEE/PES Transmission and Distribution Conference and Exhibition, Yokohama, Japan, 2002, pp. 1038-1043 vol.2, doi: 10.1109/TDC.2002.1177620.

[171] B. Singh, V. Verma and J. Solanki, "Neural Network-Based Selective Compensation of Current Quality Problems in Distribution System," in IEEE Transactions on Industrial Electronics, vol. 54, no. 1, pp. 53-60, Feb. 2007, doi: 10.1109/TIE.2006.888754.

[172] N. Gotherwal, S. Ray, N. Gupta and D. Saxena, "Performance comparison of PI and fuzzy controller for indirect current control-based shunt active power filter," 2016 IEEE 1st International Conference on Power Electronics, Intelligent Control and Energy Systems (ICPEICES), Delhi, India, 2016, pp. 1-6, doi: 10.1109/ICPEICES. 2016.7853460.

[173] P. Shah, I. Hussain and B. Singh, "Fuzzy Logic Based FOGI-FLL Algorithm for Optimal Operation of Single-Stage Three-Phase Grid Interfaced Multifunctional SECS," in IEEE Transactions on Industrial Informatics, vol. 14, no. 8, pp. 3334-3346, Aug. 2018, doi: 10.1109/TII.2017.2786159.

[174] P.C Loh, Y. Tang, F. Blaabjerg and P. Wang, "Mixed-frame and stationery-frame repetitive control schemes for compensating typical load and grid harmonics" Vol. 4, Issue-2 February 2011, PP. 218-226, DOI: 10.1049/iet-pel.2009.0222 , Print ISSN 1755-4535, Online ISSN 1755-4543.

[175] Yamina Simhamed, Farid Ykhlef, Abdelhamid Iratni, "A New Classification Scheme Based on Extended Kalman Filter and Support Vector Machine," Electric Power Systems Research, Volume 210, 2022, 108153, ISSN 0378-7796, https://doi.org/10.1016/j.epsr.2022.108153.

[176] B. Singh and S. R. Arya, "Back-Propagation Control Algorithm for Power Quality Improvement Using DSTATCOM," in IEEE Transactions on Industrial Electronics, vol. 61, no. 3, pp. 1204-1212, March 2014, doi: 10.1109 /TIE.2013.2258303.

[177] P.C. Loh, Y. Tang, F. Blaabjerg and P. Wang, '' Mixed- frame and stationary-frame repetitive control scheme for compensating typical load and grid harmonics," in IET power electronics, vol. 4, no. 2, pp. 218-226, February 2011.doi: 10.1049/iet-pel.2009.0222.

[178] R. Cardoso, J. Kanieski, H. Pinheiro and H. A. Grundling, "Reference Generation for Shunt Active Power Filters Based on Optimum Filtering Theory," 2007 IEEE Industry Applications Annual Meeting, New Orleans, LA, USA, 2007, pp. 1621-1627, doi: 10.1109/07IAS.2007.250.

[179] S. Agrawal, P. Kumar and D. K. Palwalia, "Artificial neural network based three phase shunt active power filter," 2016 IEEE 7th Power India International Conference (PIICON), Bikaner, India, 2016, pp. 1-6, doi: 10.1109/POWERI.2016.8077153.

[180] Yongtao, Dai1 Wenjin, and Dai "Harmonic and Reactive Power Compensation with Artificial Neural Network Technology "Proceedings of the 7th World Congress on Intelligent Control and Automation June 25 - 27, 2008, Chongqing, China.

[181] Ali, Munazama & Joshi, Deeraj. (2018). Analysis of Shunt Active Filter with ANN based Controller. International Journal of Computer Applications. 182. 27-32. 10.5120/ijca2018918241.

[182] Rachid, Dehini & Bassou, Abdesselam & Ferdi "Artificial neural networks application to improve shunt active power filter" 33. 1058-1065, 2009.

[183] C. Benachaiba, B. Ferdi, "A Comparative Study of IEC 61000 Part 3-2 & 3-4 and IEEE 519-1992 Standards in Low Voltage Applications'', International Review of Electrical Engineering (IREE) December 2007, pp. 771-776.

[184] Chen Ke, Ai Wu, Chen Bing and Liu Yi," Measuring and reconstruction algorithm based on improved second-order generalised integrator configured as a quadrature signal generator and phase locked loop for the three-phase AC signals of independent power generation systems" IET Power Electronics, Volume 9, Issue 11, 07 September 2016, p. 2155 – 2161,

[185] S. Kumar, I. Hussain, B. Singh, A. Chandra and K. Al-Haddad, "An Adaptive Control Scheme of SPV System Integrated to AC Distribution System," in IEEE Transactions on Industry Applications, vol. 53, no. 6, pp. 5173-5181, Nov.-Dec. 2017, doi: 10.1109/TIA.2017.2722978.

[186] C. Jain and B. Singh, "An offset reduction second order generalized integrator-based control algorithm for single-phase S-DSTATCOM," 2015 39th National Systems Conference (NSC), Greater Noida, India, 2015, pp. 1-6, doi: 10.1109/NATSYS.2015.7489076.

[187] B. Singh, S. Kumar and C. Jain, "Damped-SOGI-Based Control Algorithm for Solar PV Power Generating System," in IEEE Transactions on Industry Applications, vol. 53, no. 3, pp. 1780-1788, May-June 2017, doi: 10.1109/TIA.2017.2677358.

[188] Chandran, Vineet & Murshid, Shadab & Singh, Bhim, "Design and analysis of improved second order generalized integrator-based voltage and frequency controller for permanent magnet synchronous generator operating in small-hydro system feeding single-phase loads". International Transactions on Electrical Energy Systems.,2019,29. e2827. 10.1002/2050-7038.2827.

[189] C. Jain and B. Singh, "A SOGI-FLL based control algorithm for single phase grid interfaced multifunctional SPV under non ideal distribution system," 2014 Annual IEEE India Conference (INDICON), Pune, India, 2014, pp. 1-6, doi: 10.1109/INDICON.2014.7030368.

[190] B. Singh and V. Verma, "Selective Compensation of Power-Quality Problems Through Active Power Filter by Current Decomposition," in IEEE Transactions on Power Delivery, vol. 23, no. 2, pp. 792-799, April 2008, doi: 10.1109/TPWRD.2007.911108.

[191] Saxena, H., Singh, A. & Rai, J.N. Enhanced Third-Order Generalized Integrator-Based Grid Synchronization Technique for DC-Offset Rejection and Precise Frequency Estimation. Arab J Sci Eng 46, 9753–9762 (2021). https://doi.org/10.1007/s13369-021-05559.

[192] Vineet P. Chandran, Shadab Murshid & Bhim Singh, "Improved TOGI-Based Voltage and Frequency Control for PMSG Feeding Single-Phase Loads in Isolated Pico-Hydro Generation", IETE Journal of Research, 2021, 67:6, 882-898, DOI: 10.1080/03772063.2019.1571953.

[193] Priyank Shah, Ikhlaq Hussain and Bhim Singh, " Multi-resonant FLL-based control algorithm for grid interfaced multi-functional solar energy conversion system", Volume 12, Issue 1, January 2018, p. 49 – 62, 10.1049/iet-smt.2017.0096.

[194] P. Shah, I. Hussain and B. Singh, "A Novel Fourth-Order Generalized Integrator Based Control Scheme for Multifunctional SECS in the Distribution System," in IEEE Transactions on Energy Conversion, vol. 33, no. 3, pp. 949-958, Sept. 2018, doi: 10.1109/TEC.2018.2806191.

[195] N. Kumar, I. Hussain, B. Singh and B. K. Panigrahi, "Implementation of Multilayer Fifth-Order Generalized Integrator-Based Adaptive Control for Grid-Tied Solar PV Energy Conversion System," in IEEE Transactions on Industrial Informatics, vol. 14, no. 7, pp. 2857-2868, July 2018, doi: 10.1109/TII.2017.2777882.

[196] P. Shah, I. Hussain and B. Singh, "FOGI-QSG based control of multifunctional grid tied SECS," 2016 IEEE 7th Power India International Conference (PIICON), Bikaner, India, 2016, pp. 1-6, doi: 10.1109/POWERI.2016.8077293.

[197] P. Shah, I. Hussain and B. Singh, "Fuzzy Logic Based FOGI-FLL Algorithm for Optimal Operation of Single-Stage Three-Phase Grid Interfaced Multifunctional SECS," in IEEE Transactions on Industrial Informatics, vol. 14, no. 8, pp. 3334-3346, Aug. 2018, doi: 10.1109/TII.2017.2786159.

# APPENDIX A

## SYSTEM DATA FOR THREE PHASE GRID CONNECTED SOLAR PV SYSTEM

SPV power =32 kW, open circuit voltage= 32.9 V, short circuit current= 8.21A, Vmp= 26.3, cells per module= 96, parallel string (Np)= 6, series module (Ns)= 27, Parameters:- AC grid voltage, Vgabc(V) = 415V; DC bus voltage Vdc (V) = 700V; ripple filter:- R= 5Ω, C= 50 μF; interfacing inductor= 2.5 mH; nonlinear load, R= 5 Ω, L= 8 mH.

# APPENDIX B

## SYSTEM DATA FOR HYBRID POWER GENERATING SYSTEMS

G1=1.41 and G2=1.75, $L_{B1}$ = $5e^{-3}$H, $L_{B2}$ = $.5e^{-4}$ H, $L_f$ =$.1e^{-3}$H, ripple filter (R,C) = 5 ohm, $20e^{-6}$ F, DC link Voltage = 690 V, linear load $P_L$= 30 Kw, nonlinear load $R_L$=5 ohm, $L_L$=$8e^{-3}$ H

# APPENDIX C

## SYSTEM DATA FOR ADAPTIVE CONTROL ALGORITHMS FOR GRID-TIED PV SYSTEM

Grid voltage $(L-L, RMS) = 425V, 50Hz$, Interfacing inductor $(L_p) = 6.4mH$, DC-link capacitor $(C_{dc}) = 4000\mu F$, Non-linear load: Rectifier with $R_L = 40\Omega, \mathrm{L_L} = 80mH$, Linear load: $R_{L1} = 20\Omega, L_{L1} = 40mH$, PV array: No. of series panels = 22, Maximum Power of array=5.954kW, Maximum power of panel = 270.66W, Open-circuit voltage $(V_{oc}) = 44V$, Short-circuit current $(I_{sc}) = 8.1A$, Voltage at MPP $(V_{mp}) = 34.7V$, Current at MPP $(I_{mp}) = 7.8A$, Step-size for P&O MPPT $\Delta V = 0.025V$, Sampling Time $(Ts) = 10\mu s$.